Model-Based External Forcing of Nonlinear Dynamics in Chemical and Biochemical Reaction Systems *via* Optimal Control

D I S S E R T A T I O N

submitted to the

Combined Faculties for the Natural Sciences and for Mathematics
of the Rupertus-Carola University of Heidelberg, Germany
for the degree of
Doctor of Natural Sciences

presented by
Osman Shahi Shaik, M.Eng.
born in Sitarampuram, India

Examiners: Priv. Doz. Dr. Dirk Lebiedz
Prof. Dr. Jerzy Górecki

Heidelberg, January 24, 2008

Interdisziplinäres Zentrum für Wissenschaftliches Rechnen
Ruprecht - Karls - Universität Heidelberg
2008

D I S S E R T A T I O N

submitted to the

Combined Faculties for the Natural Sciences and for Mathematics
of the Rupertus-Carola University of Heidelberg, Germany
for the degree of
Doctor of Natural Sciences

presented by
Osman Shahi Shaik, M.Eng.
born in Sitarampuram, India

Heidelberg, January 24, 2008

Model-Based External Forcing of Nonlinear Dynamics in Chemical and Biochemical Reaction Systems *via* Optimal Control

Gutachter: Priv. Doz. Dr. Dirk Lebiedz
Prof. Dr. Jerzy Górecki

January 24, 2008

Abstract

Detailed quantitative understanding by modeling and the possibility for specific external control of cellular behavior are general long-term goals of modern bioscience research activities in systems biology. Self-organization might be a general principle in cellular organization as many dynamic properties of cellular structures are consistent with a role for self-organization in their formation, maintenance, and function. Controlling self-organized dynamics provides an avenue for exploring dynamical behavior as well as generating particular desired behavior. Towards realizing this goal the central aim of this thesis is on target oriented manipulation of these systems by optimal control methods. The optimal control approach offers a great deal of flexibility in formulating objective functions, and we use a direct multiple shooting based numerical optimization approach, which is particularly suitable for nonlinear self-organizing systems. Here, we demonstrate how model-based optimal control methods can be exploited for inducing desired system dynamics which is not system inherent by time varying control parameters in the case of Circadian rhythms and the Belousov-Zhabotinsky (BZ) reaction as model systems.

Circadian rhythms governed by the oscillating expression of a set of genes based on feedback regulation by their products have become an important issue in biology and medicine. Here, we study a circadian oscillator model of the central clock mechanism for the fruit fly *Drosophila* and show how model-based optimal control allows for optimal phase resetting, design of chronomodulated pulse-stimuli schemes for achieving circadian rhythm restoration in mutants and optimal phase synchronization between the clock and its environment. We refer to both open-loop and feedback optimal control approaches. Circadian rhythms can significantly affect the timing and entry of the cell cycle. A detailed coupled circadian cycle and the cell cycle model has been developed in a mammalian system, for investigating the model-based optimal control scenarios. Initial numerical simulation results for the coupled circadian cycle and the cell cycle model are shown here.

Easily accessible test-tube chemical systems like the BZ reaction are particularly well suited for studies of controlling self-organized dynamics, and they offer a means for characterizing behavior that is relevant to more complex biological systems. Here, we develop a novel detailed model for the photosensitive BZ reaction based on an elementary step reaction mechanism and reduce the model explicitly with quasi-steady-state (QSSA) and partial-equilibrium-approximations (PEA). Systematic analysis and model-based control for stabilizing unstable steady states, and obtaining periodic orbits with a desired time period are carried out. The results are analyzed and compared with a very simple 3-variable Oregonator model from the literature.

Keywords:

Self-organization; optimal control; direct multiple-shooting; nonlinear model predictive control (NMPC); mixed-integer optimal control; bang-bang controls; periodic control; circadian rhythms; BZ reaction; Cell cycle; phase resetting; phase tracking and entrainment.

Zusammenfassung

Ein ausführliches, quantitatives Verständnis, welches durch Modellieren erzielt wird, sowie das Ermöglichen einer spezifischen externen Steuerung des zellularen Verhaltens sind allgemeine langfristige Ziele der modernen biowissenschaftlichen Forschung in der Systembiologie. Selbstorganisation ist möglicherweise ein allgemein gültiges Prinzip für die zelluläre Organisation, da viele dynamische Eigenschaften zellulärer Strukturen sowohl hinsichtlich ihrer Bildung, Aufrechterhaltung und Funktion diesem folgen. Die Steuerung selbstorganisierter Dynamiken eröffnet einen Weg zur Untersuchung von dynamischem Verhalten sowie zur Generierung des gewünschten Verhaltens. Um dieses Ziel zu verwirklichen, konzentriert sich diese Dissertation in erster Linie auf die gezielt orientierte Beeinflussung dieser Systeme durch optimale Steuerungsmethoden. Der Ansatz optimaler Steuerung bietet große Flexibilität hinsichtlich der Bestimmung der Zielfunktionen. Wir verwenden eine direkte, auf den Multiple-Shooting-Ansatz basierende numerische Optimiermethode, welche insbesondere auf nichtlineare selbstorganisierende Systeme verwendbar ist. Die vorliegende Arbeit zeigt, wie auf Modellen basierende optimale Steuerungsmethoden zum Erzeugen der gewünschten Systemdynamiken verwertet werden können. Im Fall des Circadischen Rhythmus und der Belousov-Zhabotinsky (BZ) Reaktion als Modellsysteme sind diese bezüglich der zeitabhängigen Steuerungsparameter nicht systemimmanent.

Wir analysieren ein Circadisches Oszillatormodell des zentralen Uhrmechanismus für die Fruchtfliege *Drosophila* und zeigen, wie auf Modellen basierende optimale Steuerung Phasenneueinstellung, Design von chronomodulierten Puls-Stimuli-Schemata zur Wiederherstellung des Circadischen Rhythmus in den Mutanten und optimale Phasensynchronisierung zwischen der Uhr und ihrer Umgebung erlaubt. Wir beziehen uns sowohl auf die optimalen Open-Loop- als auch auf die Rückkopplungssteuerungsmethoden. Circadische Rhythmen können das Timing und den Eintritt des Zellzyklus erheblich beeinflussen. Zur Untersuchung der auf Modellen basierenden optimalen Steuerungsszenarios sind ein detaillert gekoppelter Circadischer Zyklus und das Zellzyklusmodell für ein Säugetiersystem entwickelt worden. Erstergebnisse der numerischen Simulationen für den gekoppelten Circadischen Zyklus und das Zellzyklusmodell werden gezeigt.

Insbesondere leicht zugängliche chemische Testrohrsysteme wie die BZ Reaktion sind für Untersuchungen der Steuerung selbstorganisierter Dynamiken sehr gut geeignet. Denn sie bieten ein Mittel für die Charkterisierung des Verhaltens, das für kompliziertere biologische Systeme relevant ist. Wir entwickeln ein ganz neuartiges detaillertes Modell für die lichtempfindliche BZ Reaktion, das auf einem Elementarreaktionsmechanismus beruht und reduzieren dieses aufgrund der Quasi-Steady-State- (QSSA) und partielle Gleichgewichtsnäherungen (PEA) explizit. Zur Stabilisierung instabiler stationärer Zustände sind systematische Analysen und auf Modellen basierende Steuerungen durchgeführt worden, woraus periodische Bahnen mit einer gewünschten Periode resultieren. Die Ergebnisse werden diskutiert und mit einem sehr einfachen 3-Variablen-Oregonator-Modell aus der Literatur verglichen.

Contents

Chapter 1

Introduction and Overview

Living organisms are thermodynamically open systems that continuously exchanging energy and matter with their environment. They are characterized by a complex organization, which results from a vast network of molecular interactions involving a high degree of nonlinearity, giving rise to variety of dynamical behavior. In physical and biological systems alike, properties such as openness and nonlinearity may express themselves through spontaneous formation of long-range correlated, macroscopic dynamical patterns in space and time - the process of *self-organization* [1].

The concepts of self-organization and dissipative structures goes back to Schrödinger and Prigogine [2, 3, 4, 5]. In open systems, mechanisms such as positive or negative feedback, auto catalysis and time delays might generate self-organized dynamical behavior. Energy is continuously dissipated during the generation of such self-stabilizing states or dissipative structures. In cells, these dissipative structures and openness prevents the biochemical reactions reaching thermodynamic equilibrium [5] as formulated by Schrödinger [4] 'living matter evades the decay to equilibrium'. The research in nonlinear dynamics has substantially contributed to a more detailed understanding of self-organization phenomena far from equilibrium [6].

Although the self-organization of macroscopic patterns, including temporal oscillations and spatiotemporal wave patterns, was first studied and theoretically understood in physical and chemical systems, numerous examples are now known at all levels of biological organization [7,8]. For example, calcium waves [9], oscillations in neuronal signals [10], oscillations in cyclic AMP in the slime mould *Dictyostelium discoideum* [11], yeast glycolytic oscillations [12], circadian rhythm [13] and cell cycle [14, 15]. A very good overview concerning oscillatory phenomena in cells and biological rhythms is given in [7]. These periodic oscillatory phenomena can be a function of time (glycolytic oscillations), space (striping in *Drosophila melanogaster* embryos), or both (*D. discoideum*, calcium waves, neuronal oscillations) depending on the mechanism of the oscillator [16]. Some of these oscillatory phenomena (for example, neuronal oscillations which reflects the temporally precise interaction of neural activities – is a likely mechanism for neural communication [17]; calcium and endocrine oscillations appear to function as information-transfer pathways [18,7,19]) are crucial in living systems in which they occur. External forcing and nonlinear

control of these self-organizing oscillating biosystems might be of great benefit [1], for example in drug development to cure diseases caused by dynamical malfunction of cellular systems or to understand which molecular defects result in pathological disturbance in oscillations.

The study of self-organizing biological systems increasingly requires the application of modeling, mathematical methods and interdisciplinary approaches. The new research area of systems biology [20, 21] aims at a system level understanding of these biological processes, how the interactions between the components give rise to the function and behavior of that system. These studies are based on detailed reaction mechanisms with nonlinear couplings, feedforward, feedback loops between components, can serve for a quantitative study of system behavior in numerical simulations and control tasks. Model-based external control allows us to explore the response of a self-organizing chaotic or non-chaotic system to a defined stimulus, and gain insight on how information is encoded and decoded and associated inherent control mechanisms in these systems. Such studies are particularly important to understand the behavior of natural systems subjected to external driving forces. Bifurcation and sensitivity analysis might reveal the qualitative and quantitative changes in the behavior of these systems to external perturbations that can be exploited for practical purposes. Controlled perturbations by pharmacological intervention are promising approaches here, that might be used to further advance our understanding and control of these self-organizing biological systems.

Literature on external control of self-organizing dynamical systems in space and time is rich in content [22, 23, 24, 25]. Many different approaches for controlling such behavior have been pursued. Some, such as those based on feedback techniques, make use of the system sensitivity to perturbations displayed by nonlinear dynamical systems [26, 23]. Global feedback, for example gives rise to a rich variety of spatiotemporal dynamics, including behavior not observed in autonomous systems [25]. Local feedback, such as variations of excitability gradients, allows directional control of propagating waves to yield a desired pattern [24]. However, systematic approaches, strictly aiming at control of self-organizing systems with respect to general predefined control aims and subject to constraints, are rare [27, 28] and optimal control is considered to be a promising approach here.

An optimal control problem formulates the control aim as an objective functional to be minimized for a given system dynamics described by ODE or DAE subject to system constraints (e.g. bounds on controls, positive concentrations). This particular formulation offers a broad flexibility for formulating different control objectives that are treated in this thesis. The present work is focused on modeling of self-organizing systems based on detailed reaction mechanisms and its response to the time varying external control inputs. The objective essentially is manipulating the desired functional behavior (generally properties of the system) by changing the

parameter values. In context of this thesis, 'control' refers to excitation or suppression of oscillations, entrainment and synchronization, or transitions from simple to aperiodic oscillations and *vice-versa*. Here, chemical model systems are suitable to provide insight into similar mechanism in the biochemical context. In the present work, we treat circadian rhythms and Belousov-Zhabotinsky (BZ) reaction system as two prototypical examples for controlling the self-organized dynamics.

The circadian clock is found in different organisms, from unicellular [29] to mammals [30]. It enhances the fitness of various organisms by improving their ability to adapt to external influences, specifically daily changes in environmental factors, such as light and temperature. The central circadian clock is an autonomous biochemical oscillator with a period close to 24 hours. Clock-controlled genes facilitate the modulation of many physiological properties during the course of one day. In human beings, blood pressure, mental performance, and hormone levels are some of the properties that change during the day. Although the existence of a circadian clock in humans had been postulated for decades, an understanding of the molecular mechanisms are becoming clear only recently in case of *Drosophila* [31] and more recently in case of mammals [30]. Mass-action kinetics models have been popular and successful for simulating bio(chemical) systems, though there are certain limitations. Several mathematical models with different levels of complexity have been proposed recently to describe different clock systems [32, 33, 34, 35]. As most of the interesting properties of the circadian systems are directly related to their oscillatory behavior, sensitivity analysis of these oscillations is an active area of research, in particular for limit cycle oscillators [36, 37, 38].

A prominent example of a pattern forming chemical system is the BZ reaction [39], which is a homogeneously catalyzed reaction in aqueous solution. It involves several reagents and various intermediate species; the central reaction step is the oxidation of malonic acid by bromate, catalyzed by metal ions. Chemical oscillations in the BZ system were first reported by Belousov (in 1951) and then by Zhabotinsky (in 1961) in a continuously stirred reactor. A decade later, Zhabotinsky and Winfree observed traveling waves of chemical activity in an unstirred reactor [40, 41]. Since then, the BZ reaction has became paradigmatic for pattern formation in chemical systems [39, 42]. The behavior of the Ru-catalyzed BZ reaction [43] is affected by exposure to visible light. The excitability is reduced in proportion to the illumination intensity, which leads to the inhibition of oscillatory behavior in reaction mixtures with appropriate reactant concentrations. This effect provides a useful tool for studies of self-organized dynamics of BZ system in presence of light [44] as an external control parameter which can be conveniently suppressed either locally or globally.

Organization of the thesis.

The thesis is divided into four parts. The first part (chapter 2-3) of this thesis deals with the mathematical background necessary for the application of numerical optimization and optimal control. In chapter 2, we introduce the basic terminology of nonlinear dynamics and fundamental mathematical background for optimal control problems. All problem types relevant for this thesis, their characteristics and solution concepts are briefly discussed. In chapter 3, we review a powerful numerical approach to optimal control problems which is based on the direct multiple-shooting method. The multiple-shooting structure reduces the effects of nonlinearity and instability by breaking down the global optimal control problem into several localized problems, which is crucial for optimal control of highly unstable systems. The latter approach is applied for the numerical solution of all kinds of optimal control problems arising in this thesis.

In chapter 4, we introduce the basic clock architecture of the circadian rhythms in *Drosophila* and mammals. Similarities between the basic clock mechanism between mammals and *Drosophila* are drawn. Medical implication of the circadian rhythms are immense and are briefly reviewed. In this chapter, we treat the first comprehensive application of various types of optimal control problem formulation and their numerical solution for external control of the self-organized circadian rhythms. In particular, here we study circadian rhythms in *Drosophila* as a model organism. Restoration of altered rhythms for therapeutic purposes can generally be viewed as an open-loop control problem. We show how a model-based optimal control allows the design of chronomodulated stimuli schemes achieving circadian rhythm restoration from altered rhythms; optimal recovery of phase synchronization between the clock and its environment; suppression and subsequent restoration of rhythms by optimal light pulses. Both open-loop and closed-loop control of circadian rhythms are treated. Insight gained from such model-based specific manipulation may be promising in biomedical applications.

In chapter 5, we introduce another important oscillator in biology, the cell cycle. Several links are reported in literature between the circadian cycle and the cell cycle, however there are no detailed molecular models available coupling these two cycles. As a first step, we try to model a coupled circadian cell cycle model *via* WEE1 kinase [45]. Initial simulation results are shown for coupled circadian cell cycle oscillator model.

In chapter 6 we treat another example of oscillatory phenomena in chemical systems, the Belousov-Zhabotinsky (BZ) system. A novel detailed model for the photosensitive BZ reaction is developed based on an elementary reaction mechanism. However, mathematical analysis and numerical simulations particularly for spatially non-homogeneous systems, are difficult tasks with detailed mechanistic models. So, model reduction techniques are widely applied to obtain representations in lower-

dimensional phase space which is more suitable for mathematical analysis, efficient numerical simulation, and model-based control tasks. In this chapter, we exploit a recently implemented numerical algorithm [46] for error-controlled computation of the minimum dimension required, to represent the detailed full scale model to a reduced model. The algorithm is based on automatic time scale decomposition and relaxation of the fast modes. The algorithm is applied to the detailed model for Ru-catalyzed BZ reaction and the results are exploited in combination with quasi-steady-state and partial-equilibrium approximations for explicit model reduction of a novel chemical mechanism. We derive such a maximally reduced model from the detailed elementary-step mechanism and demonstrate that, it reproduces quantitatively the dynamical features of the full model within a given accuracy tolerance. Induction of specific oscillatory behavior characterized by amplitude, frequency and mean value of the oscillating species; stabilizing unstable steady states; finding the periodic orbits with desired period are some of the control scenarios that are investigated in the BZ reaction system. Control results in case of the reduced model of BZ system are compared with a classical 3-variable Oregonator model.

Chapter 2

Introduction to Nonlinear Dynamics and Optimal Control

In this chapter, we briefly discuss some basic concepts in nonlinear dynamics and introduce terms like bifurcation, limit cycle oscillations which arise in later chapters. Different optimization methods are reviewed in later sections of this thesis with special emphasis on the choice of method used for controlling the self-organized dynamics modeled by *differential algebraic equations* (DAE).

2.1 Basics of nonlinear dynamics

The coupled rate equations that govern the dynamics of a homogeneous and isothermal chemical reaction follow from its reaction mechanism. In compact form, they are written as

$$\frac{dx}{dt} = F(x;p) \tag{2.1}$$

where F is the rate function, $x(t) = (x_1(t), x_2(t), \cdots, x_n(t))$ is the vector of dynamic variables in n-dimensional phase space, and $p = (p_1, p_2, \cdots, p_m)$ is the vector of control parameters. In a chemical context, $x(t)$ represent concentrations and p the parameters (i.e., rate constants, temperature, reactant composition, flow rate, etc.).

2.1.1 Limit sets, linear stability, and bifurcations

The concepts of phase space and phase portrait are important tools for visualizing the evolution of system (2.1). *Phase space* is the n-dimensional space with coordinates $(x_1, x_2, \cdots, x_n)$. A *phase portrait* is a geometric representation of the trajectories of a dynamical system in the phase plane. A dissipative system (e.g., where conservation laws for energy do not exist) is characterized by the contraction of flow in phase space and by the convergence of all initial conditions to the same region. The subsets of phase space that are approached by the trajectories as $t \longrightarrow \pm\infty$ are called *limit sets*. Of particular importance are the limit sets for $t \longrightarrow +\infty$, which are called *attractors*. Examples of attractors are the stable steady states or stable fixed-point x^* (zero-dimensional manifold), the stable limit cycle (one-dimensional manifold), and the strange attractor (a fractal, with a higher dimensional manifold) [47, 48].

The stationary limit sets (fixed points) x^* of the system (2.1) fullfill the condition $\dfrac{dx}{dt} = 0$. A linear stability analysis of a given fixed point x^* reveals whether it is stable or unstable by perturbing it slightly, $x = x^* + \delta x$, this means whether perturbations from the fixed points decay or grow. After linearization at x^*, the pertubration then evolves according to the equation

$$\dot{\delta x} = J(x^*)\delta x, \quad \text{with} \quad J_{ij} = \frac{\partial F_i}{\partial x_j} \tag{2.2}$$

The eigenvalues $\lambda_i (i = 1, \cdots, n)$ of the Jacobian J evaluated at the fixed point x^* determines the stability of the system given by Eq. 2.1. The fixed point is stable if the real parts of all eigenvalues λ_i are negative and is unstable if the real part of at least one eigenvalue is positive.

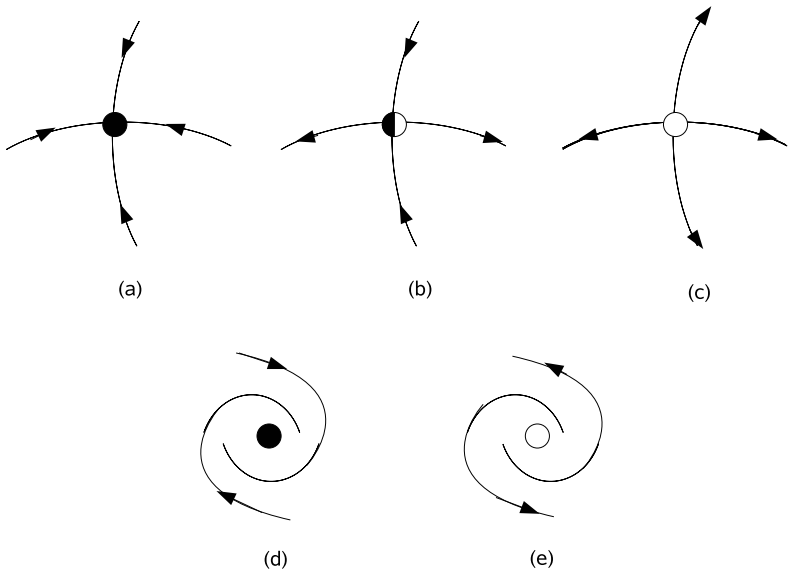

Figure 2.1: Fixed points in two-dimensional phase space: (a) stable node, (b) saddle point, (c) unstable node, (d) stable focus, and (e) unstable focus.

In two-dimensional phase space, the eigenvalues λ_1 and λ_2 may either be real or complex conjugated. Thus, the fixed points that can occur in such a system are either stable and unstable foci, stable and unstable nodes, and saddle point (see Figure 2.1). Two real negative eigenvalues correspond to a stable node and positive eigenvalues corresponds to a unstable node. A saddle point is a combination of real eigenvalues with different signs. Complex conjugated eigenvalues correspond to a focus, whose stability depends on the real parts.

The type of limit sets (fixed points) depends on the chemical kinetic term $F(x; p)$ and on the dimension n of phase space. While fixed points are the only possible attractor in one-dimensional phase spaces, another important type of attractor

is possible in two-dimensional phase spaces, namely the limit cycle. A limit cycle on a plane or a two-dimensional manifold is a closed trajectory in phase space having the property that at least one other trajectory spirals into it as time $t \longrightarrow +\infty$. In case where all the neighboring trajectories approach the limit cycle as time $t \longrightarrow +\infty$, it is referred as a stable limit cycle (see Figure 2.2). Stable limit cycles imply self sustained oscillations. Any small perturbation from the closed trajectory would cause the system to return to the limit cycle, making the system stick to the limit cycle.

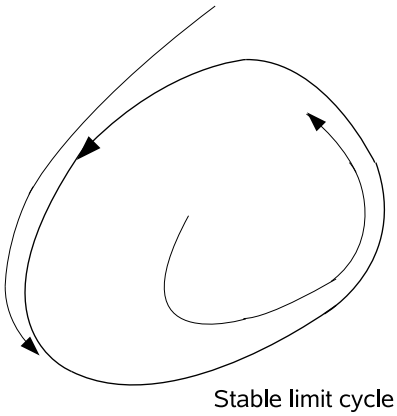

Figure 2.2: Phase space portrait of the stable limit cycle.

The stability of a fixed point may be changed when at least one of the eigenvalues changes its sign, this event is called bifurcation. The simplest example of bifurcation leading to time periodic behavior is the supercritical Hopf bifurcation (see Figure 2.3). As an appropriate parameter p is varied beyond its critical value p_c, a stable focus becomes unstable and simultaneously a stable limit cycle is born. Sufficiently close to the bifurcation point, the oscillations are harmonic and amplitude follows a square root dependence $A \sim \sqrt{p - p_c}$. Far from the Hopf bifurcation, the amplitude may become large and strongly anharmonic depending on the properties of the system. Supercritical Hopf bifurcation does not depend on the direction of the parameter change.

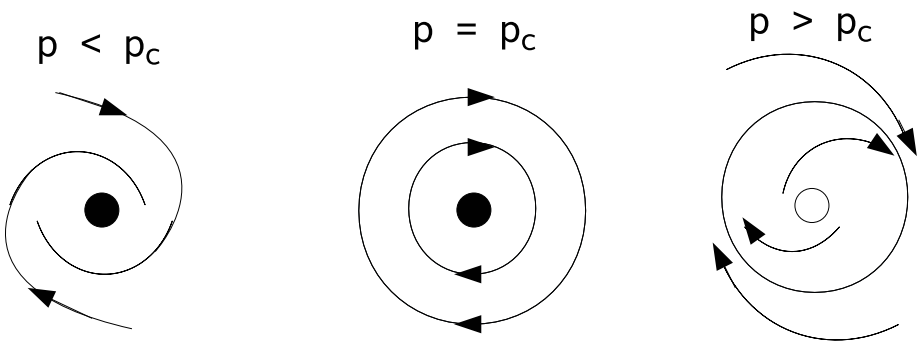

Figure 2.3: Phase space portraits in the vicinity of a supercritical Hopf bifurcation.

Further examples of local bifurcation include the subcritical variant of Hopf bifurcation. Supercritical and subcritical Hopf bifurcations are displayed in Figure 2.4. In the subcritical case, the oscillations are born suddenly with finite amplitude at one critical parameter value. Figure 2.4(b) illustrates the situation when an unstable limit cycle born in a subcritical Hopf bifurcation and is stabilized in a saddle-node bifurcation (a stable node and a saddle point appear at the bifurcation point) of limit cycles. In subcritical Hopf bifurcation, when the parameter is scanned in the opposite direction, the oscillations disappear at another critical parameter value: hysteresis occurs. More detailed discussions of limit sets and their stability can be found in [49].

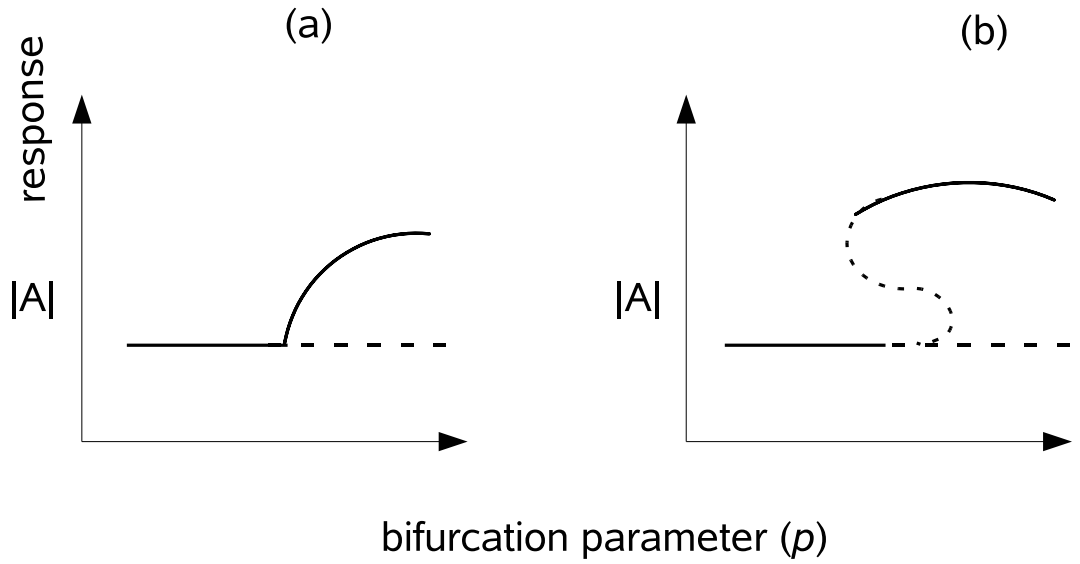

Figure 2.4: The amplitude $|A|$ of the limit cycle is shown as a function of the control parameter p in supercritical Hopf bifurcation (a), and subcritical Hopf bifurcation with stabilized limit cycle (b). Solid line (dashed) lines denote stable (unstable) states.

2.1.2 Excitable, bistable and oscillatory systems

Depending on the number and kind of limit sets, the dynamical behavior of many systems of the form Eq. 2.1 can be classified as monostable, bistable, excitable, or oscillatory [50]. This can be illustrated by considering nullclines of a two dimensional system with variables x_1 and x_2. Nullclines are defined as the lines in phase space obeying $\frac{dx_1}{dt} = 0$ and $\frac{dx_2}{dt} = 0$. The steady states are defined by the nullcline intersections, while the flow field in the phase space (x_1, x_2) can be identified by analyzing the signs of the derivatives, $\frac{dx_1}{dt}$ and $\frac{dx_2}{dt}$. Schematic drawings of the phase space in case of excitable, bistable, and oscillatory dynamics are shown in Figure 2.5.

Excitable systems are characterized by two properties: (1) it has a unique, globally attracting stationary state, and (2) a large enough stimulus can send the

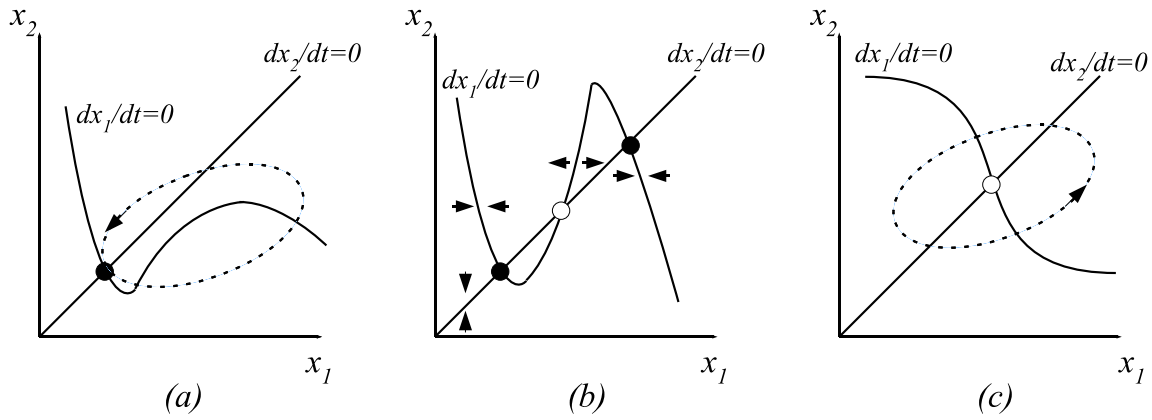

Figure 2.5: Schematic phase space drawings illustrating (a) excitable, (b) bistable, and (c) oscillatory dynamics.

system on a long excursion through phase space before it returns to the stationary state. The trajectory of such an excitation is shown in Figure 2.5(a). The rising branch of the nullcline $\frac{dx_1}{dt} = 0$ acts as excitation threshold. The time needed to recover from excitation is called the refractory period of the system. Typically, within this period excitable elements cannot be excited again.

In bistable systems, nullclines typically possess three intersection points, which corresponds to two stable fixed points separated by a saddle point as illustrated in Figure 2.5(b). The direction of flow is indicated by small arrows. The declining branches of the nullcline $\frac{dx_1}{dt} = 0$ are stable and rising middle branch is unstable with respect to changes in x_1. The straight nullcline $\frac{dx_2}{dt} = 0$ is attracting with respect to x_2; the value of x_2 decreases above the nullcline, whereas it increases below. A sufficiently strong perturbation that crosses the middle branch of the nullcline $\frac{dx_1}{dt} = 0$ is needed to carry over the system state from one stable fixed point to another.

Periodic oscillatory systems are characterized by an unstable fixed point and a stable limit cycle (dashed line) as shown in the Figure 2.5(c). For a limit cycle to exist, the chemical mechanism should have at least one autocatalytic stage and a negative feedback [3]. Autocatalysis provides accelerating growth of one species, and the negative feedback terminates the autocatalytic reaction. In oscillations, this sequence repeats periodically. More complex dynamics like deterministic chaos is possible in systems with three or more variables [47, 48]. Throughout this work, only homogenous systems which display periodic oscillations are considered.

2.2 DAE-Constrained Optimal Control Problems

Differential-Algebraic Equation Models

Let us assume that a general DAE that we would like to control is of the following form:

$$\begin{aligned} \dot{x}(t) &= f(x(t), z(t), u(t), p, t) \\ 0 &= g(x(t), z(t), u(t), p, t), \end{aligned}$$

where, x and z denote the differential and algebraic state vectors respectively, u is a vector-valued control function and p is a vector of constant system parameters such as reaction rates. We assume that the Jacobian $\frac{\partial g}{\partial z}$ is invertible, so that the DAE is of index-one. Numerical methods for the solution of index-one DAE will be briefly discussed in Section 3.4.2.

Objective Functional

The general Bolza-type objective functional on a time horizon [0,T] is given by

$$\Phi = \int_0^T L(x(t), z(t), u(t), p, t)\mathrm{d}t + E(x(T), z(T), p, T)$$

L is called Lagrange term, and E the Mayer term. This objective functional is to be minimized in optimal control problems and allows to formulate most optimal control problems arising in applications treated in this thesis.

Least Square Minimization and Tracking Problems

An important subclass of optimal control problems are tracking problems that aim at driving the system close to some reference state or trajectory $(x_r(t), z_r(t))$ on the interval $t \in [0, T]$ (e.g. phase tracking of a system to the predefined reference trajectory). Here, the distance from the reference trajectory is often measured by the geometrically motivated L^2-norm in the Lagrange term, Mayer term or both:

$$\int_0^T \|(x(t), z(t), u(t), p, t) - (x_r(t), z_r(t), u(t), p, t)\|_2^2 \mathrm{d}t + \|e(x(T), z(T), p, T)\|_2^2$$

with a vector-valued residual function e(x(T),z(T),p,T) at the end point.

Path Constraints and Boundary Conditions

Sometimes the state and control trajectories are required to satisfy additional *path constraints* which are often physically motivated in the case of (bio)chemical kinetic models (e.g. positive concentrations):

$$h(x(t), z(t), u(t), p, t) \geq 0, \quad t \in [0, T],$$

as well as terminal equality and/or inequality constraints

$$\begin{aligned} r^e(x(T), z(T), p, T) &= 0, \\ r^i(x(T), z(T), p, T) &\geq 0. \end{aligned}$$

In particular, for periodic boundary value problems, which are involved in our optimal control applications to (bio)chemical oscillators, similar equality constraints of the form x(0) = x(T) are particularly important.

2.2.1 Problem Formulation

A general class of optimal control (OC) problems which covers all problem types treated in this thesis can be formulated as

$$P_{oc}: \min_{u(\cdot), x(\cdot), z(\cdot), (T)} \int_0^T L(x(t), z(t), p, u(t))\mathrm{d}t + E(x(T), z(T), p) \tag{2.3a}$$

subject to

$$\begin{aligned} \dot{x}(t) - f(x(t), z(t), p, u(t)) &= 0, \quad t \in [0, T], && \text{(2.3b)} \\ g(x(t), z(t), p, u(t)) &= 0, \quad t \in [0, T], && \text{(2.3c)} \\ x(0) - x_0 &= 0, && \text{(2.3d)} \\ r^e(x(T), z(T), p) &= 0, && \text{(2.3e)} \\ r^i(x(T), z(T), p) &\geq 0, && \text{(2.3f)} \\ h(x(t), z(t), p, u(t)) &\geq 0, \quad t \in [0, T]. && \text{(2.3g)} \end{aligned}$$

The time horizon length T may be either fixed or enter the optimization as an additional degree of freedom. Solving the above optimal control problem (2.3) for an initial value x_0, we obtain optimal trajectories $x^*(t, x_0)$ and $z^*(t, x_0)$ and an open-loop optimal control $u^*(t; x_0)$, for $t \in [0, T(x_0)]$. In the following Section 2.3, we introduce different solution strategies available in the literature for solving the optimal control problem (2.3).

2.3 Optimal control methods

The techniques available to solve optimal control problem (2.3) fall into two broad categories: direct and indirect methods. Extensive solution strategies for both approaches are available in literature [51, 52, 53, 54].

2.3.1 Indirect Method

The indirect or variational approach is based on the optimal control theory and can be classified into three basic strategies. Calculus of variations developed by Euler, minimum principle developed by Pontryagin [51], and dynamic programming developed by Bellman [52] and are closely related to each other.

In optimal control terminology, Pontryagin's Maximum Principle (PMP) states that a minimizing path must satisfy the Euler-Lagrange equations (i.e. first order necessary conditions for a stationary solution) where the optimal controls maximize the Hamiltonian H within their bounded region at each point along the path

$$H(x, z, \lambda, u, t) = \lambda^T(t) \cdot f(x, z, u, t) + L(x, z, u, t)$$

where, the constraints on the system dynamics can be adjoined to the Lagrangian L by introducing time varying Lagrange multiplier vector $\lambda(t)$, whose elements are called the adjoint states of the system. The necessary optimality conditions formulated in PMP lead to a multi-point boundary value problem. Several numerical schemes like multiple shooting, collocation and gradient methods are available to solve the resulting problem. Despite the availability of these methods, multipoint boundary value problems (MPBVP) are demanding problems with limited robustness with respect to changes in the problem formulation (e.g., modification of the model equations or low differentiability properties of the model function). Suitable initial guesses of the state and adjoint variables must be provided at the start of iterative methods and initial values for adjoint variables do not always have physical significance making it arbitrary to guess.

The Hamilton-Jacobi-Bellman (HJB) equation is a partial differential equation based on the theory of dynamic programming developed by Bellman [52]. The solution of the HJB equation is the so called value function $V(x, z, t)$, which gives the optimal feedback control $u^*(x, z, t)$ for a given dynamical system with an associated objective functional. Hence, another name for dynamic programming might be *nonlinear feedback control*. The partial derivative of $V(x, z, t)$ with respect to x are identical to Lagrange's multipliers, and a very simple derivation of the Euler-Lagrange equations can be made using dynamic programming [55].

The PMP is inherent in dynamic programming since the HJB equation includes finding controls that minimize the Hamiltonian at each point in the state space. The PMP deals with one extremal at a time, while dynamic programming deals with families of extremals. However, in practice the HJB partial differential equation can be solved numerically for very small state dimension only ("curse of dimensionality"). The inequality constraints on the state variables as well as dynamical systems with switching points lead to discontinuous partial derivatives which are hard to be included. Because of these practical drawbacks, indirect methods are difficult to apply in practice especially for large-scale systems.

2.3.2 Direct Method

Direct methods are simple to set up and has considerable practical advantages when compared to indirect methods. In *direct methods*, the original infinite dimensional problem is approximated by a finite dimensional nonlinear programming problem [56, 54]. It is based on parameterization of the original optimization problem and can be classified basically into two approaches. A *sequential approach*, where simulation and optimization are carried out in a sequential manner and the *simultaneous approach*, where simulation and optimization are carried out simultaneously. In case of *sequential methods*, the control inputs alone are parameterized, while both states and control inputs are parameterized in the *simultaneous approach*.

Sequential Approach

This method is also referred to as control vector parameterization in literature [57], as the control inputs alone are parameterized using a finite set of decision variables. The infinitely many degrees of freedom of $u(t)$ are reduced by a control parameterization (e.g., by polynomial approximation or piecewise constant representation) that depends upon a finite dimensional vector, say q. Given the initial conditions and the parameter vector q, the system of DAEs is solved numerically. This gives the value of the objective functional, which the optimization routine then iteratively uses to find the optimal parameters in the control parameterization. The sequential method is of *feasible* path type, as in every iteration the system equations are feasible during the calculation of objective functional value.

The solution of the NLP requires sensitivity information of the states with respect to the control parameters q. Many DAE solvers exist that can efficiently compute sensitivities according to the principle of *internal numerical differentiation* (IND) (see Section 3.4.1) [58, 59, 60]. Given the sensitivity of the system states with respect to the parameters, the derivative of the objective functional and the constraints with respect to parameters are easily calculated. Several efficient optimization algorithms for sequential methods are available in literature [61, 62]. Sequential methods can use efficient state-of-the-art ODE or DAE solvers for numerical simulations, but for highly unstable systems (i.e. initial value problems with strong dependence on initial conditions) the optimization algorithm inherits the ill-conditioning of the initial value problems. While the sequential approach is straightforward to implement, it tends to be slow due to the fact that it requires repeated and expensive solution of the DAEs even when the control values are far from optimal. The numerical effort to solve the NLP is determined to a large extent by the type of parameterization of the control vector. A piecewise constant parameterization with an uniform mesh length might not be the best for general problems such that adaptive parameterization schemes should be employed to resolve the trajectory at the right place. However, it is not trivial to generate such a problem

adapted meshes *a priori*, i.e. before the actual optimal solution is known [63].

Simultaneous Approach

In *simultaneous approaches* the continuous time problem is parameterized into a NLP by approximating both the state and control variables as a family of polynomial on finite elements. Various polynomial representations are used in the literature for differential and algebraic profiles [64]. As a result, this method directly couple the solution of DAE system with the optimization problem; the DAE system is solved only once, at the optimal point, and therefore can avoid intermediate solutions that may not exist or may require excessive computational effort.

Full parameterization of both the state and control variables leads to a large scale NLP problem which usually require special solution strategies [65, 66]. These NLPs are usually solved using variations of Successive Quadratic Programming [67], which exploits the sparsity and the special block diagonal structure of the DAE optimization problems. A very good review of dynamic optimization methods using simultaneous methods is provided by Biegler *et al.* [66]. Simultaneous method has several advantages; control variables can be parameterized at the same level of accuracy as the differential and algebraic state variables and finite elements allow for discontinuities in control profiles. It also has advantages for problems with path constraints and with instabilities that occur for a range of inputs. Because they can be seen as extensions of robust boundary value solvers, they are able to pin down unstable modes by enforcing the appropriate boundary condition. On the other hand, there are some disadvantages to the simultaneous approach. First, for optimal control problems where control variables are discretized at the same level as the state variables, there are number of open questions related to convergence to the solution of the original variational problem [68]. Several studies report stability problems due to poor discretization and singular arcs. A second disadvantage arises from the need to solve large nonlinear programs; specialized methods are required to solve them efficiently.

2.3.3 Direct Multiple Shooting (DMS)

The direct multiple shooting method [53] serves as a bridge between sequential and simultaneous approaches. In this approach, the total time is divided into several shooting intervals along with control vector parameterization. Except for the first interval, the initial conditions of the various intervals are considered as decision variables along with continuity constraints stating that the initial values of every interval should match the final values of the preceding interval. This is an *infeasible* path method as in simultaneous methods, where the continuity of the system trajectory is only fulfilled at the solution, while the integration is accurate as in sequential methods.

The original optimal control problem can be formulated as a large-scale nonlinear programming (NLP) problem with a favorable block sparse structure. The resulting NLP problem can be solved with a specifically tailored sequential quadratic programming (SQP) method which fully exploits the inherent structure [69]. The optimization of highly unstable or even chaotic systems is possible by this approach [70]. For self-organizing oscillating systems studied here, the aspect of reducing the effects of nonlinearity and instability by introducing multiple-shooting time intervals is crucial for the numerical computation of optimal control funcitons [27,28,53]. This method can be easily parallelized as the initial value problems and derivative computations can be decoupled on each multiple shooting interval. Initial guesses on each of these multiple shooting nodes are required and can be pre-specified if the desired state trajectory is known *a priori*. This aspect is useful especially in case of stabilizing an arbitrary trajectory in phase space for oscillating systems or for highly unstable systems.

Due to above reasons, we chose the direct multiple shooting based optimization method for solving the optimal control problem Eq. (2.3). A mathematical overview of the problem formulation in a multiple-shooting context is described in Chapter 3. An efficient implementation of the described method is the software package MUSCOD-II [69], which is used for the results presented in this work. The main difference to the other all-at-once approach, i.e. simultaneous method, lies in the fact that the differential equations are still solved by integration. This allows the usage of state-of-the-art error controlled DAE integrators. Efficient generation of derivatives of the differential equation model is crucial for the successful implementation of this method, and is done according to the principle of IND (see Section 3.4.1). A comparison of the above direct methods is given in Table 2.1.

	Sequential method	Simultaneous method	Direct multiple shooting
States	continuous	parameterized	parameterized
Control inputs	parameterized	parameterized	parameterized
Use of DAE solvers	yes	no	yes
Initial guess for system states	initial state	all nodes	all multiple shooting nodes
Applicability to highly unstable systems	no	yes	yes

Table 2.1: Comparison of direct methods

2.4 Optimal Feedback Control

Optimization methods discussed in the previous Section 2.3, involve one underlying assumption: the mathematical model used in the method and the parameters

associated with the model are accurate and truly represent the system under consideration. However, such accurate models are seldom available in reality, especially for biological systems. Parameters involved with the modeling, kinetics and thermodynamics are not completely established for most biological systems and their dynamic nature is often not very well understood. For this reason, the optimal solution obtained by using the mathematical models may not remain valid. When applied to the real process/system, in addition to inaccurate model parameters due to errors in measuring signals, there may also be some variations in operating conditions contributing to the uncertainty. In order to overcome these uncertainties in measurements and modeling errors, one needs to incorporate a feedback control mechanism into the system. Feedback control might help in stabilizing unstable processes, reduces the sensitivity of parameter variations and improves reference tracking performance.

Let us assume that for all x_0, we can precompute the optimal control trajectories $u^*(\cdot; x_0)$ and corresponding optimal state trajectories $x^*(\cdot; x_0)$, $z^*(\cdot; x_0)$, of problem $P_{oc}(x_0)$ on $t \in [0, T(x_0)]$. Here, T is regarded as free parameter open to optimization and $T(x_0)$ denote the optimal time for $P_{oc}(x_0)$. According to *Bellman's principle of optimality*, if a decision forms an optimal solution at one stage in a process, then any remaining decisions must be optimal with respect to the outcome of the given decision [71]. From the above *principle of optimality*, for $t_1 \in [0, T(x_0)]$ and the corresponding state $x_1 := x^*(t_1; x_0)$ it holds $T(x_1) = T(x_0) - t_1$, and the optimal solution trajectory and optimal control of $P_{oc}(x_1)$ coincide with the remaining part of the solution of the original problem $P_{oc}(x_0)$ after t_1, i.e.,

$$u^*(t; x_1) = u^*(t_1 + t; x_0)$$

By choosing $t = 0$, we can get the optimal control trajectory $u(\cdot; x_0)$ for all $t_1 \in [0, T(x_0)]$ by

$$u^*(t_1; x_0) = u^*(0; x^*(t_1; x_0))$$

Thus, a precomputed *optimal feedback control* [72] function u^f for a *closed-loop* optimal control of DAE systems can be defined as:

$$u^f(x_0) := u^*(0; x_0) \tag{2.4}$$

In principle, this function could be pre-calculated off-line on a sufficiently fine grid for all relevant x_0 and store the optimal control function $u^*(t; x_0)$, $t \in [0, T(x_0)]$ for $P_{oc}(x_0)$, thus eliminating the need for any on-line calculations. Computation of such a feedback control is provided by dynamic programming [52] or a related approach using the Hamilton-Jacobi-Bellman (HJB) equation [73]. However, the number of state variables in these methods is restricted to a very small number, say 3 or 4 or less, even for moderate state dimensions (n_x=10 in case of circadian rhythms treated here) this would require a prohibitively large computational effort

and is therefore usually not feasible for large scale models [57].

It is possible to approximate the optimal feedback control $u^f(x(t))$ in the vicinity of a reference trajectory by *linearized neighboring feedback control* [72]). The approximation holds good if the distance $||x(t) - x^*(t; x_0)||$ of the real trajectory $x(t)$ to the reference trajectory $x^*(\cdot; x_0)$ remains small. However, if the real system has moved farther away from the reference trajectory during process dynamics, the approximation of the optimal feedback control may become very poor and even drive the system into directions opposite to what is desired [74].

In contrast to the above approaches, the applications treated in this work are based on an efficient way to calculate optimal feedback control via model predictive control (MPC) in real time.

2.4.1 Model Predictive Control

Model Predictive Control (MPC) is a methodology that refers to a class of control algorithms in which a dynamic model of the system is used to predict and optimize the future behavior of the process. This is done by estimating the uncertain parameters and the actual states of the system from measurements and incorporating it in future control moves.

MPC is based on iterative, finite horizon optimization problem subject to a process model. At time t, the current system state is sampled and a cost minimizing control strategy is computed (via a numerical minimization algorithm) for a relatively short-time horizon in the future: $[t, t + T]$. Specifically, an online calculation is to explore state trajectories that emanate from the current state and find a cost-minimizing control strategy until time $t + T$. In closed loop framework, only the first step of the control strategy is implemented, then the system states are sampled again and the calculations are repeated starting from the now current state, yielding a new control and new predicted state path. The prediction horizon keeps being shifted forward and for this reason MPC is also called *receding horizon control*. MPC has been used in chemical industry for more than 30 years, and has become an industry standard (mainly in the petrochemical industry [75]) due to its intrinsic capability for dealing with constraints and with multivariable systems. Most commercially available MPC technologies are based on a linear process models.

In general, linear models are often inadequate to describe the process dynamics (e.g. many bio(chemical) systems are inherently nonlinear). This has motivated the development of Nonlinear Model Predictive Control (NMPC), where a more accurate (nonlinear) model of the plant is used for prediction and optimization. Since our applications of self-organizing systems with inherent unstable dynamical modes require the ability to deal with larger perturbations and nonlinear effects online during the process runtime, our approach is based on a real-time iteration scheme

for nonlinear model predictive control (NMPC) that has recently been introduced by Diehl [74, 76]. For the state-of-the-art and future directions on NMPC, we refer Refs. [77, 78] for further reading.

2.5 Mixed-Integer Optimal Control

Many problems in plant operation and design involve variables that are not continuous but instead have integer values. This means that some of the control functions are restricted to take integer values from the set $\{0, 1\}$ or $\mathbb{Z}$ respectively. The most general case is a *mixed-integer programming* (MIP) problem, in which the objective functional depends on two sets of variables, ν_i and p_i; ν_i is the vector of integer variables and p_i denotes the continuous variables. If only integer variables are involved ($p_i = 0$), we have an *integer programming* (IP) problem. A special case of IP is *binary integer programming* (BIP), where all variables ν_i are either 0 or 1. Variables that switches values from one extreme to the other extreme at certain times are referred to as bang-bang control problems. Many MIP problems are linear in the objective functional and constraints, are subject to solution by linear programming. These problems are called MILP problems. Several algorithms exist for mixed integer and integer programming (linear problems) and we refer to Ref. [79] for a comprehensive review.

2.5.1 Mixed-Integer Nonlinear Programming

Finite-dimensional static optimization problems that involve continuous as well as integer variables are referred to as mixed-integer nonlinear programs (MINLPs). Most of the techniques that have been proposed for nonlinear discrete optimization are centered around one or more of the following basic concepts [57]: (1) rounding-off the continuous problem, (2) adaptation of nonlinear optimization techniques, (3) linear approximation, (4) binary representation of variables, (5) direct search. The relative effectiveness of any technique is quite problem-dependent and no single procedure can claim a uniform advantage over all others or all problems, or even claim to be generally effective. The most common approach to solving nonlinear discrete-value problems in practice has been to treat the variables as continuous ones. Once the continuous optimum has been determined by one of the methods outlined in earlier sections, you select a feasible set of values of the discrete variables near the optimal point for the continuous variables.

Chapter 3

Direct Multiple shooting (DMS)

In this chapter, we review the direct multiple shooting (DMS) method which was introduced by Bock and Plitt [53] in the context of optimal control problem Eq. (2.3). The direct multiple-shooting parameterization projects the original infinite optimal control problem $P_{oc}(\mathrm{x}_0)$ Eq. (2.3) to a finite dimensional nonlinear program (NLP), which can then subsequently be solved by a finite NLP solver, e.g. using sequential quadratic programming methods. The DMS method has been implemented in the optimal control package MUSCOD-II by Leineweber [80], which is used for simulations and controlling the oscillatory dynamics addressed in this thesis.

3.1 DMS Parameterization

As discussed in Section 2.3.3, direct multiple shooting method reformulate the original infinite dimensional optimization problem Eq. (2.3) as a finite NLP problem by the parameterization of both control functions and states.

3.1.1 Control Parameterization

The continuous problem Eq. (2.3) has to be replaced by a discretized one, where the control functions are approximated by a suitable parameterization using a finite set of parameters, whose optimal values can then be found by NLP techniques. In principle, one can think of global representation of the controls on the whole interval $[0, T]$ by higher order control parameterization like linear or cubic polynomials, but this approach restricts the flexibility (one should know too much about how the solution look) and makes very difficult to deal with discontinuities especially in case of bang-bang control problems treated in this thesis. It is crucial that these control parameterizations have a local influence only and does not change the partial separable structure of the problem that can be efficiently exploited numerically [81]. Therefore, a piecewise representation of the control functions is sought on the horizon $[0, T]$ with N subintervals and can be introduced as

$$0 = t_0 < t_1 < t \ldots t_N = T, \tag{3.1}$$

The control vector $u(\cdot)$ is approximated on every subinterval by a finite set of parameters using a basis function (e.g., piecewise constant approximation q_i, see Figure 3.1)

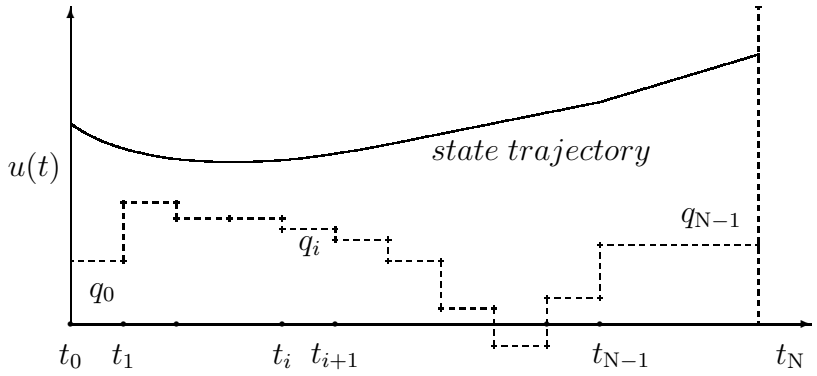

Figure 3.1: Illustration of DMS method (control discretization) with N multiple shooting intervals with piecewise constant controls.

$$u(t) := q_i \;\text{ for }\; t \in [t_i, t_{i+1}], \quad i = 0, 1, \ldots N-1, \;\; u(T) := q_N = q_{N-1} \tag{3.2}$$

where the vector q_N is introduced for notational convenience only and will not be regarded as a new parameter. In case of variable time horizon T, it can be treated as a free parameter by introducing an additional differential equation $\dot{T}(t) = 0$ with free initial value.

3.1.2 State Parameterization

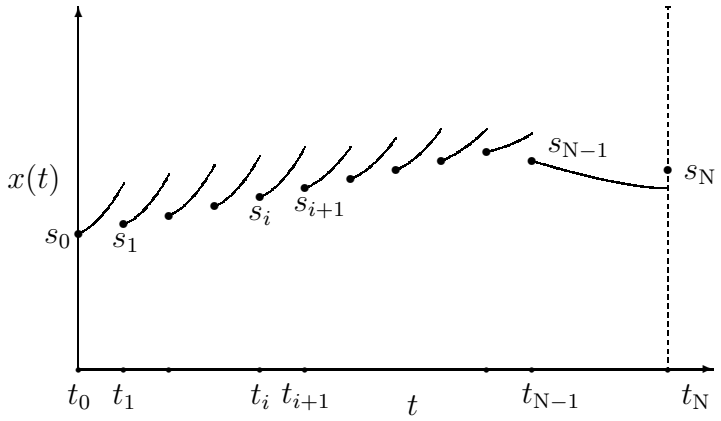

Figure 3.2: Illustration of DMS method (state discretization) with N multiple shooting intervals.

The approach of simple-shooting plus nonlinear programming frequently fails even with very good initial values [81]. The key reason for these difficulties is that the problem Eq. (2.3) has to be integrated over the whole interval $[0, T]$. Thus, the error introduced by the poor initial data, discretization, or roundoff errors may be propagated by inherent instabilities of the DAE system and grow very large. The situation can be considerably improved by using the multiple-shooting method instead of simple-shooting. We decouple the DAE solution on the N intervals $[t_i, t_{i+1}]$ by

introducing the initial values s_0^x, s_1^x,...,s_N^x and s_0^z, s_1^z,...,s_N^z (combines into vectors $s_i := (s_i^x, s_i^z)$) of differential and algebraic states as additional optimization variables (see Figure 3.2). On each subinterval $[t_i, t_{i+1}]$ we compute the trajectories $x_i(t)$ and $z_i(t)$ as the solution of an initial value problem:

$$\begin{aligned} \dot{x}_i(t) &= f(x_i(t), z_i(t), p, q_i), && (3.3)\\ 0 &= g(x_i(t), z_i(t), p, q_i) - \alpha(t) g(s_i^x, s_i^z, p, q_i) && (3.4)\\ x_i(t_i) &= s_i^x && (3.5) \end{aligned}$$

Here, the term -α in Eq. 3.4 is deliberately introduced to allow an efficient DAE solution for initial values and controls s_i^x, s_i^z, q_i that may violate temporarily the consistency conditions in Eq. 2.3c. Therefore, we require for the scalar damping factor α that $\alpha_i(t_i) = 1$. For more details on the relaxation of the DAE we refer to Schulz *et al.* [82] and Leineweber [80].

The trajectories $x_i(t)$ and $z_i(t)$ on interval $[t_i, t_{i+1}]$ are functions of the initial values, controls and parameters s_i, q_i and p only. By substituting the independent trajectory pieces $x_i(t)$, $z_i(t)$ into the Lagrange term L in Eq. 2.3a, we can simultaneously calculate the integral objective contributions $L_i(s_i, p, q_i)$ on each multiple-shooting interval

$$L_i(s_i, p, q_i) := \int_{t_i}^{t_{i+1}} L(x_i(t), z_i(t), p, q_i) \mathrm{d}t. \tag{3.6}$$

The introduction of the values s_i^x and s_i^z on each multiple-shooting point during discretization generates artificial degrees of freedom that have to be removed in order to obtain an equivalent problem by corresponding equality constraints in the NLP. The relaxation terms in the Eq. 3.4 should also vanish, i.e., *algebraic consistency* has to be assured for the optimal solution

$$g(s_i^x, s_i^z, p, q_i) = 0, \quad i = 0, 1, \ldots, N, \tag{3.7}$$

and continuity of the differential state is enforced by formulating *matching conditions* which require that each differential node value s_{i+1}^x should equal the final value of the preceding trajectory x_i:

$$s_{i+1}^x = x_i(t_{i+1}; s_i, p, q_i), \quad i = 0, \ldots, N-1, \;\; s_0^x = x_0. \tag{3.8}$$

The constraints in Eq. (3.7) and (3.8) removes the additional degrees of freedom. These constraints do not have to be satisfied during the optimization iterations and thus the direct multiple-shooting method is an infeasible path method, which can deal with and typically uses *infeasible* initial guesses of the variables s_i [69].

3.1.3 Path Constraints in DMS

Control and path constraints are imposed pointwise at the multiple shooting nodes

$$h(s_i^x, s_i^z, p, q_i) \geq 0, \quad i = 0, 1, \ldots, N. \tag{3.9}$$

as well as the terminal point

$$r^e(s_N^x, s_N^z, p) \quad = 0, \tag{3.10}$$
$$r^i(s_N^x, s_N^z, p) \quad \geq 0, \tag{3.11}$$

For bio(chemical) systems the conditions of the type in Eq. 3.9 can be used to enslave concentrations of the system variables to remain positive.

3.2 The Nonlinear Programming Problem (NLP)

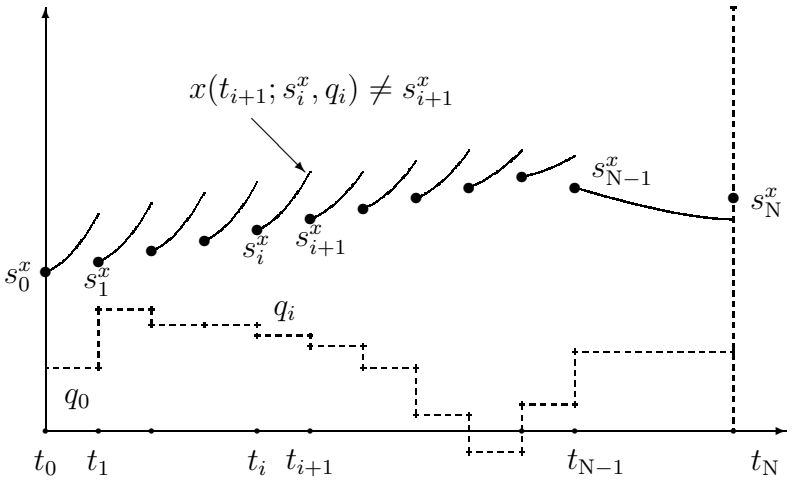

Figure 3.3: Illustration of direct multiple shooting during SQP iterations. The controls are discretized, the corresponding states obtained by piecewise integration. The matching conditions are violated in this scheme — the overall trajectory is not yet continuous.

The parameterization of the problem Eq. (2.3) as shown in Figure 3.3 using multiple-shooting nodes and piecewise constant control representation leads to the following structured NLP problem :

$$\min_{q_0,\ldots,q_{N-1},s_0,\ldots,s_N} \sum_{i=0}^{N-1} L_i(s_i^x, s_i^z, p, q_i) + E(s_N^x, s_N^z, p) \tag{3.12a}$$

subject to

$$s_{i+1}^x - x_i(t_{i+1}; s_i^x, s_i^z, p, q_i) \quad = 0, \quad i = 0, \ldots, N-1, \tag{3.12b}$$
$$g(s_i^x, s_i^z, p, q_i) \quad = 0, \quad i = 0, \ldots, N, \tag{3.12c}$$
$$s_0^x - x_0 \quad = 0, \tag{3.12d}$$
$$r^e(s_N^x, s_N^z, p) \quad = 0, \tag{3.12e}$$
$$r^i(s_N^x, s_N^z, p) \quad \geq 0, \tag{3.12f}$$
$$h(s_i^x, s_i^z, p, q_i) \quad \geq 0, \quad i = 0, \ldots, N. \tag{3.12g}$$

The NLP can be summarized as

$$\min_{w} F(w) \text{ subject to} \left\{ \begin{array}{l} G(w) = 0, \\ H(w) \geq 0. \end{array} \right\} \tag{3.13}$$

where w contains all the multiple-shooting state variables and controls as well as the model parameters:

$$w = (s_0^x, s_0^z, p, q_0, s_1^x, s_1^z, p, q_1, \cdots, s_N^x, s_N^z, p, q_N)$$

and $F(w) := \sum_{i=0}^{N-1} L_i(s_i, p, q_i) + E(s_N, p)$. The discretized dynamic model is included in the equality constraints $G(w) = 0$.

The above NLP problem (3.13) is solved by a Sequential Quadratic Programming (SQP) method tailored to the multiple-shooting structure [83, 84].

3.3 Sequential Quadratic Programming (SQP)

SQP method is an iterative technique to find a Karush-Kuhn-Tucker (KKT) (KKT conditions are the necessary first order optimality conditions for a solution of the NLP to be optimal) point of an NLP. Starting with an initial guess w^0, the SQP algorithm iterates

$$w_{k+1} = w_k + \alpha_k \Delta w_k, \quad k = 0, 1, \ldots, \tag{3.14}$$

with step directions Δw_k and relaxation factor $\alpha_k \in (0, 1]$ until a prespecified convergence criteria is satisfied. The method evaluates the NLP functions (i.e. $F(w_k)$, $G(w_k)$ and $H(w_k)$) and their derivatives with respect to w at k-th SQP iteration. Linearizations of the original nonlinear NLP are used to build a *quadratic programming* (QP) subproblem. The QP subproblem solved at the k-th SQP iteration can be written as

$$\begin{array}{c} \min\limits_{\Delta w \in \Omega_k} \nabla_w F(w_k)^T \Delta w + \frac{1}{2} \Delta w^T A_k \Delta w \\ \text{subject to} \quad \left\{ \begin{array}{l} G(w_k) + \nabla_w G(w_k)^T \Delta w = 0, \\ H(w_k) + \nabla_w H(w_k)^T \Delta w \geq 0. \end{array} \right\} \end{array} \tag{3.15}$$

Where A_k denotes an approximation of the Hessian matrix of the Lagrangian function L of the NLP.

L is defined as

$$L(w, \lambda, \mu) := F(w) - \lambda^T G(w) - \mu^T H(w). \tag{3.16}$$

where λ and μ are lagrange multipliers. The QP problem is then solved and results in a direction Δw_k that helps to determine next iterate $w_{k+1} = w_k + \alpha_k \Delta w_k$. SQP methods mainly differ in the choice of the step-length α_k, the choice of the (approximations of) the Hessian matrix A_k and the choice of the set Ω_k. For the

new values of the multiple-shooting variables, all NLP functions and derivatives are again evaluated, a new approximation for the Hessian matrix is provided and a new QP problem is solved for the next SQP iteration. The iterations form a sequence that is expected to converge towards a KKT point of the NLP. In practice, the iterations are stopped when a pre-specified convergence criterion, the KKT tolerance, is fulfilled. For a detailed description of implementation of the SQP algorithm used in the framework of MUSCOD-II, we refer to [80, 81] for further reading.

3.4 Numerical Integration

In this section, we briefly describe the numerical methods used for sensitivity generation and numerical integration in the optimal control software MUSCOD-II.

3.4.1 Numerical Differentiation

Currently, three different numerical approaches are employed in practice in order to compute sensitivity functions for DAE systems. These are *numerical differentiation* (finite difference approximations) [85], *integration of the adjoint equations* [86], *integration of the sensitivity equations* [87]. Numerical algorithms for the approximations of sensitivity matrices can be divided into two classes [58].

1. **External numerical differentiation methods (END)**:
   The sensitivity functions for END method are basically obtained independent from the numerical integration of the original state variable trajectories (for example, the sensitivity equations may be integrated independently from the model equations). This approach has the advantage that the integrator may be used as a black box. However, such an integrator contains many adaptive components which usually cause non differentiabilities or discontinuities of the numerical result of an integration. For this reason, the results of END are generally inaccurate, unless a very low integration tolerance is imposed.

2. **Internal numerical differentiation method (IND)**:
   An approach which avoids the drawbacks of END is the so called *Internal Numerical Differentiation* (IND) described by Bock [88]. In the IND approach, the integrator scheme employed for the numerical integration of the model equations is differentiated. This allows for suitable approximation to the sensitivities of the numerical solution even for low accuracy integration.

IND is implemented in the code DAESOL that is used for all numerical integration and sensitivity computations performed in this work, which is integrated in the optimal control package MUSCOD-II.

3.4.2 Backward Differentiation Formulae (BDF)

backward differentiation formulae (BDF) methods are implicit linear multi-step methods for the numerical solution of DAEs. The BDF method offers particular

advantages when dealing with stiff and unstable dynamical systems when compared to explicit methods like explicit Runge-Kutta and extrapolation methods. In particular, BDF methods have superior stability properties [89], which allow them to take much larger step sizes than would be possible with explicit methods. A BDF method with variable order and variable step-size has been implemented in the code DAESOL which is used for numerical solution of stiff differential equations arise in modeling the self-organizing systems here.

3.5 Nonlinear Model Predictive Control

In many applications of feedback control, the process runs for infinitely long ($T = \infty$), but these infinite horizons problems are difficult to treat in case of nonlinear constraints like that arise in chemical and biological modeling. Therefore, a *moving horizon approach* is often used in practice where the final time T progresses with initial time t_0 with *control horizon* (T_c) fixed for all subsequent optimization problems. This approach is called a optimal moving-horizon feedback control [63] or Nonlinear Model Predictive Control (NMPC).

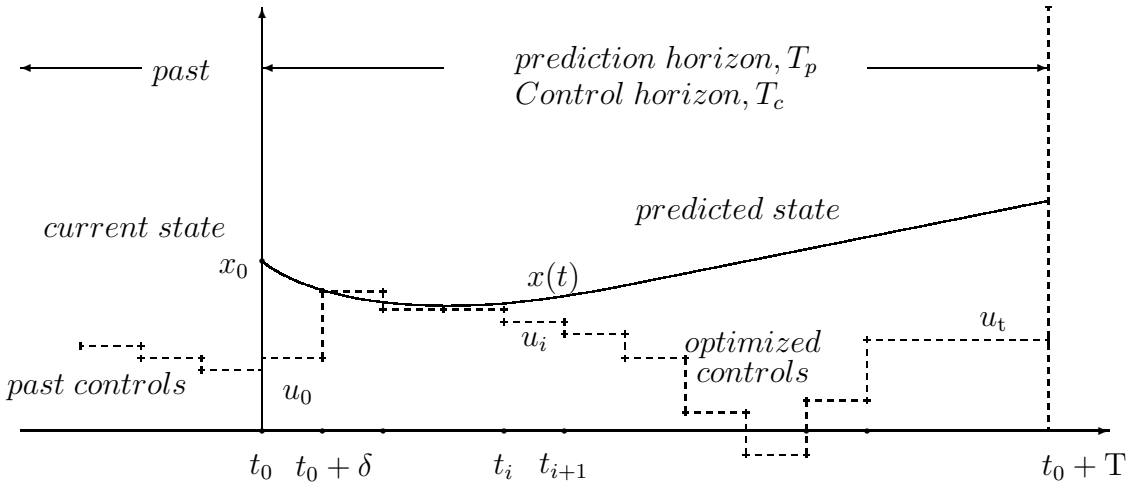

Figure 3.4: The principle of nonlinear model predictive control (NMPC) on a moving time horizon for the state x(t), T: prediction horizon, δ: sampling time horizon, u_i: piecewise constant control function parameterized on multiple-shooting intervals of length δ.

In general, the model predictive control problem is formulated as solving online a finite horizon open-loop optimal control problem subject to system dynamics and constraints involving states and controls. Figure 3.4 shows the basic principle of model predictive control. Based on the measurements obtained at time t, the controller predicts the future dynamical behavior of the system over a prediction horizon (T_p) and determines the input such that a predetermined open-loop performance objective functional is optimized. The open-loop manipulated input function will be implemented until the next measurement becomes available and the measurement will take place every δ sampling time units. Using the new measuremts at time $t + \delta$, the cost function over a certain prediction horizon is minimized and the

procedure is repeated to find a new input function with the control and prediction horizons moving forward. The inputs can be approximated as piecewise constant over the sampling time δ.

Here, we consider an finite horizon open-loop control problem as of the form

$$\min_{(x,z,u)} \int_{t_0}^{t_0+T} L(x(t), z(t), u(t))\mathrm{d}t + E(x(t_0+T), z(t_0+T)) \tag{3.17a}$$

subject to

$$\begin{aligned}
\dot{x}(t) - f(x(t), z(t), u(t)) &= 0, \quad t \in [t_0, t_0+T], && \text{(3.17b)}\\
g(x(t), z(t), u(t)) &= 0, \quad t \in [t_0, t_0+T], && \text{(3.17c)}\\
x(t_0) - \tilde{x}(t_0) &= 0, && \text{(3.17d)}\\
r^e(x(t_0+T), z(t_0+T)) &= 0, && \text{(3.17e)}\\
r^i(x(t_0+T), z(t_0+T)) &\geq 0, && \text{(3.17f)}\\
h(x(t), z(t), u(t)) &\geq 0, \quad t \in [t_0, t_0+T]. && \text{(3.17g)}
\end{aligned}$$

The Mayer-term in Eq. 3.17a plays an important role in the theory of stabilizing NMPC schemes [90]. Solving the open loop control problem Eq. (3.17) with a current initial value $\tilde{x}(t_0)$ yields an optimal control trajectory $u^*(t_0, x(t_0))$ on the horizon $[t_0, t_0+T]$. For a perfect model without any disturbances it would suffice to apply this control trajectory to the process. In NMPC closed-loop framework, only a first part of the solution u^* with the length of the sampling time is applied to the process. Then the optimal control problem (3.17) is solved again with another new initial value from the process. The time between the advent of a new $\tilde{x}$ and the response of the NMPC algorithm in the form of feedback control u^* creates a feedback delay. Generally a feedback delay of one sampling time cannot be avoided even with the fastest and most efficient algorithms. In the following, we define Diehl's algorithm [74, 76] scheme for NMPC that delivers feedback control law very quickly. It is based on the DMS algorithm as explained for the problem (2.3) in this chapter. DMS approach offers several advantages in the context of real-time process applications [91]. It allows to exploit solution information in controls, states and derivatives in subsequent optimization problems by suitable embedding techniques.

3.5.1 Real-time Iteration Scheme

The conventional approach in NMPC is to solve the NMPC problem (3.17) to desired accuracy at every time t_0 with initial value $x_0 \equiv \tilde{x}(t_0)$ and the optimal control solution of problem (3.17) is instantaneously given to the real process at t_0. Unfortunately, this is not possible with finitely fast computers. In the following, we describe a scheme for nonlinear model predictive control that delivers feedback quickly based

on a real-time iteration scheme [74].

In real-time iteration scheme, one exploits the fact that in NMPC optimization a sequence of neighboring optimization problems has to be solved, which differ only by the estimated state x_0 and parameter vector p, and possibly by a change in the reference trajectory $x_r(t)$. Solution information of the previous problem can be exploited for initialization of the following problem by an efficient initial value embedding strategy [74]. This initialization procedure in conjunction with the DMS method is so efficient for neighboring problems that it allows to perform only one single optimization iteration per optimization problem, without sacrificing much solution accuracy. A more detailed description of the real-time iteration scheme and its convergence properties can be found in Ref. [74].

The NLP is solved by a SQP algorithm as described in Section 3.3. The necessary computations during real-time iterations are divided into two phases. A long *preparation phase* in which the calculations are performed without the knowledge of $\tilde{x}$ and a shorter *feedback phase* which can be computed once the measurements are available. The computation time is reduced significantly between measurement $\tilde{x}$ and feedback control response u^* by performing only one SQP iteration for each new optimization problem. Thus the feedback delay between measurement of $\tilde{x}$ and control u^* is typically smaller than the sampling time δ_i and can be neglected. Derivative generation is the most expensive part in SQP procedure and we use advanced DAESOL [59] based on BDF method for efficient sensitivity calculations. The least square structure of the objective functional can be exploited within the optimization procedure to provide an excellent Hessian approximation at negligible computational cost [74]. This modification of the SQP procedure is equivalent to a *Gauss-Newton* method. The particular choice of the least square objective functional (L^2-norm) is crucial for the application of the highly efficient *Gauss-Newton* approach.

3.5.2 Extended Kalman Filter

The Kalman filter is a stochastic filter that allows the estimation of the states of a system based on a linear state space model. The Extended Kalman Filter (EKF) uses local linearization to extend the scope of the Kalman filter to systems described by nonlinear differential equations [92]. The main advantages of the EKF are its simplicity, the fact that it is a recursive algorithm and so its computational load is modest when compared to moving horizon estimation [93]. The EKF is suitable for many real-time applications. For this reasons, we selected EKF for estimating the states from measurements in our work. The state estimation problem for nonlinear DAEs using the Kalman filter has been studied by Becerra *et al.* [94]. Here we use the variant of the Extended Kalman Filter (EKF) algorithm developed by Diehl in [74] for the state estimation in the numerical experiments in Section 4.9.1. In contrast to the standard EKF, this variant EKF allows us to treat bounds on the

systems states. Given the measurement sequence at each sampling time for the optimization problem (2.3) with additional knowledge on system bounds, the problem here is to infer the actual states from this given information.

3.6 Integer Control Functions

The DMS concept for control and state discretization presented in Section 3.1.1 is based on fixed discretization of controls giving a constant number of optimization variables which is insufficient for bang-bang solutions if the switching points are not known *a priori*. However, DMS-based optimal control can be adapted to the needs for finding a bang-bang solution.

In the next section, we briefly present a novel algorithm implemented by Sager [79] for mixed-integer optimization based on DMS approach for treating the problems presented in this thesis (Sections 4.6,4.7 and 4.8).

3.6.1 Mixed Integer Optimization Algorithm

If the optimal control problem (2.3) under consideration contains control functions $w(\cdot)$ with a restriction to values in a disjoint set, say to $\{0,1\}^{n_w}$, then the methods in Sections 3.1-3.3 have to be extended. We say that a trajectory $\mathcal{T} = (x, w, u, p)$ is binary admissible, if all constraints are fulfilled and $w(t) \in \{0,1\}^{n_w}$ for all $t \in [0, T]$. For the application treated in this thesis, we apply the novel algorithm MSMINTOC introduced in [79] that can be sketched as follows. We relax the control functions to $w(\cdot) \in [0,1]^{n_w}$. We solve the relaxed problem for a given control discretization $\mathcal{G}^0$ and obtain the grid–dependent optimal function value $\Phi^{\mathrm{RL}}_{\mathcal{G}^0}$. We iterate on a refinement of the grid for n_{ext} steps with the idea to extrapolate towards $n_{\mathrm{ms}} \mapsto \infty$. We obtain $\Phi^{\mathrm{RL}} = \Phi^{\mathrm{RL}}_{\mathcal{G}^{n_{\mathrm{ext}}}}$ as the objective function value on the finest grid $\mathcal{G}^{n_{\mathrm{ext}}}$. This objective function value serves as a lower bound that can be approximated up to any user–specified tolerance $\varepsilon > 0$ by a binary admissible trajectory, for a proof see [79]. If the optimal trajectory on $\mathcal{G}^{n_{\mathrm{ext}}}$ is already binary admissible then stop. Otherwise, apply a rounding or penalty heuristics on the grid. If the trajectory is binary admissible, obtain an upper bound Φ^{ROU}. If $\Phi^{ROU} < \Phi^{\mathrm{RL}} + \varepsilon$ then stop. Otherwise, optimize the switching times for a fixed switching structure, initialized with the trajectory obtained by heuristics. Again, if the obtained trajectory is binary admissible, obtain an upper bound Φ^{STO} and if $\Phi^{STO} < \Phi^{\mathrm{RL}} + \varepsilon$ then stop. For most practical problems and the model under consideration in our study, a modest iteration on n_{ext} is sufficient to obtain a binary admissible trajectory that is within a certain tolerance to the reachable objective function value. For details, proofs and applications of the algorithm we refer to the work of Sager (see Ref. [79]).

Chapter 4

Circadian Rhythms

In this chapter, we present an application of advanced optimal control methods for target-oriented manipulation of circadian rhythms. A brief introduction of the molecular mechanisms of circadian rhythms is presented along with mathematical analysis of the model considered in this study. We discuss the results related to nonlinear model based external control aimed at suppressing, phase resetting, phase tracking and restoration of altered circadian rhythms. Both open and closed-loop control results are presented in this work.

4.1 Introduction

What we experience as time is related to a reference point and hence, relative. Living on earth has made us use the sun as reference and the 24-hour succession of light and darkness is probably the most pervasive epigenetic influence in the evolution from a single cell organism to man. This periodic succession of light and darkness provided the base for relative timing of biological processes over the 24 hours of a day. As energy supply is the limiting parameter for survival, a system for optimal timing of energy expenditure and uptake is developed. The mechanism of this system took the shape of a cycle reflecting the recurrence of sunrise and sunset, and is termed as "circadian clock" - a clock with a period of about one day (latin: *circa diem*). The internalization of environmental time within the organism not only allows organization of biological processes along the 24-hour time scale but also prediction of recurring events, such as availability of food and emergence of predators.

The underlying principle of circadian clocks is successive gene activation in form of a cycle. The initial gene activation is regulated by the last one in the sequence, making up an auto-regulatory feedback loop for which one cycle takes about 24 hours. This principle is illustrated in Figure 4.1. Positive elements activate the expression of negative elements, which in turn stop the activity of the positive elements. Although the genes involved in this mechanism can differ in various organisms the principle illustrated in Figure 4.1 is common to all of them (reviewed in Bell-Pedersen et al., [96]; Young and Kay [97]).

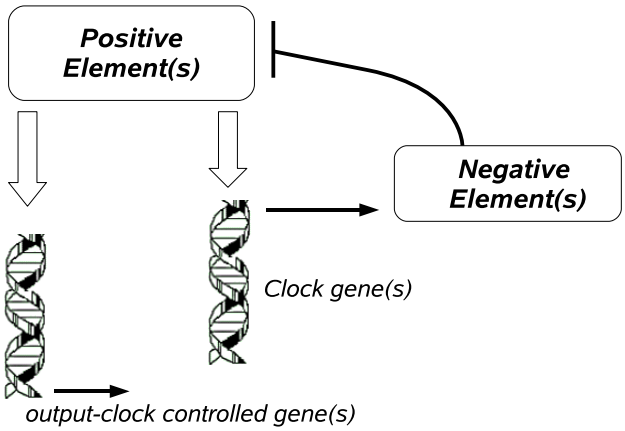

Figure 4.1: General mechanism of the circadian clock. Positive elements activate expression of negative elements that inhibit the action of positive elements, thereby establishing an auto-regulatory feedback loop. The positive elements of the clock additionally activate clock-controlled genes transmitting time information to the whole organism.

The earth's orbit around the sun leads to seasons that manifest themselves, besides the temperature changes, in an altered length of a day's light period. To adapt to these changes the circadian clock is connected to mechanisms that allow it to stay in tune with nature. Temporal information coded in this clock mechanism is only of use for the organism if it is translated into a physiological meaning. This is achieved through coupling of the clock mechanism to biological pathways that are themselves composed of sequential gene activation. Sensory organs communicate environmental time information *via* signaling pathways to the clock, thereby synchronizing the internal circadian oscillators with the environment [95]. The existence of such an input pathway in the circadian system (Figure 4.2) is the reason why humans can adapt to different time zones and overcome jet lag. The circadian timing system of mammals influences most physiological activities, including sleep and wakefulness, body temperature, intestinal peristaltics, hepatic activity, cardiovascular activity, hormonal secretion and precision of the sensory system (reviewed in Schibler et al. [98]) which will be discussed in detail in next Section 4.1.1.

4.1.1 Health issues

In this section, we discuss the medical implications of circadian rhythms that are immense, and can be broadly classified into the following three groups [31].

Effects imposed by external conditions on otherwise healthy individuals:

This group can be further divided into symptoms that arise from acute changes in external time cues, such as transmeridian flight (jet lag), and those that result from continual changes in lightdark cycles, most notably arising from shift work. Performing tasks during times in the day when psychomotor capabilities are suboptimal

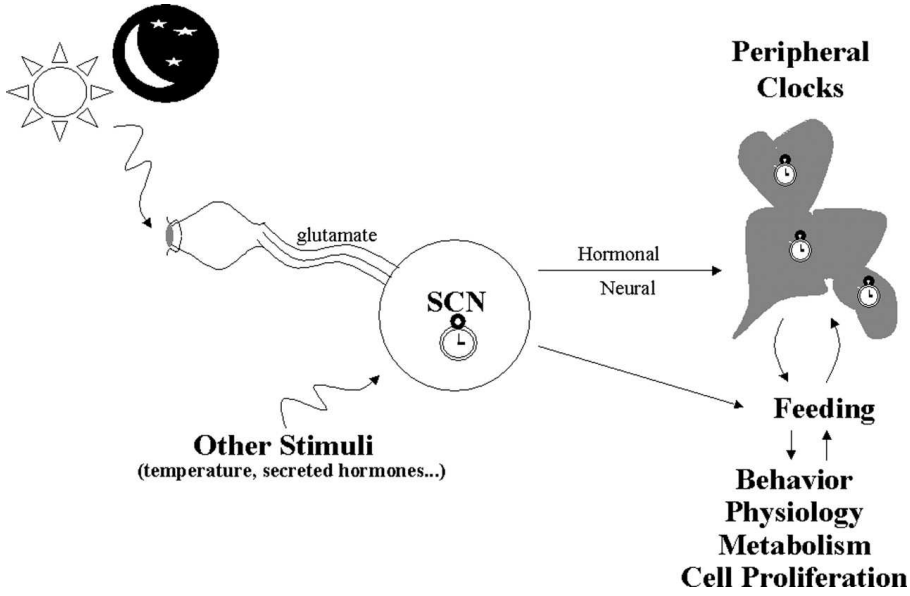

Figure 4.2: The mammalian circadian timing system. The light/dark cycle resets the activity of the master pacemaker located in the suprachiasmatic nucleus (SCN) via the retina and the retinohypothalamic tract. Other environmental stimuli such as temperature and hormone secretion can also entrain the central oscillator. The SCN then processes environmental inputs and, in turn, provides timing cues that will synchronize other slave oscillators located in peripheral tissues (heart, liver, and kidney). Control of the peripheral clocks by the central pacemaker occurs via a combination of neural and hormonal signals. Peripheral oscillators can also be reset by changing the feeding time. As an ultimate result of this synchronization, mammals will display circadian rhythms in physiology and behavior. Cellular metabolism and cell proliferation also show circadian coordination in tissues, which can largely modulate the tolerability and the efficacy of cancer treatments (The figure is taken from the Ref. [95].)

is associated with many serious consequences. For example, nurses on a repetitive shift work schedule are two-to three fold more likely to misdiagnose and wrongly treat patients than their daytime counterparts [99].

The effects of transmeridian flight and shift work on the human circadian timing system likely occur at two levels. The photic input to the circadian timing system is transduced *via* the retinohypothalamic tract (RHT) to the SCN (as shown in Figure 4.2 and reviewed in Ref. [100]), which in turn conveys time-of-day information to peripheral clocks that have tissue-specific regulatory features (e.g., see Ref. [101]). Desynchronization not only occurs between the external environment and the SCN rhythm generator but also affects phase alignments between the different peripheral clocks [102]. Different rates of resynchronization amongst the cellular clocks in the SCN and those found in the various tissues likely contribute to the dysfunction associated with jet lag and other abrupt changes in light-dark cycles [102].

Melatonin, a naturally produced hormone that is under circadian regulation, has been used to alleviate disorders associated with jet lag and shift work (reviewed

in Ref. [103]). Another successful approach to treat health problems associated with jet lag and shift work has been the use of phototherapy ([104,105]). An explanation for this noninvasive treatment is based on earlier work in model organisms showing that depending on when during the night a short pulse of light is administered, it can evoke either a delay or advance in the phase of the clock. Ideally, by correctly timing the phototherapeutic treatment, the rate of resynchronization to local time can be accelerated.

Issues related to diagnosis and treatment:
Many physiological and behavioral variables change in a rhythmic manner over the course of a day. Sampling at different times of the day and knowing the natural rhythm of the variables in question would allow physicians a more precise account of the status of the patient. However, in addition to the inherent problem of feasibility in round-the-clock sampling, other factors such as exposure to "unnatural" light conditions or malfunctions in circadian timing system might lead to rhythms that are altered, rendering the observed variables unreliable as a diagnostic indicator.

Efficacy of certain drugs is dependent on time of delivery (e.g. in treatment of cancer (reviewed in Ref. [106])). It is possible to increase the therapeutic potential and minimize toxic side effects by optimizing schedules for administering drugs. Many drugs used in chemotherapy affect the function and replication of normal and malignant cells. By targeting times when normal cells are less likely to perform DNA synthesis, higher levels of chemotherapeutic drugs can be tolerated, increasing the effectiveness of the treatment ([107, 15]). Rates of absorption, metabolism, target susceptibility, and excretion vary throughout the day, contributing to time-of-day differences in the beneficial and toxic effects of drugs.

Disorders or disease states that appear to be causally linked to malfunctions in the circadian timing system:
Malfunctions in the circadian timing system are associated with several disorders such as chronic sleep disturbances, manic-depression and seasonal affective disorders (SAD) or winter depression (reviewed in Ref. [108]). Many of the symptoms associated with certain chronic sleep problems and affective disorders can be alleviated by alterations in light-dark schedules [109].

4.2 Molecular biology of circadian rhythms

There has been remarkable progress in understanding the molecular underpinnings governing circadian rhythms of cynobacteria, *Neurospora*, *Arabidopsis*, *Drosophila*, zebrafish, amphibians and mammals in the last few years. *Drosophila* and mice are the two best studied animal model systems for understanding the neural circadian pacemakers. Both organisms show remarkable similarities in clock components and overall molecular mechanisms.

4.2.1 Drosophila circadian clock

Like many other organisms, the fruit fly *Drosophila melanogaster* operates on a 24-hour schedule maintained by environmental input to an internal body clock. The molecular basis of the clock relies on oscillations in the activation of particular genes at certain times of the day. The key feature of these molecular oscillations is a negative feedback loop in which the protein products of genes actually turn off production of more protein. This process is possible in all cells of *Drosophila*; however, the highest concentrations of the essential molecules are found in lateral neurons of the central nervous system. These lateral neurons, or pacemaker cells, are the *Drosophila* equivalent of mammalian neurons in the suprachiasmatic nucleus (SCN). The first clock gene to be identified and molecularly characterized was the *period (per)* gene in that species [110] and later several other genes like *tim*, dClock (*dClk*) and cycle (*cyc*) have been identified [111, 112, 113].

The identification of these genes resulted in the following model (see Figure 4.3) for the generation of molecular and the resultant behavioral rhythmicity. The negative feedback loop that forms the basis of the *Drosophila* molecular clock occurs at the level of gene transcription (reviewed in Panda et al., [30]). The basic-helix-loop-helix (bHLH)-PAS heterodimeric pair, dCLK and CYC, reside in the nucleus on the E-box elements in the *per* and *tim* structural genes, positively regulating their transcription. PER and TIM protein levels continue to rise throughout the day to their peak levels in the early evening - a few hours after the peak level of *per* and *tim* mRNAs. The two proteins heterodimerize and translocate into the nucleus where they inhibit the transcriptional activity of the dCLK/CYC complex, thus repressing their own transcription. As both PER and TIM proteins are degraded before dawn, this process is relieved, lifting repression of the dCLK/CYC complex, thereby starting another cycle of PER and TIM accumulation. This core mechanism and several of the above mentioned components are conserved between flies and mammals [112, 111].

4.2.2 Mammalian circadian clock

The fundamental anticipatory and light-responsive properties of the circadian pacemaker are conserved among flies and rodents, raising the possibility that the underlying timekeeping mechanism might also be conserved. A combination of forward mutagenesis screening in mice and the use of sequence comparisons with known components of the fly clock has produced a picture of the functional clock in mammals that is highly similar to that in flies (see Figure 4.4). The most similar components are CLOCK and BMAL1/MOP3, which are mammalian orthologues of fly dCLK and CYC, respectively [30]. CLOCK and BMAL1/MOP3 were shown to heterodimerize, bind the E-box element (functionally conserved between flies and mammals), and

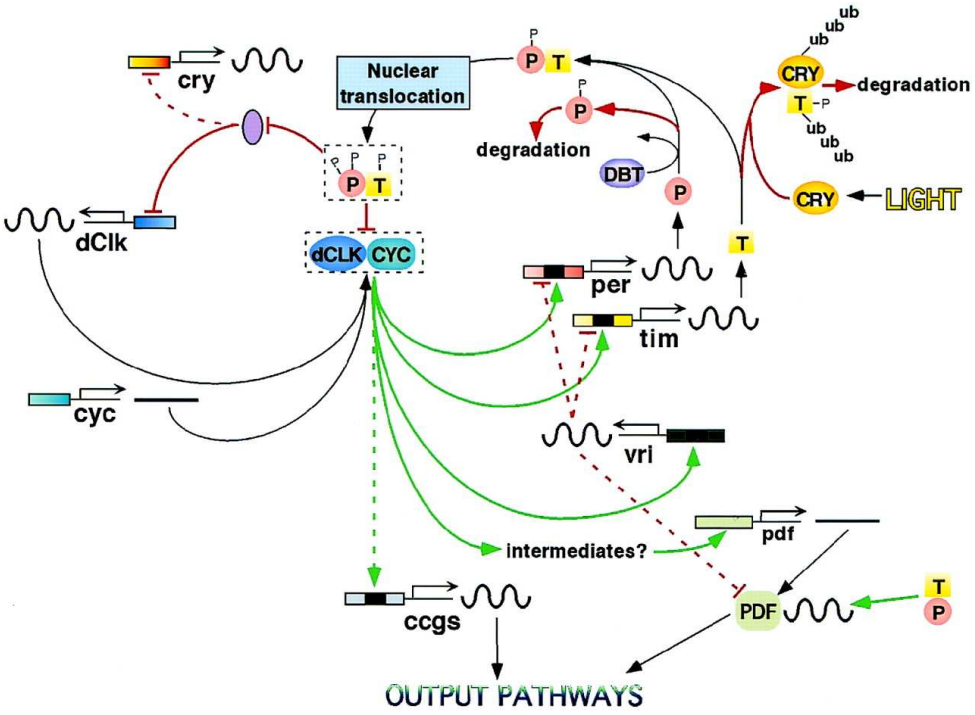

Figure 4.3: Model of circadian clock in *Drosophila melanogaster* showing photic input pathway (light; CRY) and two downstream effector pathways (ccgs, clock-controlled genes; PDF, pigment-dispersing factor). During the late day/early night, the levels of PER (indicated by large P) and TIM (indicated by T) reach critical concentrations that favor dimerization, an event that stabilizes PER and stimulates the nuclear entry of the PER-TIM complex. The enhanced degradation of monomeric PER in the cytoplasm as a result of DBT-mediated phosphorylation events and the light-induced degradation of TIM, contribute to a delay in the nuclear accumulation of PER and TIM. In the nucleus, PER, TIM, or both 1) interact with dCLK:CYC, blocking its ability to stimulate transcription of per, tim, vri, and possibly ccgs and 2) by a mechanism that is not clear, upregulate expression of dClk and cry. Green lines, pathways leading to upregulation; red lines, pathways leading to downregulation; dashed lines, uncertain pathways. Small black boxes indicate E-box elements; small P, phosphorylation; ub, ubiquitin (The figure is taken from the Ref. [31]).

transactivate mammalian genes that harbor this element [114]. The *Clock* mutant (a splice-site mutation resulting in a deletion of a portion of the transactivation surface) reduces $mPer$ expression and lengthens the overt activity rhythm eventually turning arrhythmic [115], whereas a loss-of-function $Bmal1/MOP3$ mutant abolishes mPer expression and eliminates activity rhythms altogether [116]. Mutation of two of the three PER orthologues, $mPer1$ and $mPer2$, results in aberrant circadian activity, and the double mutant abolishes rhythmicity [117, 118]. Table 4.1 shows different clock gene mutations in mice and the corresponding alteration in circadian rhythmic behavior.

Although the clock components are conserved across species, their genetic and biochemical roles have diverged. For example, in the mouse mPER2 seems to activate transcription of $Bmal1$, and exactly opposite to that in flies, BMAL1 cycles in mice whereas CLOCK does not. Therefore, PER positively regulates the rhyth-

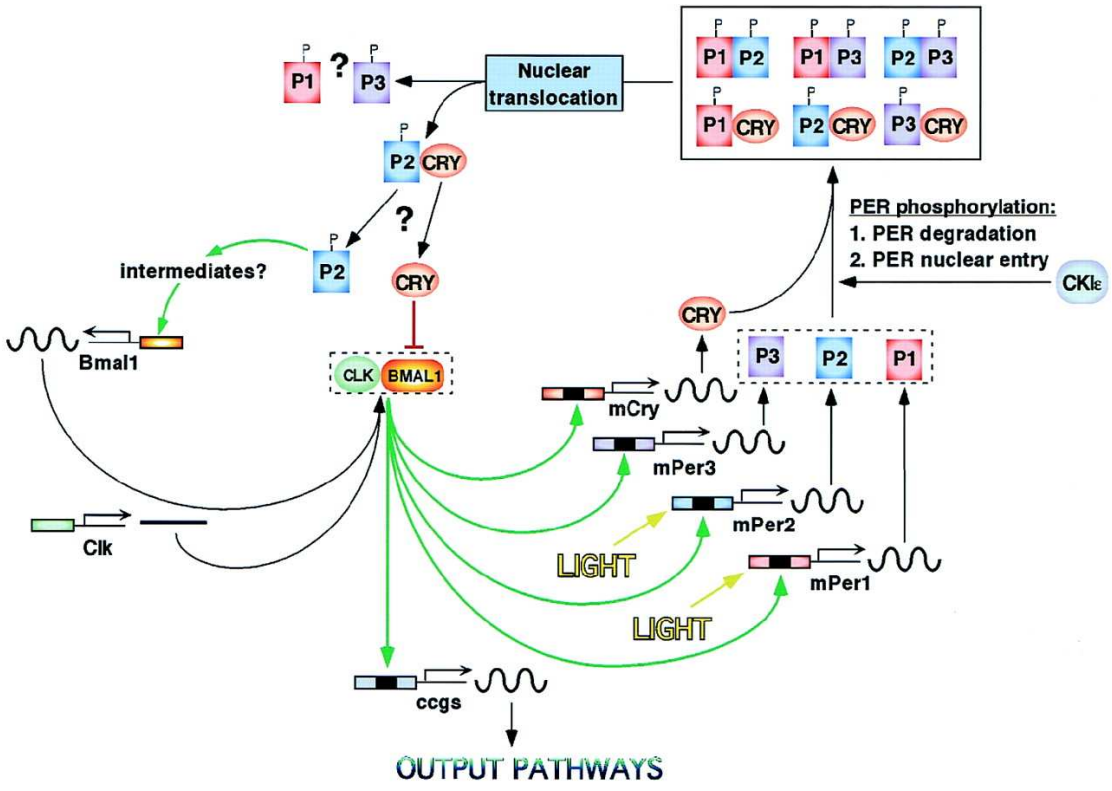

Figure 4.4: Model of circadian clock in an individual SCN neuron. Three different mPERs (mPER1, P1; mPER2, P2;and mPER3, P3) interact with each other and with two different mCRYs (only one is shown for simplicity). These presumed heterodimers regulate the nuclear entry and/or stability of the mPERs (much like the effect of TIM on PER in Drosophila). Casein kinase I epsilon (CKIe) phosphorylates the mPERs, leading to increased degradation of the mPERs (much like the effect of DBT on PER in Drosophila) and also presumably influencing the nuclear entry of the mPERs. Once in the nucleus, mCRY1, mCRY2, or both interact with CLOCK:BMAL1, blocking its ability to stimulate transcription. Light evokes rapid increases in the levels of mPer1 and mPer2 transcripts, an event likely relevant for photic entrainment of circadian pacemakers in the SCN. Green lines, pathways leading to up regulation; red lines, pathways leading to downregulation; dashed lines, uncertain pathways. Small black boxes indicate E-box elements; small P, phosphorylation; CLK, mCLOCK (The figure is taken from Ref. [31]).

mic production of CLOCK/BMAL1 complexes in both mice and flies, although its target has switched. Finally, PER protein products have been shown to weakly suppress CLOCK/BMAL1-dependent $mPer1$ transcription in cultured mammalian cells [115]. These results would seem to support a role very similar to that seen for PER (PER/TIM complex) in *Drosophila*, as a negative regulator of its own transcription and a positive regulator of the dCLK/CYC complex. The putative orthologue of *Drosophila timeless*, $mTim$, was found to be a closer orthologue of a second fly gene, *timeout*, which is apparently not involved in maintenance of circadian rhythmicity. Instead, deletion of the mTim gene in the mouse causes lethality [120]. Finally, better repressors of CLOCK/BMAL1 molecular activity were isolated with the orthologues of a Drosophila photoreceptor called cryptochrome (CRY).

Clock gene mutations

Gene	Type	Behavioral type
Clock	Deletion	Long period to arrhythmic
*BMAL*1	Null	Arrhythmic
*Per*1	Null	Var. period to arrhythmic
*Per*2	Null	Var. period to arrhythmic
*Per*3	Null	Short period
*Per*1/2	Null/Null	Arrhythmic
*Cry*1	Null	Short period
*Cry*2	Null	Long period
*Cry*1/2	Null/Null	Arrhythmic

Table 4.1: Mutations alter circadian behavioral rhythms in mice. For the *Period* and *Crytochrome* gene families, partial redundancy of function is apparent. (Adapted from Reppert et al. [119]).

4.2.3 Resetting the clock

The stability of TIM protein is light sensitive – even a brief light pulse can trigger its degradation – and this change in TIM level can reset the molecular clock and result in resetting of activity rhythm [121]. During early subjective night when TIM protein levels rise, light-induced TIM degradation promoted by dCRY delays the accumulation of TIM, which in turn delays the subsequent molecular events of the oscillator machinery, resulting in a phase delay. Conversely, light pulses administered during the late night, when TIM levels are decreasing, facilitates the rapid decline in TIM protein, and causes phase advances. This clock function of cryptochromes may be conserved in mammals [30, 122, 123]. Although dCRY and its interacting partner TIM are not functionally conserved among flies and mammals, their activity in flies elucidated the integration of two simple molecular mechanisms – a feedback loop and a simple light response to produce a seemingly complex time-of-day-dependent response of circadian behavior to light. This also establishes a model for circadian photoresponses in mammals.

4.3 Modeling of circadian rhythms in Drosophila

Model organisms such as the fly offer readily available genetic tools, rapid generation (or acquisition from public stock centres) of mutants, RNA interference technologies, and automated, quantitative phenotypic assay to rapidly go through these hypotheses. The exciting possibility that complex behavior can be described at the molecular level, and is well conserved across species, underscores the importance of

the use of model organisms and comparative behavioral genomics. In view of the

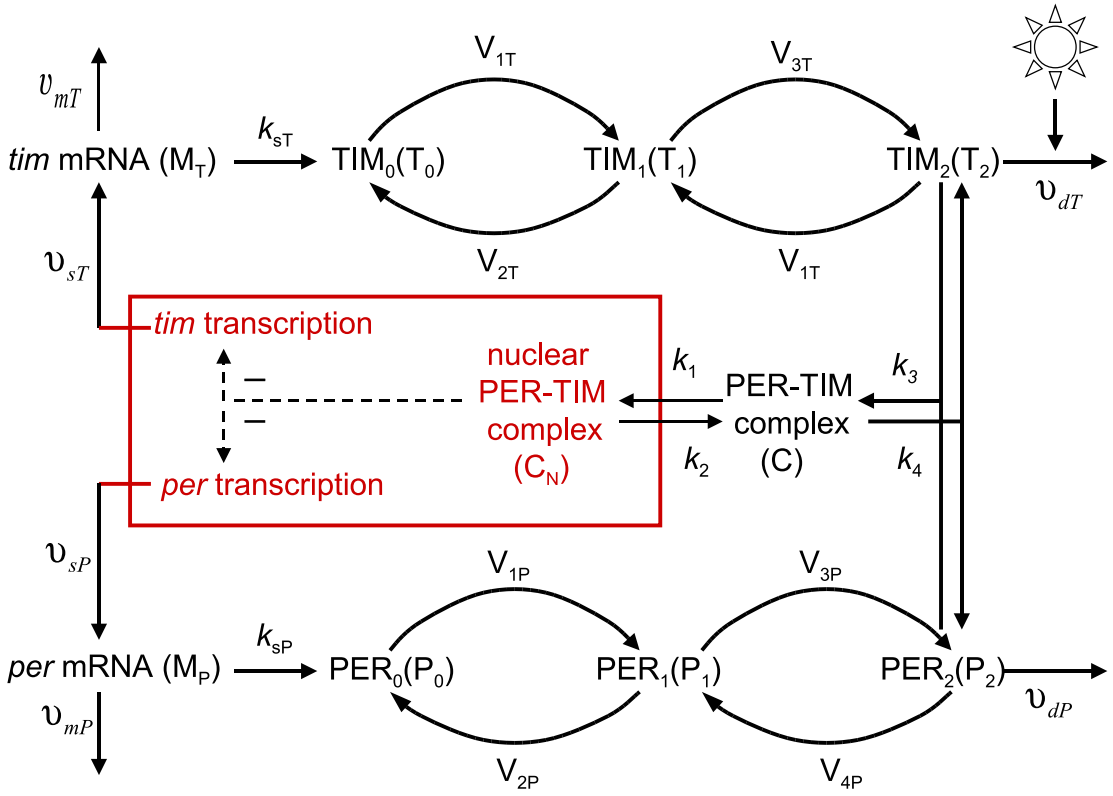

Figure 4.5: Model for circadian oscillator in *Drosophila* involving negative regulation of gene expression by PER and TIM. *per* (M_P) and *tim* (M_T) mRNAs are synthesized in the nucleus and transferred into the cytoplasm, where they accumulate at the maximum rates ν_{sP} and ν_{sT}, respectively. There they are degraded enzymatically at the maximum rates, ν_{mP} and ν_{mT}, with the Michaelis-Menten constants, K_{mP} and K_{mT}. The rates of synthesis of the PER and TIM proteins are proportional to M_P and M_T characterized by the apparent first-order rate constants k_{sP} and k_{sT}. Parameters $V_{iP}(V_{iT})$ and $K_{iP}(K_{iT})$ (i = 1,...4) denote the maximum rate and Michaelis constant of the kinases and phosphatases involved in the reversible phosphorylation of P_0 (T_0) into P_1 (T_1) and P_1 (T_1) into P_2 (T_2), respectively. The fully phosphorylated forms (P_2 and T_2) are degraded by enzymes with maximum rate ν_{dP} and ν_{dT} and Michaelis-Menten constants K_{dP} and K_{dT} and reversibly form a complex C (association and dissociation are characterized by the rate constants k_3 and k_4), which is transported into the nucleus at a rate characterized by the apparent first-order rate constant k_1. Transport of the nuclear form of the PER-TIM complex (C_N) into the cytoplasm is described by the apparent first-order rate constant k_2. The negative feedback exerted by the nuclear PER-TIM complex on *per* and *tim* transcription is modeled by a Hill-type equation. For the full kinetic model equations see Eqs. 4.1. (The figure is redrawn following Ref. [33]).

large number of variables involved and of the complexity of feedback processes that generate oscillations, mathematical models and numerical simulations are needed to fully grasp the molecular mechanisms and functions of biological rhythms. These models could be used to explore syndromes or pathological conditions resulting from disorders of circadian rhythms like familial advanced sleep phase syndrome (FASPS). Disorders of the circadian system may be viewed as "dynamical disease" [124], i.e.

physiological dysfunctions resulting from changes in dynamic behavior because of a shift outside the physiological range of control parameters. Simulations will allow rapid determination of the qualitative and quantitative effects of each parameter, and thereby can help to identify key parameters that have most profound effect on system's dynamics. Molecular mathematical models in case of *Drosophila* are readily available in literature [32, 33], and we choose the model proposed by Leloup *et al.* [33](see Figure 4.3) for our numerical studies.

4.3.1 Drosophila model-equations and rate-constants

Molecular models for circadian rhythms were proposed initially for circadian oscillations of the period (PER) protein and its mRNA in *Drosophila* [32]. It is governed by a set of five kinetic equations based on the negative control exerted by the PER protein on the expression of *per*. This early model did not account for the effect of light on the circadian system. An extended, 10-variable model in which the negative regulation is exerted by PER-TIM complex has been proposed [33] (schematized in Figure 4.3) is centered around negative auto-regulation of gene expression.

$$\frac{dM_\mathrm{p}}{dt} = v_\mathrm{sP}\frac{{K_\mathrm{IP}}^\mathrm{n}}{{K_\mathrm{IP}}^\mathrm{n}+{C_\mathrm{N}}^\mathrm{n}} - v_\mathrm{mP}\frac{M_\mathrm{P}}{K_\mathrm{mP}+M_\mathrm{P}} - k_\mathrm{d}M_\mathrm{P} \tag{4.1a}$$

$$\frac{dP_0}{dt} = k_\mathrm{sP}M_P - V_\mathrm{1P}\frac{P_0}{K_\mathrm{1P}+P_0} + V_\mathrm{2P}\frac{P_1}{K_\mathrm{2P}+P_1} - k_\mathrm{d}P_0 \tag{4.1b}$$

$$\begin{aligned}\frac{dP_1}{dt} &= V_\mathrm{1P}\frac{P_0}{K_\mathrm{1P}+P_0} - V_\mathrm{2P}\frac{P_1}{K_\mathrm{2P}+P_1} - V_\mathrm{3P}\frac{P_1}{K_\mathrm{3P}+P_1} \\ &\quad + V_\mathrm{4P}\frac{P_2}{K_\mathrm{4P}+P_2} - k_\mathrm{d}P_1\end{aligned} \tag{4.1c}$$

$$\begin{aligned}\frac{dP_2}{dt} &= V_\mathrm{3P}\frac{P_1}{K_\mathrm{3P}+P_1} - V_\mathrm{4P}\frac{P_2}{K_\mathrm{4P}+P_2} - k_3P_2T_2 + k_4C \\ &\quad - v_\mathrm{dP}\frac{P_2}{K_\mathrm{dP}+P_2} - k_\mathrm{d}P_2\end{aligned} \tag{4.1d}$$

$$\frac{dM_\mathrm{T}}{dt} = v_\mathrm{sT}\frac{{K_\mathrm{IT}}^\mathrm{n}}{{K_\mathrm{IT}}^\mathrm{n}+{C_\mathrm{N}}^\mathrm{n}} - v_\mathrm{mT}\frac{M_\mathrm{T}}{K_\mathrm{mT}+M_\mathrm{T}} - k_\mathrm{d}M_\mathrm{T} \tag{4.1e}$$

$$\frac{dT_0}{dt} = k_\mathrm{sT}M_\mathrm{T} - V_\mathrm{1T}\frac{T_0}{K_\mathrm{1T}+T_0} + V_\mathrm{2T}\frac{T_1}{K_\mathrm{2T}+T_1} - k_\mathrm{d}T_0 \tag{4.1f}$$

$$\begin{aligned}\frac{dT_1}{dt} &= V_\mathrm{1T}\frac{T_0}{K_\mathrm{1T}+T_0} - V_\mathrm{2T}\frac{T_1}{K_\mathrm{2T}+T_1} - V_\mathrm{3T}\frac{T_1}{K_\mathrm{3T}+T_1} \\ &\quad + V_\mathrm{4T}\frac{T_2}{K_\mathrm{4T}+T_2} - k_\mathrm{d}T_1\end{aligned} \tag{4.1g}$$

$$\begin{aligned}\frac{dT_2}{dt} &= V_\mathrm{3T}\frac{T_1}{K_\mathrm{3T}+T_1} - V_\mathrm{4T}\frac{T_2}{K_\mathrm{4T}+T_2} - k_3P_2T_2 + k_4C - \\ &\quad v_\mathrm{dT}\frac{T_2}{K_\mathrm{dT}+T_2} - k_\mathrm{d}T_2\end{aligned} \tag{4.1h}$$

$$\frac{dC}{dt} = k_3P_2T_2 - k_4C - k_1C + k_2C_\mathrm{N} - k_\mathrm{dC}C \tag{4.1i}$$

$$\frac{dC_N}{dt} = k_1C - k_2C_\mathrm{N} - k_\mathrm{dN}C_\mathrm{N} \tag{4.1j}$$

The total (nonconserved) quantities of PER and TIM proteins, P_t and T_t are given by

$$\begin{aligned} P_t &= P_0 + P_1 + P_2 + C + C_N \\ T_t &= T_0 + T_1 + T_2 + C + C_N \end{aligned}$$

Kinetic parameter	Parameter value	Kinetic parameter	Parameter value
v_{sP}	1 nMh^{-1}	k_d	0.01h^{-1}
v_{sT}	1 nMh^{-1}	k_{dC}	0.01h^{-1}
v_{mP}	0.7 nMh^{-1}	k_{dN}	0.01h^{-1}
v_{mT}	0.7 nMh^{-1}	V_{1P}	8 nMh^{-1}
K_{mP}	0.2 nM	V_{1T}	8 nMh^{-1}
K_{mT}	0.2 nM	V_{2P}	1 nMh^{-1}
k_{sP}	0.9 h^{-1}	V_{2T}	1 nMh^{-1}
k_{sT}	0.9 h^{-1}	V_{3P}	8 nMh^{-1}
v_{dP}	2 nMh^{-1}	V_{3T}	8 nMh^{-1}
v_{dT}	2 nMh^{-1}	V_{4P}	1 nMh^{-1}
k_1	0.6 h^{-1}	V_{4T}	1 nMh^{-1}
k_2	0.2 h^{-1}	K_{4T}	2.0 nM
k_3	1.2 nM^{-1}h^{-1}	K_{4P}	2.0 nM
k_4	0.6h^{-1}	K_{3T}	2.0 nM
K_{IP}	1.0 nM	K_{3P}	2.0 nM
K_{IT}	1.0 nM	K_{2T}	2.0 nM
K_{dP}	0.2 nM	K_{2P}	2.0 nM
K_{dT}	0.2 nM	K_{1T}	2.0 nM
n	4	K_{1P}	2.0 nM

Table 4.2: Rate constants for the *Drosophila* model.

The model takes into account nuclear transcription of the *per* and *tim* genes and transport of the *per* and *tim* mRNAs into the cytoplasm, where they are translated into PER and TIM proteins. The latter can be multiply phosphorylated and form a complex that enters the nucleus and represses *per* and *tim* transcription. The model incorporates degradation of the PER and TIM proteins and their mRNAs. Light influences the *Drosophila* clock by triggering TIM degradation [97], the maximum rate of TIM degradation ν_{dT} increases with increasing light intensity. (In mammals, where *per* and *tim* genes are also found, light acts by enhancing the rate of *per* expression ν_{sP}.) The *Drosophila* model is described by a set of 10 ordinary differential equations (ODE) that govern the time evolution of *per* and *tim* mRNAs and of the various forms of PER and TIM proteins and the PER-TIM complex [33]. The model can reproduce circadian oscillations in continuous darkness, entrainment by light-dark cycles, and phase shifting by light pulses (see Figure 4.9 and 4.11).

4.4 Mathematical analysis of the circadian model

4.4.1 Characteristics of circadian oscillators

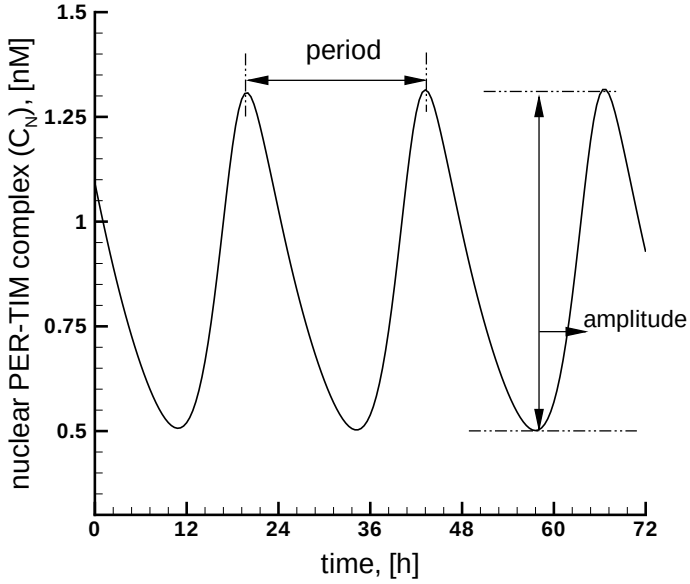

Figure 4.6: Characteristics of circadian oscillators.

Three key properties of a circadian oscillator are its period, amplitude and phase [125]. *Period* may be expressed as the time interval between peak state values (see Figure 4.6). The amplitude of the circadian oscillations relates to the difference between maximum and minimum values of mRNA or protein concentrations (see Figure 4.6). The phase of a circadian rhythm reflects where the peak and the trough occur, for example, the peak and trough of performance within the 24 hour. *Phase shift* is defined as the measure of time capturing a system's advance or delay relative to a nominal reference (see Figure 4.7).

Starting from an unstable steady state, the trajectory of the state variables towards limit cycle is shown in Figure 4.8 as a projection onto the plane spanned by the concentrations of per mRNA and total PER protein. For a given set of parameter values, the limit cycle shown in Figure 4.8 is generally unique regardless of initial conditions. As perturbations do not change the circadian period or amplitude in the long run, limit cycle oscillations represent particularly stable mode of periodic behavior. Such stability is in accordance with the robust nature of circadian clocks which have to maintain their amplitude and period in a changing environment while retaining the capability of being phase shifted by light or temperature.

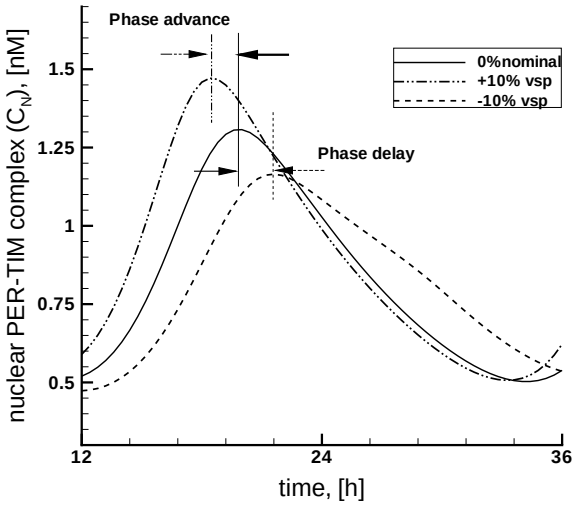

Figure 4.7: Circadian phase shift: In circadian rhythms, for e.g., the *per* transcription rate, ν_{sP} is perturbed $\pm 10\%$ of its nominal value. This disturbance causes the amplitude of oscillation to either increase (dash-dotted line in case of $+10\%$ of ν_{sP}) or decrease (dashed line in case of -10% ν_{sP}), respectively. If the peak of the perturbed trajectory crosses a time point before the peak of the nominal (solid line), there exists a phase advance (i.e., in case of dash-dotted line). The reverse yields a phase delay (i.e, in case of dashed line).

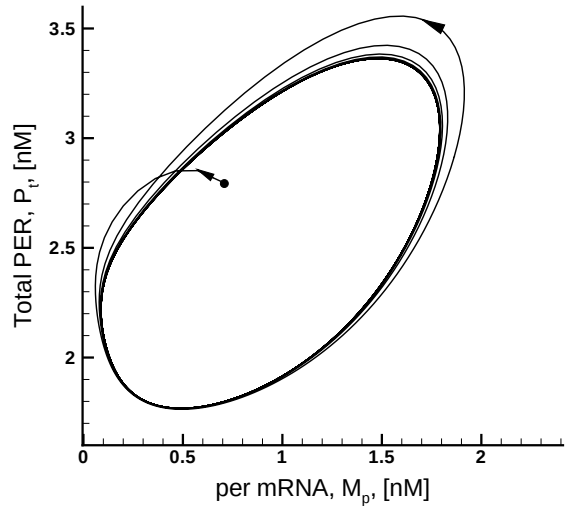

Figure 4.8: Evolution towards a limit cycle corresponding to sustained oscillations in the model for circadian oscillations in *Drosophila*. The oscillations are those observed in conditions of continuous darkness of Figure 4.9 (left). The limit cycle is reached here from initial conditions (solid circle) located near the unstable steady state. The arrow indicates the direction of movement along the limit cycle.

4.4.2 Control of circadian oscillations by light

Circadian rhythms are necessarily endogenous. By definition, these rhythms persist with stable 24 hour periods even in the absence of daily environmental cues but importantly can be synchronized (or entrained) by these cues, most notably the day-night cycles. Accordingly, the model schematized in Figure 4.3 predicts the occurrence of sustained oscillations in constant darkness (DD) and is taken hereafter as the nominal circadian oscillations. The left panel of Figure 4.9 shows the oscillations of total PER protein (P_t), per mRNA (M_p), and nuclear PER-TIM complex (C_N) observed in conditions corresponding to DD; such conditions are achieved in the *Drosophila* model by holding the parameters ν_{dT}, which measures the maximum rate of TIM degradation, at a constant low value (see Figure 4.9 (*left*)). Although the environmental conditions remain constant, the PER-TIM control system generates autonomous oscillations with a period close to 24 hours for the set of parameter values considered as observed experimentally [110]. As expected from mechanisms

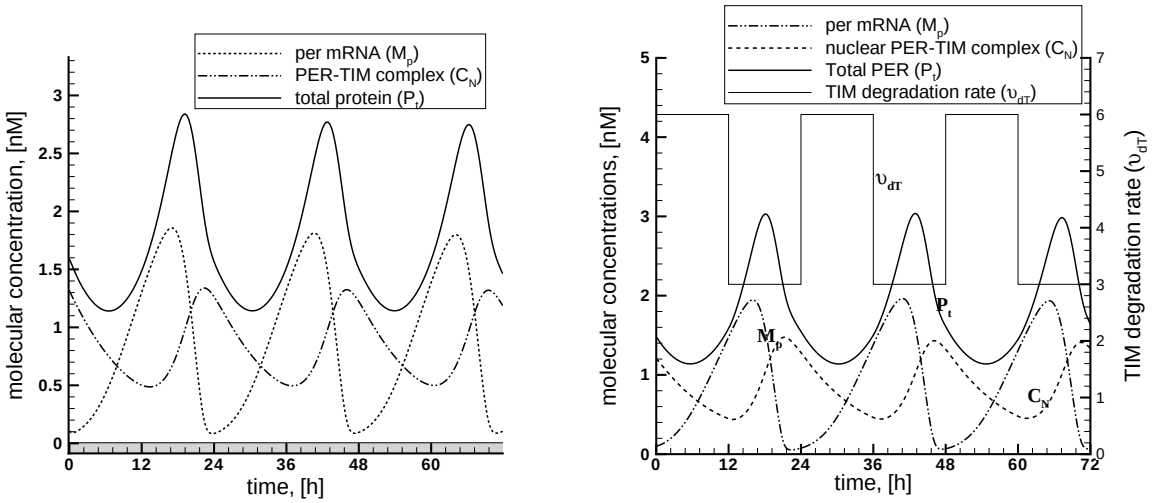

Figure 4.9: Oscillations in continuous darkness and entrainment by LD cycles for circadian rhythms in *Drosophila*. The left panel corresponds to continuous darkness and the right panel corresponds to entrainment by a light-dark cycle of 24 hour period (12:12LD). The LD cycle is symbolized by the alteration of white and black bars. The curves are obtained by numerical integration of the 10 kinetic equations governing the dynamics of the model schematized in Figure 4.3; the equations are listed in (4.1). The temporal variations in per mRNA (M_p) and in the total amount of PER protein (P_t) are shown, together with the variation in nuclear PER-TIM complex (C_N). Parameter values are taken from Table 4.2. ν_{dT} remains constant and equal to 3 in the left panel and is equal to 3 and 6 in the middle panel during dark and light phases, respectively.

in which a protein represses the transcription of its gene [126], the *Drosophila* model predicts that the peak in mRNA levels precedes the peak in protein by several hours. Moreover, the peak in total PER and TIM precedes the peak in nuclear PER-TIM complex (Figure 4.9 (*left*) panel).

Light triggers degradation of the TIM protein in *Drosophila* [121, 127]. Including a periodic variation of the light-controlled parameter into the model of the *Drosophila* circadian clock allows us to simulate the entrainment of circadian oscillations by light-dark (LD) cycles, which is shown in Figure 4.9 (*right* panel). In such conditions, the maximum TIM degradation rate ν_{dT} varies in a square-wave manner. The duration of both the light and dark phases is equal to 12 hours in the case considered (this particular light-dark cycle is denoted by 12:12 LD), the system is entrained precisely to the 24 hours external periodicity. The effect of continuous light (LL) is simulated by holding ν_{dT} at a constant high value. As observed experimentally [128], the oscillations in the model are readily damped in LL by increasing ν_{dT} to a sufficiently high value (Figure 4.10).

The induction of a phase shift by light pulses represents one of the most conspicuous properties of circadian rhythms. Biological oscillators are generally stable within a defined parameter space, a finite stimulus will force the oscillator's trajectory to deviate from its periodic orbit and return to the limit cycle asymptotically

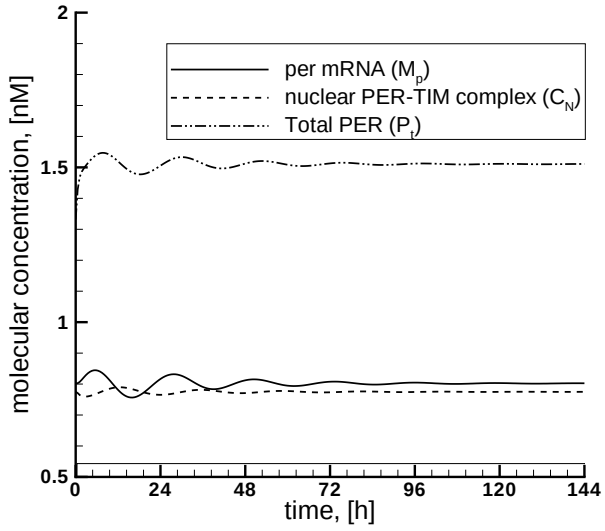

Figure 4.10: Oscillations in continuous light in the model for circadian rhythms in *Drosophila*. The temporal variations in per mRNA (M_p) and in the total amount of PER protein (P_t) are shown, together with the variation in nuclear PER-TIM complex (C_N). ν_{dT} remains constant and equal to 6.

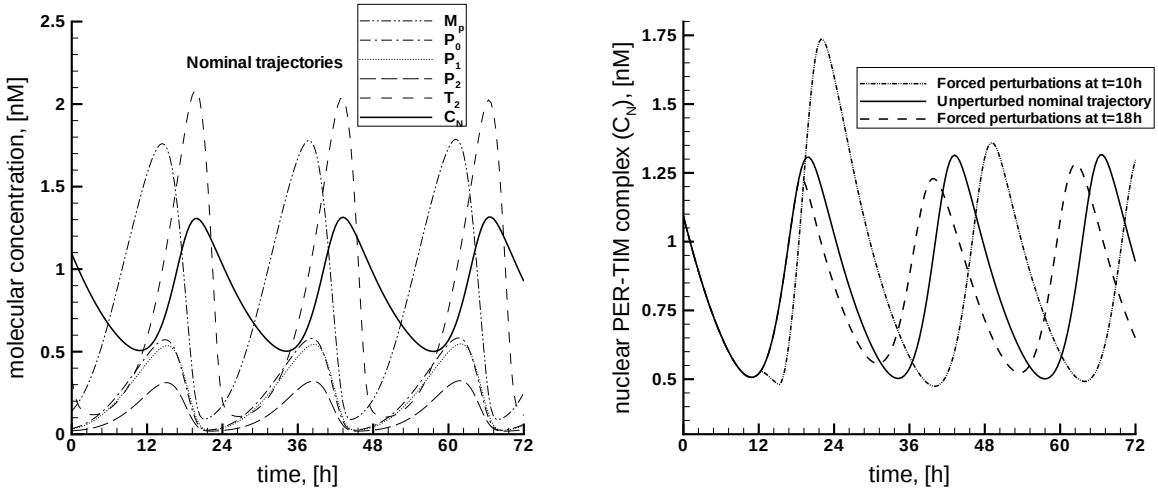

Figure 4.11: Open loop circadian dynamics with forced perturbations. The plot (*left*) depicts the nominal behavior of the circadian 10-state model over a three-day period. The heavy-weight line denotes concentrations of the PER-TIM complex within the nucleus, C_N. This complex is tracked in the plot (*right*) as a light pulse is applied to the system at 10-hours and 18-hours respectively. This disturbance temporarily represses the complex by increasing the maximum degradation rate of the TIM protein. The first perturbation recovers from the repression by gaining the amplitude and delaying its relative phase; in other words, by acquiring a negative phase shift. The second perturbation decreases amplitude, gains a relative advance, and acquires a positive phase shift.

with a phase shift. If this initial stimulus of light is applied at different times throughout the period, the resulting change in phase will vary accordingly. As depicted in Figure 4.11, a stimulus applied at 10-hours results in different change of phase relative to the same stimulus applied at 18-hours.

4.4.3 Sensitivity analysis of the circadian model

Sensitivity analysis plays an important role in the study of biochemical systems [36, 37, 129]. Parameter sensitivities yield a quantitative measure of the deviations in characteristic system properties resulting from the perturbation of system parameters. Analysis of parameter sensitivities can, hence, provide clues on the importance of individual regulatory processes on the function of clock.

For a circadian clock model described by ordinary differential equations of the form $\frac{dx}{dt} = f(x(t), p, t)$ with $t \geq t_0$, the n_S-dimensional vector of state variables x, the n_P-dimensional vector of model parameters p, and initial conditions $x(t_0) = x_0$, parameter sensitivity of the system's states along a specific trajectory $S \in \mathbb{R}^{n_s \times n_p}$ matrix of state sensitivities) with respect to a parameter is defined by

$$S_{i,j} = \frac{\partial y_i}{\partial p_j}$$

where $S_{i,j}$ is the sensitivity coefficient of the i^{th} system output y_i with respect to the j^{th} parameter p_j. Considerable work has been done on sensitivity analysis of the selected 10-variable *Drosophila* model (see Ref. [37]). The robustness analysis for the model shows that parameters could be segregated into two broad groups: "Global" parameters, like transcription and translation rates, that affect many processes in addition to the circadian clock and "local" parameters that pertian to the clock exclusively [130]. In addition, a third category of "mixed" parameters, which are neither entirely global nor local, are identified [37]. It has been found that the 10-variable *Drosophila* model is sensitive to perturbations in its global parameters but less sensitive to perturbations in its local or mixed parameters. The sensitivity analysis identified phosphorylation/dephosphorylation rates as insensitive parameters when compared to rates of degradation, transport, translation and transcription [131]. In general processes of gene regulation, transcription, and translation turned out to influence predominantly the amplitude of circadian rhythms. These sensitive elements have evolved as natural control inputs which will be used in control scenarios in Section 4.5.

4.4.4 Bifurcation Analysis

To explain the underlying dynamics of the described model with respect to sensitive control parameters and for a better understanding of our control approach, we use a bifurcation analysis with respect to the light-sensitive parameter ν_{dT}, which is shown in the Figure 4.12. It represents the dynamic behavior of the oscillatory system by a single state variable, the fully phosphorylated form of the TIM protein (T_2), as a function of ν_{dT}. At low values of ν_{dT}, a stable steady state is obtained. As ν_{dT} increases, the steady state becomes unstable at $\nu_{\mathrm{dT}} = 2.02226$, and sustained limit cycle oscillations occur. In Figure 4.12 the envelope of oscillations giving the minimum and maximum levels of T_2 at different values of ν_{dT} are shown. Beyond

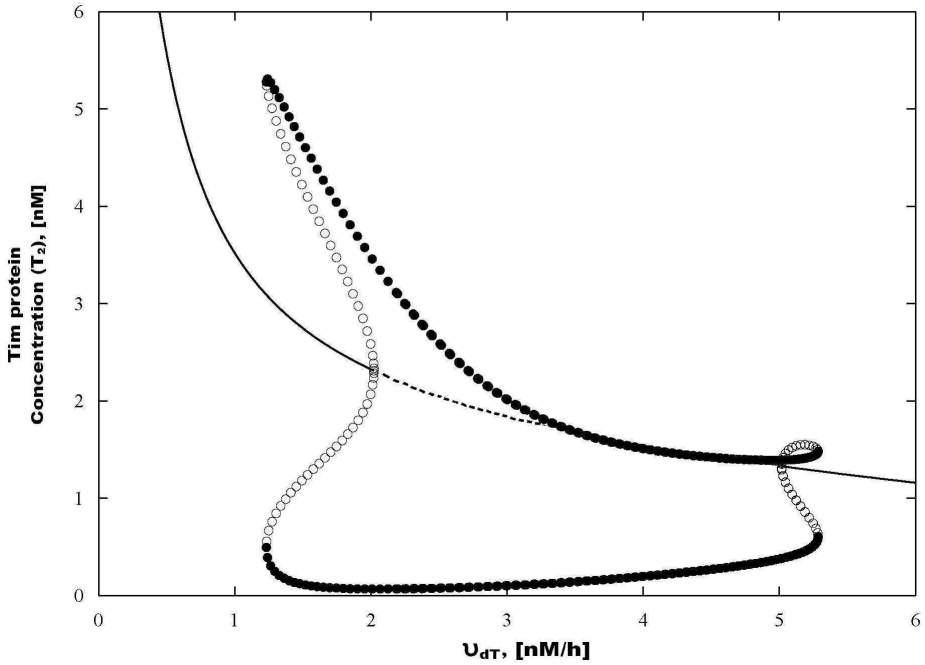

Figure 4.12: Bifurcation diagram showing the range of sustained oscillations as a function of the light-controlled parameter in the molecular model for the circadian clock [33]. The diagram represents the stable (solid line) or unstable (dashed line) steady-state value of a state variable (phosphorylated TIM form), as well as its envelope (maximum and minimum oscillation value) in the course of stable (solid circles) or unstable (open circles) sustained oscillations, as a function of ν_{dT}. Numerical computations for the bifurcation diagram were performed with the software package AUTO [132].

a second bifurcation point at large $\nu_{\mathrm{dT}} = 5.27036$, the steady state recovers its stability. For some parameter values, coexistence of a stable steady state and a stable regime of limit cycle oscillations is observed. This situation is important to obtain stability in our open-loop control scenarios aimed at switching between the periodic and stationary states.

4.5 Control of circadian rhythms

An inability to entrain circadian rhythms to the environment causes many functional disorders [124]. Circadian disorders include non-24-hour sleep-wake syndrome, seasonal affective disorders (SAD) or winter depression, general malaise associated with jet-lag and shift-work, advanced or delayed phase sleep syndrome, and irregular sleep-wake pattern syndrome [133]. Many researchers have studied the clock in an attempt to both understand and correct for existing discrepancies. Analysis of the circadian clock demonstrates that control inputs, such as light can be used to

manipulate the system dynamics. The use of such light pulses as artificial entraining agents along with natural light/dark cycles may help to reduce the recovery time of circadian rhythms when they are disturbed due to rapid time-zone change because of traveling and shift work. Boulos *et al.* performed experiments establishing bright light treatment as a means to accelerate circadian re-entrainment following trans-meridian travel [134]. Daan *et al.* discussed light-induced phase shifts as a function of circadian time and the role phase response curves play in achieving entrainment [135, 136]. Watanabe *et al.* confirmed Daan *et al.* work through experimental procedures proving that the basis for phase adjustment involves rapid resetting of both advance and delay components of the phase response curve [137]. Entrainment and robust properties of circadian rhythms with respect to environmental cues (light/dark cycles) are studied by Takeuchi *et al.* in a molecular model for *Drosophila* [138]. Despite decades of work put forth in understanding circadian phase and entrainment properties, the idea of optimally controlling circadian properties via open and closed-loop control algorithms for molecular models is a recent area of interest (e.g. see Refs. [139, 140, 141, 142, 130]).

4.5.1 Formulation of optimal control problems

The aim of our approach is to change the behavior of the dynamical system by a time variant external control such as the maximum rate of protein degradation (ν_{dT}), translation frequency (k_s) or transcription rate (ν_s). We will denote the corresponding functions ν_{dT}, k_s and ν_s by $u(t)$. We want to minimize the integrated difference between the state trajectory $x(t)$ of the system and a reference trajectory $x_r(t)$. This reference trajectory is obtained by solving a boundary value problem that includes a periodicity constraint

$$x_r(0) = x_r(T)$$

with $T = 24$. Under free running conditions, the oscillations has a period of about 23.8 hours, which is different from the entrained period of 24 hours. However, we fix the parameters to the values given in Table 1, which corresponds to a "darkness scenario" except ν_{dT} for obtaining the reference trajectory with a period of 24 hours as in case of entrained conditions. We apply the optimal control software package MUSCOD-II [143] that implements the direct multiple-shooting method, see Chapter 3. As a result of the numerical optimization we obtain the value of the parameter $\nu_{\mathrm{dT}} = 3$ for which the system shows the desired periodic behavior with a period of exactly 24 hours. The number of multiple-shooting nodes $N = 1$ here, with final time T and initial conditions as free parameters. As can be seen in Figure 4.12, for the value $\nu_{\mathrm{dT}} = 3$ the system is characterized by an unstable steady state surrounded by stable limit cycle oscillations respresented in solid dots. Therefore the calculated reference orbit $x_r(t)$ corresponding to $\nu_{\mathrm{dT}} = 3$ is stable.

Our optimization problem now consists of minimizing the deviation from this reference trajectory for given initial values $x(0) = x_0$ over a given time horizon,

$$\begin{aligned} \min_{u,x} \quad & \int_0^T \|x(t) - x_r(t)\|_2^2 \, \mathrm{d}t \\ \text{subject to} \quad & \dot{x} = f(x, u, p), \\ & x(0) = x_0, \\ & u_{min} \leq u \leq u_{max}. \end{aligned} \tag{4.2}$$

The function f represents the differential equation model given in Eq. 4.1; control constraints $u \in [u_{\min}, u_{\max}]$ and concentrations $x_i(t) \geq 0$. $\|.\|_2$ denotes the Euclidean norm and p a parameter vector. Problem (4.2) is a standard optimal-control problem and can be solved by direct multiple-shooting (DMS) method with a piecewise-constant control parameterization $u(t) = u_i$, $t \in [t_i, t_{i+1}], i = 1, \cdots, N$ on multiple-shooting intervals $[t_i, t_{i+1}] \subset [0, T]$, where T is total time of simulation. For numerical integration we use the BDF method implemented in the solver DAESOL [59]. We have investigated the control scenarios for circadian rhythms with three different control parameters.

In the first two control scenarios, for phase resetting and phase tracking of circadian rhythms, we use ν_{dT} as a control parameter and other parameter values are fixed to the values given in Table 1. In the third control scenario, for restoration of altered rhythms, we use translation frequency (k_s) of PER and TIM proteins or transcription rates (ν_s) of *per* and *tim* mRNA as the control parameters. We choose translation frequency/transcription rates as control parameter because the system dynamics turned out to be very sensitive with respect to k_s and ν_s [37]. In practice, the light sensitive parameter ν_{dT}, and the translation frequency/transcription rates are easier to control as a switching off-on-off control function than a function with continuous values over time. Mathematically this means that we have to restrict the control function $u(t)$ to take values in $\{u_{\min}, u_{\max}\}$ only. This can be reformulated via $u(t) = u_{\min} + w(t)(u_{\max} - u_{\min})$ into a binary valued control function $w(t) \in \{0, 1\}$.

The solution that minimizes the objective function for a given differential equation model, set of initial conditions and constraints is solved with the optimal control software package MUSCOD-II [143, 80]. MUSCOD-II implements an SQP method for solving the NLP problem that arise after discretizing problem 4.2 as discussed in Section 3.3. A DAE solver DAESOL is used with the BDF method for the solution of the DAEs and the generation of derivatives and accuracies of 10^{-6} for the KKT condition and 10^{-7} for the integration.

4.6 Optimal phase resetting of circadian rhythms by critical light pulses

One of the most intriguing observations on circadian rhythms is that they can be suppressed in a prolonged manner by a single pulse of light. Long-term suppression has been reported for a variety of organisms including insects [144] and mammals [145, 146]. The abolished rhythm can often be restored by a second light pulse [145]. For limit cycle attractors surrounding a steady state, Winfree has proven via topological arguments under very general assumptions that a critical stimulus with appropriate timing, length and strength corresponding to a so called phase singularity must exist which takes the system immediately to steady state, meaning instantaneous suppression of the oscillations [147].

The model considered here allows us to address this issue explicitly, given that the effect of light in this model is included in the molecular mechanism of circadian oscillations. The situation schematized in Figure 4.12 has distinct dynamical consequences regarding the possibility of suppressing the circadian rhythmicity by light pulses. In the situation when the control parameter ν_{dT} lies between the two critical values 1.25 nM/h and 2 nM/h, a stable steady state coexists with a stable limit cycle. An unstable limit cycle separates the basins of attraction of these two stable regimes. Such a situation, observed in the model for circadian rhythms in Drosophila [33] is schematized in the upper left panel in Figure 4.13. The arrow from the stable limit cycle (solid curve) symbolizes the effect of a light pulse that brings the system across the unstable limit cycle (dashed curve) into the basin of attraction of the stable steady state. The consequence of such a light pulse applied at the appropriate phase with the appropriate duration and magnitude is illustrated in the left bottom panel of Figure 4.13. The light pulse has suppressed the rhythm permanently. The analysis of the Drosophila model indicates that the phases at which the light pulse permanently suppresses the rhythm correspond roughly to the portion of the limit cycle associated with the rise in TIM.

In the more common situation, in which a stable limit cycle does not coexist with a stable steady state (see Figure 4.12 in the interval ν_{dT} between 2 nM/h and 5.2 nM/h), the effect of a light pulse is different. As illustrated in the upper right panel of Figure 4.13, a light pulse applied at the appropriate phase with the appropriate duration and magnitude can bring the system into the close vicinity of the steady state, but because the latter is unstable the system will eventually return to the limit cycle, possibly after skipping a number of oscillations, as illustrated for a higher value of ν_{dT} in the Drosophila model in the bottom right panel of Figure 4.13. In such conditions, suppression of the circadian rhythm by the light pulse is only transient. Both transient and permanent suppression of circadian rhythms by single, critical perturbations have been observed experimentally [128]. However, neither the phase at which the stimulus have to be applied nor the characteristics of the critical stimulus strength for suppression or restoration of oscillations are a *priori* clear.

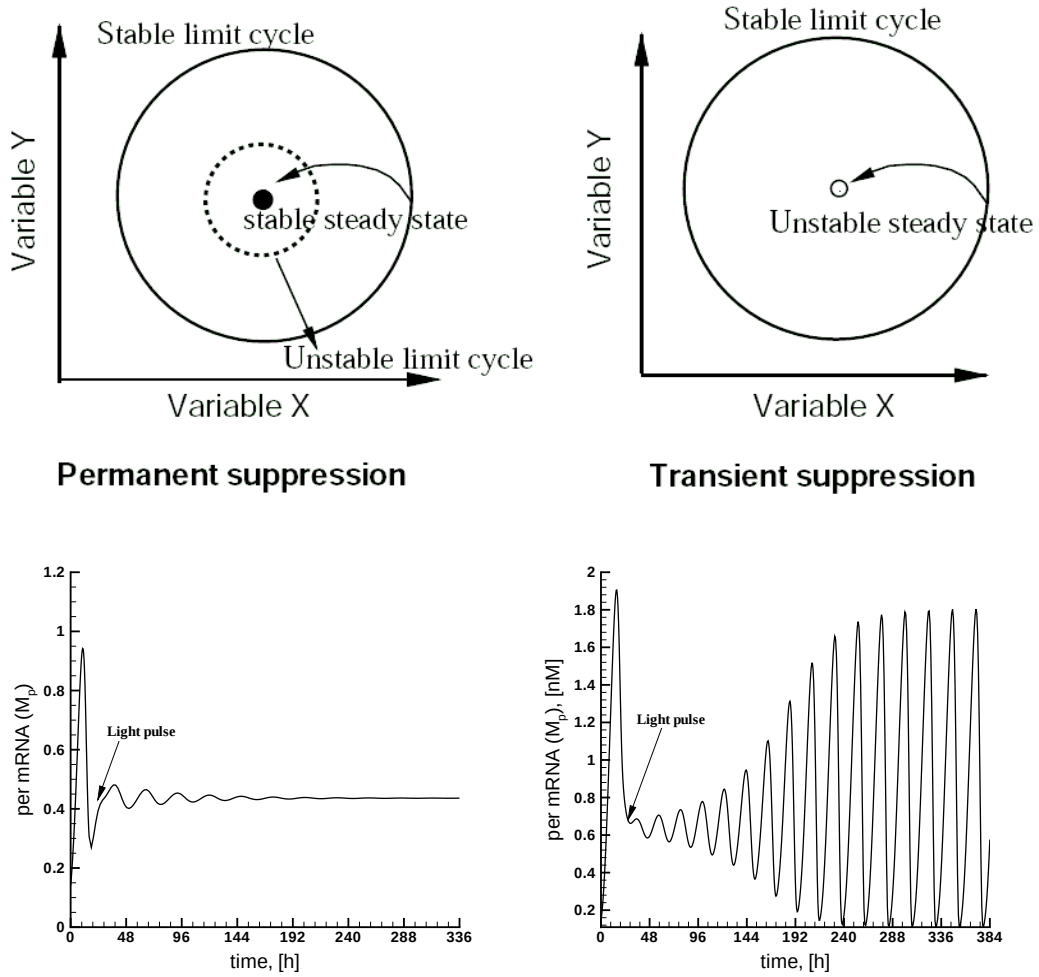

Figure 4.13: Permanent and transient suppression of circadian rhythmicity by light pulses in the *Drosophila* clock model. The upper left panel schematically depicts to the coexistence between a stable limit cycle (solid curve) and a stable steady state (dot) which are separated by an unstable limit cycle (dashed line). The upper right panel portrays the situation of a stable limit cycle surrounding an unstable steady state. The (stable or unstable) steady state is often referred to as singularity. The curves in the bottom panels have been obtained by numerical integration of kinetic equations governing the evolution of the *Drosophila* circadian clock model 4.1. Lower left panel: permanent suppression of the circadian rhythm. Parameter ν_{dT} is increased, at the time indicated by vertical arrow, during a 2-hour from the basal value of 1.3nMh^{-1} upto 4.0nMh^{-1}. Lower right panel: transient suppression of the circadian rhythm in the *Drosophila* clock model. At the time indicated by the arrow, parameter ν_{dT} is increased during a 3.8-hour from the basal value of 3.5nMh^{-1} up 6.7nMh^{-1}. The basal value of 1.3nMh^{-1} and 3.5nMh^{-1} correspond to the situations depicted in the upper left and right panels, respectively. Other parameter values are taken from the Table 4.2

Winfree proposed an approach to determine these parameters by probing the phase resetting response for various stimulus intensities and corresponding phase relations between stimulus and system state and construction of so-called phase resetting curves [147]. However, in complex multi-component systems occurring in biology, the overwhelming variety of the kind, strength and timing of possible stimuli make

simulation based approaches via phase resetting curves impractical [28]. For this reason, a systematic and automatic algorithmic procedure for identification of the phase singularities is attractive. Here, we demonstrate how model-based optimal control of mixed-integer type can be exploited for the task of systematically finding appropriate strength and timing of critical external stimuli leading to specific suppression and restoration of circadian rhythms [140]. It is crucial that we use the underlying direct multiple-shooting method for our numerical studies, a method that has shown to be suitable for complex self-organizing behavior before in Lebiedz *et al.* [27, 148, 149, 150].

On the basis of the *Drosophila* model presented in Section 4.3, we consider suppression of circadian rhythmicity by directly controlling the light-sensitive parameter ν_{dT}. We address this problem by model-based mixed-integer optimal control via formulation of the control objective as the minimization of the system state deviation from the desired steady state integrated over time. The corresponding mixed-integer optimal control problem is

$$\min_{w(t)} J(x, w(t)) := \int_0^T \sum_{\mathrm{i}=1}^{10} (x_i(t, w(t)) - x_{\mathrm{i}}^s)^2 dt \tag{4.3}$$

subject to the ODEs in Eq. (4.1), the integer constraints $w(t) \in \{0, 1\}$, positive valued concentrations $x_i(t)$ and initial conditions. The vector x_i^s denotes the steady state coordinates and is obtained by using the XPPAUT software [132]. The objective functional (4.3) is minimized for suppressing the circadian rhythms with control parameter ν_{dT}. For restoration of suppressed circadian rhythms, the maximization of the same objective functional (4.3) turned out to be suitable.

We apply a novel approach based on the DMS method [53] which can treat bang-bang control scenarios with a piecewise constant control parameterization to obtain such an optimal light stimulus to suppress and subsequently restore the circadian rhythmicity in the *Drosophila* model at *a priori* defined time points. We compute an optimal control $\nu_{\mathrm{dT}}(\mathrm{t})$ as a solution of problem (4.3) via convex relaxation of the integer constraints (see Section 3.6.1). The result is shown in Figure 4.14, (*left*). Obviously the rhythm can be suppressed and restored by adjustable time-varying light pulses (see Figure 4.15 *left*). However, these are difficult to realize in practice, therefore, we go on to compute a bang-bang solution of problem (4.3) (see Figure 4.14, *right*). Figure 4.15 shows the corresponding controlled system state trajectory for the TIM protein concentration. Obviously, it is possible to achieve a desired optimal switching between stationary and oscillatory states on the basis of the circadian rhythm model. Figure 4.16 shows the bang-bang control solution and corresponding state trajectories for permanent suppression of circadian rhythms with a single light pulse.

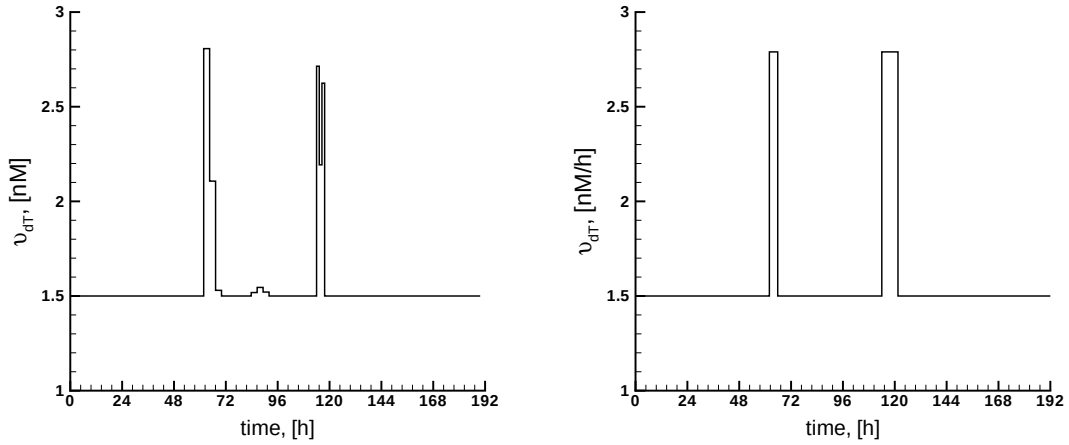

Figure 4.14: Optimal control for the relaxed problem (*left):* and the bang-bang problem *(right):* of circadian rhythm suppression by light and subsequent restoration of the rhythm based on the *Drosophila* model. Control input: light-sensitive maximum rate of protein degradation ν_{dT} as a function of time.

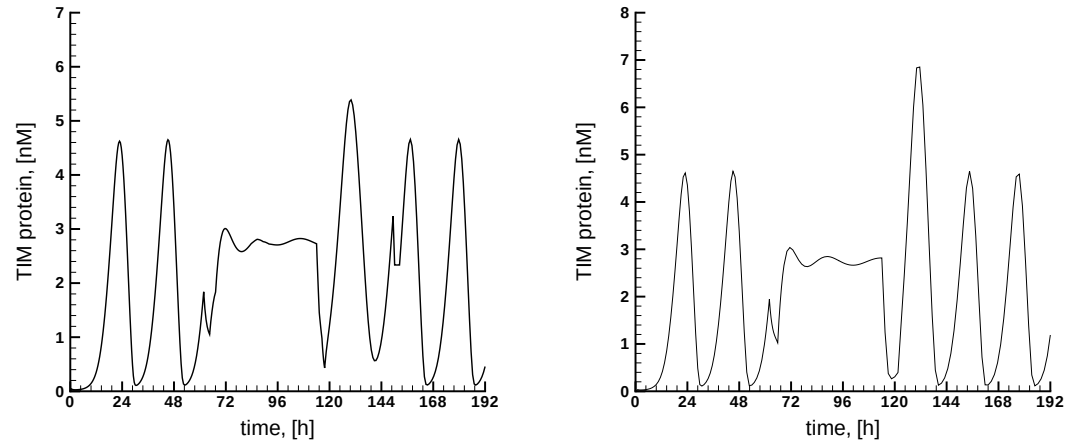

Figure 4.15: Rhythm suppression and restoration by a light stimuli corresponding to the optimal control functions in Figure 4.14, *(left):* relaxed control scenario, *(right):* bang-bang control scenario. The plot shows the TIM protein in nM as a function of time.

4.7 Optimal phase tracking of circadian rhythms

Circadian rhythm desynchronization and disruption are the result of a living systems being out of sync with the environmental cycles. Depending on at what time an organism is exposed to the entraining agent, one can set the clock forward, set back, or not changed at all. In case of light as entraining agent, during the middle of subjective day when light is expected, it has no effect on circadian phase. However, a light pulse administered around subjective dusk (or early night) causes a phase delay, whereas a light pulse near subjective dawn (or early morning) causes a phase advance. Plotting the direction and magnitude of the phase shift as a function of

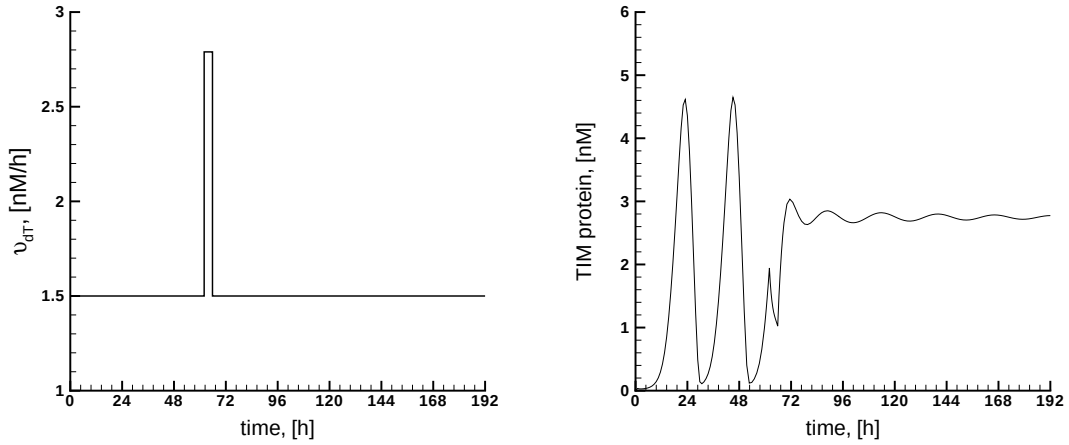

Figure 4.16: Bang-bang control solution *(left)* for permanent suppression of circadian rhythms and the corresponding TIM protein accumulation*(right)*. Control input: light-sensitive maximum rate of protein degradation ν_{dT} as a function of time.

the phase of the rhythm, when the perturbation is timed, yields the phase-response curve. In nature, this property allows the clock to function as a timing device to measure day length, enabling organisms to synchronize their physiology with changing seasons (it also enables jet travelers to adjust to new time zones). Molecular models have been used to obtain theoretical phase-response curves that can be compared with experimental observations [33, 151].

Instead of using the phase response curves, here the aim of our optimal control approach is to automatically identify strength and timing of the light-induced parameter changes for TIM degradation which synchronize the system with a desired reference trajectory. We use the light-sensitive control parameter $\nu_{\mathrm{dT}}(t)$ as a control function. Our optimization problem now consists of minimizing the deviation of actual circadian rhythm $x(t)$ from a reference trajectory $x_r(t)$ with a phase difference with respect to $x(t)$ for given initial values $x(0) = x_0$ over a given time horizon,

$$\min_{\nu_{\mathrm{dT}}(t)} \quad \int_0^{72} \|x(t) - x_r(t)\|_2^2 \mathrm{d}t \tag{4.4}$$

subject to

$$\begin{aligned} &\dot{x} = f(x, \nu_{\mathrm{dT}}, p), \\ &x(0) = x_0, \\ &\nu_{\mathrm{dT}_{\min}} \leq \nu_{\mathrm{dT}} \leq \nu_{\mathrm{dT}_{\max}}. \end{aligned}$$

The function f represents the differential equations of the model given in Eq. 4.1; control constraints $\nu_{\mathrm{dT}} \in [\nu_{\mathrm{dT}_{\min}}, \nu_{\mathrm{dT}_{\max}}]$ and concentrations $x_i(t) \geq 0$. Two cases of

reference trajectories $x_r(t)$ are considered here, one with a phase advance of 6 hours and another with 12 hours with respect to $x(t)$. A more relevant issue would be to achieve total PER protein level restoration rather than mRNA level approximate restoration. So in our objective function Eq. (4.4), we tracked all the variable concentrations in the model. For simplicity, we show only the results of PER-TIM complex in nucleus (C_N) here, but as formulated in objective function (4.4), we tracked all the variable concentrations to the reference trajectory.

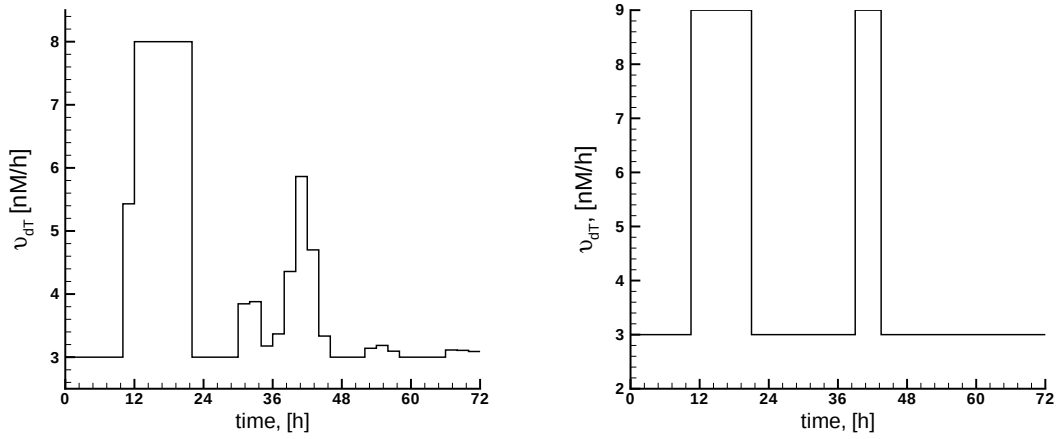

Figure 4.17: Optimal control functions for the relaxed problem (*left*) and the bang-bang problem (*right*) of circadian rhythm tracking with a 6-hour phase difference by light based on the *Drosophila* model. The control input is the light-sensitive maximum rate of protein degradation (ν_{dT}) as a function of time. The values of the control function ν_{dT} are required to be in the interval $\nu_{\mathrm{dT}} \in [3, 9]$.

We compute a relaxed optimal control $\nu_{\mathrm{dT}}(t)$ as a solution of problem (4.4) using piecewise linear control parameterization. Total simulation time in this case is T=72 hours with 36 multiple shooting points i.e. with 2 hours time on each shooting interval. The result is shown in Figure 4.17 (*left*). The controller is able to recover a maximum 6-hours phase difference within 23-hours with 0.5 hours accuracy (see Figure 4.18). Obviously the rhythm can be successfully tracked by piecewise constant time varying light stimuli. However, these are difficult to realize in practice and therefore, like in previous section, we go on to compute a pulse control in terms of a bang-bang solution of problem (4.4) as in the case (4.3) that switches between a maximal and minimal value of the control parameter. We reformulate the optimal control problem as

$$\min_{w(t)} J(x, w(t)) := \int_0^{72} (x_i(t, w(t)) - x_{\mathrm{ir}}(t))^2 dt \tag{4.5}$$

by setting $\nu_{\mathrm{dT}}(\mathrm{t})=\nu_{\mathrm{dTmin}}+w(t)(\nu_{\mathrm{dTmax}}\text{-}\nu_{\mathrm{dTmin}})$, this can be formulated assuming a binary-valued control function $w(t)$ which can take only boundary values low or up

of a relaxed feasible domain $[0, 1]$. x_{ir} is the reference trajectory for i^{th} variable corresponding to x_i. The value of ν_{dT} is restricted in the interval of [3,9], ν_{dT}=3 corresponds to the continuous darkness case and ν_{dT}=9 is a 50% increase in the value ν_{dT}=6 under continuous light. In Figure 4.17 (*right*) shows the bang-bang problem computed via mixed-integer optimal control. Figure 4.18 (*right*) shows the corresponding controlled system state trajectory of the PER-TIM protein complex in the nucleus for the pulse control. Solid lines symbolize reference trajectories while dashed lines symbolize the controlled and uncontrolled PER-TIM complex. From Figure 4.18, it is obvious that there is hardly a difference between the tracked system trajectories in relaxed and the mixed integer results but the corresponding control inputs differ significantly from each other in Figure 4.17. It is easier to implement in practice, a pulsatile solution obtained from bang-bang control problem than the relaxed solution which can take any value inbetween minimum and maximum, which is evident from the Figure 4.17.

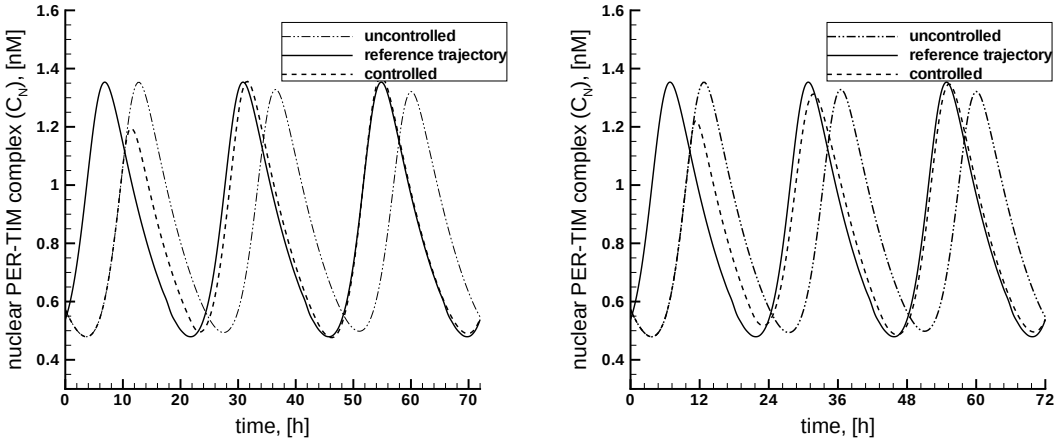

Figure 4.18: Phase tracking by light stimuli corresponding to the optimal control functions in Figure 4.17, *left:* relaxed control scenario, *right:* bang-bang control scenario. The plot shows the PER-TIM protein concentration as a function of time.

Optimization problem (4.5) is solved with $x_r(t)$ having a initial phase difference of 12 hours with 36 multiple shooting points on total time T=72. The results for tracking a 12 hours phase difference are shown in Figure 4.19. The controller is able to recover a maximum 12-hours initial phase difference within 28-hours with 0.5 hours accuracy (see Figure 4.20). In Figure 4.19 (*left*) shows the protein degradation parameter ν_{dT} as function of time for relaxed control for recovering the 12 hours phase difference and bang-bang solution (*right*) computed via mixed-integer optimal control. The corresponding controlled state trajectories for tracking a rhythm with initial phase difference of 12 hours with respect to $x(t)$ is shown in Figure 4.20 with relaxed solution (*left*) and bang-bang solution on (*right*). The plot depicts the concentrations PER-TIM protein complex in the nucleus for uncontrolled and

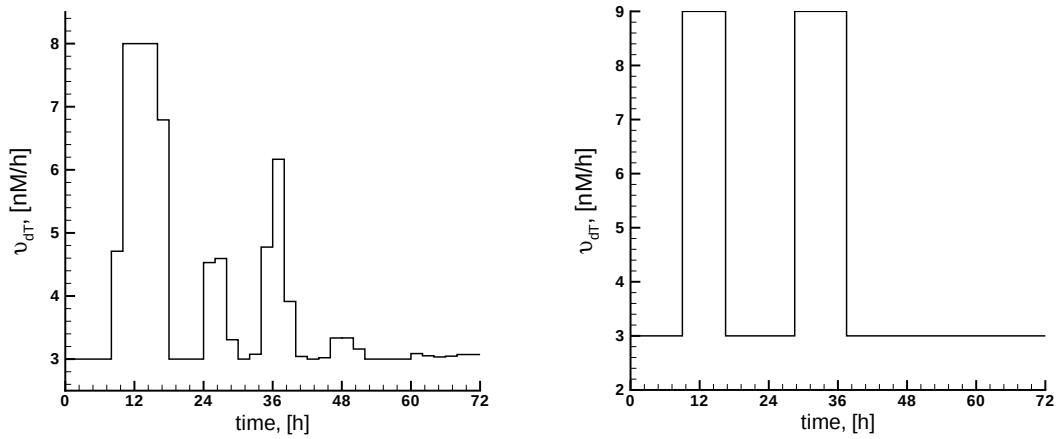

Figure 4.19: Optimal control for the relaxed problem (*left*) and the bang-bang problem (*right*) of circadian rhythm tracking of 12-hour phase difference by light based on the *Drosophila* model. The control input is the light-sensitive maximum rate of protein degradation ν_{dT} as a function of time. The values of the control function ν_{dT} are required to be in the interval $\nu_{\mathrm{dT}} \in [3, 9]$.

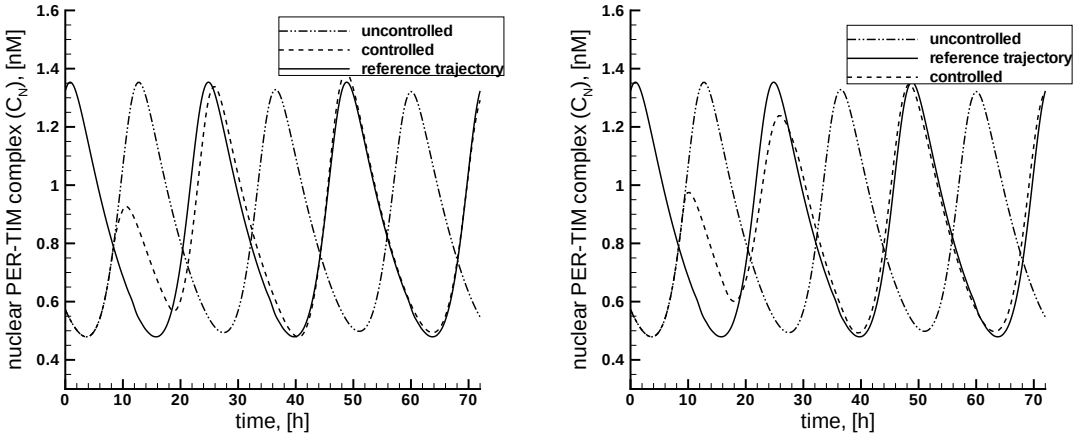

Figure 4.20: Phase tracking by light stimuli corresponding to the optimal control functions in Figure 4.19, *left:* relaxed control scenario, *right:* bang-bang control scenario. The plot shows the PER-TIM protein concentration as a function of time.

controlled cases along with the reference trajectory. Similar to the above phase advance tracking examples, one can calculate the recovery time required for tracking the system with initial phase delay. However, the maximum phase advance one can obtain with a 1 min light pulse is about 4.5 hours when compared to the maximum phase delay of 3.2 hours with the same light pulse [152,142]. Due to this asymmetric property of phase response curve for phase advance and phase delay with the same light pulse, the time required to track a phase advanced curve and phase delayed curve for the same phase difference may differ and it also crucially depends upon the initial conditions of the system.

4.8 Restoration of altered circadian rhythms

Chronotherapy can be viewed as a therapeutic control operated through drug injection schedules or modifications of the environment (e.g., exposure to light or feeding). Cancer is one field of medicine where chronotherapeutic approaches have been developed and tested [153]. Chronomodulated injection for example allows to lower considerably the side effects of highly toxic anticancer drugs [154] in chemotherapy. Clinical observations indicate that circadian rhythms may be altered in many types of cancer [155]. It has also very recently been established that the circadian clock plays a key role in tumor suppression [156] and that rhythm alteration itself might even cause cancer. Thus an additional goal of cancer therapy beyond the destruction of tumor cells might be the restoration of the endogenous circadian time structure because such a restoration could improve the prospects of patient recovery [157].

The issue of restoring normal rhythmic behavior by means of external perturbations has been addressed in models admitting sustained oscillations of the limit cycle type. An abstract nonlinear model has been proposed for the rhythmic evolution of vasopressin and cortisol. Two sets of conditions are considered, yielding oscillations characterized by the same circadian period but corresponding to different relative levels of the two hormones [158]. The model was used to determine the type of periodic perturbation by which "pathological" oscillations could be reverted optimally to the "normal" pattern of oscillation. A simplified *Drosophila* model has recently been studied from a control point of view in [159], where the authors theoretically investigate periodic activation/inhibition schemes of the translation frequency of messenger RNA of a clock gene. Flatness based control methods have been applied to control protein concentration oscillations in [160]. However the use of optimal pulsatile activation/inhibition schemes have not been studied so far. We use mixed-integer optimization for obtaining such pulsatile solutions for restoration of altered rhythm.

The *Drosophila* circadian rhythm model studied here can be used for studying possibilities to modify pathological rhythms, e.g. to restore the normal characteristics of the circadian time structure, bearing in mind possible applications in pharmacokinetics. In this case, the aim of our control problem is to determine the type of perturbation by which pathological oscillations could be reverted optimally to the normal pattern of oscillation.

We model the altered pathological rhythm by changing the parameters $\nu_{\mathrm{dP}} = 2.4nMh^{-1}$ and $\nu_{\mathrm{dT}} = 2.4nMh^{-1}$, the maximal degradation of PER and TIM proteins. These parameter values represents the nonmutant or "wild-type" *Drosophila*, with an oscillation period of close to 24 hours. By changing the parameter values to $\nu_{\mathrm{dP}} = 4.5nMh^{-1}$ and $\nu_{\mathrm{dT}} = 4.5nMh^{-1}$, we model the mutant *Drosophila*, called per^l, and with $\nu_{\mathrm{dP}} = 1.25nMh^{-1}$ and $\nu_{\mathrm{dT}} = 1.25nMh^{-1}$, mutant *Drosophila*, called

per^s, with altered amplitude and endogenous oscillation period of 29 hours and 19 hours respectively. Such mutants with long period of about 29 hours and short period of about 19 hours are well known in case of *Drosophila* [110].

For optimal control, we consider the problem of shifting a mutant *Drosophila* PER cycles towards a wild-type *Drosophila* PER cycle, setting its period precisely back to 24 hours. We assume that the alteration, caused by changing the parameters cannot be recovered by direct pharmacological access of ν_{dP} and ν_{dT}, and that we have to find an indirect way to change the period and geometric characteristics of the limit cycle characterzing the the wild-type *Drosophila* PER cycle. Progress in gene manipulation techniques make it reasonable to think of modifying transcription rates by constant activation or inhibition. However translation rates can be acted upon by more conventional means: drugs like antibiotics, substances like interferons or toxines are known to have influence on translation frequency. Here we use both translation frequency k_{sP} and k_{sT} of PER and TIM proteins and transcription rates ν_{sP} and ν_{sT} of *per* and *tim* mRNA as control parameters which may be influenced by suitable drugs. It is possible to achieve the objective of a 24-hour periodicity for mutant rhythms by activation/inhibition of translation/transcription rates to a constant value. However, other circadian characteristics like amplitude and phase of oscillations cannot be recovered well for the mutant rhythms by constant stimulation strategy. So we use translation/transcription rates as time varying controls. Time varying drug injecting pumps with constant inputs could be used for the purpose of chronomodulated drug administration. The control objective here is to restore the nominal 24 hours period and the characteristics of the oscillations (shape and amplitude) close to the wild-type *Drosophila* PER cycle by activation/inhibition of translation/transcription rates.

4.8.1 Restoration of altered *per^l* mutant rhythm

per^l mutant rhythm is characterized by large amplitude long period oscillations with a period of about 29 hours. Starting from the mutant *Drosophila* per^l, we focus on changing the translation frequency k_s of mRNAs into the nonphosphorylated form of proteins. Here we assume the translation frequency of PER k_{sP} and TIM protein k_{sT} are the same and equal to k_s. In our case the constraints on k_s are minimum and maximum values of the parameter, as k_s is supposed to switch between $k_{\min}$ and $k_{\max}$.

$$\min_{w(t)} J(x, w(t)) := \int_0^{72} (x_i(t, w(t)) - x_{\mathrm{ir}}(t))^2 dt \tag{4.6}$$

The mixed-integer optimal control problem Eq. (4.6) is solved with piecewise constant control inputs $k_s(t)$ after relaxing the integer constraints is shown in Figure 4.21 (*left*). The rhythm can be tracked by suitable variation of the translation frequencies of PER and TIM proteins. The controller is able to restore a period of

24 hours, phase and amplitude of nominal oscillations very well for the long period mutant per^l. The parameter value of k_s is allowed to vary in the interval of [0.8,1.6]. In Figure 4.21 (*right*), the mixed integer solution of the optimal control problem Eq. (4.6) is shown, which has been computed starting from the relaxed solution as discussed in Section 3.6.1. The corresponding controlled state trajectories are shown in Figure 4.22 for the mixed-integer solution. In Figure 4.22 (*left*) accumulation of per mRNA is plotted as a function of time for controlled, non mutant wild type x_r(t) and uncontrolled mutant type per^l. The controller is able to restore both the period and amplitude of the mutant oscillations close to the desired trajectory x_r(t) with bang-bang controls. We plotted per mRNA *vs* PER-TIM complex in nucleus on right side of Figure 4.22, to visualize the control result in a state space projection.

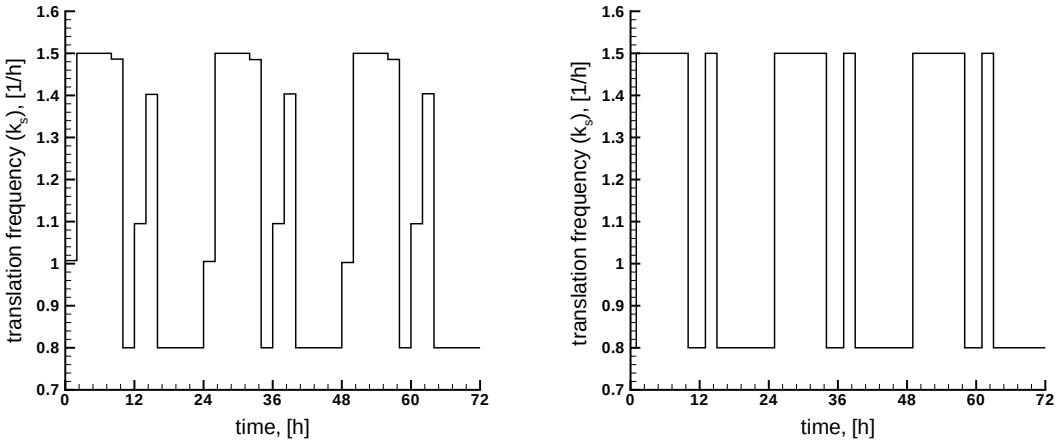

Figure 4.21: Optimal control inputs for the relaxed problem (*left*) and the bang-bang problem (*right*) of circadian rhythm restoration of mutant per^l in *Drosophila* by varying the translation frequency k_s as control input.

We studied control of transcription rates of *per* and *tim* mRNAs in our control scenarios for restoration of per^l mutant rhythm. The transcription rates of *per* (ν_{sP}) and *tim* (ν_{sT}) are not the equal in this case and we have two control parameters for the optimal control problem Eq. 4.6. The constraints on transcription rates are minimum and maximum values of individual parameters ν_{sP} and ν_{sT}, and are supposed to switch between their minimum and maximum for mixed-integer case. The mixed-integer solution of the optimal control problem Eq. (4.6) is shown in Figure 4.23 with transcription rates (ν_{sP} and ν_{sT}) as control parameters. By varying the transcription rates of *per* and *tim* we are able to achieve the same results for per^l mutant rhythm restoration as in case of using translation rates as control parameters.

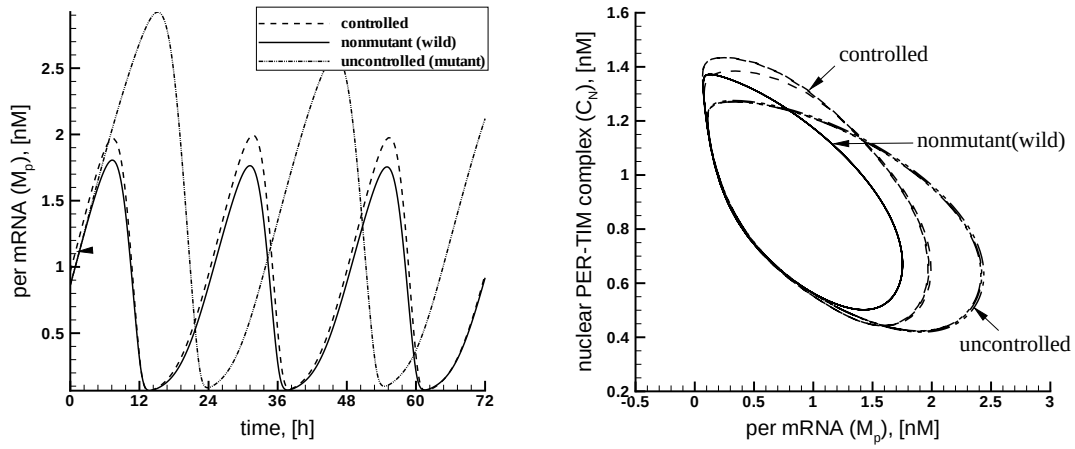

Figure 4.22: Rhythm restoration of mutant *Drosophila* per^l by the optimal bang-bang control functions from Figure 4.21. The (*left*) plot shows the per mRNA protein as a function of time in case of above control scenarios and (*right*) plot shows the corresponding limit cycles for the per^l mutant restoration in a state space projection.

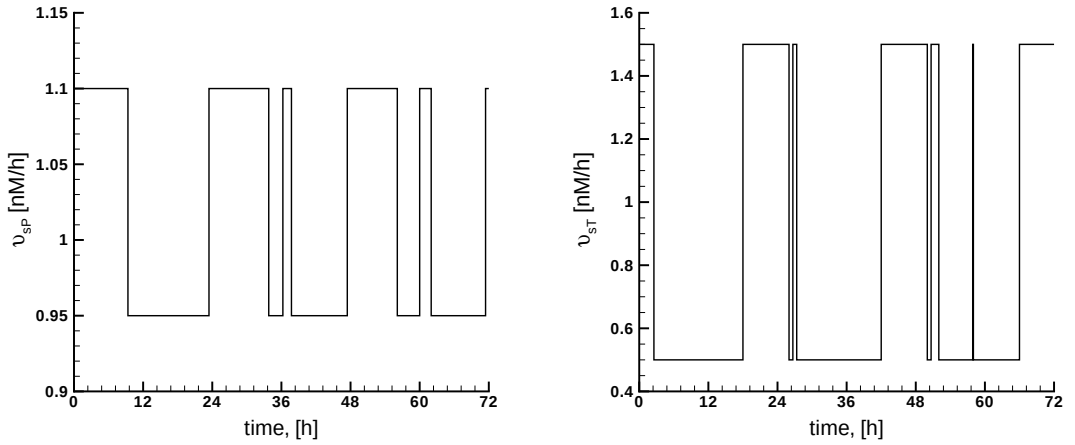

Figure 4.23: Optimal control inputs of bang-bang problem for circadian rhythm restoration of mutant per^l in *Drosophila* model by varying the transcription rates ν_{sP} and ν_{sT} as control parameters.

4.8.2 Restoration of altered *per*^{s} mutant rhythm

per^s mutant rhythm is characterized by small amplitude short period oscillations with a period of about 19 hours. Our control objective is again to restore the nominal 24 hours period and the characteristics of the oscillations (shape and amplitude) close to the nominal values by inhibition of translation rates of PER and TIM. In Figure 4.24 (*left*), the control input $k_s(t)$ as a solution of problem (4.6) with relaxation of the integer constraints is shown. The parameter value of k_s is allowed to vary in the interval of [0.2,1.2].

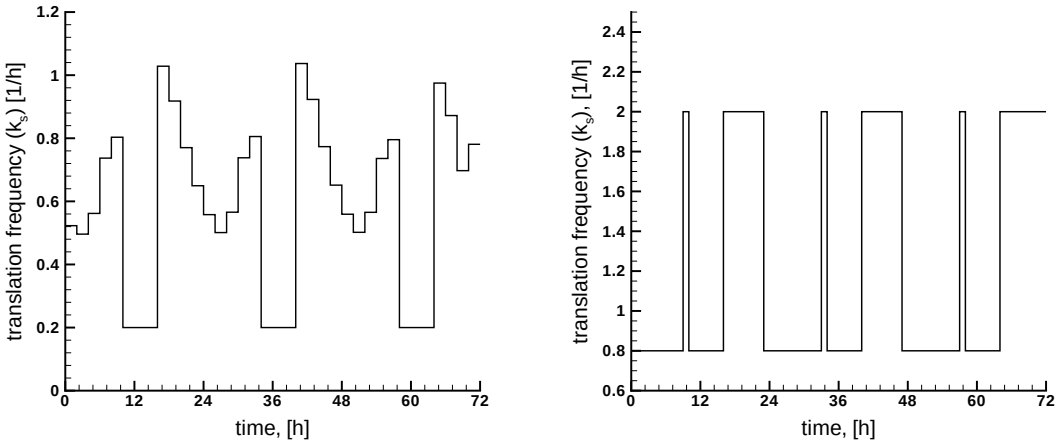

Figure 4.24: Optimal control inputs for the relaxed problem (*left*) and bang-bang control solution (*right*) for circadian rhythm restoration of mutant per^s in *Drosophila* by varying the translation frequency k_s as a function of time.

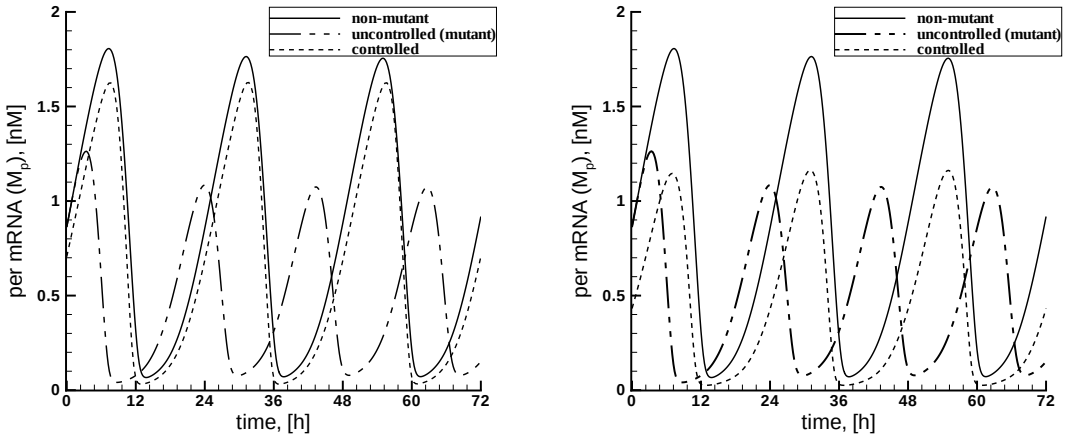

Figure 4.25: Restoration of per^s mutant rhythm by optimal relaxed solution (*left*) and bang-bang control solution (*right*) by varying the translation frequency k_s as a function of time. The plot shows the corresponding *per* mRNA as a function of time.

The rhythm can be tracked by suitable variation of the translation frequencies. The controller is able to restore a period of 24 hours, phase and amplitude of nominal oscillations very well for the short period mutant per^s and the corresponding state trajectory of per mRNA concentration is shown in Figure 4.25 (*left*). Starting with the relaxed solution we tried to calculate the bang-bang solution for the problem (4.6) for per^s case. But a bang-bang numerical solution within the control intervals of $k_s \in [0.2,1.2]$ cannot be achieved, which is evident from the structure of the relaxed solution of Figure 4.24(*left*). We modified the control intervals of $k_s \in [0.8,2.0]$ for obtaining a bang-bang numerical solution.

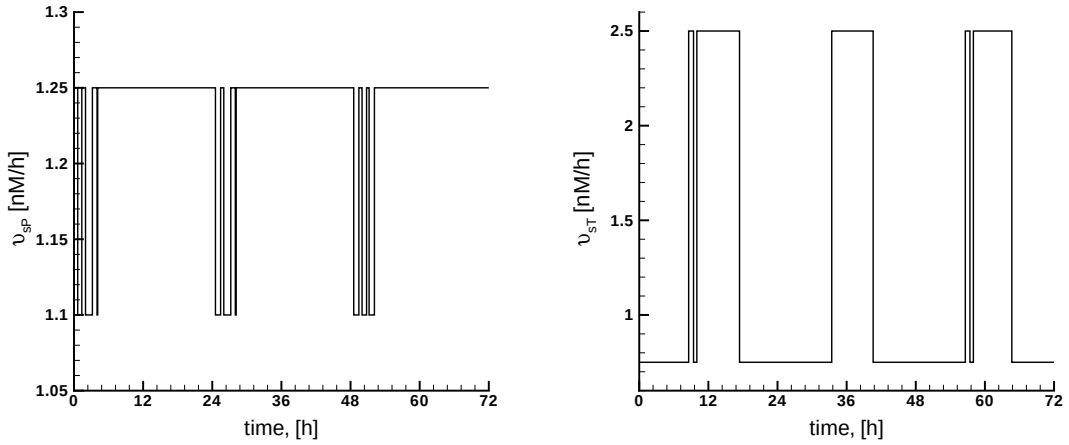

Figure 4.26: Optimal control inputs for the bang-bang problem of circadian rhythm restoration of mutant per^s in *Drosophila* by varying the transcription rates ν_{sP} and ν_{sT} as control parameters.

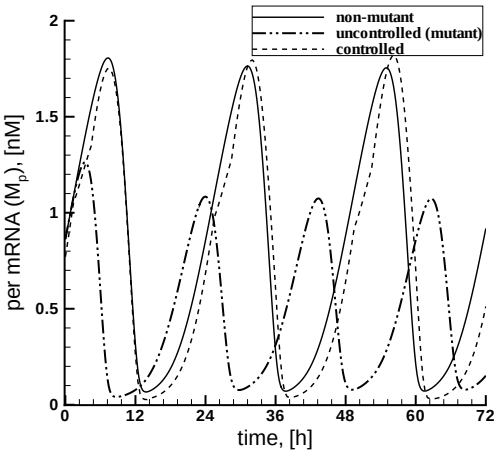

Figure 4.27: Restoration of *per*^{s} mutant rhythm with bang-bang control solution by varying the transcription rates (ν_{sP} and ν_{sT}) as a function of time. The plot shows the corresponding *per* mRNA concentration as a function of time.

The mixed integer control inputs k_s(t) for restoration of per^s mutant rhythm is shown in Figure 4.24 (*right*) and controlled per mRNA concentration as a function of time in Figure 4.25 (*right*). The controller is able to restore the period of oscillations to 24 hours but the amplitude of oscillations are not restored well within the control limits of $k_s \in [0.8,2.0]$. This might be due to the fact that one has to inhibit the translation rates in order to recover the amplitude and period of *per*^{s} mutant rhythm. But the choice of control intervals $k_s \in [0.8,2.0]$ for mixed-integer solution allows very little freedom for the controller to inhibit the translation rates from its nominal value of $k_s = 0.9$.

We also studied the control of transcription rates of *per* and *tim* mRNAs

in our control scenarios for restoration of per^s mutant rhythm. The mixed-integer solution of the optimal control problem Eq. (4.6) is shown in Figure 4.26 with transcription rates (ν_{sP} and ν_{sT}) as control parameters. By varying the transcription rates of *per* and *tim* we are able to achieve a better restoration results for per^s mutant rhythm when compared to using translation frequency as control parameter. The corresponding controlled state trajectory for *per* mRNA is shown in Figure 4.27.

4.9 Optimization based Feedback: Nonlinear Model Predictive Control

In this section, we present the NMPC real-time iteration scheme [74,76,91] for restoring the altered circadian rhythms online using circadian rhythms in *Drosophila* as a model system. We extend the concept of offline control approach presented in Section 4.8, to restore the characteristics of mutant rhythms at a given time points in real time by feedback tracking of such altered rhythms. The optimization problem is numerically solved by the *real-time iteration* scheme realized within the software package MUSCOD-II [80] as discussed in Section 3.5. NMPC real-time iteration scheme along with an EKF state estimation algorithm allows us to estimate the actual state values from noisy measurements of system states and parameters. The algorithm has been successfully applied for NMPC of a real pilot-plant distillation column modeled by a large scale DAE systems [161].

4.9.1 Control of circadian rhythms with NMPC

Mott *et al.* used model predictive control to shift the biological clock within a constrained environment (maintaining an astronaut's rhythm in space) by finding a set of optimal light pulses [162]. Their methods were applied to a modified *Van der Pol* oscillator with a free-running period of just over 24 hours. The *Van der Pol* system was transformed into a linear model through use of both a nonlinear state feedback compensation block and a nominal linear approximation. Bagheri *et al.* used model-specific data which was calculated a priori (i.e. through phase and transient response curves) and used in combination with a cost function to determine the next control move, simulating an iterative closed-loop look-up table problem [142]. Recent studies again by Bagheri *et al.* showed how to effectively reset the circadian rhythms in a model of mammalian circadian system using NMPC [141]. Laroche *et al.* used a flatness-based control method for controlling the PER protein oscillations in a five variable *Drosophila* model using translation frequency as control parameter [160]. Most of these methods are based either on linear approximation of the model or assume that there is no mismatch between the actual process and the model considered, which is clearly not the case in reality. In the present work here, we demonstrate exemplarily the application of an efficient nonlinear model predictive control (NMPC) algorithm for real-time optimal feedback control of altered circadian rhythms in a *Drosophila* model system in case of measurement noise and process-model mismatch.

Here we use translation frequency as the control parameter $u(t) = k_s$ as in case of open-loop control in Section 4.8, which is assumed to be piecewise constant on small intervals and can be controlled *online* by a drug delivery pump. By controlling the translation frequency rates via NMPC, we show numerically how one can restore the amplitude and period of mutant circadian rhythms back to the nonmutant rhythms online.

The objective functional here is the minimization of deviation of the mutant rhythm from that of the desired reference trajectory $x_r(t)$ (nonmutant wild-type rhythm). Here we choose the L^2-norm to quantify the deviation leading to the following Lagrange-type objective function:

$$\Phi = \int_{t_0}^{t_0+T} (\|x_i(t) - x_{ir}(t)\|_2^2 \ + \|k_s(t) - k_{\mathrm{sr}}(t)\|_2^2)\ dt \tag{4.7}$$

where $x_{ir}(t)$ is the desired reference trajectory corresponding to x_i to be induced by the control function k_s. We added an additional term $(\|k_s(t) - k_{\mathrm{sr}}(t)\|_2^2)$ to our objective functional in order to penalize the control moves with reference to a set point $k_{sr}(t)$. The least-squares form of this type of objective function can be exploited for an efficient solution of the optimization problem by using a *Gauss-Newton* approach of the constrained nonlinear optimization problem [74]. Due to low computational cost, the later approach is particularly useful for real-time optimization. At time t $= t_0$ the system is assumed to be in the initial state with the following structure,

$$\dot{x}(t) = \ f(x(t), k_s(t), p), \tag{4.8}$$

$$x(t_0) = \ \tilde{x}(t_0). \tag{4.9}$$

$$k_{\mathrm{s_{min}}} \leq k_{\mathrm{s}} \leq k_{\mathrm{s_{max}}} \tag{4.10}$$

where $\tilde{x}(t)$ denotes the current differential states that are either measured or estimated. Objective functional (4.7) has to be solved with respect to the constraints (4.8-4.10).

In biology the operating conditions for the model organisms varies from one experiment to other experiment and it is reasonable to include a feedback strategy for incorporating the model inefficiencies into an online optimal control algorithm. This could be done by real-time measurements of concentrations of mRNA and proteins involved in circadian system together with system estimation techniques. At every sampling time t, the concentrations of mRNA and proteins are measured and the actual values are updated accordingly in the optimization algorithm. We simulate numerically disturbances and uncertainties in measurements of actual system states by adding a Gaussian white noise at each sampling point, there by simulating the system under more realistic conditions.

Solving the NLP resulting from direct multiple-shooting reformulation of Eqs. 4.7-4.10 as in Section 3.5 with a current initial value $\tilde{x}(t_0)$ yields an optimal solution $u^*(t_0, \tilde{x}(t_0))$ on the horizon $[t_0, t_0 + T_p]$, where T_p is the prediction horizon (T_p =120 hour in the present case). In the closed-loop framework, however only a first of u^* with the length usually depending on the sampling time ($\delta = 1$ hour) is applied to the process. Based on the measurements at $t + \delta$, the concentrations of variables are estimated with the variant of EKF (as discussed in Section 3.5.2) and the new values of states and control moves are updated. Then the optimal control problem Eq. (4.7) is solved again with the new initial values obtained from the estimator. The time between the advent of a new $\tilde{x}$ and the response of the NMPC in form of a corresponding u^* creates a feedback delay which can be minimized by real-time iteration scheme with initial value embedding strategy as described in Section 3.5.1. The control horizon (T_c) and the prediction horizon (T_p) both have the same time length in our applications treated here. In general one can have a prediction horizon which is longer than the control horizon. In this case, the controls u for any time beyond the control horizon are fixed to the last value of the control horizon.

In the following sections, we present the results aiming at restoration and feedback tracking of a mutant rhythms in a *Drosophila* model to that of nonmutant rhythms. We present and discuss NMPC results for two scenarios: (1) Restoration of per^l mutant rhythm; (2) Restoration of per^s mutant rhythm. The NMPC schemes are simulated within a Matlab control environment that calls the DAE solver, DAESOL [59], to simulate the process for one sampling time and delivers the current states and parameters to the controller. The control environment is waiting for the results of the dynamic optimization performed by MUSCOD-II. It reads the available results from a communication file and gives the new controls to the DAE solver for the simulation of the next sampling period. This procedure is repeated for each sampling interval until the end of simulation time is reached.

4.9.2 Restoration of altered per^l mutant rhythm by NMPC

We assume the translation frequency of PER/TIM proteins are equal in this case as well(i.e. $k_{sP} = k_{sT} = k_s$) for restoring the circadian periodicity and amplitude of the per^l mutant rhythms. An approximate choice of bounds for control values (k_s) are taken from offline solution of per^l mutant rhythm restoration from Section 4.8.1. In order to recover the high amplitude long period oscillations, translation frequency (k_s) of PER/TIM proteins has to be activated from its nominal value of k_s=0.9. So, we set the control set point $k_{sr}(t) = 1h^{-1}$ which is higher than the nominal k_s value for nonmutant rhythm.

We assume that the measurements of two differential variables x_1, x_{10} are available at each sampling instant with a sampling time of 1 hour. We have implemented a variant of an EKF in order to estimate the differential states x from these two measurements x_1, x_{10}. We added a normally distributed random perturbation

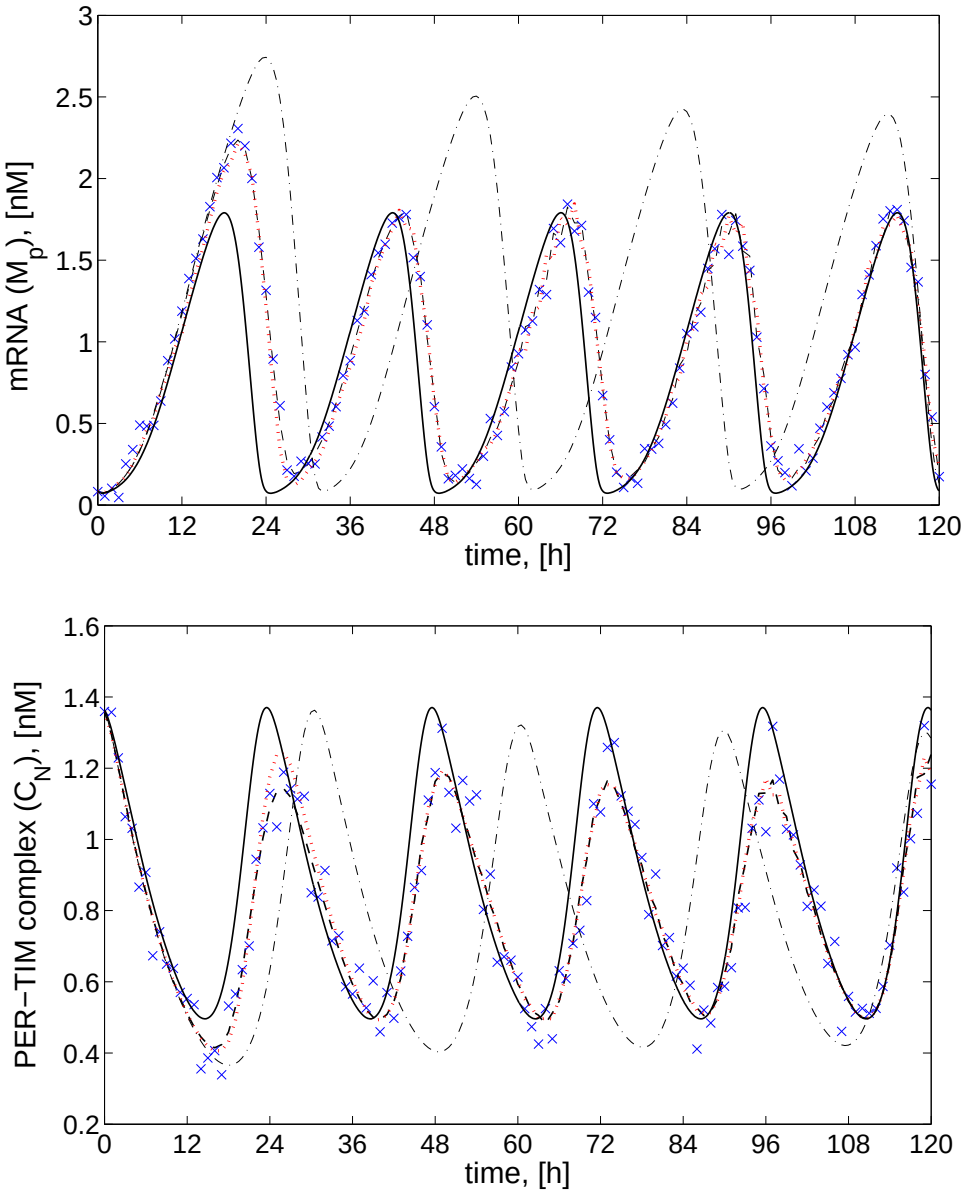

Figure 4.28: Rhythm restoration of mutant *Drosophila* per^l by nonlinear model predictive control. The (*top*) plot shows the per mRNA (M_p) concentration and (*bottom*) plot shows PER-TIM complex (C_N) protein concentration as a function of time. Solid line: Reference trajectory of a nonmutant rhythm. Dash-dot line: Long period mutant rhythm with a period of about 29 hrs. Small $\times$-symbols: System states after Gaussian perturbations of the actual predicted states. Dotted line: Model-based numerical prediction of the states for the controlled model system. Dashed line: Controlled mutant rhythm with NMPC.

(Gaussian white noise) of 1% mean and 4% variance to the numerically simulated concentration values of x_1, x_{10} on each sampling interval in this application. It is important that the process model assumed is perfect, i.e. there is no process-model mismatch. However, this assumption is clearly not satisfied in most cases as the parameters in modeling of biological systems are not quantitative enough. A remedy is to additionally estimate a sufficient number of model parameters along with the

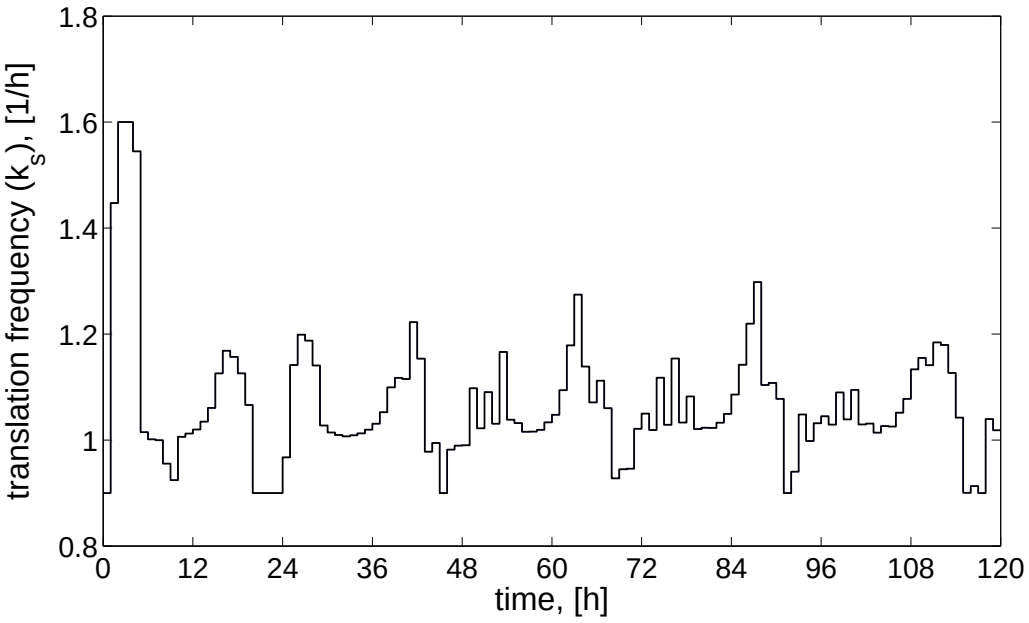

Figure 4.29: Optimal control inputs for circadian rhythm restoration of mutant per^l by NMPC in *Drosophila* model system by varying the translation frequency k_s of PER/TIM proteins as a function of time.

system states or use EKF formulation including process noise. Here, we incorporate such process noise in our system for parameters ν_{dP}, ν_{dT} and ν_{sP} with Gaussian white noise of zero mean and 3% variance of actual values of model parameters. This process noise along with measurement noise is updated to the EKF estimation algorithm at each sampling interval of 1 hour.

The control and EKF state estimation results are summarized in Figure 4.28. The numerical NMPC scheme needs a relatively constant computation time of less than one sec for delivering the feedback control. It compares the measured (Small $\times$-symbols), estimated (dotted line) and true states (dashed line) of *per* mRNA and nuclear PER-TIM protein complex (C_N) under controlled conditions. Despite the noise levels in measurements and process, the NMPC scheme tracks the concentrations of *per* mRNA and nuclear PER-TIM protein complex very well, which demonstrate good filtering properties of the EKF algorithm. In Figure 4.28, it also depicts reference trajectory nonmutant rhythm ("wild-type") (*solid line*) and the mutant uncontrolled rhythm (*dash-dot line*), so that one can view how much we steered the system from its original behavior. To visualize the results in state space, we plotted *per* mRNA vs PER-TIM complex (C_N) in Figure 4.30. The NMPC controller is able to react very well to the process and measurements noise, and follows a desired limit cycle closely. The necessary piecewise constant change in translation frequency of PER/TIM proteins for restoration altered long period mutant rhythm is shown in Figure 4.29. By activation of translation rates of protein PER and TIM from its nominal value of $k_s = 0.9$, one can decrease the period of oscillations and

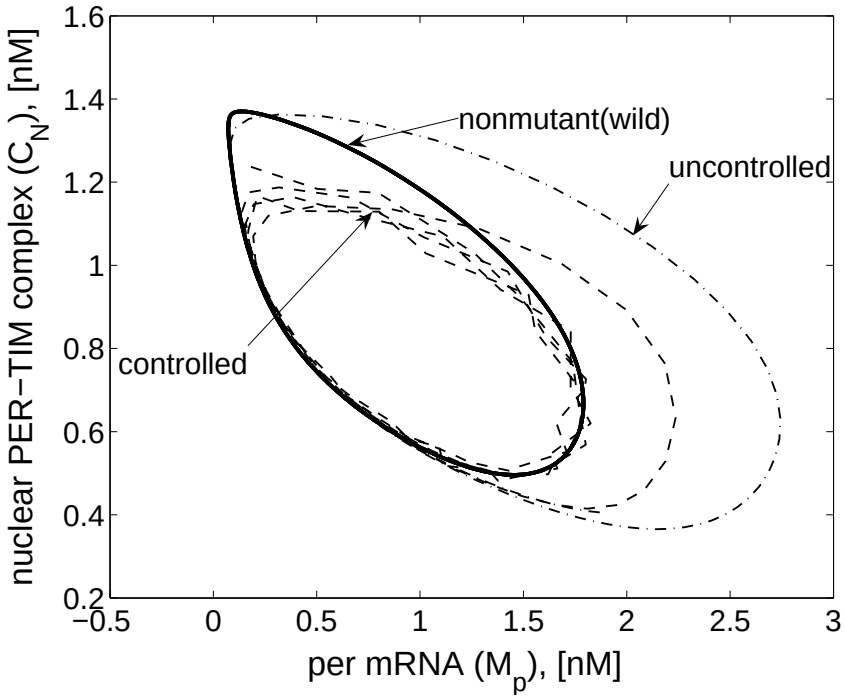

Figure 4.30: The corresponding limit cycles for the per^l mutant restoration in a phase space projection of *per* mRNA and nuclear PER-TIM protein complex. Solid line: Reference trajectory of a nonmutant rhythm. Dash-dot line: Long period mutant rhythm with a period of about 29 hrs. Dashed line: Controlled limit cycle oscillations under measurement and process noise.

restore the circadian characteristics like amplitude and phase very well within the control limits of $k_s \in [0.8,1.6]$ for per^l mutant rhythm.

4.9.3 Restoration of altered per^s mutant rhythm by NMPC

In order to recover the period and amplitude of per^s mutant rhythms, one need to inhibit the translation rates of PER/TIM proteins. We fix the control set point k_{sr}(t) at 0.44, where the system actually recovers the circadian period in per^s mutant rhythm. We assume that the measurements of the two differential variables x_1, x_{10} are available at every sampling interval in this case as well. All measurements are perturbed with Gaussian white noise of 1% mean and 4% variance to the numerically simulated concentration variables x_1, x_{10} and with zero mean 3% variance for the parameters ν_{dP}, ν_{dT} and ν_{sP} on each sampling interval.

The results in case of per^s restoration are summarized in Figure 4.31. It compares the measured (Small $\times$-symbols), estimated (dotted line) and true states (dashed line) along with reference trajectory of nonmutant rhythm (solid line) and per^s mutant rhythm (dash-dot line) of *per* mRNA and nuclear PER-TIM protein complex (C_N) under controlled conditions. Like in previous case for restoration of per^l mutant rhythm, the NMPC algorithm here for per^s mutant rhythm reacts well to the process and measurement noise and tracks the concentrations of mRNA and

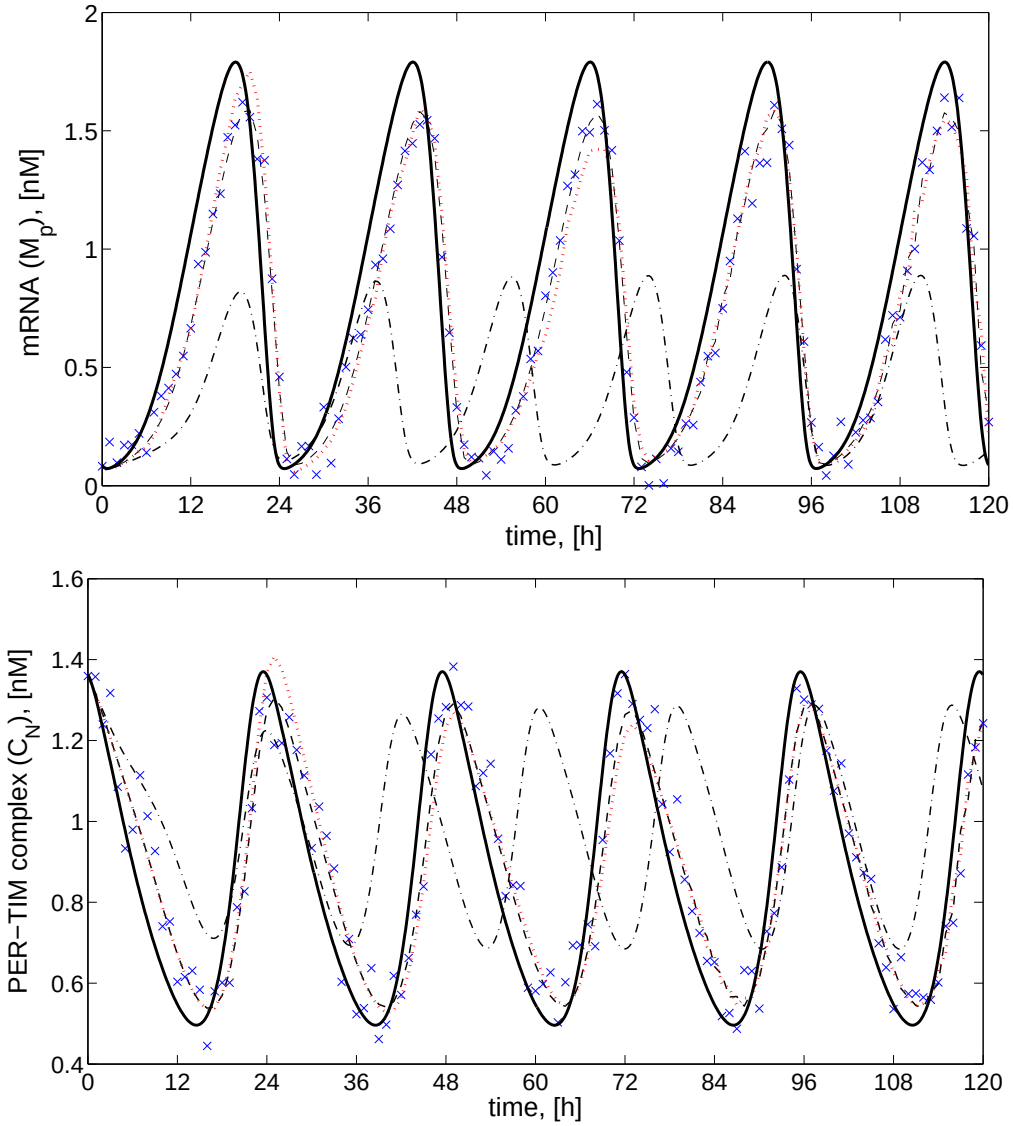

Figure 4.31: Rhythm restoration of mutant *Drosophila* per^s by nonlinear model predictive control. The (*top*) plot shows the per mRNA (M_p) concentration and (*bottom*) plot shows PER-TIM complex (C_N) protein concentration as a function of time. Solid line: reference trajectory of a nonmutant rhythm. Dash-dot line: Short period mutant rhythm with a period of about 19 hrs. Small $\times$-symbols: System states after Gaussian perturbations of the actual predicted states. Dotted line: Model-based numerical prediction of the states for the controlled model system. Dashed line: Controlled mutant rhythm with NMPC.

proteins very well with in control limits $k_s \in [0.4, 0.6]$. In Figure 4.33, it depicts the results of per^s mutant rhythm restoration in state space of *per* mRNA vs PER-TIM complex (C_N). The controller is able to react well to the noise levels and follows a desired limit cycle closely. The necessary piecewise constant changes in translation frequency of PER/TIM proteins for restoration of altered per^s mutant rhythm with noise levels is shown in Figure 4.32. By inhibiting the translation rates from its nominal value of (k_s=0.9), one can increase the oscillation period in per^s mutant case and restore its circadian characteristics like amplitude and phase.

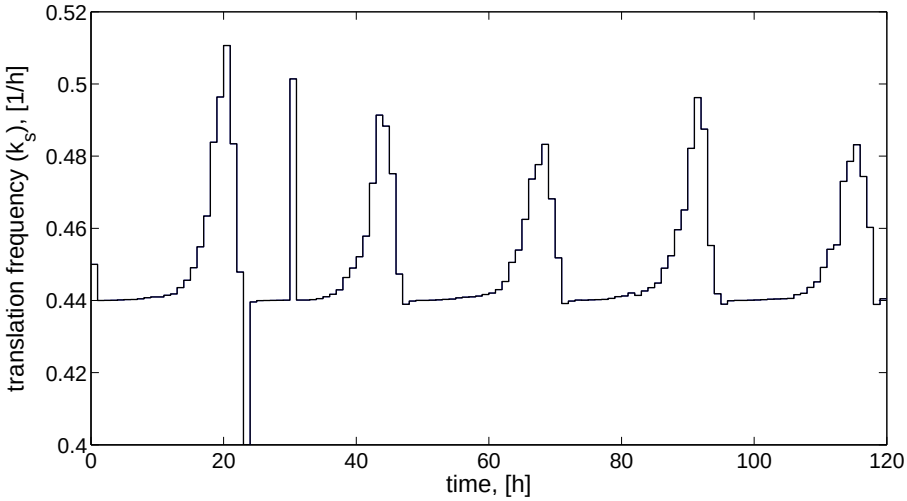

Figure 4.32: Optimal control inputs for circadian rhythm restoration of mutant per^s calculated by NMPC in *Drosophila* model system by varying the translation frequency k_s of PER/TIM proteins as a function of time.

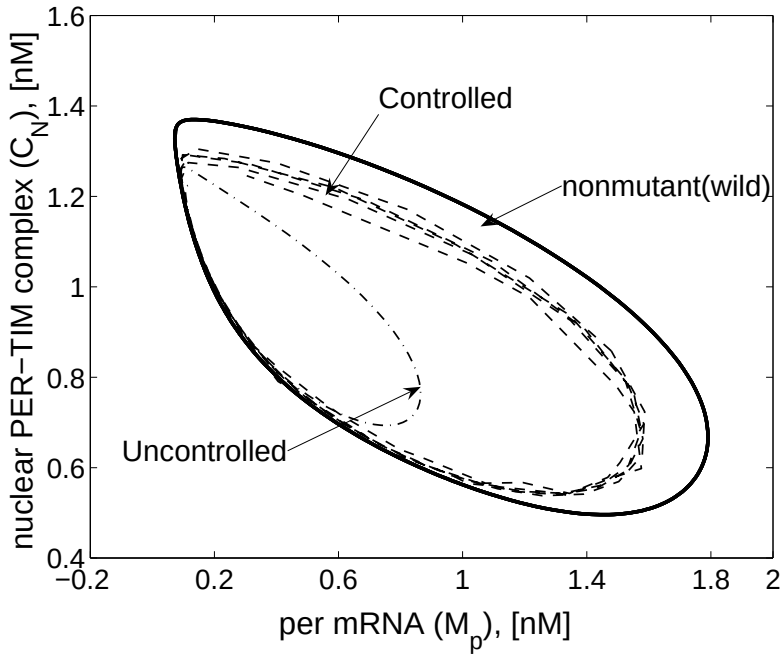

Figure 4.33: The corresponding limit cycles for the per^s mutant restoration in a phase space projection of *per* mRNA and nuclear PER-TIM protein complex. Solid line: Reference trajectory of a nonmutant rhythm. Dash-dot line: Short period mutant rhythm with a period of about 19 hrs. Dashed line: Controlled limit cycle oscillations under measurement and process noise.

NMPC controller allows restoration of approximate level of mRNA and protein concentrations in case of both *per*^{l} and *per*^{s} mutant rhythms under measurement and process noise in the present study.

Chapter 5

Circadian Cycle and Cell Cycle

Circadian cycle and the cell cycles are two global regulatory systems that have pervasive effects on organismal and cellular physiology. It has been quite clear for many years that there is an interaction between the cell division and the circadian cycles [45, 163, 164, 165]. Disruption of the circadian rhythm may cause defects in regulation of cell proliferation. Model studies addressing the mechanisms through which the circadian clock regulates the cell cycle might help Chronotherapy. Chronotherapy takes into account the biological time to improve cancer treatments caused by the malfunction of the cell cycle, by optimizing the chronomodulation of drugs into the system. A detailed molecular level model between the circadian cycle and the cell cycle might help to understand the timing of the cell cycle events. In this chapter, we try to model the coupled mammalian circadian cycle with cell cycle at molecular level linking via WEE1 kinase. We briefly describe different phases of the cell cycle and the mathematical models of cell cycle and circadian cycle considered here with some experimental evidences of links between these two cycles.

5.1 Cell Cycle

Cell cycle is the period of time that is needed for a cell to double its genetic content and distribute it to its two daughter cells. In most cells, this time is coupled to the duplication of other cell contents and cells can divide only after doubling their size [166]. A typical cell goes through a precise DNA replication and mitosis (doubling and distributing genetic information) while its ribosome number and cell mass approximately doubles. Duplication of cell mass is usually the slower process, which creates special phases into the cell cycle. Between S-phase (DNA replication) and M-phase (mitosis) growing, genetically resting phases G1 and G2 are incorporated. So the typical somatic eukaryotic cell cycle is ordered in G1, S, G2 and M-phases. Special checkpoints of the cell cycle coordinate cell growth with the DNA cycle, the cells have to reach a critical size to start S-phase and have to complete DNA replication and might need to reach another critical size to initiate mitosis. Before subsequent S-phase, the proper finish of M-phase is also checked. In homeostasis, cell growth and the DNA cycle, balance each other with the help of extended G1 and G2 phases, hence individual cell cycle times in a population of cells will be equal to the mass doubling time (MDT) of the population. Molecular mechanisms

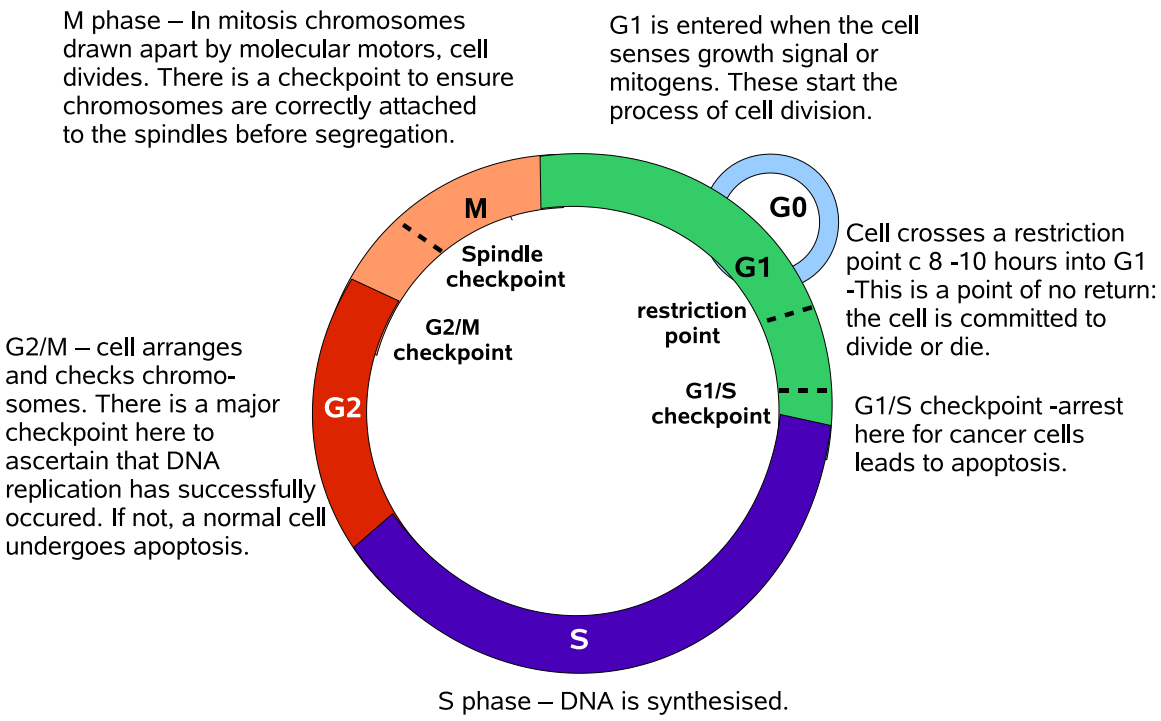

Figure 5.1: The phases of the cell cycle

that ensure the correct progression of the cell cycle have been described. Interlocked feedback loops constitute an essential pre-requisite for the regulation of molecular components of the cell cycle machinery [167, 168]. As a result of this tight regulation, defects in cell cycle check-points may be responsible for an uncontrolled and continuous proliferation leading to cancer development [169].

5.1.1 A Computational model for the cell cycle

The molecular controls of cell division are fundamentally similar in all eukaryotes [171]. Major events of the eukaryotic cell cycle are choreographed by periodic activation of several cyclin-dependent kinases (Cdks) and the enzymes and inhibitors that effect their activities. Unlike unicellular organisms, like yeast, the cells of multicellular organisms proliferate only when permitted by specific growth factors (GFs). If GFs are deprived, cells early in G1-phase leave the cycle and enter a resting state (G0); older cells finish the ongoing cycle and enter the resting state after mitosis. The point in G1, before which cells enter directly into the resting state is called the *restriction point* [172].

Here we use the model proposed by Novák and Tyson on restriction point control of mammalian cell cycle [170]. A schematic wiring diagram of the cell cycle model is shown in Figure 5.2. For a detailed description of the reaction mechanisms and different processes involved, we refer to the Novák and Tyson article [170]. The

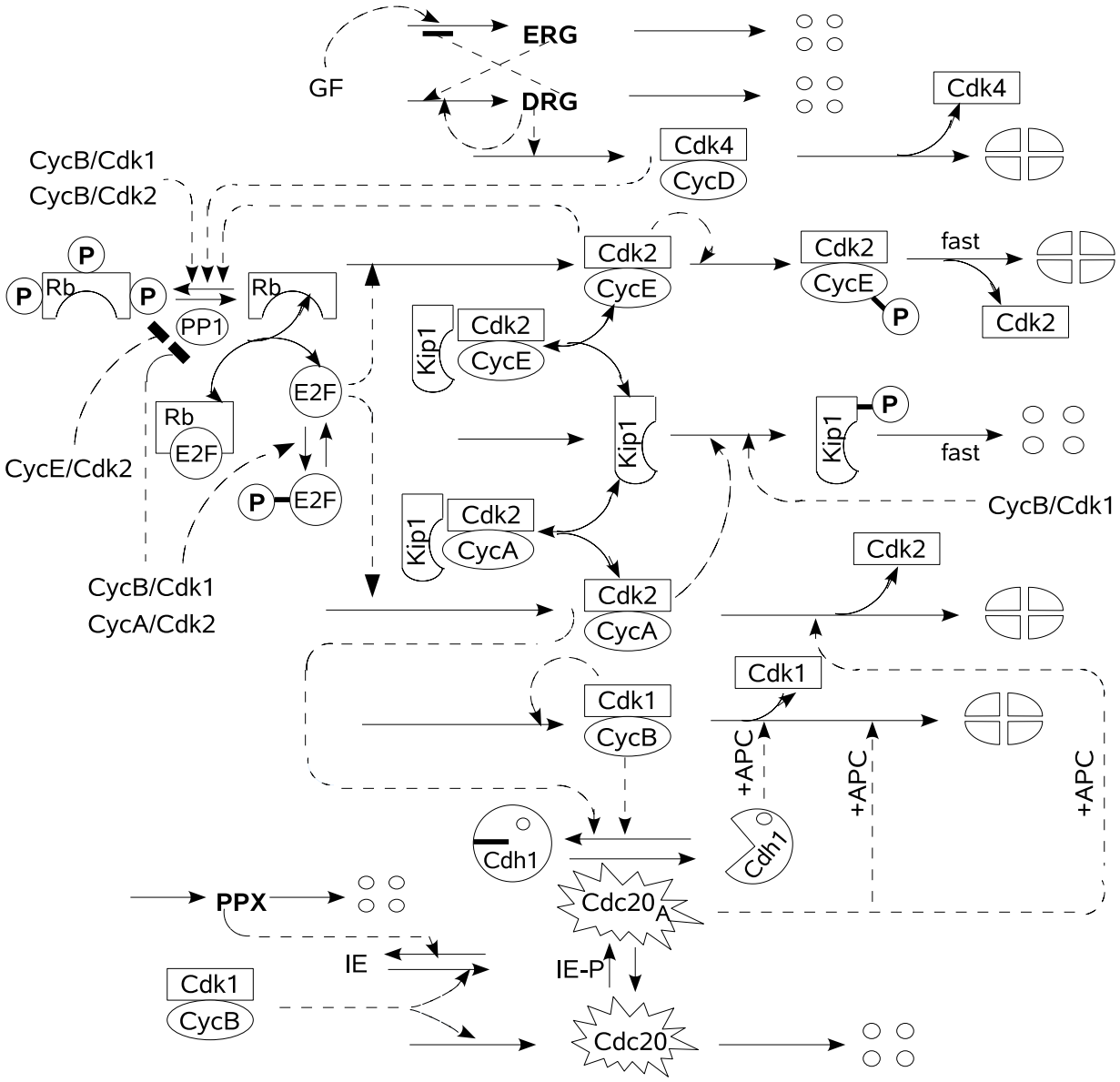

Figure 5.2: Schematic diagram of molecular network regulating the progression of mammalian cells through the cell cycle (The figure is redrawn following the Ref. [170]).

model consists of a set of nonlinear differential equations (Eq. A.2-A.27) based on realistic molecular events underlying progression through different phases of cell cycle. In this part of the thesis, we will be concentrating more on coupling aspects of this cell cycle model with circadian cycle through WEE1 in G2-M phase.

Figure 5.3 and 5.4 show numerically simulated cell cycles of normal mammalian cells, growing exponentially in the presence of GFs, based on the differential equations (A.2-A.27). The parameter values are tabulated in Table A.1 and dimensionless constants in Table A.2.

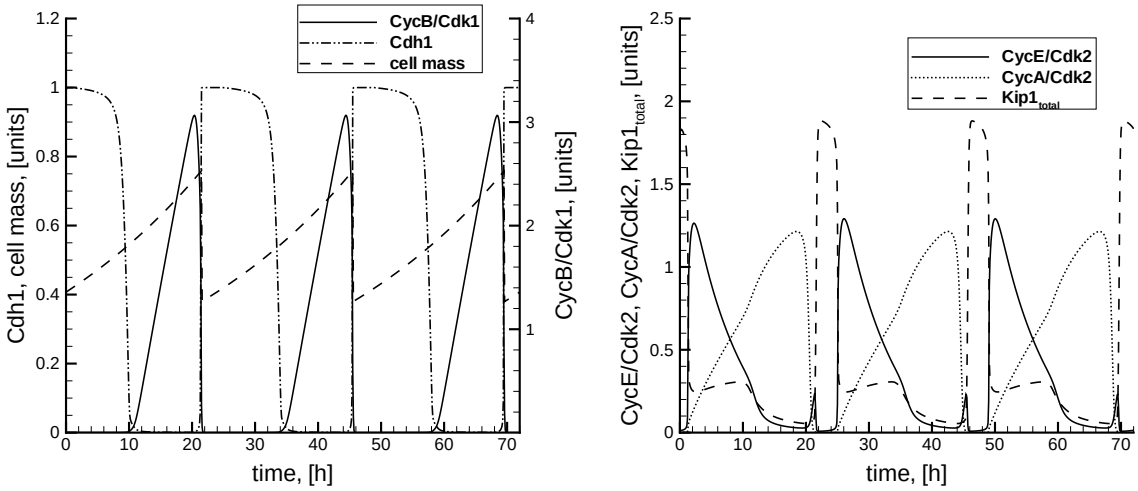

Figure 5.3: Numerical simulations of the mammalian cell cycle. Three full cycles are shown. Cells are accumulating cytoplasmic mass exponentially (*left*: dashed line) and dividing when Cdc20 and Cdh1 are activated at the end of the cycle. The curves in the (*right*) panels represent the cellular concentration of different cell-cycle regulators, total Kip1 level(free and in complex with cyclins A, D and E), and the active forms of CycA and CycE associated kinase (not in complex with Kip1). (Results are reproduced following [170])

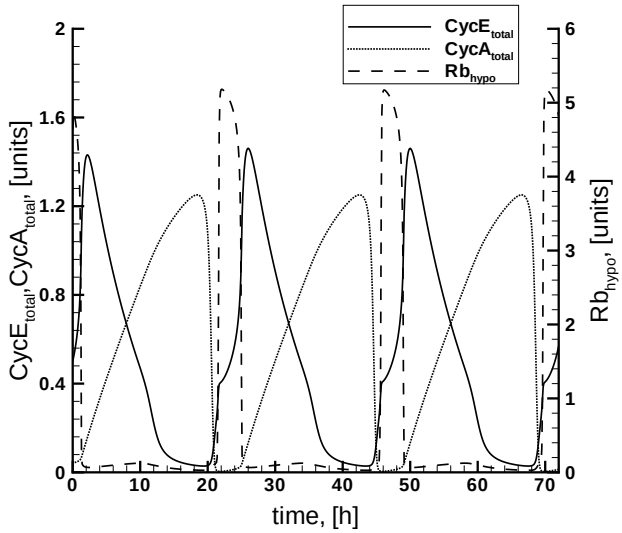

Figure 5.4: Numerical simulations of the mammalian cell cycle. The curves in the plot represent the cellular concentration of different cell-cycle regulators. Total CycA and CycE levels (dimers with Cdk2 and trimers with Cdk2 and Kip1) and the hypophosphorylated form of Rb.

5.2 A Computational model for the mammalian circadian clock

Overview of how the mammalian molecular clock works is described in Section 4.2.2. A family of closely related models can be built based on the mechanisms described in Figure 4.4. Here, we focus on one particular model proposed by Leloup and

Goldbeter [34] which is schematized in Figure 5.5 . The model for circadian oscillations in mammals involves interlocked negative and positive regulations of *Per*, *Cry*, *Bmal*1 genes by their protein products. For a detailed description of molecular processes involved in the considered model, we refer to the original article (see Ref. [34]).

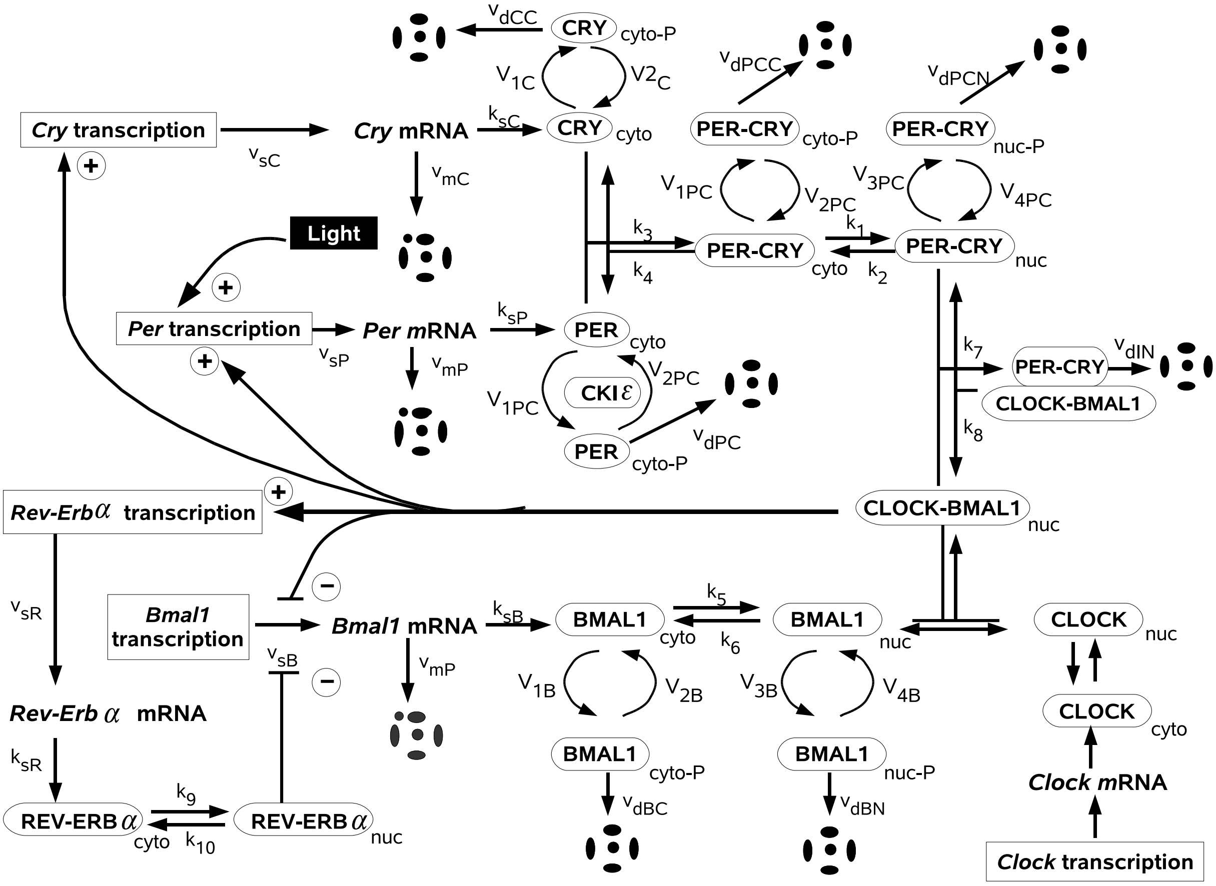

Figure 5.5: Model for circadian oscillations in mammals involving interlocked negative and positive regulations of *Per*, *Cry*, *Bmal*1 genes by their protein products. *Per*, *Cry*, and *Bmal*1 mRNAs are synthesized in the nucleus and transferred into the cytosol. There they are degraded and translated into the PER, CRY, and BMAL1 proteins, which undergo reversible phosphorylation that leads to their degradation. The complex formed by the cytosolic unphosphorylated forms of PER and CRY, and the cytosolic BMAL1 protein are reversibly transported into the nucleus. It assumes that once in the nucleus, unphosphorylated BMAL1 immediately forms a complex with CLOCK. Nuclear BMAL1 activates *Per* and *Cry* transcription and inhibits Bmal1 transcription. These regulations are counteracted by the reversible formation of an inactive complex between the nuclear, unphosphorylated PER-CRY and CLOCK-BMAL1 complexes. The effect of light is to increase the rate of expression of the *Per* gene. (The figure is redrawn following the Ref. [34])

Figure 5.6 numerically simulates circadian oscillations based on the differential equations (Eqs. B.1- B.16) and parameter values in Table B.1. The model accounts for the occurrence of sustained oscillations, in the conditions corresponding to continuous darkness. This is achieved by keeping the ν_{sP} value at a constant low level of $1.5nMh^{-1}$. In agreement with experiments, the model predicts an antiphase rela-

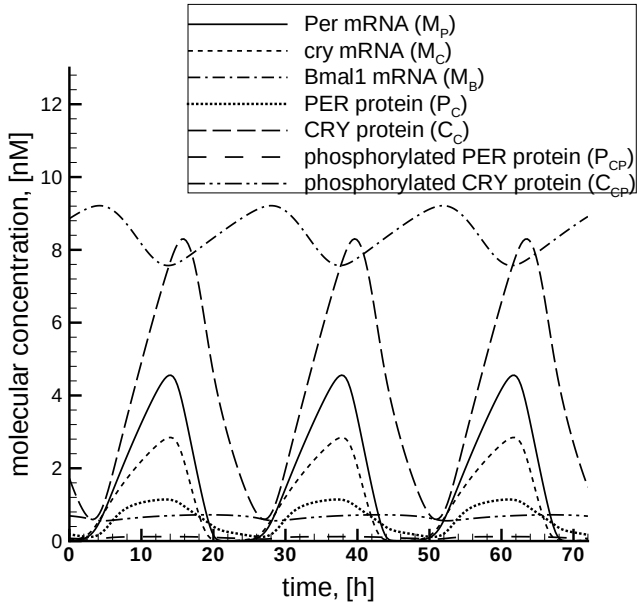

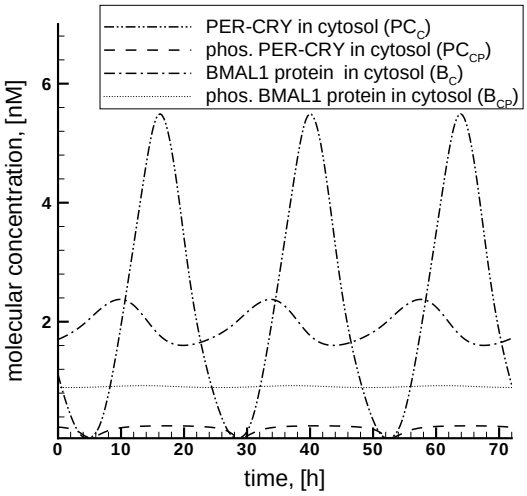

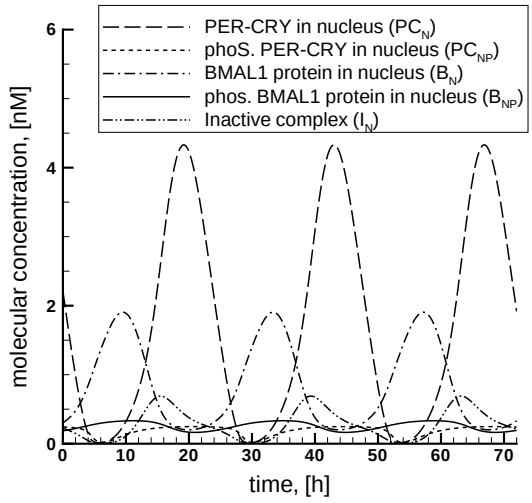

Figure 5.6: Circadian oscillations in continuous darkness. Time evolution of mRNAs, phosphorylated and non-phosphorylated proteins in cytosol and nucleus are shown in the figures. *Per*, *Cry* and *Bmal1*, phosphorylated and non-phosphorylated proteins PER and CRY in the cytosol are shown in the (*side*) figure. Plot in the bottom (*left*) panel shows the phosphorylated and non-phosphorylated form of PER-CRY complex and BMAL1 protein in cytosol. Plot in the bottom (*right*) panel shows the phosphorylated and non-phosphorylated form of PER-CRY complex and BMAL1 protein along with inactive complex in nucleus respectively. The curves are obtained by the numerical integration of Eqs. (B.1-B.16) for the parameters listed in Table B.1

tionship between the oscillations of *Per* and *Cry* mRNAs on one hand, and *Bmal*1 mRNA on the other. When incorporating the light-induced gene expression of the *Per* gene, the model accounts for entrainment of the oscillations by the light-dark cycles.

5.3 Coupling the circadian cycle and the cell cycle

The circadian cycle and the cell cycle are regulated by common factors like metabolites, hormones, or nutrients, that affect food intake [173] (see Figure 5.7). For example, glucose is able to reset peripheral clocks and regulate genes involved directly

in cell cycle progression [174]. Melatonin is a chronobiotic regulator that relays the circadian rhythm to the peripheral organs for physiological regulations [175]. While

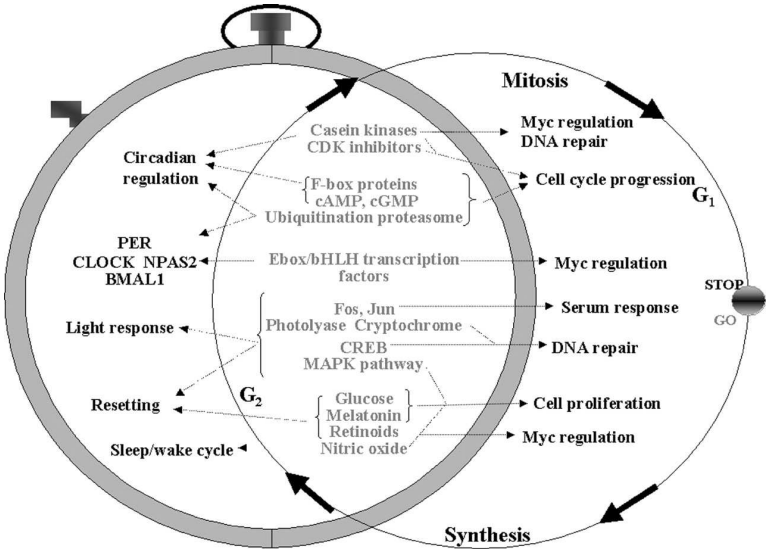

Figure 5.7: Common elements shared by biological clocks and cell cycle. (The figure is taken from the Ref. [95]

these two regulatory systems involve distinct mechanisms, there is some evidence that these cycles are linked. Most mammalian diploid cells exhibit an approximately 24-hour cell cycle period, and the circadian clock has been implicated in regulation of the phases of cell division [176]. For example, in humans, the major peak of *per1* expression coincides with the G1 phase, whereas the peak of *bmal1* expression coincides with M-phase [177, 178]. Of special interest was the demonstration that the cell proliferation and apoptosis in rapidly renewing tissues are circadianly synchronized [176, 179]. It has been observed that phase shifting of mice leads to a corresponding shift in the timing of the cell cycle events in both gut and bone marrow [180]. Such phase shifting is associated with a shift in the circadian expression of *per1* in the rat SCN and in peripheral tissues [102].

Matsuo *et al.* [45] measured the expression of proteins involved in the cell cycle mechanism at different hours of the day in regenerating liver cells, especially the WEE1 kinase and its target, the cyclin-dependent kinase *cdc2*. According to them, mutations of circadian genes have a direct impact on *wee1* mRNA and protein patterns (e.g. a *cry* deficient mutant exhibits high levels of *wee1* mRNA throughout regeneration) suggesting that WEE1 is regulated by some components of the circadian cycle. The change in CDC2 activity might be a consequence of the change in WEE1 [181]. The *wee1* gene promoter is believed to be activated by the complex CLOCK/BMAL1 and inhibited by CRY. The WEE1 kinase seems to be a good candidate to establish a link between the cell and circadian cycles during the G2-M transition (see Section 5.3.1). Other links are also reported in literature by which circadian rhythms influence the cell cycle, for example, PER2 regulates the

transcription of *c-myc*, and in a moderate way that of *mdm2* [165], links through *tim* (timeless) are also hypothesized [163, 164]. However, the precise mechanisms involved are still not completely clear and require a very detailed description of the cell cycle and circadian cycle that distinguishes between PER1, PER2 and PER3, etc. All of these data thus suggest the existence of complex indirect influences of circadian rhythms on the mechanisms controlling cell proliferation. In this work, we restrict our study to the link established through WEE1, which will allow us to rely on a simpler and more generic models of the cell cycle and circadian cycle.

5.3.1 Linking the cell cycle and the circadian cycle via WEE1 kinase

Many models have been developed to describe both of these cycles, but only a few have described a real interaction between them [181, 182]. In the coupled circadian cycle and cell cycle model proposed by Calzone *et al.* [181], the focus is on a single phase of the cell cycle i.e. the G2-M transition. The model proposed by Zámborszky *et al.* [182] is based on full cell cycle model but the circadian model they considered doesnot distinguish between different genes and proteins. Here, we try to couple the two numerical models presented in the previous sections, one for the circadian cycle in Section 5.2 and other for the generic cell cycle model in Section 5.1.1. We will try to establish a relation at molecular level through WEE1 kinase. In a way, the present model is an extension to the model proposed by Zámborszky *et al.* [182] with detailed molecular level model for the circadian clock.

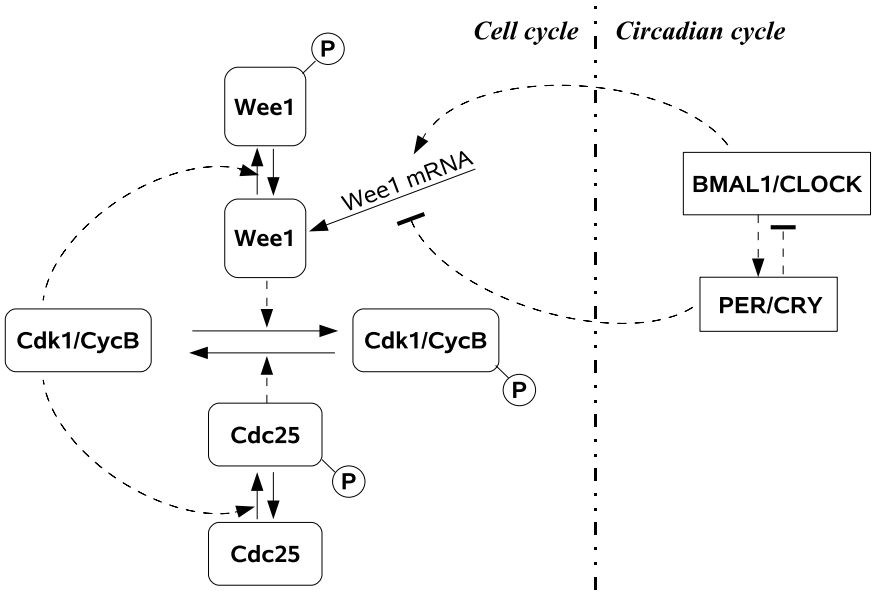

Figure 5.8: Linking the circadian and the cell cycles via WEE1.

The two models are linked through the transcription of WEE1. In addition to the equations of both models (Eq. A.2-A.27) and (Eq. B.1-B.16) a set of equations for WEE1, WEE1P protein, phosphorylated form of Cdk1/CycB and CDC25 are

added. We didn't consider the equation for *wee*1 mRNA as in case of cell cycle model under the assumption of rapid message turnover [170], such that mRNAs in cell cycle are always in steady state. The proteins chosen to illustrate in coupling these two models are shown in Figure 5.8.

$$\begin{aligned}\frac{d[Wee1]}{dt} &= (kw5' + kw5''[B_N]) - kw6[Wee1] + \frac{kw1[Wee1p]}{(Jw1 + [Wee1p])} \\ &\quad - \frac{((kw2' + kw2''[CycB])[Wee1])}{Jw2 + [Wee1]} \qquad (5.1)\\ \frac{d[Wee1P]}{dt} &= \frac{(kw2' + kw2''[CycB])[Wee1]}{Jw2 + [Wee1]} \\ &\quad - \frac{kw1[Wee1P]}{Jw1 + [Wee1P]} - kwd[Wee1P] \qquad (5.2)\end{aligned}$$

$$\begin{aligned}\frac{d[cycBP]}{dt} &= (kwee1' + kwee1''[Wee1])[cycB] - V_2[CycBP] \\ &\quad -(kcdc25' + kcdc25''[Cdc25a])[cycBP] \qquad (5.3)\\ \frac{d[Cdc25a]}{dt} &= \frac{(kc3' + kc3''[CycB])(1 - [Cdc25a])}{Jc3 + 1 - [Cdc25a]} - \frac{kc4[Cdc25a]}{Jc4 + [Cdc25a]} \qquad (5.4)\end{aligned}$$

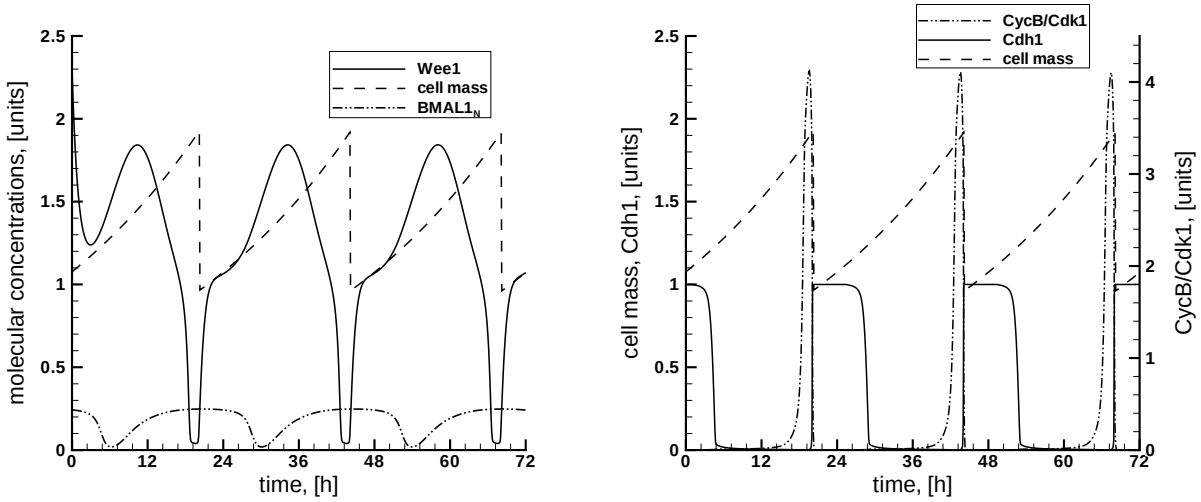

Figure 5.9: Numerical simulation of coupled circadian cell cycle model. Plots shows the variation of WEE1 concentration along with cell mass and circadian BMAL1$_N$ concentration (*left*). Cells accumulate cytoplasmic mass exponentially and divide when Cdh1 crosses 0.2 from below (*right*: dashed line).

Early in the cycle, Cdk1/CycB is kept inactive because the cyclin is not synthesized and WEE1 is present. As the cyclin is slowly synthesized, Cdk1/CycB activates and reaches a threshold that both inactivate WEE1 and activate CDC25 which maintains Cdk1/CycB in its active state [181]. The model is composed of two positive feedback loops (CDC25 activates Cdk1/CycB which in turn activates CDC25,

and WEE1 inactivates Cdk1/CycB which in turn inactivates WEE1). The production of WEE1 is a function of the nuclear form of the complex BMAL1/CLOCK (B_N) and the unphosphorylated nuclear form of the complex PER/CRY(P_{CN}). The negative effect of PER/CRY(P_{CN}) does not need to appear in the equation as it already has an influence on the activity of BMAL1/CLOCK (B_N). The degradation of proteins are considered to be linear for WEE1, WEE1P. The parameter values for the coupled circadian cell cycle model are chosen from the Refs. [181,182,34,170].

Figure 5.9 shows the numerical simulation results in case of coupled circadian cell cycle model. For the selected values of parameters the model has mass doubling time = circadian oscillation time period of 24 hour revealing an entrainment of the cell cycle through WEE1 activity. As observed in experiments [183] after the DNA replication is complete, the G2 cells must await a circadian time window when the WEE1 protein is expressed at low levels before they can enter the mitosis. When expressed at higher cellular concentrations, WEE1 inactivate the Cdk1/CycB complex there by preventing the transition from G2 to M. BMAL1/CLOCK (B_N) and Cdk1/CycB show a stable limit cycle behavior but with antiphasic behavior.

Chapter 6

Belousov-Zhabotinksy (BZ) reaction

Introduction

Oscillating chemical reactions are among the most important examples for the presence of nonlinear dynamic laws in chemical systems [184]. The famous Belousov-Zhabotinsky (BZ) reaction [185] is a thoroughly investigated model system for many kinds of complex dynamical behavior ranging from simple oscillations to chaotic behavior in continuously stirred tank reactor (CSTR) and to spatiotemporal pattern like propagating waves in un-stirred media [40]. The BZ systems is often referred to as a chemical prototype for complex self-organizing dynamics in biological systems which are seldom directly accessible to direct experimental investigation and manipulation. In this chapter we present the numerical results for target-oriented manipulation of self-organized dynamics in BZ reaction. Firstly, we developed a novel detailed model for BZ reaction based on elementary reaction mechanism and applied nonlinear control techniques aiming at, stabilizing unstable steady states and induction of specific oscillatory behavior characterized by amplitude, frequency and mean value of the oscillating species. Control results of the newly developed model are compared with a simple 3-variable Oregonator model available in literature for BZ reaction.

The BZ reaction system typically consists of malonic acid or a similar organic compound which is oxidized by an acidified bromate solution in the presence of a metal ion catalyst. $Ru(bpy)_3^{2+}$ as a catalyst [43] plays an important role in the investigation of self-organizing dynamics in the presence of light [44] as an external control parameter. This ruthenium-catalyzed system has become increasingly important during the last years, particularly in studies related to external control of the system dynamics by modifying the medium's excitability through adjusting the illumination intensity [24]. Detailed kinetic models are required for quantitative numerical simulation of experimental results and an in-depth understanding of the underlying mechanism.

6.1 Construction of a detailed photo-BZ model

Several mechanisms have been proposed to account for the light sensitivity of the $Ru(bpy)_3^{2+}$-catalyzed BZ reaction [186, 187, 188]. These consist of number of el-

ementary reaction steps for most of which kinetic parameters are available from experimental data. The primary photochemical process is absorption of visible light by the $Ru(bpy)_3^{2+}$ complex [189]. The excited state of the complex $Ru(bpy)_3^{2+*}$, is an extremely strong reducing agent, for the inorganic part of the BZ reaction the main effect of the light is the production of $BrO_2^{\cdot}$ via (R1)-(R3) [190].

$$\begin{aligned} &Ru(II)+h\nu \rightarrow Ru(II)^* && \nu && (R1)\\ &Ru(II)^* \rightarrow Ru(II) && k_2 && (R2)\\ &Ru(II)^*+BrO_3^-+2H^+ \rightarrow Ru(III)+BrO_2^{\cdot}+H_2O && k_3 && (R3) \end{aligned}$$

which is coupled to the auto catalytic cycle

$$\begin{aligned} &Ru(II)+ BrO_2^{\cdot}+H^+ \rightarrow Ru(III)+HBrO_2 && (R4)\\ &BrO_3^-+HBrO_2 +H^+ \rightarrow 2BrO_2^{\cdot}+H_2O && (R5) \end{aligned}$$

A complete list of the reactions for the photosensitive BZ system with corresponding kinetic parameters we use here can be found in Table 6.1. The concentration of water molecules is taken into account in the rate constants of the reactions R16, R22, R23, R24 and R30. The rate of reaction R1 depends on the intensity and power spectrum of light used to illuminate the reagents. For the xenon lamp, an approximate expression derived in [191] has the form

$$\nu = \nu_{max}\frac{[Ru(II)]}{(k_1 + [Ru(II)])} \tag{6.1}$$

where ν_{max} contains information on the characteristics of the light source. As in [191] we use the values $k_1 = 4.0 \times 10^{-5}M$ and $H = 0.5M$. Building on the core mechanism described in [191] we included also the role of dibromomalonic acid (Br_2MA) in the photo sensitivity of the BZ system (R9). According to Försterling [193], the concentration of Br_2MA can be quite high if the sum of the initial bromide and bromate concentrations are comparable with those of malonic acid (MA) which is the case in many pattern formation experiments.

Modern experimental techniques with high spatiotemporal resolution, increasingly allow the construction of detailed, quantitative kinetic models on a firm data basis. There are numerous models available in literaure based on the above mechanisms [194, 195, 188], However from model based control point of view, they are far from accurate. Here we model the complete reaction system using the detailed elementary-step mechanism given in Table 6.1 in a CSTR case which leads to a set of ordinary differential equations. We have 20 chemical species but due to the fact that CO_2 is only produced and not consumed in the BZ system the dimension of the state space reduces to 19.

$$\frac{dc_i}{dt} = r_i + k_f(c_{mf} - c_i) \tag{6.2}$$

$c_{i=1\ldots19}$: concentration of species, $r_{i=1\ldots19}$: reaction rates, c_{mf}: mixed feed concentration, k_f: flow rate.

Reaction	Rate constants	Reference
(R1) $Ru(II) + h\nu \longrightarrow Ru(II)^*$	$k_1 = 4.0 \times 10^{-5} M^b$	[191]
(R2) $Ru(II)^* \longrightarrow Ru(II)$	$k_2 = 1.7 \times 10^{+6} s^{-1}$	[191]
(R3) $Ru(II)^* + BrO_3^- + 2H^+ \longrightarrow Ru(III) + BrO_2^{\cdot} + H_2O$	$k_3 = 2.105 \times 10^8 M^{-3} s^{-1}$	[187]
(R4) $Ru(II) + BrO_2^{\cdot} + H^+ \longrightarrow Ru(III) + HBrO_2$	$k_4 = 4.0 \times 10^6 M^{-2} s^{-1}$	[192]
(R5) $BrO_3^- + HBrO_2 + H^+ \longrightarrow 2BrO_2^{\cdot} + H_2O$	$k_5 = 48 M^{-2} s^{-1}$	[192]
(R6) $Ru(II)^* + BrMA \longrightarrow Ru(III) + MA^{\cdot} + Br^-$	$k_6 = 1.9 \times 10^7 M^{-1} s^{-1}$	[191]
(R7) $Ru(III) + BrMA \longrightarrow Ru(II) + BrMA^{\cdot} + H^+$	$k_7 = 55 M^{-1} s^{-1}$	[191]
(R8) $Br_2 + BrMA \longrightarrow Br_2MA + H^+ + Br^-$	$k_8 = 53 M^{-1} s^{-1}$	[191]
(R9) $Ru(II)^* + Br_2MA + H^+ \longrightarrow Ru(III) + Br_2 + MA^{\cdot}$	$k_9 = 1.48 \times 10^8 M^{-2} s^{-1}$	[191]
(R11) $Br_2 + MA \longrightarrow BrMA + H^+ + Br^-$	$k_{11} = 29 M^{-1} s^{-1}$	[191]
(R12) $Ru(III) + MA \longrightarrow Ru(II) + MA^{\cdot} + H^+$	$k_{12} = 0.2 M^{-1} s^{-1}$	[191]
(R15) $2Br^{\cdot} \longrightarrow Br_2$	$k_{15} = 1.0 \times 10^8 M^{-2} s{-}1$	[191]
(R16) $Ru(III) + Br_2MA + H_2O \longrightarrow Ru(II) + Br^{\cdot} + H^+ + BrTA$	$k_{16} = 0.2 M^{-1} s^{-1}$	[191]
(R17) $Ru(III) + Br^- \longrightarrow Ru(II) + Br^{\cdot}$	$k_{17} = 0.17 M^{-1} s^{-1}$	[191]
(R18) $BrTA \longrightarrow MOA + Br^- + H^+$	$k_{18} = 1 s^{-1}$	[191]
(R20) $Br^{\cdot} + MA^{\cdot} \longrightarrow BrMA$	$k_{20} = 1.0 \times 10^9 M^{-1} s^{-1}$	[191]
(R21) $Br^{\cdot} + BrMA^{\cdot} \longrightarrow Br_2MA$	$k_{21} = 3.0 \times 10^9 M^{-1} s^{-1}$	[191]
(R22) $2BrMA^{\cdot} + H_2O \longrightarrow BrMA + BrTA$	$k_{22} = 5.0 \times 10^7 M^{-1} s^{-1}$	[191]
(R23) $2MA^{\cdot} + H_2O \longrightarrow MA + TA$	$k_{23} = 4.2 \times 10^8 M^{-1} s^{-1}$	[191]
(R24) $MA^{\cdot} + BrMA^{\cdot} + H_2O \longrightarrow MA + BrTA$	$k_{24} = 1.0 \times 10^9 M^{-1} s^{-1}$	[191]
(R25) $MA^{\cdot} + Br_2 \longrightarrow BrMA + Br^{\cdot}$	$k_{25} = 1.5 \times 10^8 M^{-1} s^{-1}$	[191]
(R26) $MA^{\cdot} + Br_2MA^{\cdot} + H_2O \longrightarrow BrMA + BrMA^{\cdot}$	$k_{26} = 2.0 \times 10^5 M^{-1} s^{-1}$	[191]
(R27) $MA^{\cdot} + BrMA \longrightarrow MA + BrMA^{\cdot}$	$k_{27} = 1.0 \times 10^5 M^{-1} s^{-1}$	[191]
(R28) $Br^{\cdot} + MA \longrightarrow Br^- + MA^{\cdot} + H^+$	$k_{28} = 2.0 \times 10^5 M^{-1} s^{-1}$	[191]
(R29) $Br^{\cdot} + BrMA \longrightarrow Br^- + BrMA^{\cdot} + H^+$	$k_{29} = 1.0 \times 10^5 M^{-1} s^{-1}$	[191]
(R30) $Br^{\cdot} + MOA + H_2O \longrightarrow Br^- + OA + {}^{\cdot}COOH + H^+$	$k_{30} = 2.0 \times 10^3 M^{-1} s^{-1}$	[191]
(R31) $Br^{\cdot} + {}^{\cdot}COOH \longrightarrow Br^- + CO_2 + H^+$	$k_{31} = 1.0 \times 10^9 M^{-1} s^{-1}$	[191]
(R32) $Br^{\cdot} + OA \longrightarrow Br^- + {}^{\cdot}COOH + CO_2 + H^+$	$k_{32} = 2.0 \times 10^3 M^{-1} s^{-1}$	[191]
(R33) $Ru(III) + {}^{\cdot}COOH \longrightarrow Ru(II) + CO_2 + H^+$	$k_{33} = 1.0 \times 10^8 M^{-1} s^{-1}$	[191]
(R34) ${}^{\cdot}COOH + {}^{\cdot}COOH \longrightarrow OA$	$k_{34} = 1.0 \times 10^9 M^{-1} s^{-1}$	[191]
(R35) $Br_2 \longrightarrow HOBr + H^+ + Br^-$	$k_{35} = 80 s^{-1}$	[191]
(R36) $HOBr + H^+ + Br^- \longrightarrow Br_2$	$k_{36} = 8.0 \times 10^9 M^{-2} s^{-1}$	[191]
(A2) $HBrO_2 + Br^- + H^+ \longrightarrow 2HOBr$	$k_{i2} = 2.5 \times 10^{-6} M^{-2} s^{-1}$	[191]
(A3) $2HBrO_2 \longrightarrow HOBr + BrO_3^- + H^+$	$k_{i3} = 3.0 \times 10^3 M^{-1} s^{-1}$	[191]

Table 6.1: Reaction mechanism of the photosensitive BZ reaction and corresponding rate constants, [b]An approximate rate expression for R1 is given in Eq. 6.1.

$\dot{X}$=-R5+R4-2A3-A2+A1-A_{i1}+k_f(X_{mf}-X)
$\dot{Y}$=-R36+R35-A1+A_{i1}-A2+R6+R18+R11+R8+R28+R29+R30+R31+R32+k_f(Y_{mf}-Y)
$\dot{P}$=A3+2A2+A1-A_{i1}+R35-R36+k_f(P_{mf}-P)
$\dot{A}$=-R3-R5+2*A3-A1+A_{i1}+k_f(A_{mf}-A)
$\dot{V}$=-R6-R7+R11-R8+R20+R22+R25+R26-R27-R29+k_f(V_{mf}-V)

$\dot{G}$=-R1+R2-R4+R12+R7+R16+R17+R33+k_f(G_{mf}-G)
$\dot{E}$=R1-R2-R3-R6-R9+k_f(E_{mf}-E)
$\dot{Z}$=R3+R4+R6+R9-R12-R7-R16-R17-R33+k_f(Z_{mf}-Z)
$\dot{W}$=R3-R4+2R5+k_f(W_{mf}-W)
$\dot{Q}$=-R9-R16+R8+R21-R26+k_f(Q_{mf}-Q)
$\dot{S}$=R6+R9+R12-R20-2*R23-R24-R25-R26-R27+R28+k_f(S_{mf}-S)
$\dot{T}$=R7-R21-2*R22-R24+R26+R27+R29+k_f(T_{mf}-T)
$\dot{F}$=R16+R17-2*R15-R20-R21+R25-R28-R29-R30-R31-R32+k_f(F_{mf}-F)
$\dot{MA}$=-R12-R11+R23+R24+R27-R28+k_f(MA_{mf}-MA)
$\dot{I}$=R15-R11-R8-R25-R35+R36+k_f(I_{mf}-I)
$\dot{J}$=R16-R18+R22+R24+k_f(J_{mf}-J)
$\dot{L}$=R18-R30+k_f(L_{mf}-L)
$\dot{M}$=R30-R31+R32-R33-R34+k_f(M_{mf}-M)
$\dot{N}$=-R32+R34+k_f(N_{mf}-N)

where X=$HBrO_2$, Y=Br^-, P=HOBr, A=BrO_3^-, V=BrMA, G=Ru(II), E=Ru(II)*, Z=Ru(III), W=$BrO_2^{\cdot}$, Q=Br_2MA, S=$MA^{\cdot}$, T=$BrMA^{\cdot}$, F=$Br^{\cdot}$, MA (malonic acid), I=Br_2, J=BrTA (tartronic acid), L=MOA (mesoxalic acid), M=$^{\cdot}$COOH, N=OA (oxalic acid) denote the species concentrations c_i, k_f=flow rate and c_{mf} refers to mixed feed concentrations, the dots meaning time derivative $\dot{c}_i = \frac{dc_i}{dt}$. R1-R9a, R11-R12, R15-R18, R20-R36 and A1-A3 are rate expressions for the reactions listed in Table 1. The concentrations in the mixed feed stream are zero for intermediate species and products, only A_{mf},V_{mf},G_{mf},Q_{mf} and MA_{mf} have non-zero initial values. The parameter values of light intensity and inflow rate are chosen such that the system is in oscillatory mode, advanced DAESOL [59] based on BDF method is used for accurate error-controlled numerical simulation.

By varying the parameters flow rate (k_f) and level of illumination (here ν_{max}= ϕ), different kinds of dynamical behavior are found which correspond semi-quantitatively well with experimental results [191]. Figure 6.1 shows numerically simulated uniform oscillation behavior of the variables $HBrO_2$, Br^-, Ru(III) and Br_2 in the full model based on the set of differential equations and parameter values from Table 6.1. The model reaches a stable limit cycle after initial transient response starting from arbitrary initial conditions. Figure 6.2 shows the simulated time series of bromide ion concentration for parameter values ($\phi = 3.8 \times 10^{-8} Ms^{-1}, 3.8 \times 10^{-6} Ms^{-1}$) and $k_f = 0.1 s^{-1}$. By increasing ϕ the system undergoes a Hopf bifurcation and reaches a steady state. The commonly observed steady state at high ϕ-value is due to the excessive production of Br^- ion, which acts as an effective inhibitor for the auto catalytic reaction.

6.2 Control of BZ reaction system

In this study, we examine the control of temporal oscillation patterns by controlling the light intensity and flowrate in the Ru-catalyzed BZ system. For our numerical simulations, we employ the system of differential equations listed in Eq. 6.2 as a

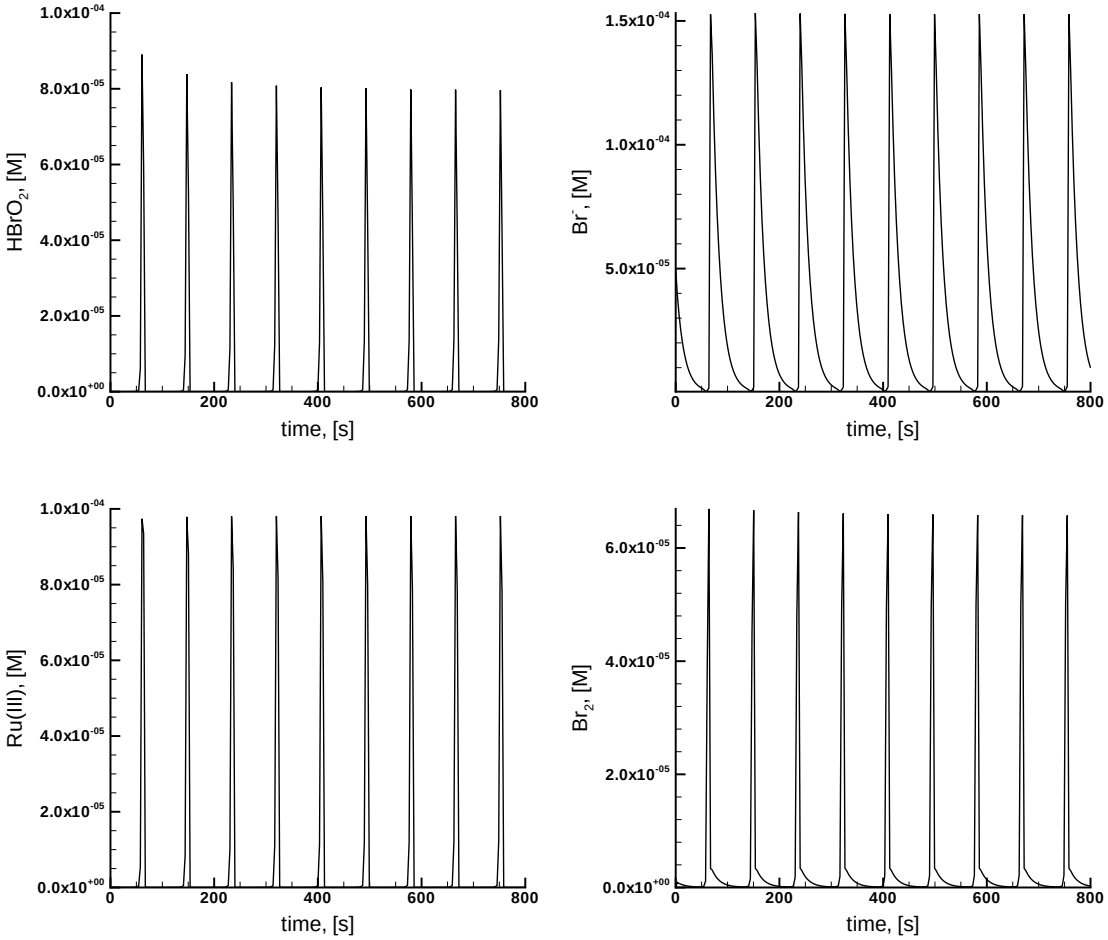

Figure 6.1: Numerical simulation of BZ reaction with the Eq. 6.2. For ϕ= 3.8 $\times 10^{-8}$ Ms^{-1} and $k_f = 0.01\mathrm{s}^{-1}$ the system exhibits uniform oscillations. Plot shows the time varying concentrations of $HBrO_2$ [M], Br^- [M], Ru(III) [M] and Br_2 [M] respectively.

model system. We treat light intensity (ϕ) and flow rate (k_f) as control parameters to compute time varying control inputs which gives rise to a particular output behavior of the system. This output behavior $x_r(t)$ is a predetermined desired temporal dynamics of the system. The corresponding input signals ϕ and k_f are numerically computed as solutions of the optimal control problem to minimize the deviation of the actual system behavior from that of the desired reference trajectory. In a mathematical formulation the optimal control problem here is

$$\begin{aligned} \min_u := \quad & \int_0^T \|x(t) - x_r(t)\|^2 \mathrm{d}t \qquad (6.3) \\ \text{subject to} \quad & \dot{x} = f(x, \phi, k_f, p), \\ & x(0) = x_0, \end{aligned}$$

$$\phi_{min} \leq \phi \leq \phi_{max}$$
$$k_{f_{min}} \leq k_f \leq k_{f_{max}}$$

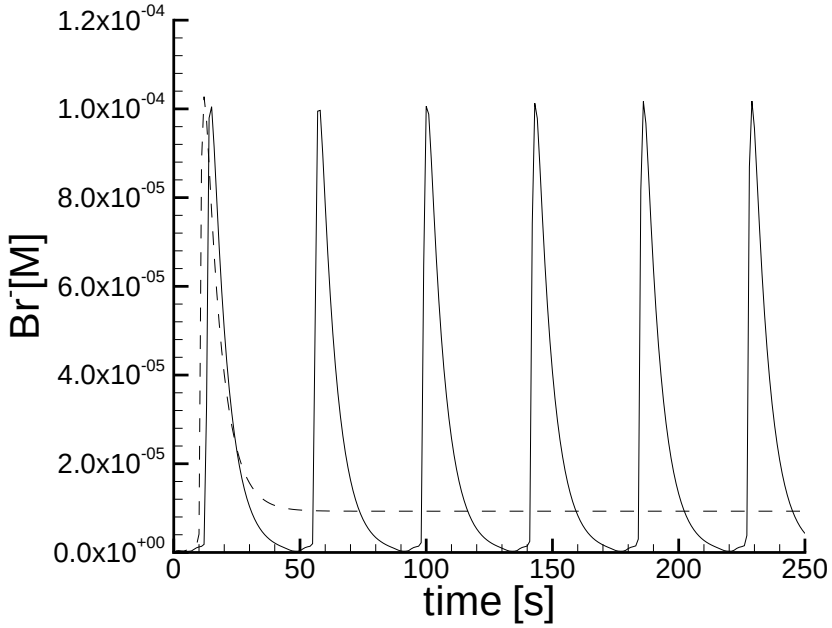

Figure 6.2: Simulated time series of bromide concentration in the BZ reaction system model as specified in Table 6.1. For the chosen inflow rate k_f=0.1/s the system dynamics is characterized by uniform oscillations(solid line) at light intensity ϕ=3.8×10^{-8}M/s and steady state behavior(-dashed line) at $\phi = 3.8 \times 10^{-6}$M/s.

where $x_r(t)$: predetermined desired temporal dynamics, (ϕ, k_f) : Control functions, and the dynamic constraints are given by the ODE system (6.2). The ODE system (6.2) is highly nonlinear with unstable parts of its dynamics and multiple time scales that become obvious in the relaxation oscillations. The aspect of reducing the nonlinearity and instability in highly nonlinear systems by multiple-shooting structure is crucial for the sensitive generation required in gradient based optimization. Therefore MUSCOD-II is a suitable tool for numerical control of complex self-organizing oscillating system like BZ reaction.

6.2.1 Stabilization of unstable steady states

The aim here is to stabilize the unstable steady states by the optimal control approach. We use ϕ and k_f as our control parameters, and the optimal control problem here is

$$\min_{phi,k_f} := \int_0^{800} (x_i(t) - x_i^s)^2 \mathrm{d}t \tag{6.4}$$

$$\begin{aligned} \text{subject to} \quad & \dot{x} = f(x, \phi, k_f, p), \\ & x(0) = x_0, \\ & \phi_{min} \leq \phi \leq \phi_{max}. \\ & k_f min \leq k_f \leq k_f max. \end{aligned}$$

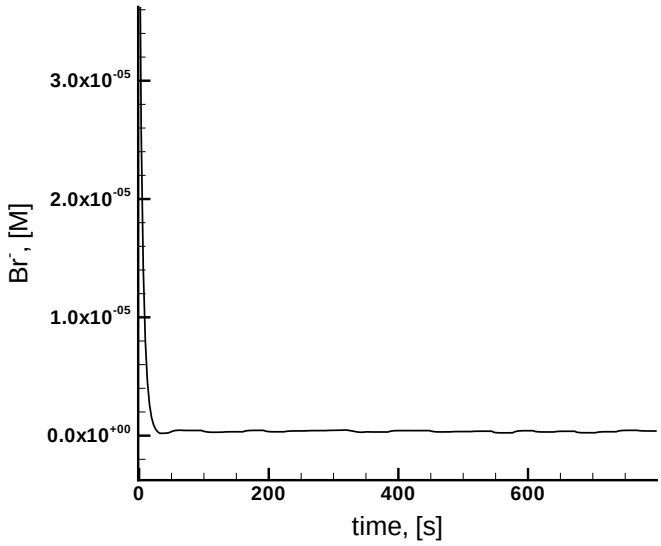

Figure 6.3: Stabilization of unstable steady states in BZ reaction corresponding to Br^- concentration of 2.32×10^{-7}M. Plot shows the stabilized unstable steady state of Br^- ion concentration.

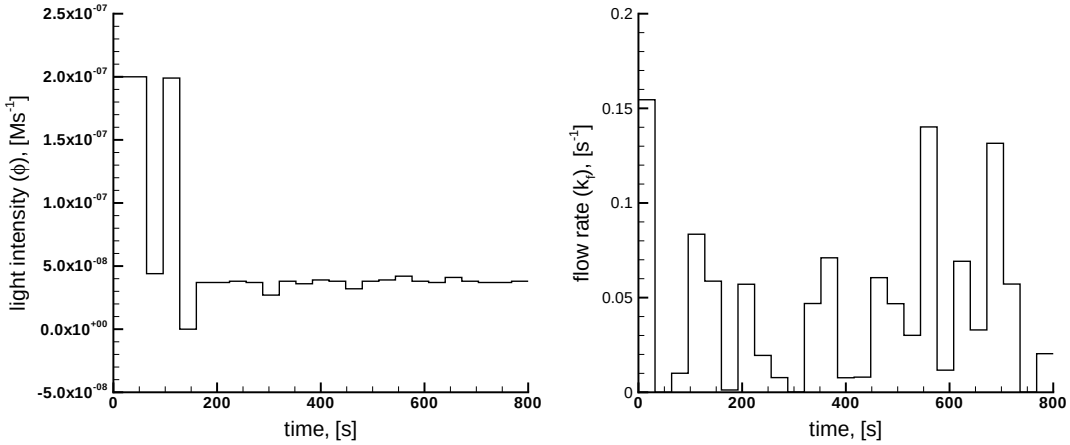

Figure 6.4: Stabilization of unstable steady states in BZ reaction corresponding to Br^- concentration of 2.32×10^{-7}M. Plot shows the piecewise constant control functions ϕ and k_f obtained as the solution of the optimal control problem (6.4).

The vector x_i^s denotes the unstable steady state coordinates for the system of equations 6.2. As a first control scenario we try to stabilize unstable steady state corresponding to bromide ion concentration of 2.32×10^{-7}M. For the given initial conditions x_0, the optimal control problem (6.4) is solved by direct multiple-shooting method [53] implemented in MUSCOD-II [143]. Here the final T for optimization is 800 seconds and we used $N = 25$ multiple shooting points.

In the model of BZ reaction studied here, small multiple shooting time intervals are crucial for efficient numerical computation of optimal control functions

for ϕ and k_f. Figure 6.3 shows the stabilized unstable steady state of Br^- ion concentration in the BZ system and corresponding step changes in control functions ϕ and k_f for obtaining the desired trajectory are shown in Figure 6.4. The minimum and maximum values of the control parameters $\phi \in [0, 2 \times 10^{-7}]Ms^{-1}$ and $k_f \in [0, 0.3]s^{-1}$ are chosen such that the system remains in oscillatory domain.

6.2.2 Driving the BZ system at a desired frequency and amplitude

Self-organized dynamical systems offer a great flexibility for encoding complex input responses in nonlinear chemical and biochemical systems. Lebiedz and Brandt-Pollmann has shown how tuning of temporal self-organization in a model of CO oxidation on Platinum catalyst by input signals in a simple nonlinear chemical reaction exhibiting oscillations can be used for both processing complex information and specific control of dynamical behavior [148]. In the following, we analyze this aspect for the complex BZ reaction as an example by using ideas from optimal control theory. As discussed in Chapter 1, the more interesting and demanding control tasks would be to drive the system to arbitrary regions in phase space which are not stable attractors. One such a case is to formulate the objective functional for obtaining a desired trajectory with a shape of a sinusoidal harmonic oscillator with certain frequency and amplitude in the BZ system. Forced or tuned oscillators for example are not only considered to be important in cellular rhythms, but also in technical applications involving chemical reaction systems [196].

The optimal control problem here is

$$\begin{aligned} \min_{phi,k_f} := \quad & \int_0^T \|x(t) - x_r(t)\|^2 \mathrm{d}t \qquad (6.5) \\ \text{subject to} \quad & \dot{x} = f(x, \phi, k_f, p), \\ & x(0) = x_0, \\ & \phi_{min} \leq \phi \leq \phi_{max}. \\ & k_{f_{min}} \leq k_f \leq k_{f_{max}}. \end{aligned}$$

where $x_r(t) = x_a + Asin(2\pi\nu t)$ is the reference trajectory with x_a , A, and ν as the predetermined parameters corresponding to the bromide ion concentration, amplitude and frequency of a desired sine function.

The objective essentially here is to compute input controls, which tune the oscillatory behavior such that the resulting bromide ion concentration is a harmonic sine function with predetermined fixed parameters: A, and ν. The resulting problem is solved using MUSCOD-II [143] with 25 multiple shooting points on total T=100 seconds. In the first case as shown in Figure 6.5, we try to induce a sinusoidal shape for Br^- ion with $x_a = 5 \times 10^{-5}$, $A = -5 \times 10^{-5}$, and $2\pi\nu$ =0.05. The controller is able to induce the desired dynamics into the system. Under constant illumination of light with $\phi = 3.8 \times 10^{-6}$M/s and k_f=$0.3s^{-1}$, the oscillations in the

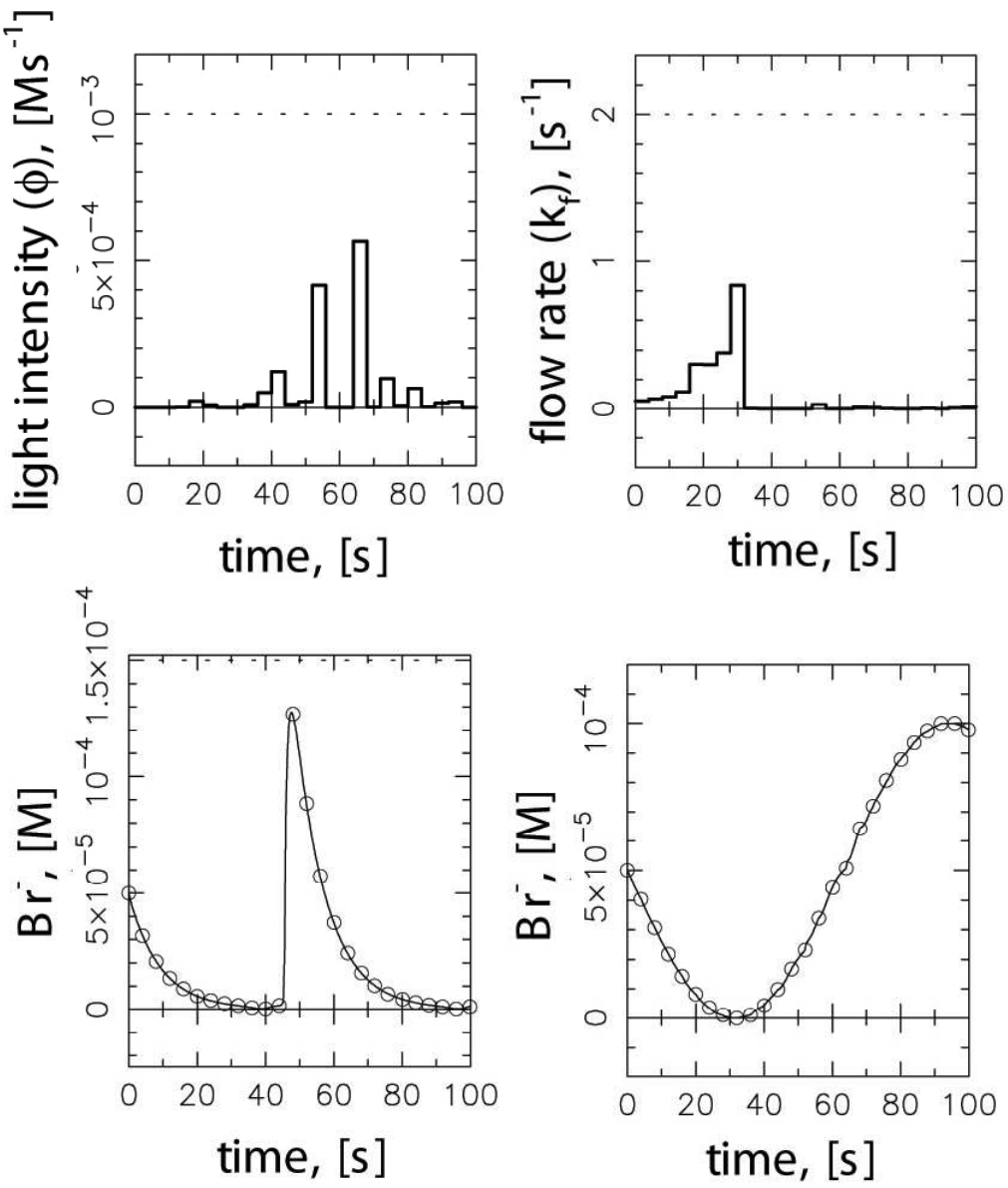

Figure 6.5: Control inputs ϕ and k_f (top) for the desired oscillatory output behavior $x_r(t) = x_a + Asin(2\pi\nu t)$ (bottom) characterized by the three parameters x_a, A, and ν. There are computed as solutions of the optimal control problem (6.5) for different parameter value $x_a = 5 \times 10^{-5}$, $A = -5 \times 10^{-5}$, and $2\pi\nu$ =0.05. Plot on (*bottom left*) shows actual Br^- concentration profile and (*bottom right*) after the control.

BZ system reaches the steady state. However, the maximum values of the control parameters required to induce the desired sine function dynamics in bromide ion concentration are higher than the values at which the system reaches steady state. In our optimal control problem (6.5), the maximum values of control parameters used are $\phi = 1.0 \times 10^{-3}$M/s and k_f=1.0s^{-1}, which means that the system does not remain in the oscillatory regime alone to induce such a dynamics. Figure 6.6 shows another example of inducing sine function dynamics in Br^- ion concentration in BZ system with different oscillation frequency. Here $x_a = 5 \times 10^{-5}$, $A = -5 \times 10^{-5}$, and $2\pi\nu$ =0.075. Parameters in $x_r(t)$ can be varied arbitrarily within a certian range

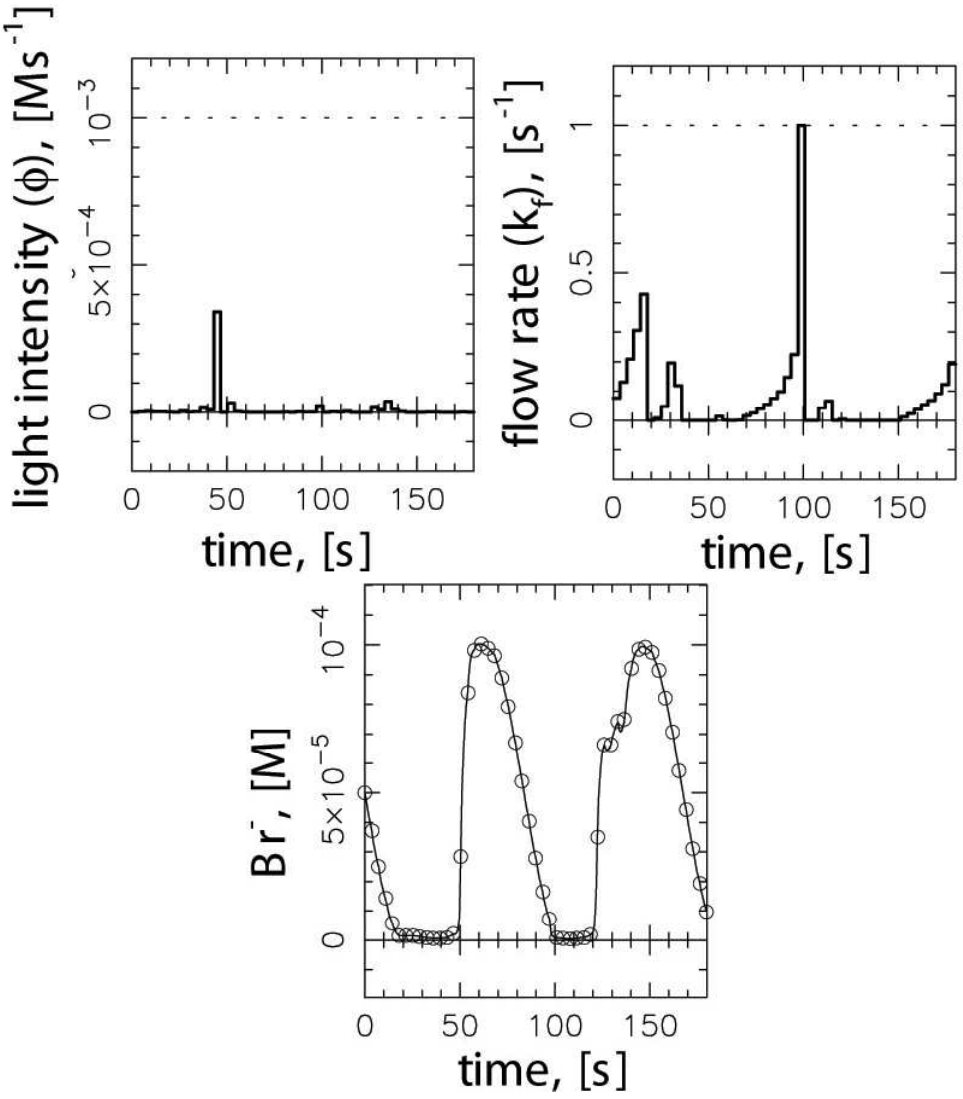

Figure 6.6: Control inputs ϕ and k_f (top) for the desired oscillatory output behavior $x_r(t) = x_a + Asin(2\pi\nu t)$ (bottom) characterized by the three parameters x_a, A, and ν computed as solutions of the optimal control problem Eq. 6.5 for different parameter value $x_a = 5\times10^{-5}$, $A = -5\times10^{-5}$, and $2\pi\nu = 0.075$.

for obtaining the desired oscillatory behavior in bromide ion concentration by using light intensity and flow rate as control parameters.

6.3 Reduction of the detailed model

In many situations the high spatiotemporal resolution of modern experimental techniques provides an accurate data basis for the construction of detailed chemical reaction mechanisms for systems with highly complex dynamical behavior. However, both mathematical analysis and numerical simulations are difficult tasks in high dimensional phase space associated with detailed mechanistic models. In particular for spatially non-homogeneous systems, numerical treatment of the underlying large scale and mostly stiff partial differential equations is still a challenge [197].

Therefore, model reduction techniques are commonly applied to reduce the dimension of the reaction mechanism by eliminating chemical species and elementary reaction steps [198, 199]. The aim is to construct a reduced model which can be treated much easier numerically and if small enough may allow even an analytic investigation of phase space topology, bifurcation behavior, attractor geometry and generally incorporation into numerically expensive simulation of spatially extended reaction-diffusion systems. Since quite a long time the well known quasi-steady-state assumption (QSSA) and the partial-equilibrium-approximation (PEA) are used for model reduction [200]. Both of them implicitly exploit intrinsic multiple time scales in the system under consideration. The QSSA eliminates intermediate species by approximating their rate of change to be zero if it is very small compared to the overall system dynamics, whereas the PEA assumes some fast elementary reaction steps to be relaxed to equilibrium immediately. Both assumptions are justified to some extent if the corresponding time scales are very slow in the QSSA case and very fast in the PEA case. However, for large-scale mechanisms their identification is extremely difficult and time consuming. Therefore, many automatic numerical methods have been developed for the purpose of model reduction in chemical kinetics (see Ref. [201] for a comprehensive review of model reduction techniques).

A central problem of these common approaches is that the validity of the approximations usually changes dramatically with the actual system state. Moreover, one does not have an a priori estimate of the error that is introduced by these assumptions and the extent to which the original detailed model can be reduced to yield still quantitatively accurate results for the dynamical behavior. In fact, the error can be estimated a posteriori by comparing numerical simulations of the full and reduced system, but a lower bound for the minimal dimension required for a still accurate reduced model is difficult to obtain. Nevertheless, in many cases the systems are reduced to two or three dimensions in order to make use of analytic and geometric methods exploiting the well characterized topology of these low dimensional phase spaces. However, in this case both quantitative relation to the original detailed model and physical significance of parameter values often get obscured and one is restricted to the rather qualitative study of dynamical behavior.

In practical applications relying on quantitative models like for example model based system control and optimization, the latter approach is often prohibited if the model is supposed to serve as a basis for process controller design which requires quantitative results and accurate physical modeling of the control input [91]. Therefore, an a priori estimate of the error introduced by reduction and the minimal dimension required for preserving quantitative consistency with the full model is desirable. Former validation approaches for reduced models are often restricted to error estimations for steady state behavior, but for systems with complex nonlinear behavior it is crucial to take dynamical aspects into account. Here, we exploit a novel numerical algorithm [46] based on the concept of Intrinsic Low Dimensional

Manifolds (ILDM) proposed by Maas and Pope [202] which is able to compute dynamically (during numerical integration) the minimal reduced dimension required for error-controlled consistency with the full model. For detailed description and implementation of the algorithm can be found in [201]. The algorithm uses an automatic time scale decomposition of the full system into a "slow" and a "fast" part of dynamical modes and applies an error criterion proposed by Deuflhard and Heroth which is derived from singular perturbation theory for ordinary differential equations to identify the dimension of the slow part [203].

The algorithm is applied to the detailed model for the photosensitive Belousov-Zhabotinsky reaction including 19 species and 36 elementary reaction steps presented in Section 6.1. The results are exploited for an error control motivated application of classical QSSA and PEA approaches to construct a quantitatively accurate reduced model.Our aim is to reduce the presented detailed model as much as possible while maintaining quantitative accuracy. For this purpose we apply the algorithm and analyze the time-scale decomposition results for the BZ reaction system in the oscillatory regime. The minimum dimension computed by the algorithm with an error tolerance of $TOL = 10^{-4}$ as a function of time is shown in Figure 6.8. From these results we conclude that the minimum dimension required for still accurate representation of the full model dynamics is 7-9 depending on the actual system state in the oscillatory regime. Further reduction is not possible without severe loss of such quantitative agreement.

We know try to reduce the model explicitly as much as possible to come close to the minimum dimension of 7. The first step of reduction is to eliminate those variables which are constant or decrease by only 1 or 2 % during numerical simulation of the model on the chosen time horizon. We identify three such variables A(BrO_3^-), Q (Br_2MA), MA whose values are quasi-constant.

We exploit the information provided by the component analysis output of the algorithm (see Ref. [204] for detailed component analysis of the algorithm). The analysis of the individual species contributions to the active (slow) modes shows that they are negligibly small in some cases over the complete time horizon (see exemplarily Figure 6.7 for comparison with other species sharing significant contribution). The relative contribution of Ru(II)* for example is orders of magnitude smaller than that of Ru(II) and Br^- suggesting that a quasi-steady-state approximation can be applied here. In sum, we were able to identify seven such species P, E, S, T, F, M and N whose contribution to the active modes is extremely low. In a subsequent step the outlined model reduction is carried out explicitly by applying quasi-steady-state assumption (QSSA) and solving the resulting algebraic equation system. When solving the equations explicitly using the computer algebra software package MAPLE we got huge expressions (2 GB of memory) for a representation of the seven variables in terms of remaining active ones. We tried to simplify

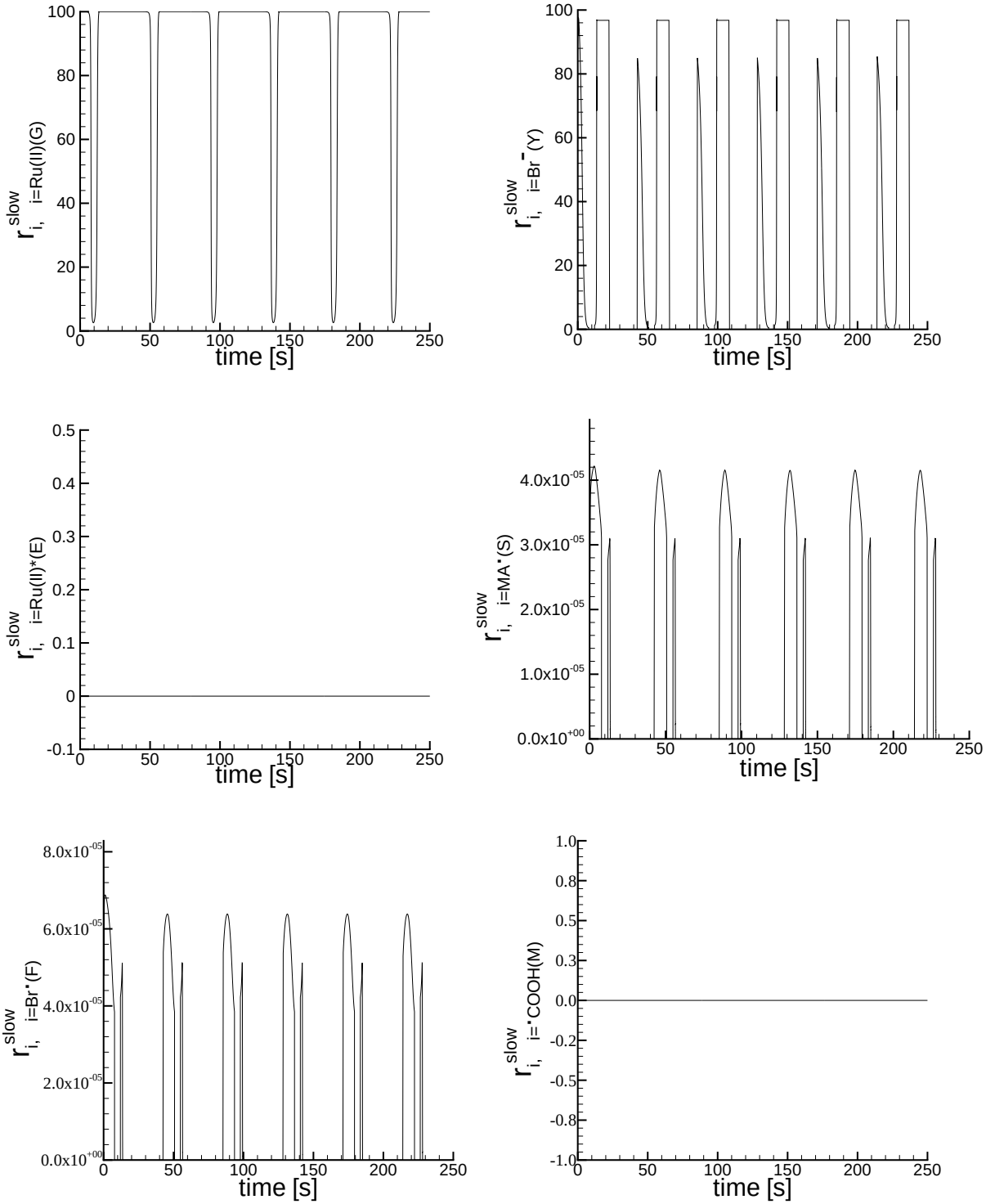

Figure 6.7: Analysis of a selection of chemical species i with respect to their contributions r_i^{slow} to the active modes in the BZ reaction system. The plots exemplarily show the contribution for i=Ru(II), Br^-,Ru(II)*,$MA^{\cdot}$,$Br^{\cdot}$ and $^{\cdot}COOH$ under conditions as in Figure 6.8.

these expressions by considering only important reactions which significantly contribute to the dynamics for these variables from the Table 6.1 and deleting all higher order terms. In fact, we deleted (R20,R23,R24),(R21,R22,R24,R26,R27,R29) and (R15,R20,R30,R31,R32) from equations for $\dot{S}$, $\dot{T}$ and $\dot{F}$ respectively and confirmed their minor contribution to the overall rates by checking the values of these terms at maximum concentration of the individual species. The remaining equations can be solved simultaneously quite easily. Finally, we come up with an explicitly reduced set of 9 differential equations with A, Q, MA as constants and values E, T, S, F, M, N and P algebraically expressed in terms of the remaining variables X, Y, V, G, Z, W, I, J and L.

X'=-R5+R4-2*A3-A2+A1-Ai1+k_f(X_{mf}-X)
Y'=-R36+R35-A1+Ai1-A2+R6+R18+R11+R8+R28+R29+R30+R31+R32+k_f(Y_{mf}-Y)
V'=-R6-R7+R11-R8+R20+R22+R25+R26-R27-R29+k_f(V_{mf}-V)
G'=-R1+R2-R4+R12+R7+R16+R17+R33+k_f(G_{mf}-G)
Z'=R3+R4+R6+R9-R12-R7-R16-R17-R33+k_f(Z_{mf}-Z)
W'=R3-R4+2*R5+k_f(W_{mf}-W)
I'=R15-R11-R8-R25-R35+R36+k_f(I_{mf}-I)
J'=R16-R18+R22+R24+k_f(J_{mf}-J)
L'=R18-R30+k_f(L_{mf}-L)

E=-ν_{max}G/(-k_2-0.5$k_9$$a$Q-0.25$k_3$A-$k_6$V-$k_f$)($k_1$+G)

T=(-k_f+sqrt(k_f^2+8$k_{22}$$k_7$VZ))/4$k_{22}$

S=-(k_{16}QZ+k_{17}YZ)/(k_{25}I)+(-k_f-k_{21}T-k_{28}MA-k_{29}V(k_{25}I(Hk_{9a}QE+k_6VE+k_{12}MA.Z)-(-k_f-k_{26}Q-k_{24}T-k_{25}I-k_{27}V)(k_{16}QZ+k_{17}YZ)))/(k_{25}I($k_{25}$$k_{28}$MAI-(-$k_f$-$k_{26}$Q-$k_{24}$T-$k_{25}$I-$k_{27}$V)(-$k_f$-$k_{21}$T-$k_{28}$MA-$k_{29}$V)))

F=-(k_{25}I(Hk_{9a}QE+k_6VE+k_{12}MA.Z)-(-k_f-k_{26}Q-k_{24}T-k_{25}I-k_{27}V)(k_{16}QZ+k_{17}YZ))/($k_{25}$$k_{28}$MAI-(-$k_f$-($k_{26}$Q)-$k_{24}$T-$k_{25}$I-$k_{27}$V)(-$k_f$-($k_{21}$T)-$k_{28}$MA-$k_{29}$V))

M=k_{30}FL/(k_{31}F+k_{33}Z+k_f)

N=$k_{30}^2$$k_{34}FL^2$/($k_{32}$($k_{31}$F+$k_{33}$Z+$k_f$)($k_{31}$F+$k_{33}$Z+$k_f$))

P=-(-2$k_{i3}$$X^2$-$k_{35}$I-2H$k_{i2}$XY-$H^2$$k_{i1}$YA)/($k_{mi1}$X+H$k_{36}$Y+$k_f$)

A dimension of 9 has been predicted by the algorithm if the model is supposed to be accurate with a tolerance of 10^{-4} on the full time horizon (see Figure 6.8). However, in large parts an even smaller dimension of 7 has been proposed. We observe in numerical integrations that the value of the variable L increases almost linearly with time and remains constant after an initial phase. For short integration times we can approximate this variable with the linear expression L=$5.714\times10^{-6}t$, where t is the integral time. The value of the constant naturally depends on the initial conditions of the system. This linear approximation is valid for time horizons smaller than

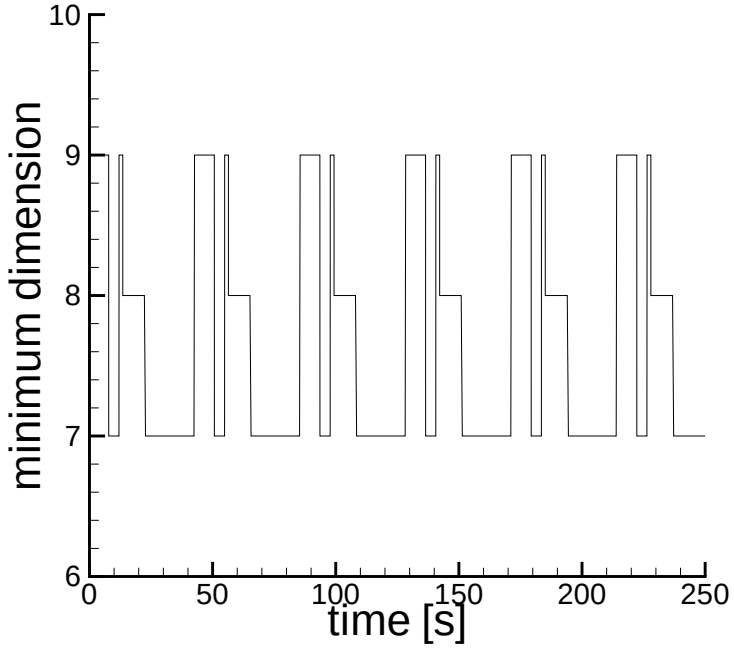

Figure 6.8: Minimum dimension of the reduced model for the BZ reaction with inflow rate k_f=0.1/s and light intensity ϕ=3.8×10^{-8} computed by the algorithm [201]. The analysis is performed in the oscillatory dynamical regime. The plot shows the number of active, 'slow' modes.

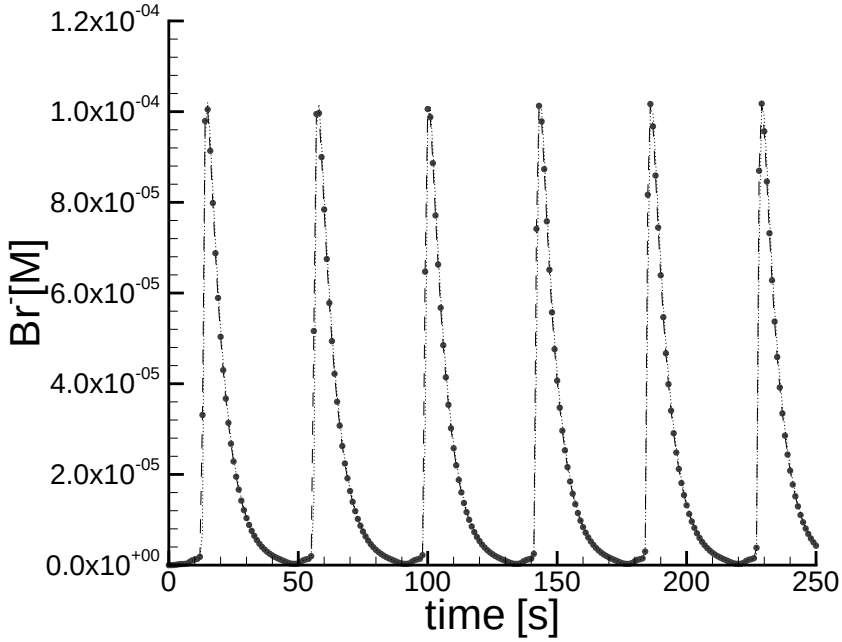

Figure 6.9: Simulated time series of bromide concentration in the BZ reaction system model, comparison between the full model(– dashed line) and the reduced 7 variable model(·) under conditions as in Figure 6.8.

T=6000s. Thus, we have an 8 variable reduced model which has effectively only 7 degrees of freedom since Ru(II)+Ru(III)+Ru(II)*=constant is obvious from the mass balance of the catalyst. The maximally reduced model shows dynamical behavior quantitatively very close to the full model in the oscillatory dynamic regimes (Figure 6.9).

6.3.1 Complex oscillations in the 8-variable model

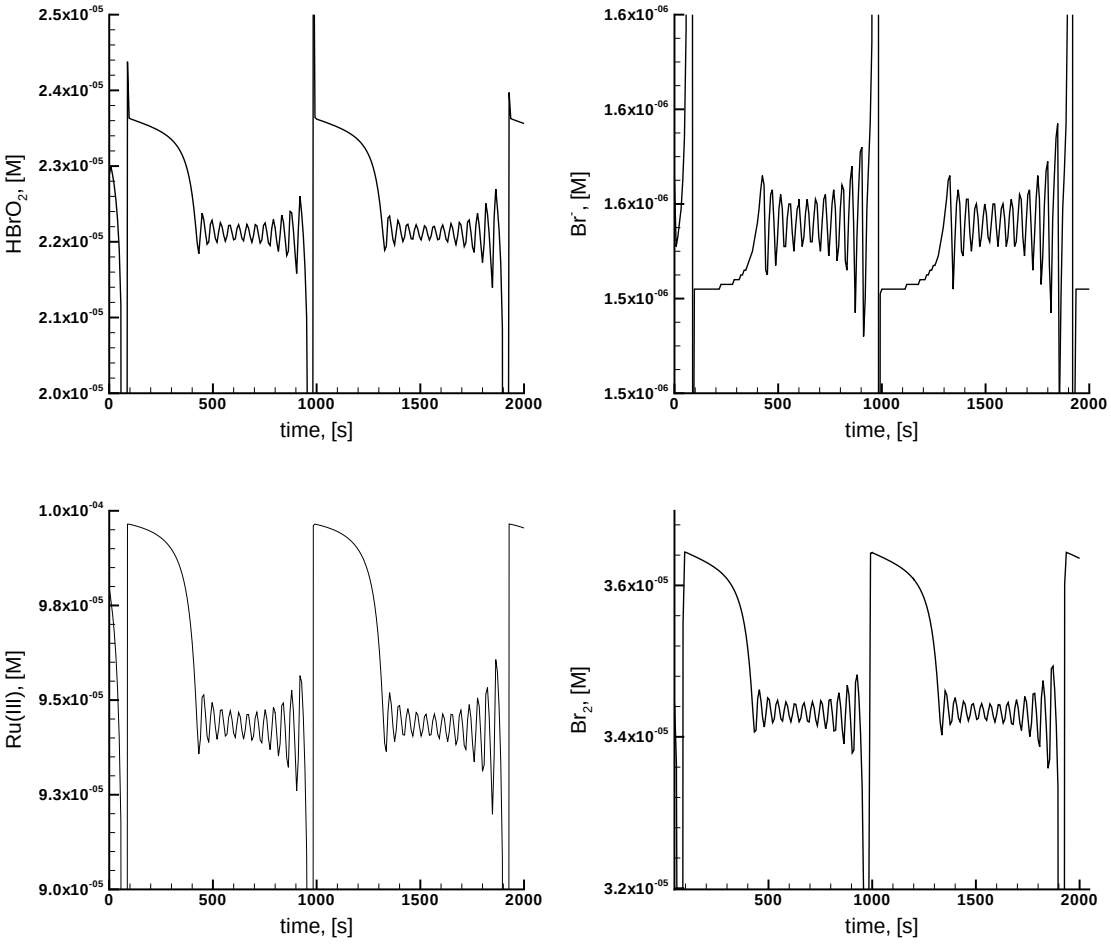

Figure 6.10: Complex oscillations in reduced 8-variable model. Initial concentrations are: $[HbrO_2]$=2.2882864×10^{-5} M; $[Br^-]$ = 1.5652838×10^{-6} M; [BrMA] = 1.1788022×10^{-2} M; [Ru(II)] = 2.0209202×10^{-6} M; $[BrO_2^*]$ = 2.0675897×10^{-5} M; $[Br_2]$ = 3.5778697×10^{-5} M; [BrTA] = 3.4178939×10^{-5} M; [MOA] = 3.0875×10^{-1} M; parameters: ϕ = 7.5 × 10^{-6} Ms^{-1}; k_f = 1.06 × $10^{-4}s^{-1}$

Parameters ϕ and k_f are varied through their phase space for finding a region where complex oscillations can be found in the BZ system. Under appropriate initial conditions and for parameter values of $\phi = 7.5 \times 10^{-6}Ms^{-1}$ and $k_f = 1.06 \times 10^{-4}s^{-1}$, the 8-variable reduced model (without the linear assumption for L) exhibits complex oscillations near Hopf bifurcation point. An oscillation time series with rich internal structure that ranges from high-amplitude and relatively high-frequency regular

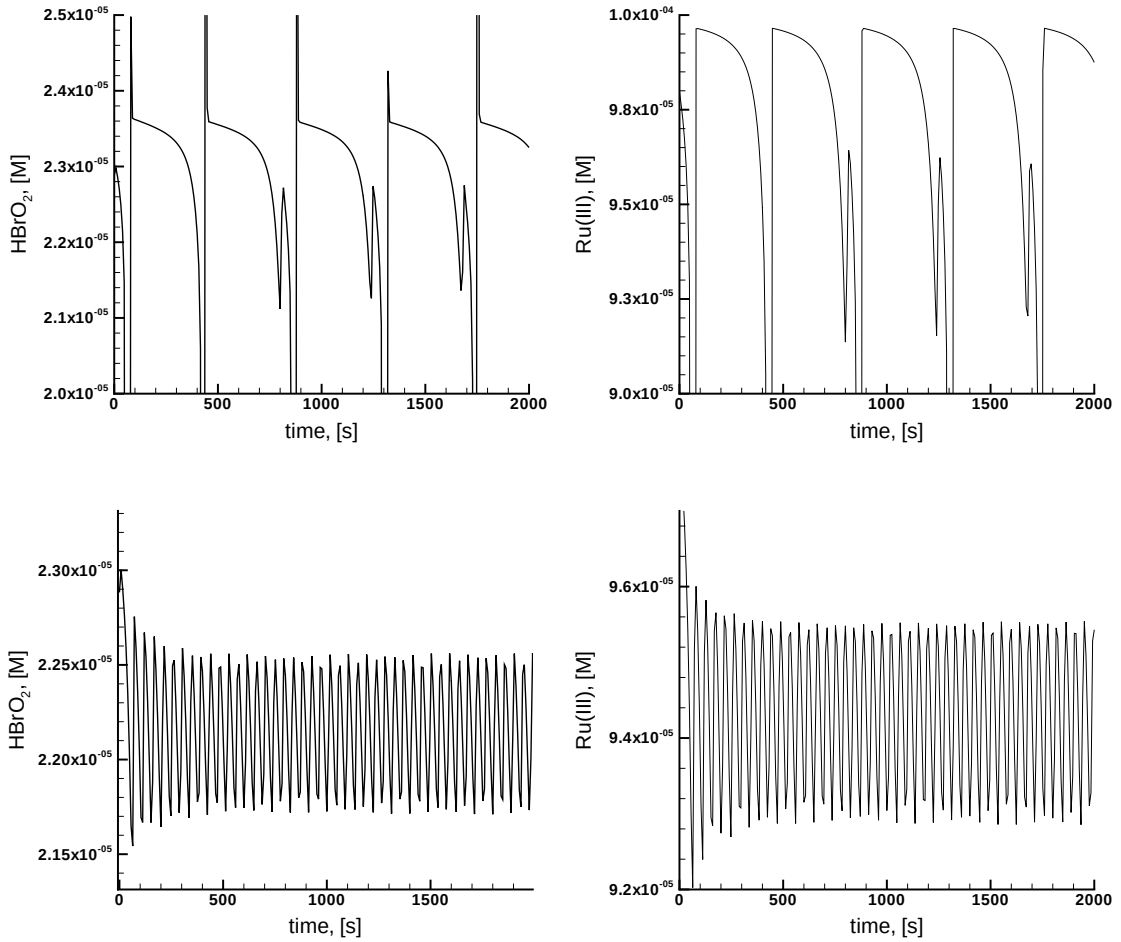

Figure 6.11: Aperiodic and uniform oscillations in the reduced 8-variable model. Initial concentrations are: $[HbrO_2]$=2.2882864×10^{-5} M; [Br$^-$] = 1.5652838×10^{-6} M; [BrMA] = 1.1788022×10^{-2} M; [Ru(II)] = 2.0209202×10^{-6} M; [BrO_2^*] = 2.0675897×10^{-5} M; [Br_2] = 3.5778697×10^{-5} M; [BrTA] = 3.4178939×10^{-5} M; [MOA] = 3.0875×10^{-1} M; parameters values for (*top*): $\phi = 7.9 \times 10^{-6}$ Ms^{-1}; $k_f = 1.06 \times 10^{-4}$s^{-1} and (*bottom*) $\phi = 7.3 \times 10^{-6}$ Ms^{-1}; $k_f = 1.06 \times 10^{-4}$s^{-1}

oscillations; a domain of highly irregular "intermittent" oscillations; low amplitude oscillations with gradual vanishing of their amplitude and finally to the cessation of oscillations.

Figure 6.10 shows one such scenario where high frequency small amplitude oscillations are followed by low frequency high amplitude oscillations. The reaction starts with an induction period during which no oscillations takes place, followed by sudden birth of small amplitude oscillations, followed by large amplitude low frequency oscillations. By slightly varying the parameter ϕ to 7.9×10^{-6}Ms^{-1} one gets aperiodic oscillations as shown in Figure 6.11 *(top)*. Each large amplitude peaks are separated by one or more small amplitude spacer peaks, whose number appears to be randomly distributed. If one decrease the value of ϕ to 7.3×10^{-6}Ms^{-1}, the aperiodic oscillations gives way to high frequency uniform oscillations as shown in

Figure 6.11 *(bottom).*

6.4 Control scenarios for reduced 8-variable model

6.4.1 Finding a periodic orbit

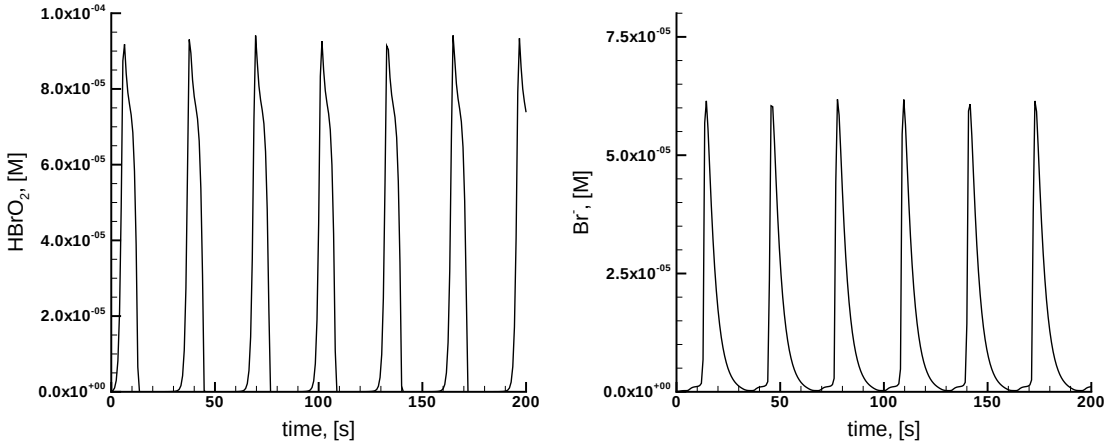

Figure 6.12: BZ system dynamics under dark conditions having a time period of 32 seconds in case of the 8-variable model. Plots shows the time varying concentrations of $HBrO_2$ and Br^- for ϕ =0; k_f =0.2s^{-1}; $[\text{BrMA}]_{in}$ = 0.05 M; $[\text{Ru(II)}]_{in} = 1.0 \times 10^{-4}$ M.

The control aim here is to induce the periodic orbits in the BZ system with a desired time period by using light intensity as control parameter. We formulate it as a boundary value problem with coupled constraints i.e. the residual of the starting point and the end point is equal to zero by varying light as a control parameter. The initial conditions of the BZ system are left as free parameters along with end time T for the optimization problem.
The objective functional here is of the form

$$\begin{aligned} \min_{phi} := \quad & \int_0^T (t_s - t)^2 \mathrm{d}t \\ \text{subject to} \quad & \dot{x} = f(x, \phi, p), \\ & x(0) = x(T), \\ & \phi_{min} \leq \phi \leq \phi_{max}. \end{aligned} \tag{6.6}$$

where t_s: predetermined desired time period; ϕ: control function and the dynamic constraints are given by ODE system (6.2). The periodic solution is computed using offline variant of MUSCOD-II [143] imposing periodicity conditions for a given t_s in the objective function (6.6). This periodic reference solution is denoted by $x_r(t)$ and is defined for all the $t \in (0, \infty)$ and satisfies the periodicity condition $x_{ir}(t+T) = x_{ir}(t)$ and $u_r(t+T) = u_r(t)$, where x_{ir} represents the reference trajectory corresponding to variable x_i.

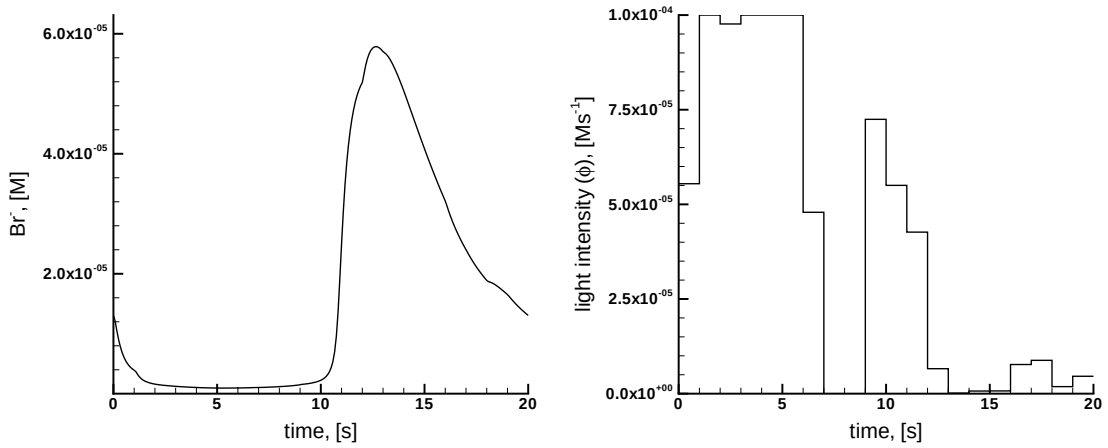

Figure 6.13: Periodic orbit with the desired time period of 20 seconds by using light intensity as control parameter. Plot shows the desired time period in Br^- ion concentration and piecewise constant control of light intensity (ϕ) to obtain the desired 20 seconds period in case of 8-variable model. The control values of ϕ are obtained by solving the boundary value problem Eq. (6.6) with t_s=20 seconds.

The effect of constant illumination of light on the reaction medium is the production of bromide ion which acts as an inhibitor, there by suppressing the oscillations. For a critical value of ϕ= 5.8×10^{-6}Ms^{-1} one can completely suppress the oscillations under constant illumination conditions. Under constant illumination of light, period of oscillations can only be increased but cannot be decreased less than that of the period under dark conditions. For the fixed values of ϕ=0, k_f=$0.2s^{-1}$, $[BrMA]_{in}$ = 0.05 M and $[Ru(II)]_{in}$ = 1.0×10^{-4} M oscillations have a period of T=32 seconds, as shown in Figure 6.12 under dark conditions. One can actually increase or decrease the period of oscillations by changing the flowrate k_f, but in our case studies we fix the value of k_f and use light intensity as the only control parameter available for the dynamic control.

In case of the 8-variable model, we would like to induce an oscillation period of 20 seconds in BZ system. We formulate the objective functional (6.6) with $t_s = 20$ seconds and light intensity(ϕ) as a control parameter. The resulting boundary value problem is solved with MUSCOD-II with 20 multiple shooting points. Results are shown in Figure 6.13(*left*) with time varying concentration of Br^- ion with the desired time period of 20 seconds satisfying the condition $Br^-(0) = Br^-(20)$. The corresponding piecewise constant control parameter light intensity required to impose such a dynamics is shown in Figure 6.13 (*right*). Please make note that the maximum value of light used for obtaining the optimal soultion is 1.0×10^{-4}Ms^{-1}, which is approximately 20 times the order of magnitude of light intensity used for suppressing the oscillations completely under constant illumination. The system is driven into the steady state and back to oscillatory regime for obtaining the desired oscillation time period. The amplitude of 20 seconds period oscillations are slightly

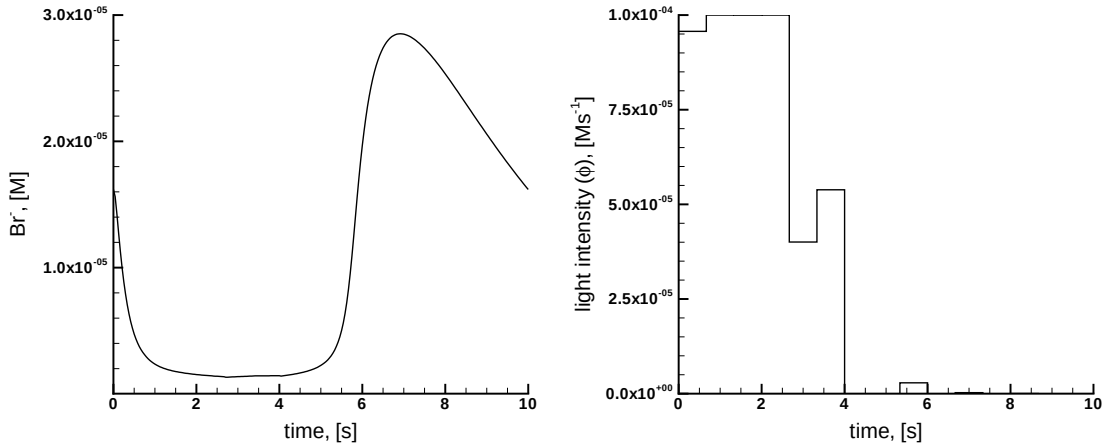

Figure 6.14: Periodic orbit with a time period of 10 seconds by using light intensity as control parameter. Plot shows the desired time period in Br^- ion concentration and piecewise constant control of light intensity (ϕ) to obtain the desired period in case of 8-variable model. The control values of ϕ are obtained by solving the boundary value problem Eq. (6.6) with t_s=10 seconds.

smaller in magnitude when compared to that of oscillations under dark conditions.

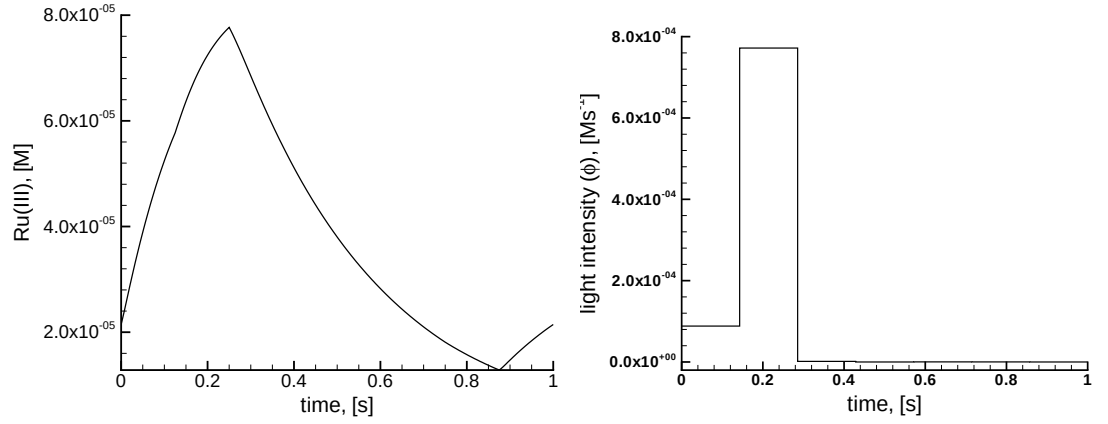

Figure 6.15: Periodic orbit with a time period of 1 second by using light intensity as control parameter. Plot shows the desired time period in Ru(III) [M] concentration and piecewise control of light intensity ϕ [Ms^{-1}] to obtain the desired period in case of 8-variable model. The control values of ϕ are obtained by solving the boundary value problem Eq. (6.6) with t_s=1 second.

By a similar formulation as in case of obtaining a 20 second periodic orbit, one can obtain a reduced 10 seconds oscillation period by solving problem (6.6) with t_s=10 seconds. Figure 6.14 shows the piecewise constant control values of light intensity (ϕ) and the corresponding concentration of Br^- ion for obtaining the desired 10 second oscillation period. The boundary value problem Eq. (6.6) is solved with MUSCOD-II with 15 multiple shooting points. One can reduce the period of oscillations subsequently as small as 1 second as shown in Figure 6.15.

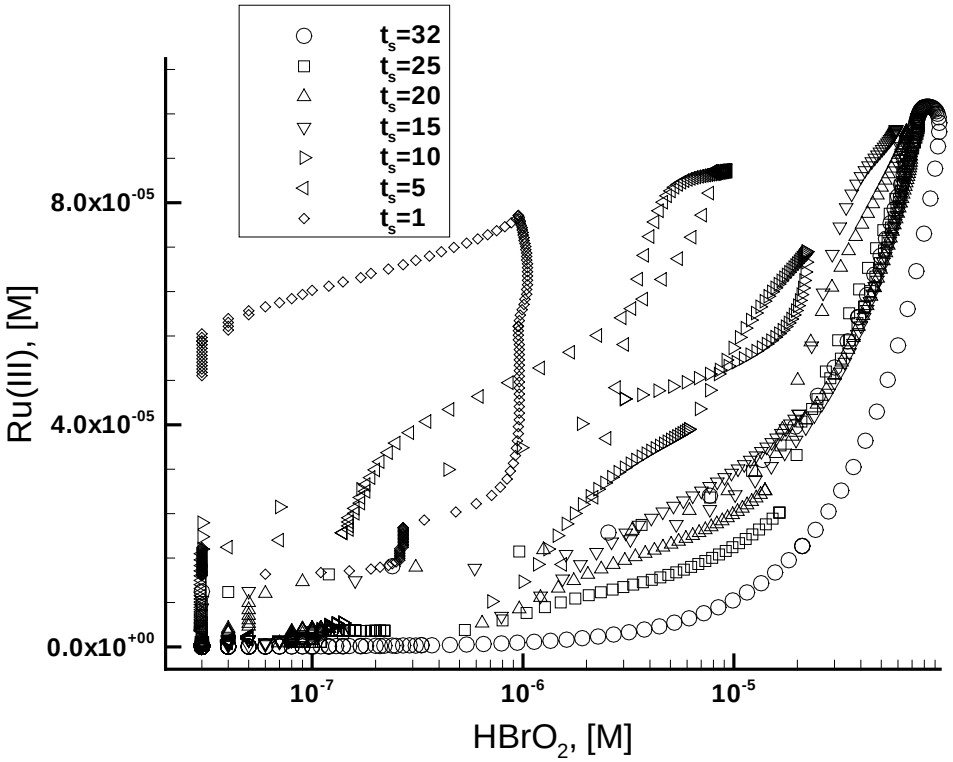

Figure 6.16: Limit cycles of different time periodic orbits obtained with time varying light intensity as control parameter. Plot shows the concentrations of logarithmic scale of $HBrO_2$ [M] vs Ru(III) [M] for different desired time periods (t_s) in case of 8-variable model.

The resultant amplitude of this short period oscillations is also reduced when compared to oscillations under dark conditions. The maximum value of light intensity ϕ_{max} required for obtaining the reduced time period oscillation gets higher as the period gets shorter. Figure 6.16 plotted on logarithmic scale of $HBrO_2$ on x-axis and Ru(III)(i.e. Ru_0-Ru(II)) on y-axis shows the limit cycle oscillations obtained with different time periods in case of the 8-variable model. The plot shows 7 such different periods from T=32 seconds to T=1 second. Large limit cycle oscillation (open circle) corresponds to the BZ system concentrations under dark conditions with T=32 seconds. As the oscillation period decreases to T=1 second, the amplitude of the oscillations also decreases and so does the size of limit cycles.

6.4.2 Response to optimal periodic stimuli in case of 8-variable model

In Section 6.4.1, in order to obtain oscillations with a desired period, we left the initial conditions as free parameters for the optimizer. In case of repetitive optimal stimuli (i.e. with the control values of light intensity obtained as in Section 6.4.1 for obtaining reduced period oscillations), irrespective of initial conditions, the system eventually reaches the stable limit cycle after initial transient response with the desired time period. Figure 6.17 shows the BZ systems response to the repetitive optimal stimuli for obtaining a desired oscillation period of 20 seconds. The control

values of the light intensity in Figure 6.17 (*right*) are calculated by offline solution of problem (6.6) by imposing a periodic constraint of t_s=20 seconds. Figure 6.17 (*left*) shows the response to the periodic optimal controls. After the initial transient response, the system eventually reaches a stable periodic orbit with a time period of 20 seconds. Initial conditions in this case are chosen randomly.

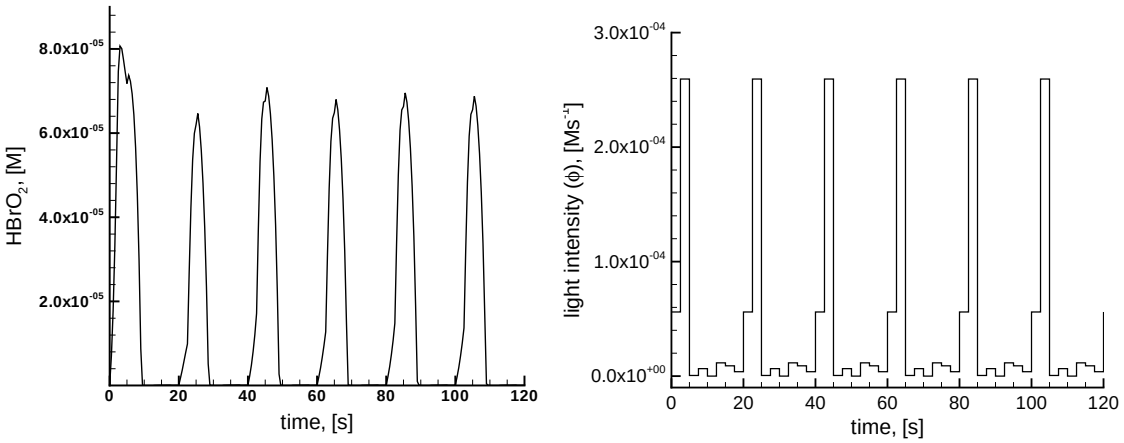

Figure 6.17: Long term simulation under the repetitive periodic forcing of control parameter light intensity with random initial conditions in case of 8-variable model. Plot shows the concentraion of $HBrO_2$ [M] with time and the corresponding variation of repetitive light stimuli [Ms^{-1}]. The control values of light intensity for 20 seconds period solution are obtained with a periodicity constraint of t_s=20 seconds in the boundary value problem Eq. 6.6.

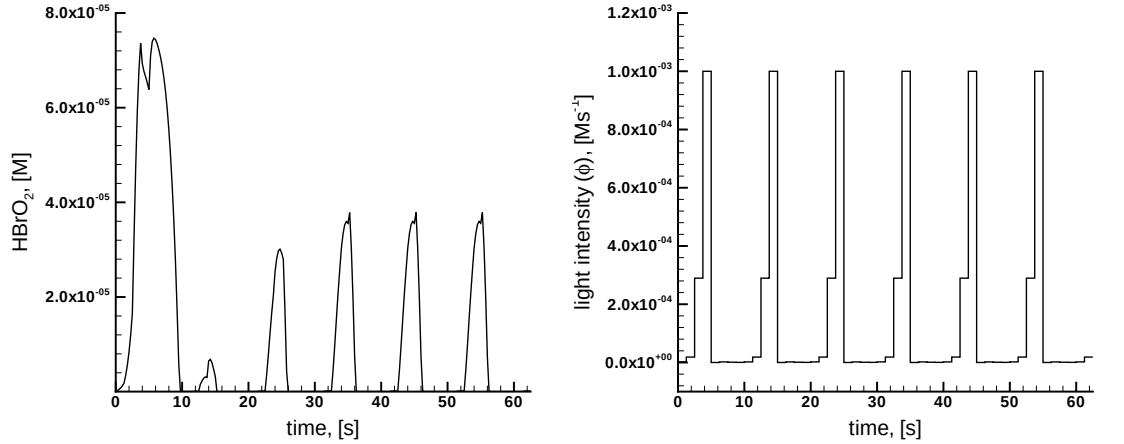

Figure 6.18: Long term simulation under the repetitive periodic forcing of control parameter light intensity with random initial conditions in case of 8-variable model. Plot shows the concentraion of $HBrO_2$ [M] with time. The control values of light intensity [Ms^{-1}] for 10 seconds period solution are obtained with a periodicity constraint of t_s=10 seconds in the boundary value problem Eq. 6.6.

We simulated the ODE system (6.2) with random initial conditions for obtaining a 10 second oscillation period, which is shown in Figure 6.18 with optimal

repetitive stimuli calculated by solving the optimal control problem Eq. (6.6) with t_s=10 seconds. The transient response in this case is very clear, nevertheless the system eventually reaches a 10 second periodic orbit. As the oscillation period to be induced in the BZ system gets smaller, the dependence of BZ system's dynamics on initial conditions gets more sensitive. For obtaining a 1 second oscillation period with repetitive stimuli, not only the control values are important but also the initial conditions of all the variables. Having a good initial condition is crucial in this case and by trial and error, we found some initial conditions for which the BZ system's dynamics is stable. Figure 6.19 *(left)* shows the concentration of $HBrO_2$ with 1 second period oscillations and Figure 6.19 *(right)* shows the corresponding repetitive periodic stimuli needed to induce such dynamics.

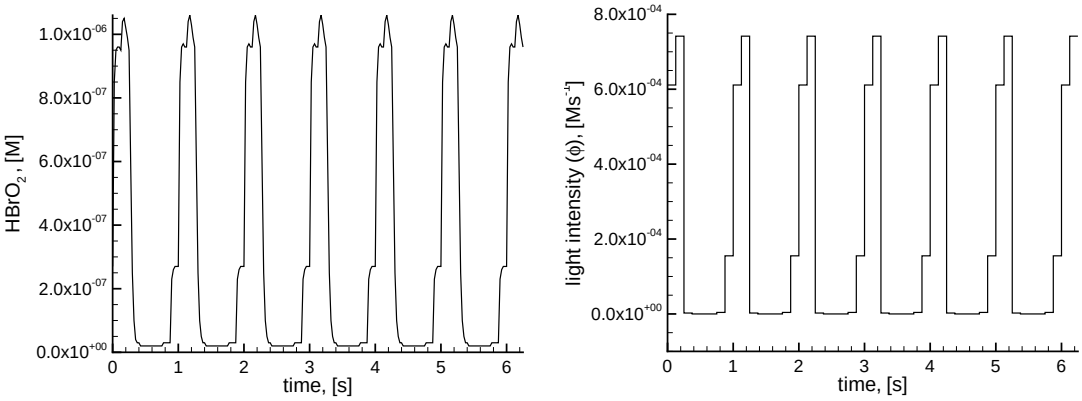

Figure 6.19: Long term simulation under the repetitive periodic forcing of control parameter light intensity with random initial conditions in case of 8-variable model. Plot shows the concentraion of $HBrO_2$ [M] with time. The control values of light intensity [Ms^{-1}] for 1 seconds period solution are obtained with a periodicity constraint of t_s=1 seconds in the boundary value problem Eq. 6.6.

6.4.3 Comparions with 3-variable modified Oregonator model

Control results in Section 6.4.1 and Section 6.4.2 for the 8-variable reduced model are compared with a simple 3-variable modified Oregonator (MO) model. The 3-variable Oregonator model has been modified to include the photosensitivity of the Ru-catalyzed BZ reaction medium [205]. The kinetic part of the model is given by the following equations for the concentrations of bromus acid $HBrO_2(u)$, the oxidized form of catalyst Ru(III)(v), and bromide(w).

$$\epsilon \frac{du}{dt} = u - u^2 - w(u - q) \tag{6.7a}$$

$$\frac{dv}{dt} = u - v \tag{6.7b}$$

$$\epsilon' \frac{dw}{dt} = fv - w(v + q) + \phi \tag{6.7c}$$

where $\epsilon = 0.08547$, $\epsilon' = 9.4428 \times 10^{-4}$ and $q = 0.002$ are scaling parameters, $f = 1.4$ is the stoichiometry parameter, and ϕ represents the photochemically induced

bromide flow which is assumed to be proportional to the applied light intensity.

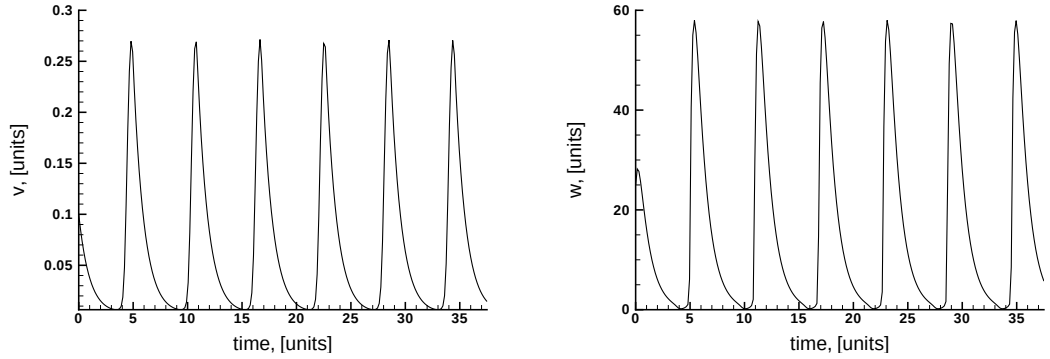

Figure 6.20: 3-variable modified Oregonator model for BZ system dynamics under dark conditions having a time period of 6.25 units. Plots shows the time varying uniform oscillations in non-dimensionalized variables v and w respectively.

In case of the 3-variable MO model, under dark conditions (ϕ=0) and at constant flowrate value of k_f=0.01, the oscillations have a period of about 6.25 units (T_{dark}=6.25) (as shown in Figure 6.20). By increasing the light intensity to a value ϕ=0.0038, one can suppress the oscillations completely. For obtaining the reduced

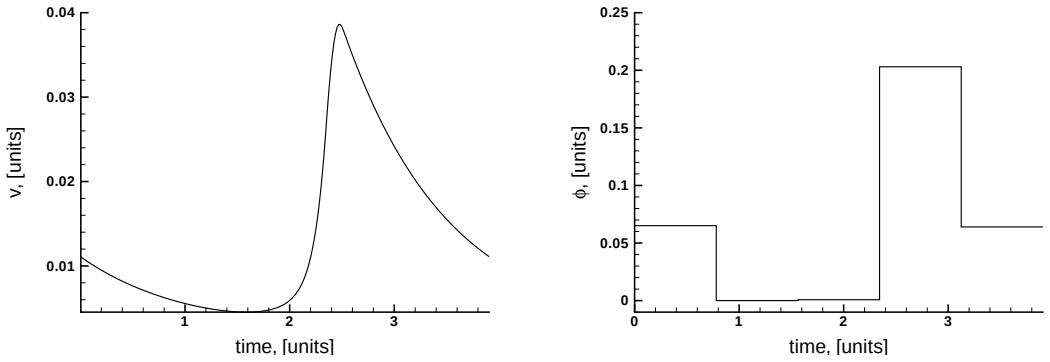

Figure 6.21: Periodic orbit with a time period of 3.90625 units by using ϕ as control parameter. Plot shows the desired time period in v and piecewise constant control of ϕ to obtain the desired period in case of 3-variable modified Oregonator model.

period oscillations in case of modified 3-variable Oregonator model, a similar control analysis as in Section 6.4.1 is done. Here, we would like to reduce the oscillation period till $\alpha = 0.03125$ ($\alpha = T/T_{dark}$), which corresponds to T=1 second in case of 8-variable model. Control results are shown in case of 3-variable MO model in the Figure 6.21 for α=0.625 (i.e. with a time period t_s=3.90625 which corresponds to T=20 seconds in case of reduced 8-variable model). Figure 6.21 *(left)* shows the non-dimensionalized variable v and the corresponding piecewise constant control values of parameter ϕ required for obtaining t_s=3.90625 oscillations on Figure 6.21 *(right)*. Amplitude of these oscillations obtained are significantly smaller when compared

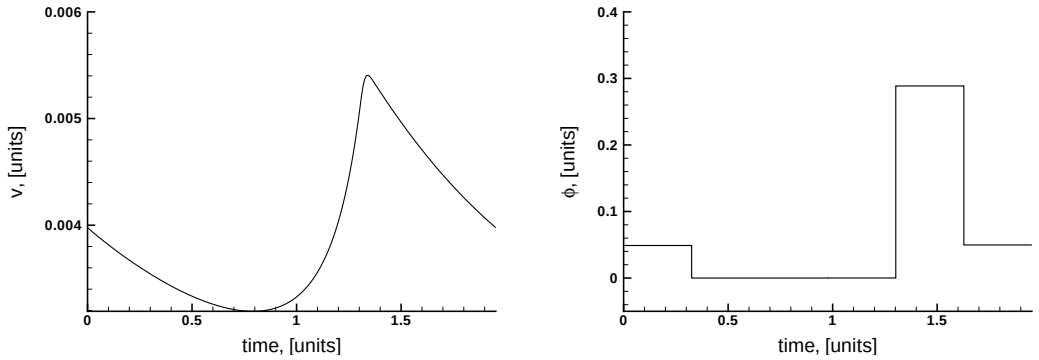

Figure 6.22: Periodic orbit with a time period of 1.953125 units by using ϕ as control parameter. Plot shows the desired time period in v and piecewise constant control of ϕ to obtain the desired period in case of 3-variable modified Oregonator model.

to dark period oscillations as in case of the 8-variable model. Figure 6.22 shows another periodic orbit of v for α=0.3125 (i.e with t_s=1.953125) with time varying control parameter ϕ. Amplitude of oscillations gets even smaller in this case. In case of 3-variable MO model we could not reduce the oscillation period less than T=1 unit. Figure 6.23 shows the plot drawn between u and v on a logarithmic scale, the bigger limit cycle corresponds to the oscillations under dark conditions and the smaller limit cycle corresponds to the solution obtained with t_s=1.953125 as periodicity constraint. Interestingly, in case of 3-variable MO model one can obtain these reduced period oscillations even with constant illumination of light. In case of 8-variable model for obtaining the reduced period of oscillations, the light intensity in all the results is time dependent.

Response of BZ system to the optimal periodic stimuli in case of 3-variable MO model is carried out as in Section 6.4.2. The objective functional here for the boundary value problem is same and is given by optimal control problem Eq. (6.6) and has to solved with respect to constraints given by Eq. 6.7 along with new bounds on ϕ. The BZ system's response in case of 3-variable MO model to the repetitive optimal stimuli obtained, as a solution of the above control problem is not stable, even if one starts the simulation with initial conditions obtained from the optimal solution.

We computed the fundamental solution and the sensitivity of the final state with respect to its initial values in case of 3-variable MO model for t_s=3.90625 and t_s=1.953125 periodic oscillations, which is called the monodromy matrix. A numerical computation of the monodromy matrix for these periodic orbits and eigenvalue decomposition yields one eigenvalue, i.e. Floquet multiplier that is greater than one in both cases. A Floquet multiplier greater than one confirms that the optimal solutions obtained in case 3-variable MO model for reduced period oscillations are not stable. Where as in case of the 8-variable model, for repetitive stimulus, irrespective of initial conditions, the system eventually reached the desired limit cycle with

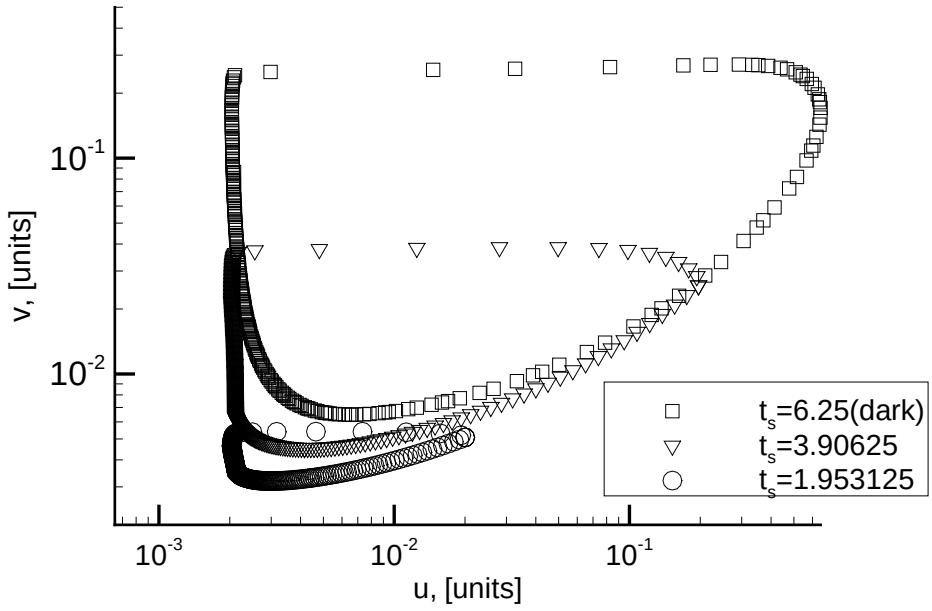

Figure 6.23: Limit cycles of different time periodic orbits obtained with time varying ϕ as control parameter. Plot shows the variables u and v on logarithmic scale for different desired time periods (t_s) in case of 3-variable modified Oregonator model.

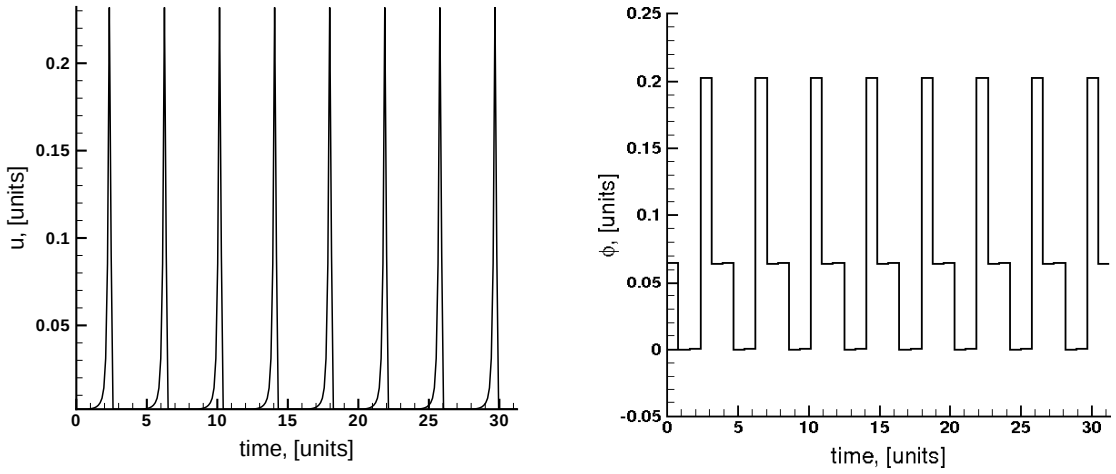

Figure 6.24: Long term simulation under the repetitive periodic forcing of control parameter light intensity with optimal initial conditions in case of 3-variable modified Oregonator model. Plot shows the variable u with non-dimensionalized time. The control values of ϕ for 3.90625 units period solution are obtained according to boundary value problem Eq. (6.6) with equation (6.7) as constraints.

a reduced oscillation period. By trail and error, we found some initial conditions in case of 3-variable MO model for obtaining the desired period oscillations with repetitive stimuli. Figure 6.24 and Figure 6.25 shows the u and the corresponding time varying repetitive ϕ required for obtaining the reduced period oscillations of t_s=3.90625 and t_s=1.953125 respectively.

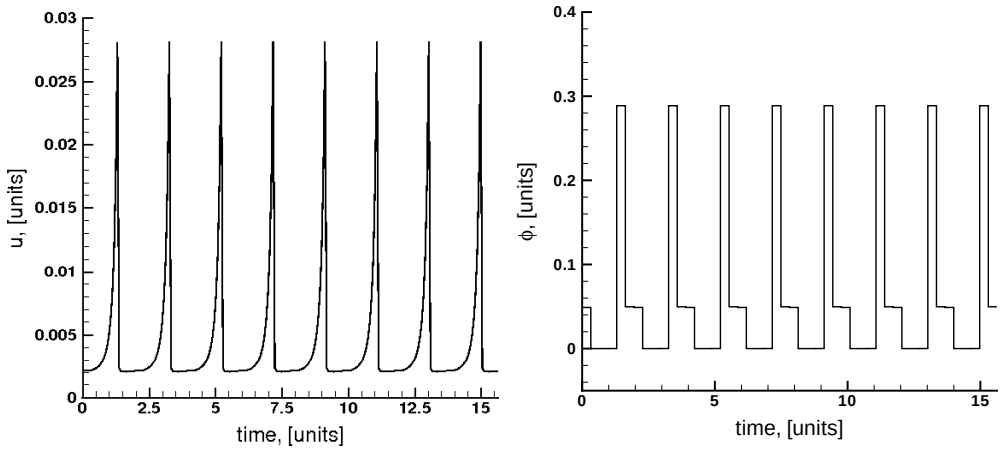

Figure 6.25: Long term simulation under the repetitive periodic forcing of control parameter light intensity with optimal initial conditions in case of 3-variable modified Oregonator model. Plot shows the concentraion of $HBrO_2$ with time. The control values of light intensity for 1.953125 units period solution are obtained according to boundary value problem Eq. (6.6) with equation (6.7) as constraints.

Chapter 7

Summary, Conclusion and Outlook

Applications of control theory to complex self-organized biological systems and model-based specific manipulation of system dynamics are promising visions in biomedical applications for systematic design of chronomodulated therapeutics. Here, we demonstrate the value of numerical optimal control for such tasks exploiting the fundamental optimization idea to force the system to desired behavior with the best possible results. As an example to demonstrate optimal control of models for circadian rhythms in *Drosophila* and BZ reaction systems to manipulate the dynamics in a systematic way.

In chapter 2, we present basic concepts of nonlinear dynamics and different approaches to solve the optimal control problems. Our optimal control problems are solved numerically using a direct multiple-shooting approach (chapter 3) implemented in MUSCOD-II [53, 69]. This method allows to efficiently treat unstable systems that arise in modeling self-organized dynamics.

In chapter 4, we considered circadian rhythms in *Drosophila* as an example of a self-organized biological system. Analysis of the circadian clock model demonstrates that control inputs, such as light that directly influences the parameter ν_{dT} and translation/transcription rates can be used to manipulate the system dynamics. The use of such artificial light pulses or drugs that activate/inhibit the translation/transcription rates, as entraining agents, may help to reduce the recovery time of circadian systems when they are disturbed by significant changes in day light patterns or malfunctioning of the cells. The results obtained here for the *Drosophila* model demonstrate that, we can successfully identify critical phase resetting stimuli, leading to the suppression and restoration of limit cycle oscillations by mixed-integer optimal control. A closed-loop nonlinear model predictive control algorithm can deal with model uncertainties and is effective at providing optimal control inputs for recovering the altered rhythms. Phase resetting, phase tracking and restoration control algorithms described in this thesis can be applied to biological oscillators in general.

The model presented in chapter 5 serves as a starting point towards a detailed modeling of the coupling between cell cycle and circadian cycle. The model should

account for the phase shifts, entrainment conditions between these two cycles and would allow to simulate both healthy and cancerous cells. Circadian rhythms can affect significantly the metabolism, the clearance, and the very action of medications on target cells. Recent research in cancer chronotherapies by Lis *et al.* has pointed out that circadian rhythms can have a very strong effect on toxicity and the efficacy of anti-tumor drugs [206]. A possible explanation is that the effect of anti-cancer drugs on a (healthy or tumorous) cell is dependent on the phase of the cell cycle in which that cell lies. It is possible to drastically reduce the toxicity of antitumor drugs by injecting them when they harm as few healthy cells as possible. The coupled cell cycle / circadian cycle model might allow to set the conditions for entrainment in phase and period by improving the efficacy/toxicity ratio.

In chapter 6, the BZ reaction, which often serves as a prototype for many biological phenomena is considered as another example oscillatory chemical system for controlling the self-organized dynamics. A new model has been developed based on detailed elementary reaction step mechanisms for photo-sensitive BZ reaction. Quantitative minimum models have computational advantage in terms of reduced stiffness and decreased simulation time in particular in spatiotemporal simulations of (bio)chemical reaction systems while retaining the accuracy of a detailed reaction mechanism. In the context of model-based control, such quantitatively accurate minimal models are of great benefit in online-controller design, in particular, if severe real-time constraints have to be fulfilled. By applying a recently developed algorithm [201], the BZ system is automatically decomposed according to time scale separation. We exploit the information provided by the component analysis of the algorithm [201] in carrying out explicit model reduction by quasi-steady-state and partial equilibrium assumptions.

We demonstrate numerically for the BZ system by use of advanced numerical optimal control strategies that a simple nonlinear chemical model system exhibiting oscillations can be forced to a particular desired and predetermined behavior by external dynamic nonlinear control. In particular, we present results on how to stabilize an unstable steady state and drive the system from arbitrary regions in phase space into a desired target state that is not a stable attractor in the uncontrolled case.

Based on the detailed kinetic models, such control strategies for complex self-organizing systems may turn out to be of great benefit in various applications ranging from physicochemical systems in technical process [196], to drug development and biomedical treatment strategies of dynamical diseases [1].

Appendix A

Cell cycle model equations and rate constants

$$\frac{d[ERG]}{dt} = \varepsilon \frac{k_{15}}{1+([DRG]/J_{15})^2} - k_{16}[ERG] \quad \text{(A.1)}$$

$$\frac{d[DRG]}{dt} = \varepsilon(k'_{17}[ERG] + \frac{k_{17}([DRG]/J_{17})^2}{1+([DRG]/J_{17})^2}) - k_{18}[DRG] \quad \text{(A.2)}$$

$$\begin{aligned}\frac{d[cycD]}{dt} &= \varepsilon k_9[DRG] + V_6[CycD:Kip1] + k_{24\mathrm{r}}[CycD:Kip1] \\ &\quad -k_{24}[CycD][Kip1] - k_{10}[CycD] \quad \text{(A.3)}\end{aligned}$$

$$\begin{aligned}\frac{d[cycD:Kip1]}{dt} &= k_{24}[CycD][Kip1] - k_{24\mathrm{r}}[CycD:Kip1] - V_6[CycD:Kip1] \\ &\quad -k_{10}[CycD:Kip1] \quad \text{(A.4)}\end{aligned}$$

$$\begin{aligned}\frac{d[cycE]}{dt} &= \varepsilon(k'_7 + k_7[E2F_{\mathrm{A}}) - V_8[cycE] - k_{25}[CycE][Kip1] \\ &\quad +k_{25\mathrm{r}}[CycE:Kip1] + V_6[CycE:Kip1] \quad \text{(A.5)}\end{aligned}$$

$$\begin{aligned}\frac{d[cycE:Kip1]}{dt} &= k_{25}[CycE][Kip1] - k_{25\mathrm{r}}[CycE:Kip1] - V_6[CycE:Kip1] \\ &\quad -V_8[CycE:Kip1] \quad \text{(A.6)}\end{aligned}$$

$$\begin{aligned}\frac{d[cycA]}{dt} &= \varepsilon k_{29}[E2FA][mass] - k_{30}[Cdc20][cycA] - k_{25}[CycA][Kip1] \\ &\quad +k_{25\mathrm{r}}[CycA:Kip1] + V_6[CycA:Kip1] \quad \text{(A.7)}\end{aligned}$$

$$\begin{aligned}\frac{d[cycA:Kip1]}{dt} &= k_{25}[CycA][Kip1] - k_{25\mathrm{r}}[CycA:Kip1] - V_6[CycA:Kip1] \\ &\quad -k_{30}[Cdc20][CycA:Kip1] \quad \text{(A.8)}\end{aligned}$$

$$\begin{aligned}\frac{d[Kip1]}{dt} &= \varepsilon k_5 - V_6[Kip1] - k_{24}[CycD][Kip1] + k_{24\mathrm{r}}[CycD:Kip1] \\ &\quad -k_{25}[Kip1]([CycE]+[CycA]) + k_{25\mathrm{r}}([CycE:Kip1] \\ &\quad +[CycA:Kip1]) + V_8[CycE:Kip1] + k_{30}[Cdc20][CycA:Kip1] \\ &\quad +k_{10}[CycD:Kip1] \quad \text{(A.9)}\end{aligned}$$

$$\begin{aligned}\frac{d[E2F]}{dt} &= k_{22}([E2FT]-[E2F]) \\ &\quad -(k'_{23}+k_{23}([CycA]+[CycB]))[E2F] \quad \text{(A.10)}\end{aligned}$$

$$\frac{d[Cdh1]}{dt} = (k'_3 + k_3[Cdh20])\frac{1-[Cdh1]}{J_3+1-[Cdh1]} - V_4\frac{[Cdh1]}{J_4+[Cdh1]} \quad (A.11)$$

$$\frac{d[Cdc20_{\mathrm{T}}}{dt} = \varepsilon(k'_{11} + k_{11}[CycB]) - k_{12}[Cdc20_{\mathrm{T}}] \quad (A.12)$$

$$\frac{d[Cdc20]}{dt} = k_{13}[IEP]\frac{[Cdc20_{\mathrm{T}}]-[Cdc20]}{J_{13}+[Cdc20_{\mathrm{T}}]-[Cdc20]} - k_{14}\frac{[Cdc20]}{J_4+[Cdc20]} - k_{12}[Cdc20] \quad (A.13)$$

$$\frac{d[PPX]}{dt} = \varepsilon k_{33} - k_{34}[PPX] \quad (A.14)$$

$$\frac{d[IEP]}{dt} = k_{31}[CycB]\frac{1-[IEP]}{J_{31}+1-[IEP]} - k_{32}[PPX]\frac{[IEP]}{J_{32}+[IEP]} \quad (A.15)$$

$$\frac{[GM]}{dt} = k_{27}[mass]H(\frac{[Rb_{\mathrm{hypo}}]}{[Rb_{\mathrm{T}}]}) - k_{28}[GM] \quad (A.16)$$

$$\frac{d[mass]}{dt} = \varepsilon\mu[GM] \quad (A.17)$$

$$\frac{d[cycB]}{dt} = \varepsilon(k'_1 + \frac{k_1([CycB]/J_1)^2}{1+([CycB]/J_1)^2})[mass] - (kwee1' + kwee1''[Wee1])[cycB] + (kcdc25' + kcdc25''[Cdc25a])[cycBP] - V_2[CycB] \quad (A.18)$$

Steady state relations

$$[PP1_{\mathrm{A}}] = \frac{[PP1_{\mathrm{T}}]}{1+K_{21}(\phi_{\mathrm{E}}([CycE]+[CycA])+\phi_{\mathrm{B}}[CycB])} \quad (A.19)$$

$$Rb_{\mathrm{hypo}} = \frac{[Rb_{\mathrm{T}}]}{1+\frac{k_{20}(\lambda_{\mathrm{D}}[CycD_{\mathrm{T}}]+\lambda_{\mathrm{E}}[CycE]+\lambda_{\mathrm{A}}[CycA]+\lambda_{\mathrm{B}}[CycB])}{k'_{19}([PP1_{\mathrm{T}}]-[PP1_{\mathrm{A}}])+k_{19}[PP1_{\mathrm{A}}]}} \quad (A.20)$$

$$E2F_{\mathrm{A}} = \frac{([E2F_{\mathrm{T}}]-[E2F:Rb])[E2F]}{[E2F_{\mathrm{T}}]} \quad (A.21)$$

$$E2F:Rb = \frac{2[E2F_{\mathrm{T}}][Rb_{\mathrm{hypo}}]}{[E2F_{\mathrm{T}}]+[Rb_{\mathrm{hypo}}]+L+\sqrt{([E2F_{\mathrm{T}}]+[Rb_{\mathrm{hypo}}]+L)^2-4[E2F_{\mathrm{T}}][Rb_{\mathrm{hypo}}]}} \quad (A.22)$$

$$V_2 = k'_2(1-[Cdh1]) + k_2[Cdh1] + k''_2[Cdc20] \quad (A.23)$$

$$V_4 = k_4(\gamma_{\mathrm{A}}[CycA]+\gamma_{\mathrm{B}}[CycB]) \quad (A.24)$$

$$V_6 = k'_6 + k_6(\eta_{\mathrm{E}}[CycE]+\eta_{\mathrm{A}}[CycA]+\eta_{\mathrm{B}}[CycB]) \quad (A.25)$$

$$V_8 = k'_8\frac{k_8(\psi_{\mathrm{E}}([CycE]+[CycA])+\psi_{\mathrm{B}}[CycB])}{J_8+[cycE_{\mathrm{T}}]} \quad (A.26)$$

$$L = \frac{k_{26r}}{k_{26}} + \frac{k_{20}}{k_{26}}(\lambda_{\mathrm{D}}[CycD]+\lambda_{\mathrm{E}}[CycE]+\lambda_{\mathrm{A}}[CycA]+\lambda_{\mathrm{B}}[CycB]) \quad (A.27)$$

Kinetic parameter	Value(h^{-1})	Kinetic parameter	Value(h^{-1})
k_1'	0.1	k_1	0.6
k_2'	0.05	k_2	20
k_2''	1	k_3'	7.5
k_3	140	k_4	40
k_5	20	k_6'	10
k_6	100	k_7'	20
k_7	0.6	k_8'	0.1
k_8	2	k_9	2.5
k_{10}	5	k_{11}'	0
k_{11}	1.5	k_{13}	5
k_{14}	2.5	k_{15}	0.25
k_{16}	0.25	k_{17}'	0.35
k_{17}	10	k_{18}	10
k_{19}'	0	k_{19}	20
k_{20}	10	k_{22}	1
k_{23}'	0.005	k_{23}	1
k_{24}	1000	$k_{24\mathrm{r}}$	10
k_{25}	1000	$k_{25\mathrm{r}}$	10
k_{26}	10	$k_{26\mathrm{r}}$	200
k_{27}	0.2	k_{28}	0.2
k_{29}	0.05	k_{30}	20
k_{31}	0.7	k_{32}	1.8
k_{33}	0.05	k_{34}	0.05
μ	0.061		

Table A.1: Rate constants for cell cycle model for Equations A.2-A.27. All the rate of synthesis terms for proteins have a factor ϵ; which represents the translation efficiency of the ribosomes. ϵ is a number between 0 and 1; its value is influenced by growth factors and by translation inhibitors like cycloheximide. In all our numerical simulations we used the value of 1. The model assumes that a cell divides, [mass]= [mass]/2, when Cdh1 crosses 0.2 from below.

Dimensionless constants	Value
J_1	0.1
J_3	0.01
J_4	0.01
J_8	0.1
J_{13}	0.005
J_{14}	0.005
J_{15}	0.1
J_{17}	0.3
J_{31}	0.01
J_{32}	0.01
K_{21}	1
$[E2F_{\mathrm{T}}]$	5
$[PP1_{\mathrm{T}}]$	1
$[Rb_{\mathrm{T}}]$	10
ϕ_{E}	25
ϕ_{B}	2
γ_{A}	0.3
γ_{B}	1
η_{E}	0.5
η_{B}	1
λ_{D}	3.3
λ_{E}	5
λ_{A}	3
λ_{B}	5
ψ_{E}	1
ψ_{B}	0.05
ε	1

Table A.2: Dimensionless constants for cell cycle model for Equations A.2-A.27

Appendix B

Circadian mammalian model-equations and rate-constants

(a) mRNAs of *Per, Cry* and Bmal1:

$$\frac{dM_{\rm P}}{dt} = \nu_{\rm sP}\frac{B_{\rm N}^{\rm n}}{K_{\rm AP}^{\rm n}+B_{\rm N}^{\rm n}} - \nu_{\rm mP}\frac{M_{\rm P}}{K_{\rm mP}+M_{\rm P}} - k_{\rm dmp}M_{\rm P}, \tag{B.1}$$

$$\frac{dM_{\rm C}}{dt} = \nu_{\rm sC}\frac{B_{\rm N}^{\rm n}}{K_{\rm AC}^{\rm n}+B_{\rm N}^{\rm n}} - \nu_{\rm mC}\frac{M_{\rm C}}{K_{\rm mC}+M_{\rm C}} - k_{\rm dmc}M_{\rm C}, \tag{B.2}$$

$$\frac{dM_{\rm B}}{dt} = \nu_{\rm sB}\frac{K_{\rm IB}^{\rm m}}{K_{\rm IB}^{\rm m}+B_{\rm N}^{\rm m}} - \nu_{\rm mB}\frac{M_{\rm B}}{K_{\rm mB}+M_{\rm B}} - k_{\rm dmb}M_{\rm B} \tag{B.3}$$

(b) Phosphorylated and non-phosphorylated proteins PER and CRY in the cytosol:

$$\begin{aligned}\frac{dP_{\rm C}}{dt} &= k_{\rm sP}M_{\rm P} - V_{1\rm P}\frac{P_{\rm C}}{K_{\rm p}+P_{\rm C}} + V_{2\rm P}\frac{P_{\rm CP}}{K_{\rm dp}+P_{\rm CP}} + k_4 PC_{\rm C}\\ &\quad -k_3 P_{\rm C}C_{\rm C} - k_{\rm dn}P_{\rm C},\end{aligned} \tag{B.4}$$

$$\begin{aligned}\frac{dC_{\rm C}}{dt} &= k_{\rm sC}M_{\rm C} - V_{1\rm C}\frac{C_{\rm C}}{K_{\rm p}+C_{\rm C}} + V_{2\rm C}\frac{C_{\rm CP}}{K_{\rm dp}+C_{\rm CP}} + k_4 PC_{\rm C}\\ &\quad -k_3 P_{\rm C}C_{\rm C} - k_{\rm dnc}C_{\rm C},\end{aligned} \tag{B.5}$$

$$\frac{dP_{\rm CP}}{dt} = V_{1\rm P}\frac{P_{\rm C}}{K_{\rm p}+P_{\rm C}} - V_{2\rm P}\frac{P_{\rm CP}}{K_{\rm dp}+P_{\rm CP}} - \nu_{\rm dPC}\frac{P_{\rm CP}}{K_{\rm d}+P_{\rm CP}} - k_{\rm dn}P_{\rm CP}, \tag{B.6}$$

$$\frac{dC_{\rm CP}}{dt} = V_{1\rm C}\frac{C_{\rm C}}{K_{\rm p}+C_{\rm C}} - V_{2\rm C}\frac{C_{\rm CP}}{K_{\rm dp}+C_{\rm CP}} - \nu_{\rm dCC}\frac{C_{\rm CP}}{K_{\rm d}+C_{\rm CP}} - k_{\rm dn}C_{\rm CP}. \tag{B.7}$$

(c) Phosphorylated and non-phosphorylated PER-CRY complex in cytosol and nucleus:

$$\begin{aligned}\frac{dPC_{\rm C}}{dt} &= -V_{1\rm PC}\frac{PC_{\rm C}}{K_{\rm p}+PC_{\rm C}} + V_{2\rm PC}\frac{PC_{\rm CP}}{K_{\rm dp}+PC_{\rm CP}} - k_4 PC_{\rm C} + k_3 P_{\rm C}C_{\rm C}\\ &\quad +k_2 PC_{\rm N} - k_1 PC_{\rm C} - k_{\rm dn}PC_{\rm C},\end{aligned} \tag{B.8}$$

$$\begin{aligned}\frac{dPC_{\rm N}}{dt} &= -V_{3\rm PC}\frac{PC_{\rm N}}{K_{\rm p}+PC_{\rm N}} + V_{4\rm PC}\frac{PC_{\rm NP}}{K_{\rm dp}+PC_{\rm NP}} - k_2 PC_{\rm N} + k_1 PC_{\rm C}\\ &\quad -k_7 B_{\rm N}PC_{\rm N} - k_8 I_{\rm N} - k_{\rm dn}PC_{\rm N}\end{aligned} \tag{B.9}$$

$$\frac{dPC_{\rm CP}}{dt} = V_{\rm 1PC}\frac{PC_{\rm C}}{K_{\rm p}+PC_{\rm C}} - V_{\rm 2PC}\frac{PC_{\rm CP}}{K_{\rm dp}+PC_{\rm CP}} - \nu_{\rm dPCC}\frac{PC_{\rm CP}}{K_{\rm d}+PC_{\rm CP}} - k_{\rm dn}PC_{\rm CP}, \quad \text{(B.10)}$$

$$\frac{dPC_{\rm NP}}{dt} = V_{\rm 3PC}\frac{PC_{\rm N}}{K_{\rm p}+PC_{\rm N}} - V_{\rm 4PC}\frac{PC_{\rm NP}}{K_{\rm dp}+PC_{\rm NP}} - \nu_{\rm dPCN}\frac{PC_{\rm NP}}{K_{\rm d}+PC_{\rm NP}} - k_{\rm dn}PC_{\rm NP}. \quad \text{(B.11)}$$

(d) Phosphorylated and non-phosphorylated protein BMAL1 in the cytosol and nucleus:

$$\frac{dB_{\rm C}}{dt} = k_{\rm sB}M_{\rm B} - V_{\rm 1B}\frac{B_{\rm C}}{K_{\rm p}+B_{\rm C}} + V_{rm2B}\frac{B_{\rm CP}}{K_{\rm dp}+B_{\rm CP}} - k_5B_{\rm C} + k_6B_{\rm N} - k_{\rm dn}B_{\rm C} \quad \text{(B.12)}$$

$$\frac{dB_{\rm CP}}{dt} = V_{\rm 1B}\frac{B_{\rm C}}{K_{\rm p}+B_{\rm C}} - V_{\rm 2B}\frac{B_{\rm CP}}{K_{\rm dp}+B_{\rm CP}} - \nu_{\rm dBC}\frac{B_{\rm CP}}{K_{\rm d}+B_{\rm CP}} - k_{\rm dn}B_{\rm CP} \quad \text{(B.13)}$$

$$\frac{dB_{\rm N}}{dt} = -V_{\rm 3B}\frac{B_{\rm N}}{K_{\rm p}+B_{\rm N}} - V_{\rm 4B}\frac{B_{\rm NP}}{K_{\rm dp}+B_{\rm NP}} + k_5B_{\rm C} - k_6B_{\rm N} - k_7B_{\rm N}PC_{\rm N} + k_8I_{\rm N} - k_{\rm dn}B_{\rm N}, \quad \text{(B.14)}$$

$$\frac{dB_{\rm NP}}{dt} = V_{\rm 3B}\frac{B_{\rm N}}{k_{\rm p}+B_{\rm N}} - V_{\rm 4B}\frac{B_{\rm NP}}{K_{\rm dp}+B_{\rm NP}} - \nu_{dBN}\frac{B_{\rm NP}}{K_{\rm d}+B_{\rm NP}} - k_{\rm dn}B_{\rm NP}. \quad \text{(B.15)}$$

(e) Inactive complex between PER-CRY and CLOCK-BMAL1 in nucleus:

$$\frac{dI_{\rm N}}{dt} = -k_8I_{\rm N} + k_7B_{\rm N}PC_{\rm N} - \nu_{dIN}\frac{I_{\rm N}}{K_{\rm d}+I_{\rm N}} - k_{\rm dn}I_{\rm N}. \quad \text{(B.16)}$$

Kinetic parameter	Parameter value	Kinetic parameter	Parameter value
k_1	$0.4h^{-1}$	n	4
k_2	$0.2h^{-1}$	V_{1B}	$0.5nMh^{-1}$
k_3	$0.4nM^{-1}h^{-1}$	V_{1C}	$0.6nMh^{-1}$
k_4	$0.2h^{-1}$	V_{1P}	$0.4nMh^{-1}$
k_5	$0.4h^{-1}$	V_{1PC}	$0.4nMh^{-1}$
k_6	$0.2h^{-1}$	V_{2B}	$0.1nMh^{-1}$
k_7	$0.5h^{-1}$	V_{2C}	$0.1nMh^{-1}$
k_8	$0.1h^{-1}$	V_{2P}	$0.3nMh^{-1}$
K_{AP}	$0.7nM$	V_{2PC}	$0.1nMh^{-1}$
K_{AC}	$0.6nM$	V_{3B}	$0.5nMh^{-1}$
K_{IB}	$2.2nM$	V_{3PC}	$0.4nMh^{-1}$
k_{dmb}	$0.01h^{-1}$	V_{4B}	$0.2nMh^{-1}$
k_{dmc}	$0.01h^{-1}$	V_{4PC}	$0.1nMh^{-1}$
k_{dmp}	$0.01h^{-1}$	V_{phos}	$0.4nMh^{-1}$
k_{dn}	$0.01h^{-1}$	ν_{dBC}	$0.5nMh^{-1}$
k_{dnc}	$0.12h^{-1}$	ν_{dBN}	$0.6nMh^{-1}$
K_d	$0.3nM$	ν_{dCC}	$0.7nMh^{-1}$
K_{dp}	$0.1nM$	ν_{dIN}	$0.8nMh^{-1}$
K_p	$0.1nM$	ν_{dPC}	$0.7nMh^{-1}$
K_{mB}	$0.4nM$	ν_{dPCC}	$0.7nMh^{-1}$
K_{mC}	$0.4nM$	ν_{dPCN}	$0.7nMh^{-1}$
K_{mP}	$0.31nM$	ν_{mB}	$0.8nMh^{-1}$
k_{sB}	$0.12h^{-1}$	ν_{mC}	$1.0nMh^{-1}$
k_{sC}	$1.6h^{-1}$	ν_{mP}	$1.1nMh^{-1}$
k_{sP}	$0.6h^{-1}$	ν_{sB}	$1.0nMh^{-1}$
M	2	ν_{sC}	$1.1nMh^{-1}$
ν_{sP}	$1.5nMh^{-1}$		

Table B.1: Rate constants for the mammalian circadian model.

Bibliography

[1] J. Walleczek (Ed.). *Self-organized biological dynamics and nonlinear control: Toward understanding complexity, chaos and emergent function in living systems.* Cambridge University Press, Cambridge, 2000.

[2] P. Glansdorff, I. Prigogine. *Thermodynamic theory of structure, stability and fluctuations.* Wiley, London, 1971.

[3] G. Nicolis, I. Prigogine. *Self-organization in nonequilibrium systems: From dissipative structures to order through fluctuations.* Wiley, New York, 1977.

[4] E. Schrödinger. *What is life?* Cambridge University Press, Cambridge, 1980.

[5] I. Prigogine, G. Nicolis. *Biological order, structure and instabilities.* Q Rev Biophys **4**, pp 107–148, 1971.

[6] J. M. T. Thompson, H. B. Stewart. *Nonlinear dynamics and chaos.* Wiley, Chichester / Weinheim, 2002.

[7] A. Goldbeter. *Biochemical oscillations and cellular rhythms: The molecular bases of periodic and chaotic behavior.* Cambridge University Press, Cambridge, 1996.

[8] B. Hess. *Periodic patterns in biology.* Naturwissenschaften **87**, pp 199–211, 2000.

[9] M. D. Bootman, T. J. Collins, C. M. Peppiatt, L. S. Prothero, L. MacKenzie, P. De Smet, M. Travers, S. C. Tovey, J. T. Seo, M. J. Berridge, F. Ciccolini, P. Lipp. *Calcium signalling–an overview.* Semin Cell Dev Biol **12**, pp 3–10, 2001.

[10] M. I. Rabinovich, H. D. Abarbanel. *The role of chaos in neural systems.* Neuroscience **87**, pp 5–14, 1998.

[11] J. Halloy, J. Lauzeral, A. Goldbeter. *Modeling oscillations and waves of cAMP in Dictyostelium discoideum cells.* Biophys Chem **72**, pp 9–19, 1998.

[12] A. Ghosh, B. Chance. *Oscillations of glycolytic intermediates in yeast cells.* Biochem Biophys Res Commun **16**, pp 174–181, 1964.

[13] F. W. Turek. *Circadian rhythms.* Horm Res **49**, pp 109–113, 1998.

[14] T. Mori, C. H. Johnson. *Circadian control of cell division in unicellular organisms.* Prog Cell Cycle Res **4**, pp 185–192, 2000.

[15] R. Smaaland. *Circadian rhythm of cell division.* Prog Cell Cycle Res **2**, pp 241–266, 1996.

[16] K. A. Reijenga, H. V. Westerhoff, B. N. Kholodenko, J. L. Snoep. *Control analysis for autonomously oscillating biochemical networks.* Biophys J **82**, pp 99–108, 2002.

[17] A. Schnitzler, J. Gross. *Normal and pathological oscillatory communication in the brain.* Nat Rev Neurosci **6**, pp 285–296, 2005.

[18] A. Goldbeter, G. Dupont, M. J. Berridge. *Minimal model for signal-induced Ca^{2+} oscillations and for their frequency encoding through protein phosphorylation.* Proc Natl Acad Sci U S A **87**, pp 1461–1465, 1990.

[19] M. D. Bootman, K. W. Young, J. M. Young, R. B. Moreton, M. J. Berridge. *Extracellular calcium concentration controls the frequency of intracellular calcium spiking independently of inositol 1,4,5-trisphosphate production in HeLa cells.* Biochem J **314**, pp 347–354, 1996.

[20] H. Kitano. *Systems biology: a brief overview.* Science **295**, pp 1662–1664, 2002.

[21] H. Kitano. *Computational systems biology.* Nature **420**, pp 206–210, 2002.

[22] E. Ott, C. Grebogi, J. A. Yorke. *Controlling chaos.* Phys Rev Lett **64**, pp 1196–1199, 1990.

[23] K. Pyragas. *Continuous control of chaos by self-controlling feedback.* Phys Lett A **170**, pp 421–428, 1992.

[24] T. Sakurai, E. Mihaliuk, F. Chirila, K. Showalter. *Design and control of wave propagation patterns in excitable media.* Science **296**, pp 2009–2012, 2002.

[25] V. K. Vanag, L. Yang, M. Dolnik, A. M. Zhabotinsky, I. R. Epstein. *Oscillatory cluster patterns in a homogeneous chemical system with global feedback.* Nature **406**, pp 389–391, 2000.

[26] T. Shinbrot, C. Grebogi, E. Ott, J. A. Yorke. *Using small perturbations to control chaos.* Nature **363**, pp 411–417, 1993.

[27] D. Lebiedz, U. Brandt-Pollmann. *Manipulation of self-aggregation patterns and waves in a reaction-diffusion system by optimal boundary control strategies.* Phys Rev Lett **91**, p 208301, 2003.

[28] D. Lebiedz, S. Sager, H. G. Bock, P. Lebiedz. *Annihilation of limit-cycle oscillations by identification of critical perturbing stimuli via mixed-integer optimal control.* Phys Rev Lett **95**, p 108303, 2005.

[29] I. Mihalcescu, W. Hsing, S. Leibler. *Resilient circadian oscillator revealed in individual cyanobacteria.* Nature **430**, pp 81–85, 2004.

[30] S. Panda, J. B. Hogenesch, S. A. Kay. *Circadian rhythms from flies to human.* Nature **417**, pp 329–335, 2002.

[31] I. Edery. *Circadian rhythms in a nutshell.* Physiol Genomics **3**, pp 59–74, 2000.

[32] A. Goldbeter. *A model for circadian oscillations in the Drosophila period protein (PER).* Proc Biol Sci **261**, pp 319–324, 1995.

[33] J.-C. Leloup, D. Gonze, A. Goldbeter. *Limit cycle models for circadian rhythms based on transcriptional regulation in Drosophila and Neurospora.* J Biol Rhythm **14**, pp 433–448, 1999.

[34] J.-C. Leloup, A. Goldbeter. *Toward a detailed computational model for the mammalian circadian clock.* Proc Natl Acad Sci U S A **100**, pp 7051–7056, 2003.

[35] D. B. Forger, C. S. Peskin. *A detailed predictive model of the mammalian circadian clock.* Proc Natl Acad Sci U S A **100**, pp 14806–14811, 2003.

[36] D. E. Zak, J. Stelling, F. J. Doyle III. *Sensitivity analysis of oscillatory (bio)chemical systems.* Comput Chem Eng **29**, pp 663–673, 2005.

[37] J. Stelling, E. D. Gilles, F. J. Doyle III. *Robustness properties of circadian clock architectures.* Proc Natl Acad Sci U S A **101**, pp 13210–13215, 2004.

[38] B. P. Ingalls. *Sensitivity analysis of autonomous oscillations: application to biochemical systems.* In Proceedings of the sixteenth international symposium on Mathematical Theory of Networks and Systems (MTNS), Leuven, Belgium. 2004.

[39] M. Burger, R. J. Field (Ed.). *Oscillations and traveling waves in chemical systems.* Wiley, New York, 1985.

[40] A. N. Zaikin, A. M. Zhabotinsky. *Concentration wave propagation in two-dimensional liquid-phase self-oscillating system.* Nature **225**, pp 535–537, 1970.

[41] A. T. Winfree. *Spiral Waves of Chemical Activity.* Science **175**, pp 634–636, 1972.

[42] M. C. Cross, P. C. Hohenberg. *Pattern-formation outside of equilibrium.* Rev Mod Phys **65**, pp 851–1112, 1993.

[43] J. N. Demas, D. J. Diemente. *An oscillating chemical reaction with a luminescent indicator.* J Chem Educ **50**, pp 357–358, 1973.

[44] L. Kuhnert. *A new optical photochemical memory device in a light-sensitive active medium.* Nature **319**, pp 393–394, 1986.

[45] T. Matsuo, S. Yamaguchi, S. Mitsui, A. Emi, F. Shimoda, H. Okamura. *Control mechanism of the circadian clock for timing of cell division in vivo.* Science **302**, pp 255–259, 2003.

[46] J. Zobeley, D. Lebiedz, J. Kammerer, A. Ishmurzin, U. Kummer. *A new time-dependent complexity reduction method for biochemical systems.* Lect Notes Comput Sc, pp 90–110, 2005.

[47] S. K. Scott. *Chemical chaos.* Clarendon, Oxford, 1991.

[48] R. J. Field, L. Gyorgyi (Ed.). *Chaos in chemistry and biochemistry.* World Scientific, Singapore, 1993.

[49] S. H. Strogatz. *Nonlinear dynamics and chaos with applications to physics, biology, chemistry and engineering.* Perseus Books Group, New York, 2001.

[50] A. S. Mikhailov. *Foundations of synergetics I: Distributed active systems.* Springer-Verlag, Berlin / Heidelberg, 1994.

[51] L. S. Pontryagin, V. G. Boltyanski, R. V. Gamkrelidze, E. F. Miscenko. *The mathematical theory of optimal processes.* Wiley, New York, 1962.

[52] R. E. Bellman. *Dynamic programming.* Princeton University Press, Princeton, New Jersey, 1957.

[53] H. G. Bock, K. J. Plitt. *A multiple shooting algorithm for direct solution of constrained optimal control problems.* In Proceedings of the ninth IFAC world congress, pp 242–247, Pergamon Press, Budapest. 1984.

[54] L. T. Biegler. *Solution of dynamic optimization problems by successive quadratic programming and orthogonal collocation.* In 97^{th} Aiche National Meeting, San Francisco. 1984.

[55] S. E. Dreyfus. *Dynamic programming and the calculus of variations.* Academic Press, New York, 1965.

[56] D. Kraft. *On converting optimal control problems into nonlinear programming problems.* In Computational mathematical programming, Vol. 15 of *NATO ASI Series*, pp 261–280, 1985.

[57] T. F. Edgar, D. M. Himmelblau. *Optimization of chemical processes.* McGraw-Hill, New York, 1988.

[58] H. G. Bock, J. P. Schlöder, V. H. Schulz. *Numerik großer Differentiell-Algebraisher Gleichunen: Simulation und Optimierung.* In Prozeßsimulation, pp 35–80, VCH, Weinheim. 1995.

[59] I. Bauer, F. Finocchi, W. J. Duschl, H. P. Gail, J. P. Schlöder. *Simulation of chemical reactions and dust destruction in protoplanetary accretion disks.* Astron Astrophys **317**, pp 273–289, 1997.

[60] T. Maly, L. R. Petzold. *Numerical methods and software for sensitivity analysis of differential-algebraic systems.* Applied Numerical Mathematics **20**, pp 57–79, 1996.

[61] L. T. Biegler, R. R. Hughes. *Process optimization: A comparative case study.* Comput Chem Eng **7**, pp 645–661, 1983.

[62] S. Storen, T. Hertzberg. *The sequential linear-quadratic programming algorithm for solving dynamic optimization problems - a review.* Comput Chem Eng **19**, pp S495–S500, 1995.

[63] T. Binder, L. Blank, H. G. Bock, R. Bulirsch, W. Dahmen, M. Diehl, T. Kronseder, W. Marquardt, J. P. Schlöder, O. v. Stryk. *Introduction to model based optimization of chemical process on moving horizons.* Online Optimization of Large Scale Systems: State of the Art, pp 295–339, Springer, Berlin / Heidelberg. 2001.

[64] J. E. Cuthrell, L. T. Biegler. *On the optimization of differential-algebraic process systems.* Aiche Journal **33**, pp 1257–1270, 1987.

[65] A. Cervantes, L. T. Biegler. *Large-scale DAE optimization using a simultaneous NLP formulation.* Aiche Journal **44**, pp 1038–1050, 1998.

[66] L. T. Biegler, A. M. Cervantes, A. Wachter. *Advances in simultaneous strategies for dynamic process optimization.* Chem Eng Sci **57**, pp 575–593, 2002.

[67] A. M. Cervantes, A. Wachter, R. H. Tutuncu, L. T. Biegler. *A reduced space interior point strategy for optimization of differential algebraic systems.* Comput Chem Eng **24**, pp 39–51, 2000.

[68] L. T. Biegler, I. E. Grossmann. *Part I: Retrospective on optimization.* Comput Chem Eng **28**, pp 1169–1192, 2004.

[69] D. B. Leineweber, I. Bauer, H. G. Bock, J. P. Schlöder. *An efficient multiple shooting based reduced SQP strategy for large-scale dynamic process optimization. Part 1: theoretical aspects.* Comput Chem Eng **27**, pp 157–166, 2003.

[70] J. Kallrath, H. G. Bock, J. P. Schlöder. *Least square parameter estimation in chaotic differential equations*. Celestial Mechanics and Dynamical Astronomy **56**, pp 353–371, 1993.

[71] B. D. O. Anderson, J. B. Moore. *Optimal control: linear quadratic methods*. Prentice-Hall, New Jersey, 1989.

[72] A. E. Bryson, Y. C. Ho. *Applied optimal control: Optimization, estimation, and control*. Hemisphere Publ. Corp., New York, 1989.

[73] E. B. Lee, L. Markus. *Foundations of optimal control theory*. Wiley, New York, 1968.

[74] M. Diehl. *Real-time optimization for large scale nonlinear processes*. Phd thesis, University of Heidelberg, Germany, 2001.

[75] S. J. Qin, T. A. Badgwell. *An overview of industrial model predictive control technology*. Fifth International Conference on Chemical Process Control- CPC V, pp 232– 256, 1996.

[76] M. Diehl, H. G. Bock, J. P. Schlöder. *A real-time iteration scheme for nonlinear optimization in optimal feedback control*. SIAM J Control Optm **43**, pp 1714–1736, 2005.

[77] S. J. Qin, T. A. Badgwell. *An overview of nonlinear model predictive control applications*. In F. Allgöwer, A. Zheng (Ed.), Nonlinear model predictive control: Theory and applications, pp 3–32, Birkhäuser, Basel. 2001.

[78] M. A. Henson. *Nonlinear model predictive control: current status and future directions*. Comput Chem Eng **23**, pp 187–202, 1998.

[79] S. Sager. *Numerical methods for mixed-integer optimal control problems*. Phd thesis, University of Heidelberg, Germany, 2005.

[80] D. B. Leineweber. *Efficient reduced SQP methods for the optimization of chemical processes described by large sparse DAE models*. In Fortschr.-Ber. VDI Reihe 3, Verfahrenstechnik, VDI Verlag, Düsseldorf. 1999.

[81] D. B. Leineweber. *The theory of MUSCOD in a nutshell*. Diploma thesis, University of Heidelberg, Germany, 1995.

[82] V. H. Schulz, H. G. Bock, M. C. Steinbach. *Exploiting invariants in the numerical solution of multipoint boundary value problems for DAEs*. SIAM J Sci Comput **19**, pp 440–467, 1998.

[83] S. P. Han. *Superlinearly convergent variable-metric algorithms for general nonlinear programming problems.* Math Program **11**, pp 263–282, 1976.

[84] M. J. D. Powell. *The convergence of variable metric methods for nonlinearly constrained optimization calculations.* In Nonlinear programming 3, Academic Press, New York. 1978.

[85] O. Buchauer, P. Hiltmann, M. Kiehl. *Sensitivity analysis of initial-value problems with application to shooting techniques.* Numer Math **67**, pp 151–159, 1994.

[86] K. R. Morison, R. W. H. Sargent. *Optimization of multistage processes described by differential-Algebraic Equations.* In Lecture notes in mathematics, Vol. 1230, pp 86–102, Springer-Verlag, New York. 1986.

[87] M. Caracotsios, W. E Stewart. *Sensitivity analysis of initial value problems with mixed ODEs and algebraic equations.* Comput Chem Eng **9**, pp 359–365, 1985.

[88] H. G. Bock. *Numerical treatment of inverse problems in chemical reaction kinetics.* Vol. 18 of *Modeling of Chemical Reaction Systems, Springer Series in Chemical Physics*, pp 102–125, Springer-Verlag, Heidelberg. 1981.

[89] P. Deuflhard, F. Boremann. *Scientific computing with ordinary differential equations.* Vol. 42 of *Texts in Applied Mathematics*, Springer-Verlag, New York. 2002.

[90] D. Q. Mayne, J. B. Rawlings, C. V. Rao, P. O. M. Scokaert. *Constrained model predictive control: Stability and optimality.* Automatica **36**, pp 789–814, 2000.

[91] M. Diehl, H. G. Bock, J. P. Schloder, R. Findeisen, Z. Nagy, F. Allgower. *Real-time optimization and nonlinear model predictive control of processes governed by differential-algebraic equations.* J Process Contr **12**, pp 577–585, 2002.

[92] P. S. Maybeck. *Stochastic models, estimation, and control.* Academic Press, New York, 1982.

[93] J. S. Albuquerque, L. T. Biegler. *Decomposition algorithms for on-line estimation with nonlinear DAE models.* Comput Chem Eng **21**, pp 283–299, 1997.

[94] V. M. Becerra, P. D. Roberts, G. W. Griffiths. *Applying the extended Kalman filter to systems described by nonlinear differential-algebraic equations.* Control Eng Pract **9**, pp 267–281, 2001.

[95] L. Canaple, T. Kakizawa, V. Laudet. *The days and nights of cancer cells.* Cancer Res **63**, pp 7545–7552, 2003.

[96] D. Bell-Pedersen, V. M. Cassone, D. J. Earnest, S. S. Golden, P. E. Hardin, T. L. Thomas, M. J. Zoran. *Circadian rhythms from multiple oscillators: lessons from diverse organisms.* Nat Rev Genet **6**, pp 544–556, 2005.

[97] M. W. Young, S. A. Kay. *Time zones: a comparative genetics of circadian clocks.* Nat Rev Genet **2**, pp 702–715, 2001.

[98] U. Schibler, J. Ripperger, S. A. Brown. *Peripheral circadian oscillators in mammals: time and food.* J Biol Rhythm **18**, pp 250–260, 2003.

[99] D. R. Gold, S. Rogacz, N. Bock, T. D. Tosteson, T. M. Baum, F. E. Speizer, C. A. Czeisler. *Rotating shift work, sleep, and accidents related to sleepiness in hospital nurses.* Am J Public Health **82**, pp 1011–1014, 1992.

[100] R. G. Foster. *Shedding light on the biological clock.* Neuron **20**, pp 829–832, 1998.

[101] L. P. Shearman, M. J. Zylka, D. R. Weaver, L. F. Kolakowski, S. M. Reppert. *Two period homologs: circadian expression and photic regulation in the suprachiasmatic nuclei.* Neuron **19**, pp 1261–1269, 1997.

[102] S. Yamazaki, R. Numano, M. Abe, A. Hida, R. Takahashi, M. Ueda, G. D. Block, Y. Sakaki, M. Menaker, H. Tei. *Resetting central and peripheral circadian oscillators in transgenic rats.* Science **288**, pp 682–685, 2000.

[103] A. Brzezinski. *Melatonin in humans.* N Engl J Med **336**, pp 186–195, 1997.

[104] Z. Boulos, S. S. Campbell, A. J. Lewy, M. Terman, D. J. Dijk, C. I. Eastman. *Light treatment for sleep disorders: consensus report. VII. Jet lag.* J Biol Rhythm **10**, pp 167–176, 1995.

[105] C. I. Eastman, Z. Boulos, M. Terman, S. S. Campbell, D. J. Dijk, A. J. Lewy. *Light treatment for sleep disorders: consensus report. VI. Shift work.* J Biol Rhythm **10**, pp 157–164, 1995.

[106] F. Lévi. *Cancer chronotherapy.* J Pharm Pharmacol **51**, pp 891–898, 1999.

[107] R. R. Klevecz, R. M. Shymko, D. Blumenfeld, P. S. Braly. *Circadian gating of S phase in human ovarian cancer.* Cancer Res **47**, pp 6267–6271, 1987.

[108] G. Copinschi, K. Spiegel, R. Leproult, E. Van Cauter. *Pathophysiology of human circadian rhythms.* Novartis Found Symp **227**, pp 143–162, 2000.

[109] M. Terman, A. J. Lewy, D. J. Dijk, Z. Boulos, C. I. Eastman, S. S. Campbell. *Light treatment for sleep disorders: consensus report. IV. Sleep phase and duration disturbances.* J Biol Rhythm **10**, pp 135–147, 1995.

[110] R. J. Konopka, S. Benzer. *Clock mutants of Drosophila melanogaster.* Proc Natl Acad Sci U S A **68**, pp 2112–2116, 1971.

[111] R. Allada, N. E. White, W. V. So, J. C. Hall, M. Rosbash. *A mutant Drosophila homolog of mammalian Clock disrupts circadian rhythms and transcription of period and timeless.* Cell **93**, pp 791–804, 1998.

[112] T. K. Darlington, K. Wager-Smith, M. F. Ceriani, D. Staknis, N. Gekakis, T. D. Steeves, C. J. Weitz, J. S. Takahashi, S. A. Kay. *Closing the circadian loop: CLOCK-induced transcription of its own inhibitors per and tim.* Science **280**, pp 1599–1603, 1998.

[113] M. P. Myers, K. Wager-Smith, C. S. Wesley, M. W. Young, A. Sehgal. *Positional cloning and sequence analysis of the Drosophila clock gene, timeless.* Science **270**, pp 805–808, 1995.

[114] N. Gekakis, D. Staknis, H. B. Nguyen, F. C. Davis, L. D. Wilsbacher, D. P. King, J. S. Takahashi, C. J. Weitz. *Role of the CLOCK protein in the mammalian circadian mechanism.* Science **280**, pp 1564–1569, 1998.

[115] X. Jin, L. P. Shearman, D. R. Weaver, M. J. Zylka, G. J. de Vries, S. M. Reppert. *A molecular mechanism regulating rhythmic output from the suprachiasmatic circadian clock.* Cell **96**, pp 57–68, 1999.

[116] M. K. Bunger, L. D. Wilsbacher, S. M. Moran, C. Clendenin, L. A. Radcliffe, J. B. Hogenesch, M. C. Simon, J. S. Takahashi, C. A. Bradfield. *Mop3 is an essential component of the master circadian pacemaker in mammals.* Cell **103**, pp 1009–1017, 2000.

[117] K. Bae, X. Jin, E. S. Maywood, M. H. Hastings, S. M. Reppert, D. R. Weaver. *Differential functions of mPer1, mPer2, and mPer3 in the SCN circadian clock.* Neuron **30**, pp 525–536, 2001.

[118] B. Zheng, U. Albrecht, K. Kaasik, M. Sage, W. Lu, S. Vaishnav, Q. Li, Z. S. Sun, G. Eichele, A. Bradley, C. C. Lee. *Nonredundant roles of the mPer1 and mPer2 genes in the mammalian circadian clock.* Cell **105**, pp 683–694, 2001.

[119] S. M. Reppert, D. R. Weaver. *Coordination of circadian timing in mammals.* Nature **418**, pp 935–941, 2002.

[120] A. L. Gotter, T. Manganaro, D. R. Weaver, L. F. Kolakowski, B. Possidente, S. Sriram, D. T. MacLaughlin, S. M. Reppert. *A time-less function for mouse timeless.* Nat Neurosci **3**, pp 755–756, 2000.

[121] C. Lee, V. Parikh, T. Itsukaichi, K. Bae, I. Edery. *Resetting the Drosophila clock by photic regulation of PER and a PER-TIM complex.* Science **271**, pp 1740–1744, 1996.

[122] K. Kume, M. J. Zylka, S. Sriram, L. P. Shearman, D. R. Weaver, X. Jin, E. S. Maywood, M. H. Hastings, S. M. Reppert. *mCRY1 and mCRY2 are essential components of the negative limb of the circadian clock feedback loop.* Cell **98**, pp 193–205, 1999.

[123] C. Lee, J. P. Etchegaray, F. R. Cagampang, A. S. Loudon, S. M. Reppert. *Posttranslational mechanisms regulate the mammalian circadian clock.* Cell **107**, pp 855–867, 2001.

[124] M. C. Mackey, L. Glass. *Oscillation and chaos in physiological control systems.* Science **197**, pp 287–289, 1977.

[125] J. C. Dunlap, J. J. Loros, P. J. DeCoursey. *Chronobiology: Biological timekeeping.* Sinauer Associates, Sunderland, 2004.

[126] P. E. Hardin, J. C. Hall, M. Rosbash. *Feedback of the Drosophila period gene product on circadian cycling of its messenger RNA levels.* Nature **343**, pp 536–540, 1990.

[127] H. Zeng, Z. Qian, M. P. Myers, M. Rosbash. *A light-entrainment mechanism for the Drosophila circadian clock.* Nature **380**, pp 129–135, 1996.

[128] J. Qiu, P. E. Hardin. *per mRNA cycling is locked to lights-off under photoperiodic conditions that support circadian feedback loop function.* Mol Cell Biol **16**, pp 4182–4188, 1996.

[129] B. P. Ingalls, H. M. Sauro. *Sensitivity analysis of stoichiometric networks: an extension of metabolic control analysis to non-steady state trajectories.* J Theor Biol **222**, pp 23–36, 2003.

[130] F. J. Doyle III, R. Gunawan, N. Bagheri, H. Mirsky, T. L. To. *Circadian rhythm: A natural, robust, multi-scale control system.* Comput Chem Eng **30**, pp 1700–1711, 2006.

[131] N. Bagheri, J. Stelling, F. J. Doyle III. *Quantitative performance metrics for robustness in circadian rhythms.* Bioinformatics **23**, pp 358–364, 2007.

[132] E. J. Doedel. *A program for the automatic bifurcation analysis of autonomous systems.* Congr Num **30**, pp 265–284, 1981.

[133] R. Y. Moore. *Circadian rhythms: basic neurobiology and clinical applications.* Annu Rev Med **48**, pp 253–266, 1997.

[134] Z. Boulos, M. M. Macchi, M. P. Stürchler, K. T. Stewart, G. C. Brainard, A. Suhner, G. Wallace, R. Steffen. *Light visor treatment for jet lag after westward travel across six time zones.* Aviat Space Environ Med **73**, pp 953–963, 2002.

[135] S. Daan, C. S. Pittendrigh. *A functional analysis of circadian pacemakers in nocturnal rodents. II. The variability of phase response curves.* J Comp Physiol A **106**, pp 253–266, 1976.

[136] S. Daan, C. S. Pittendrigh. *A functional analysis of circadian pacemakers in nocturnal rodents. IV. Entrainment: Pacemaker as clock.* J Comp Physiol A **106**, pp 291–331, 1976.

[137] K. Watanabe, T. Deboer, J. H. Meijer. *Light-Induced resetting of the circadian pacemaker: quantitative analysis of transient versus steady-state phase shifts.* J Biol Rhythm **16**, pp 564–573, 2001.

[138] T. Takeuchi, T. Hinohara, K. Uchida, S. Shibata. *Control theoretic views on circadian rhythms.* In Proceedings of the IEEE: International Conference on Control Applications, Munich. 2006.

[139] O. Shaik, S. Sager, O. Slaby, D. Lebiedz. *Phase tracking and restoration of circadian rhythms by model-based optimal control.* IET Systems Biology, (*in press*).

[140] D. Lebiedz, S. Sager, O. S. Shaik, O. Slaby. *Optimal control of self-organized dynamics in cellular signal transduction.* Math Comp Model Dyn **13**, pp 487–502, 2007.

[141] N. Bagheri, J. Stelling, F. J. Doyle III. *Circadian phase entrainment via nonlinear model predictive control.* Int J Robust Nonlin **17**, pp 1555 – 1571, 2007.

[142] N. Bagheri, J. Stelling, F. J. Doyle III. *Optimal phase-tracking of the nonlinear circadian oscillator.* In Proceedings of the American Control Conference, Vol. 5, pp 3235–3240, 2005.

[143] D. B. Leineweber, I. Bauer, H. G. Bock, J. P. Schlöder. *An efficient multiple shooting based reduced SQP strategy for large-scale dynamic process optimization - Part II: Software aspects and applications.* Comput Chem Eng **27**, pp 167–174, 2003.

[144] A. T. Winfree. *Integrated view of resetting a circadian clock.* J Theor Biol **28**, pp 327–374, 1970.

[145] S. Honma, K. Honma. *Light-induced uncoupling of multioscillatory circadian system in a diurnal rodent, Asian chipmunk.* Am J Physiol **276**, pp R1390–R1396, 1999.

[146] M. E. Jewett, R. E. Kronauer, C. A. Czeisler. *Light-induced suppression of endogenous circadian amplitude in humans.* Nature **350**, pp 59–62, 1991.

[147] A. T. Winfree. *The geometry of biological time.* Springer-Verlag, New York, 1980.

[148] D. Lebiedz, U. Brandt-Pollmann. *Dynamic control and information processing in chemical reaction systems by tuning self-organization behavior.* Chaos **14**, p 611, 2004.

[149] D. Lebiedz, U. Brandt-Pollmann. *Manipulation of surface reaction dynamics by global pressure and local temperature control: a model study.* Phys Rev E **70**, p 051609, 2004.

[150] D. Lebiedz, U. Brandt-Pollmann. *Specific external forcing of spatiotemporal dynamics in reaction-diffusion systems.* Chaos **15**, p 23901, 2005.

[151] P. Ruoff, M. Vinsjevik, C. Monnerjahn, L. Rensing. *The Goodwin model: simulating the effect of light pulses on the circadian sporulation rhythm of Neurospora crassa.* J Theor Biol **209**, pp 29–42, 2001.

[152] J. C. Leloup, A. Goldbeter. *Modeling the molecular regulatory mechanism of circadian rhythms in Drosophila.* Bioessays **22**, pp 84–93, 2000.

[153] F. Lévi. *Cancer Chronotherapy.* Lancet Oncol **2**, pp 307–315, 2001.

[154] F. Lévi, U. Schibler. *Circadian rhythms: mechanisms and therapeutic implications.* Annu Rev Pharmacol Toxicol **47**, pp 593–628, 2007.

[155] M. C. Mormont, J. Waterhouse, P. Bleuzen, S. Giacchetti, A. Jami, A. Bogdan, J. Lellouch, J. L. Misset, Y. Touitou, F. Lévi. *Marked 24-h rest/activity rhythms are associated with better quality of life, better response, and longer survival in patients with metastatic colorectal cancer and good performance status.* Clin Cancer Res **6**, pp 3038–3045, 2000.

[156] L. Fu, C. C. Lee. *The circadian clock: pacemaker and tumour suppressor.* Nat Rev Cancer **3**, pp 350–361, 2003.

[157] I. Iurisci, E. Filipski, J. Reinhardt, S. Bach, A. Gianella-Borradori, S. Iacobelli, L. Meijer, F. Lévi. *Improved tumor control through circadian clock induction by Seliciclib, a cyclin-dependent kinase inhibitor.* Cancer Res **66**, pp 10720–10728, 2006.

[158] E. Bernardweil. *A general-model for the simulation of balance, imbalance and control by agonistic antagonistic biological couples.* Mathematical Modelling **7**, pp 1587–1600, 1986.

[159] D. Claude, J. Clairambault. *Period shift induction by intermittent stimulation in a Drosophila model of PER protein oscillations.* Chronobiol Int **17**, pp 1–14, 2000.

[160] B. Laroche, D. Claude. *Flatness-based control of PER protein oscillations in a Drosophila model.* IEEE Transactions On Automatic Control **49**, pp 175–183, 2004.

[161] M. Diehl, I. Uslu, R. Findeisen, S. Schwarzkopf, F. Allgöwer, H. G. Bock, T. Büber, E. D. Gilles, A. Kienle, J. P. Schlöder, E. Stein. *Real-time optimization for large scale processes: Nonlinear model predictive control of a high purity distillation column.* Online Optimization of Large Scale Systems: State of the Art, pp 363–383, Springer-Verlag, Berlin / Heidelberg. 2001.

[162] C. Mott, D. Mollicone, M. van Wollen, M. Huzmezan. *Modifying the human circadian pacemaker using model based predictive control.* In Proceedings of the American Control Conference, Vol. 1, pp 453–458, 2003.

[163] J. W. Barnes, S. A. Tischkau, J. A. Barnes, J. W. Mitchell, P. W. Burgoon, J. R. Hickok, M. U. Gillette. *Requirement of mammalian Timeless for circadian rhythmicity.* Science **302**, pp 439–442, 2003.

[164] K. Unsal-Kaçmaz, T. E. Mullen, W. K. Kaufmann, A. Sancar. *Coupling of human circadian and cell cycles by the timeless protein.* Mol Cell Biol **25**, pp 3109–3116, 2005.

[165] L. Fu, H. Pelicano, J. Liu, P. Huang, C. Lee. *The circadian gene Period2 plays an important role in tumor suppression and DNA damage response in vivo.* Cell **111**, pp 41–50, 2002.

[166] A. Sveiczer, B. Novak, J. M. Mitchison. *The size control of fission yeast revisited.* J Cell Sci **109**, pp 2947–2957, 1996.

[167] P. Nurse. *A long twentieth century of the cell cycle and beyond.* Cell **100**, pp 71–78, 2000.

[168] L. L. Breeden. *Periodic transcription: a cycle within a cycle.* Curr Biol **13**, pp R31–R38, 2003.

[169] D. Hanahan, R. A. Weinberg. *The hallmarks of cancer.* Cell **100**, pp 57–70, 2000.

[170] B. Novák, J. J. Tyson. *A model for restriction point control of the mammalian cell cycle.* J Theor Biol **230**, pp 563–579, 2004.

[171] P. Nurse. *Universal control mechanism regulating onset of M-phase.* Nature **344**, pp 503–508, 1990.

[172] A. B. Pardee. *G1 events and regulation of cell proliferation.* Science **246**, pp 603–608, 1989.

[173] Y. Kita, M. Shiozawa, W. Jin, R. R. Majewski, J. C. Besharse, A. S. Greene, H. J. Jacob. *Implications of circadian gene expression in kidney, liver and the effects of fasting on pharmacogenomic studies.* Pharmacogenetics **12**, pp 55–65, 2002.

[174] T. Hirota, T. Okano, K. Kokame, H. Shirotani-Ikejima, T. Miyata, Y. Fukada. *Glucose down-regulates Per1 and Per2 mRNA levels and induces circadian gene expression in cultured Rat-1 fibroblasts.* J Biol Chem **277**, pp 44244–44251, 2002.

[175] J. H. Stehle, C. von Gall, H-W. Korf. *Melatonin: a clock-output, a clock-input.* J Neuroendocrinol **15**, pp 383–389, 2003.

[176] G. A. Bjarnason, R. Jordan. *Circadian variation of cell proliferation and cell cycle protein expression in man: clinical implications.* Prog Cell Cycle Res **4**, pp 193–206, 2000.

[177] G. A. Bjarnason, R. C. Jordan, R. B. Sothern. *Circadian variation in the expression of cell-cycle proteins in human oral epithelium.* Am J Pathol **154**, pp 613–622, 1999.

[178] G. A. Bjarnason, R. C. Jordan, P. A. Wood, Q. Li, D. W. Lincoln, R. B. Sothern, W. J. Hrushesky, Y. Ben-David. *Circadian expression of clock genes in human oral mucosa and skin: association with specific cell-cycle phases.* Am J Pathol **158**, pp 1793–1801, 2001.

[179] A. C. Ruifrok, M. M. Weil, H. D. Thames, K. A. Mason. *Diurnal variations in the expression of radiation-induced apoptosis.* Radiat Res **149**, pp 360–365, 1998.

[180] M. Tampellini, E. Filipski, X. H. Liu, G. Lemaigre, X. M. Li, P. Vrignaud, E. François, M. C. Bissery, F. Lévi. *Docetaxel chronopharmacology in mice.* Cancer Res **58**, pp 3896–3904, 1998.

[181] L. Calzone, S. Soliman. *Coupling the cell cycle and the circadian cycle.* INRIA, Paris, Technical Report, 2006.

[182] J. Zámborszky. *Connection between the cell cycle and the circadian clock in mammalian cells.* Diploma thesis, Budapest University of Technology and Economics, Hungary, 2007.

[183] U. Schibler. *Circadian rhythms. Liver regeneration clocks on.* Science **302**, pp 234–235, 2003.

[184] P. Strizhak, M. Menzinger. *Nonlinear dynamics of the BZ reaction: A simple experiment that illustrates limit cycles, chaos, bifurcations, and noise.* J Chem Educ **73**, pp 868–873, 1996.

[185] R. Karpal, K. Showalter (Ed.). *Chemical waves and patterns.* Kluwer, Dordrecht, 1995.

[186] S. Kadar, T. Amemiya, K. Showalter. *Reaction mechanism for light sensitivity of the Ru(Bpy)$_3^{2+}$-catalyzed Belousov-Zhabotinsky reaction.* J Phys Chem A **101**, pp 8200–8206, 1997.

[187] T. Amemiya, T. Yamamoto, T. Ohmori, T. Yamaguchi. *Experimental and model studies of oscillations, photoinduced transitions, and steady states in the Ru(Bpy)$_3^{2+}$-catalyzed Belousov-Zhabotinsky reaction under different solute compositions.* J Phys Chem A **106**, pp 612–620, 2002.

[188] H. J. Krug, L. Pohlmann, L. Kuhnert. *Analysis of the modified complete Oregonator accounting for oxygen sensitivity and photosensitivity of Belousov-Zhabotinsky systems.* J Phys Chem **94**, pp 4862–4866, 1990.

[189] M. Jinguji, M. Ishihara, T. Nakazawa. *Primary process of illumination effect on the Ru(Bpy)$_3^{2+}$-catalyzed Belousov-Zhabotinskii reaction.* J Phys Chem **96**, pp 4279–4281, 1992.

[190] A. Kaminaga, I. Hanazaki. *Transient photoresponse of the tris(2,2'-bipyridine) ruthenium(II)-catalyzed minimal bromate oscillator.* J Phys Chem A **102**, pp 3307–3314, 1998.

[191] V. K. Vanag, A. M. Zhabotinsky, I. R. Epstein. *Role of dibromomalonic acid in the photosensitivity of the Ru(Bpy)$_3^{2+}$-catalyzed Belousov-Zhabotinsky reaction.* J Phys Chem A **104**, pp 8207–8215, 2000.

[192] Y. Gao, H. D. Försterling. *Oscillations In The Bromomalonic Acid/Bromate System Catalyzed By Ru(Bpy)$_3^{2+}$.* J Phys Chem **99**, pp 8638–8644, 1995.

[193] H. D. Forsterling, L. Stuk, A. Barr, W. D. Mccormick. *Stoichiometry of bromide production from ceric oxidation of bromomalonic acid in the Belousov-Zhabotinskii reaction.* J Phys Chem **97**, pp 2623–2627, 1993.

[194] L. Gyorgyi, R. J. Field. *A 3-variable model of deterministic chaos in the Belousov-Zhabotinsky reaction.* Nature **355**, pp 808–810, 1992.

[195] T. Amemiya, T. Ohmori, T. Yamaguchi. *An oregonator-class model for photoinduced behavior in the Ru(Bpy)$_3^{2+}$-catalyzed Belousov-Zhabotinsky reaction.* J Phys Chem A **104**, pp 2144–2144, 2000.

[196] I. Z. Kiss, J. L. Hudson. *Chemical complexity: Spontaneous and engineered structures.* Aiche Journal **49**, pp 2234–2241, 2003.

[197] J. Warnatz, U. Maas, R.W. Dibble. *Combustion: Physical and chemical fundamentals, modeling and simulation, experiments, pollutant formation.* Springer-Verlag, Berlin, 2001.

[198] M. S. Okino, M. L. Mavrovouniotis. *Simplification of mathematical models of chemical reaction systems.* Chem Rev **98**, pp 391–408, 1998.

[199] A. N. Gorban, I. V. Karlin, A. Y. Zinovyev. *Constructive methods of invariant manifolds for kinetic problems.* Phys Rep **396**, pp 197–403, 2004.

[200] M. J. Pilling, P. W. Seakins. *Reaction kinetics.* Oxford University Press, Oxford, 1997.

[201] J. Kammerer. *Numerische Verfahren zur dynamischen Komplexitätsreduktion biochemischer Reaktionssysteme.* Phd thesis, University of Heidelberg, Germany, 2007.

[202] U. Maas, S. B. Pope. *Simplifying chemical kinetics: Intrinsic low-dimensional manifolds in composition space.* Combust Flame **88**, pp 239–264, 1992.

[203] P. Deuflhard, J. Heroth. *Dynamic dimension reduction in ODE models.* In F. Keil, W. Mackens, H. Voß, J. Werther (Ed.), Scientific Computing in Chemical Engineering, pp 29–43, Springer-Verlag, Heidelberg. 1998.

[204] O. S. Shaik, J. Kammerer, J. Gorecki, D. Lebiedz. *Derivation of a quantitative minimal model from a detailed elementary-step mechanism supported by mathematical coupling analysis.* J Chem Phys **123**, p 234103, 2005.

[205] H. J. Krug, L. Pohlmann, L. Kuhnert. *Analysis of the modified complete Oregonator accounting for oxygen sensitivity and photosensitivity of Belousov-Zhabotinsky systems.* J Phys Chem **94**, pp 4862–4866, 1990.

[206] C. G. Lis, J. F. Grutsch, P. Wood, M. You, I. Rich, W. J. M. Hrushesky. *Circadian timing in cancer treatment: the biological foundation for an integrative approach.* Integr Cancer Ther **2**, pp 105–111, 2003.

List of Figures

List of Tables

Nomenclature

BDF	Backward Differentiation Formulae
bHLH	Basic-Helix-Loop-Helix
BIP	Binary Integer Programming
BMAL1	Brain and Muscle Arnt-Like protein-1
BZ	Belousov-Zhabotinsky
CDK	Cyclin Dependent Kinase
CKIα	Casein Kinase
CLOCK	Circadian Locomotor Output Cycles Kaput
CRY	Cryptochrome
CSTR	Continuous Stirred Tank Reactor
DAE	Differential-Algebraic Equation
DAESOL	Differential-Algebraic Equation Solver
DBT	Double Time (Protein or gene)
DMS	Direct Multiple Shooting
DSPS	Delayed sleep phase syndrome
EKF	Extended Kalman Filter
END	External Numerical Differentiation
FASPS	Familial Advanced Phase Syndrome
GF	Growth Factors
HJB	Hamilton-Jacobi-Bellman
ILDM	Intrinsic Low-Dimensional Manifold
IND	Internal Numerical Differentiation
IVP	Initial Value Problem
KKT	Karush-Kuhn-Tucker
LP	Linear Programming
MDT	Mass Doubling Time
MILP	Mixed-Integer Linear Programming
MINLP	Mixed-Integer Nonlinear Programming
MIOC	Mixed-Integer Optimal Control
MM	Michaelis-Menten
MPC	Model Predictive Control
MPF	Mitosis Promoting Factor
NLP	Nonlinear Programming
NMPC	Nonlinear Model Predictive Control
ODE	Ordinary Differential Equation
OGY	Ott-Grebogi-Yorke
PEA	Partial-Equilibrium Approximations

Nomenclature

PER	Period (Protein or Gene)
QP	Quadratic Programming
QSSA	Quasi-Steady-State Assumption
SQP	Sequential Quadratic Programming
SCN	Suprachiasmatic nucleus
TIM	Timeless (Protein or Gene)
WEE1	Protein Kinase that control the timing of cell cycle events

Symbols

Symbol	Meaning	Introduced in
G	equality constraint function	Sec. 3.2
H	inequality constraint function	Sec. 3.2
k_f	flow rate in CSTR	Sec. 6.1
k_s	translation frequency	Sec. 4.5.1
λ	Lagrange multiplier vector for equality constraints	Sec. 3.3
μ	Lagrange multiplier vector for inequality constraints	Sec. 3.3
N	number of multiple-shooting intervals	Sec. 3.1.1
p	constant system parameter vector	Sec. 2.1
ϕ	Light intensity	Sec. 6.1
$P_{oc}(x_0)$	optimal control problem for initial value x_0	Sec. 2.2.1
q	vector of "free" NLP variables (controls $q_0, \cdots, q_{N-1}$)	Sec. 3.2
q_i	control parameter on i-th multiple-shooting interval	Sec. 3.1.1
s	vector of "dependent" NLP variables (states $s_0, \cdots, s_N$)	Sec. 3.2
s_i	state node vector $s_i = (s_i^x, s_i^z)$	Sec.3.1.2
s_i^x	differential state node value	Sec. 3.1.2
s_i^z	algebraic state node value	Sec. 3.1.2
T	length of the time horizon	Sec. 2.2.1
T_c	control horizon	Sec. 3.5
T_p	prediction horizon	Sec. 3.5
$T(x_0)$	optimal horizon length for problem $P_{oc}(x_0)$	Sec. 2.2.1
t	time	Sec 2.1
u	control vector	Sec. 2.2
$u^*(t; x_0)$	optimal control trajectory for problem $P_{oc}(x_0)$	Sec. 2.4
w	vector of NLP variables $w = (q, s, p)$	Sec. 3.2
x_0	initial value	Sec. 2.2.1
$\tilde{x}_0$	current initial value in NMPC	Sec. 3.5
ν_{dT}	light controlled protein degradation factor	Sec. 4.3
z	algebraic state vector	Sec. 2.2

Publications

- O. S. Shaik, J. Kammerer, J. Gorecki, D. Lebiedz. Derivation of a quantitative minimal model for the photosensitive Belousov-Zhabotinsky reaction from a detailed elementary-step mechanism. J Chem Phys **123**, p 324103, 2005.
- O. Slaby, S. Sager, O. S. Shaik, U. Kummer, D. Lebiedz. Optimal control of self-organized dynamics in cellular signal transduction. Math Comp Model Dyn, **13**, pp 487-502, 2007.
- O. S. Shaik, S. Sager, O. Slaby, D. Lebiedz. Phase tracking and restoration of circadian rhythms by model-based optimal control. IET Systems Biology, *in press*.

Proceedings

- D. Lebiedz, S. Sager, O. S. Shaik, O. Slaby. Optimal control of self-organized dynamics in cellular signal transduction. Proceedings of the 5th Vienna Symposium of Mathematical Modeling, Vienna, 2006. Argesim Rep. 30, 2006.

Acknowledgments

I would like to thank ···

··· my mentor PD Dr. Dirk Lebiedz suggesting a very interesting project and for his professional advice and support that made this dissertation possible.

··· Prof. Jürgen Warnatz for giving me the opportunity to prepare this work in the excellent scientific environment at IWR.

··· Prof. Jerzy Górecki my coadvisor from Polish academy of sciences, Warsaw, Poland. It was always a pleasure to work with him during my stay at ICM in Warsaw.

··· Prof. Hans Georg Bock and "Simulation and Optimization" group for providing the software MUSCOD-II, which is the basis for calculations in this thesis. I specially thank Dr. Sebastian Sager and Dr. Julia Kammerer for colloborating on this project, Peter kühl and Boris Hauska for helpful suggestions and discussions.

··· the Deutsche Forschungsgemeinschaft for financial support under the International Graduiertenkolleg IGK 710 "Complex processes: Modeling, Simulation and Optimization" at IWR, Heidelberg and ICM, Warsaw.

··· Peter kühl, Jan Albersmeyer, Oliver Slaby, Dr. Mario Mommer, Dr. Obul Reddy, Dr. KVS Badireenath and Sreejith Kuttanikkad for reading and correcting the manuscript.

··· Dr. Uwe Riedel for solving all administrative and financial hurdles during my stay at IWR.

··· my wonderful colleagues from *reaflow* group and graduiertenkolleg IGK 710 for the pleasant interaction.

··· Ingrid Hellwig, Astrid Sudmann, Ria Lynott for their assistance and a special thanks goes to Anna Trykozko from ICM for making the stay in Warsaw a pleasant one.

··· my Indian friends here in heidelberg for creating a home away from home.

··· and, last but not least my family and friends for their patience and support.

··· Is that everyone?

Erklärung:

Hiermit versichere ich, daß ich die Arbeit selbständig verfaßt und keine anderen als die angegebenen Quellen und Hilfsmittel verwendet habe.

Heidelberg, den Osman S Shaik